IASJ
المجلات الاكاديمية العراقية
KJPS
AL-Kitab Journal For Pure Sciences

AL-Kitab Journal For Pure Sciences

Volume : 8 (2024)

Issue: 2

ISSN: 2617-1260 (print)

ISSN: 2617-8141 (online)

DOI: http://10.32441/kjps

Deposit number at the Notional House of Books and Archives, Iraq, 2271 in 2017

Al-Kitab Journal for Pure Science

KJPS

ISSN: 2617-1260 (print), 2617-8141(online)
DOI: http://10.32441/kjps
https://isnra.net/index.php/kjps

An Academic Semi-Annual Journal

Volume: 08 Issue: 02 Dec. 2024

University Website: **www.uoalkitab.edu.iq**
Journal Website: **https://isnra.net/index.php/kjps**
E-mail: **kjps@uoalkitab.edu.iq**

Aims and Scope

The Al-Kitab Journal for Pure Sciences aims to provide an international forum for the publication and dissemination of original work that contributes to the understanding of the principal and related disciplines of science. Al-Kitab Journal for Pure Sciences publishes two peer-reviewed issues per year, an online and print journal, which publishes innovative research papers, literature reviews, and technical notes on the fields of Biology, Computer Sciences, Chemistry, Physics, and Mathematics.

Authors Guidelines

Rules and Instructions for Publication in Al-Kitab Journal for Pure Sciences

First: General requirements

1. The paper is submitted to the Editorial Secretariat directly in four copies with CD-ROM or E-mail of the magazine in MS Word and PDF files.
2. Research before being sent to scientific evaluators is subject to the quotation Turnitin program.
3. Research shall be accepted for publication after being judged by scientific evaluators and according to the rules.
4. The publication fee is (50$) for researchers from Iraqi Universities and (free of charge) for foreign researchers.

Second: To prepare research for publication, authors must follow the following procedures.

1. **The article:**

   The article needs to be typed on one side of A4 paper (Right margin =2.5 cm, left margin =2.5 cm, and 2cm for the top and bottom) with 1.5 space, and the pages must be numbered.

2. **The content organization:**

   MS Word is to be used as follows: "Simplified Arabic" font for the Arabic articles, and "Times New Roman" for the English articles. The Size of the title is 18 bold. The names of the authors will be typed in 11 bold in Arabic and 11 bold in English. Abbreviations, keywords, the main headings, the reference, and the acknowledgment will be typed in 14. Subheadings will be in 12 bold. The abstract will be size 12. The body of the article/paper is in size 12. The order of the paper's content will be as follows:

The article heading, the names of authors and their addresses, and the abstract (Both in Arabic and English).

3. **Research paper title:**

The title must be as short as possible and indicate the contents of the subject together with the name (names) of the authors. The names of the authors to whom correspondence is to be made should be indicated with (*) and show his / her email.

4. **The size:**

The paper should contain no more than 25 pages of journal pages including charts and diagrams.

5. **Abstract:**

The abstract should include the purpose and the means of the founding results and the conclusions. It should also contain the knowledge values of the subject of research. It is meant to be no more than 250 words. It should also emphasize the content of the subject and include the keywords used throughout the paper.

6. **Diagrams:**

Figures and diagrams must be given following the explanation referring to the diagram. Each diagram must contain its title below the diagram at the first size of 12. The diagram should be editable in terms of enlargement or reduction within the margins of the paper size. The parts of each diagram must be grouped into drawing parts.

7. **Tables:**

The tables should follow the parts of the main body and should be located below the indicated part of the text. Tables must have titles with a text size of 12. The text used inside the tables should be of size 12 and kept within the cells of the table.

8. **References:**

The references used in the paper must be given in order and their numbers given inside the square bracket **[ ]**. The following instructions are to be followed:

If the reference is a book, the First name of the reference must be given first followed by the other names. Then the title (bold and Italic) of the book, edition, year of publication, the publisher, and place of publication (year of publication).

Example: **[1]** P. Ring and P. Schuck, "**The Nuclear Many-Body Problem**", First Edition, Springer-Verlag, New York (1980).

(b) If the reference is a research paper or an article in a journal: The name of the author must be given first, the title of the article, the name of the journal, the volume (issue), page (Year). **Example:** **[1]** Ali H. Taqi, R. A. Radhi, and Adil M. Hussein,

"Electroexcitation of Low-lying Particle-Hole RPA States of ^{16}O with WBP Interaction", Communication

Theoretical Physics, 62(6), 839 (2014).

c) If the reference is an M.Sc. or Ph.D. thesis, the name of the anther must be written with the first name first followed by the surname, title of the thesis, the name of the university, and Country (Year).

Example: [1] R. A. Radhi, **"Calculations of Elastic and Inelastic Electron Scattering in Light Nuclei with Shell-Model Wave Functions**", Ph.D. Thesis, Michigan State University, USA (1983).

(d) If the reference is from the conference. Authors Name, "**Paper Title**", Conference, Country, Publisher, volume, page (Year).

Example: [1] Ali H. Taqi and Sarah S. Darwesh, **"Charge-Changing Particle-Hole Excitation of ^{16}N and ^{16}F Nuclei"**, 3rdInternational Advances in Applied Physics and Materials Science Congress, Turkey, AIP Conf. Proc., 1569, 27 (2013)

Third: Privacy Statement

1. The names and e-mail addresses entered into the journal's website will be used exclusively for the purposes stated in this journal and will not be provided for any other purpose or to any other party.
2. The editor of the journal has the right to change any statement or phrase of the research content he may find necessary to express the work suitable to the general style of the journal.
3. After publishing the paper and its presentation on the journal page, the editors' team will destroy all the scrap papers. The author has no right to ask for them in any case.

Fourth: Modernity of sources:

The percentage of modern references used in the research should not be less than 50% of the total references used in the research. Modernity is measured within the last ten years of the year of submission of the research. For example, when submitting the research in 2018, the references should be from 2008 upwards and not less than 50%. The journal prefers to have at least one of the reference types of research published in the previous journal issues.

Note: For more information, visit:

Al-Kitab University Website: www.uoalkitab.edu.iq

Or Journal Website: https://isnra.net/index.php/kjps

The Journal can also be e-mailed to kjps@uoalkitab.edu.iq

Table of Contents

Volume: 08 Issue: 02 Dec. 2024

Al-Kitab Journal for Pure Sciences (2024); 8(2):1-10.
https://doi.org/10.32441/kjps.08.02.p1

Al-Kitab Journal for Pure Sciences
ISSN: 2617-1260 (print), 2617-8141(online)

https://isnra.net/index.php/kjps

Molecular detection of Virulence Factor Genes in Candida albicans Isolated from the Oral Cavity of Local Chicken and Antifungal Susceptibility in Mosul Province

Hawraa F.H. Al-Abedi[*1], Israa Ibrahim Khalil[2], Semaa F.H. Al-Abedi[1]

[1]Department of Biology, College of Education for Pure Sciences, University of Al-Hamdaniya, Al-Hamdaniya, Iraq.
[2]Department of Microbiology, College of Veterinary Medicine, University of Mosul, Mosul /Iraq.

Corresponding Author: hawraafaisal@uohamdaniya.edu.iq

Citation: Al-Abedi HF, Khalil II, Al-Abedi SF. Molecular detection of Virulence Factor Genes in Candida albicans Isolated from the Oral Cavity of Local Chicken and Antifungal Susceptibility in Mosul Province. Al-Kitab J. Pure Sci. [Internet]. 2024 June. 01 [cited 2024 June. 01];8(2):1-10. Available from: https://doi.org/10.32441/kjps.08.02.p1.

Keywords: Candida albicans, molecular techniques, Local Chicken, Oral Cavity, Antifungal Susceptibility.

Article History

Received	11	Apr.	2024
Accepted	21	May	2024
Available online	01	June	2024

Abstract:

Candida spp. is a naturally occurring bacteria in the GI tracts of numerous species, including birds. Candidiasis is an opportunistic illness that emerges when the normal microflora is disturbed. Clinical findings include thickening mucosa and white, elevated pseudomembranous areas. Gross lesions can serve as a presumptive diagnosis. This study aimed to detect and identify Candida albicans as of oral cavity of chicken. The Seventy samples were gathered using swabbing from the oral cavity of the Chicken and transported to the Mycology laboratory, using a cool container for handling. Samples were inoculated onto sabouraud dextrose agar for presumptive identification of Candida albicans. Based on molecular techniques, regarding the consequences of PCR amplification of the 18S rRNA gene in the identification of Candida albicans, this gene has existed existing 50 samples, Metallo-aminopeptidase gene was present in 50/50 (100%) and the alkaline phosphatase sequence gene was once existing in 50/50 (100%). whilst alpha glucosidase used to be existing in 30/50 (60%) and sterol esterase genes 25/50 (50%). Antifungal sensitivity testing results showed that ketoconazole and itraconazole provided the most exceptional Sensitivity (100%) against Candida albicans isolates, followed by fluconazole and Amphotericin B. The outcomes of the present research showed that local poultry oral cavities likely contain pathogenic yeasts.

Keywords: Candida albicans, molecular techniques, Local Chicken, Oral Cavity, Antifungal Susceptibility.

الكشف الجزيئي لجينات عامل الضرواة في المبيضات البيضاء المعزولة من تجويف الفم لدى الدجاج المحلي والحساسية للمضادات الفطرية في محافظة الموصل

حوراء فيصل العابدي[١]، إسراء إبراهيم خليل [٢]، سيماء فيصل حسب الله[١]

قسم علوم الحياة/ كلية التربية للعلوم الصرفة/ جامعة الحمدانية/ الموصل/ العراق[١]

فرع الأحياء المجهرية/ كلية الطب البيطري/ جامعة الموصل/ الموصل/ العراق[٢]

hawraafaisal@uohamdaniya.edu.iq, israibrahim@uomosul.edu.iq, semaa.f@uohamdaniya.edu.iq

الخلاصة:

أجناس المبيضات هي جزء من البكتيريا الطبيعية في الجهاز الهضمي للعديد من الأنواع، بما في ذلك الطيور. داء المبيضات هو عدوى انتهازية فرصيه تحدث عند أي إعاقة للبكتيريا الطبيعية. تشمل العلامات السريرية سماكة الغشاء المخاطي مع ابيضاض وارتفاع بالغشاء الكاذب. قد يعتمد التشخيص الافتراضي على الآفات العينية. الغرض من هذه الدراسة هو عزل وتوصيف المبيضات البيضاء من تجويف الفم في الدجاج. جمعت السبعين عينة عن طريق أخذ مسحة من تجويف فم الدجاج ونقلها إلى مختبر الفطريات. باستخدام الصندوق البارد للمعالجة. وتم زراعة العينات على أكار سكر العنب من أجل التعرف الافتراضي على المبيضات البيضاء. بناءً على التقنيات الجزيئية، فيما يتعلق بأهمية تفاعل تضخيم البوليميرات المتسلسل لجين الرنا الريبوسي S١٨ لتحديد المبيضات البيضاء، كان هذا الجين موجودًا في ٥٠ عينة، وكان جين *Metallo-aminopeptidase* موجودًا في ٥٠/٥٠ (١٠٠٪) وكان جين *alkaline phosphatase sequence* موجودًا في ٥٠/٥٠ (١٠٠٪). بينما كان *alpha glucosidase* موجودًا في ٥٠/٣٠ (٦٠٪) وجين *sterol esterase25/50* (٥٠٪). أظهرت نتائج اختبار الحساسية للمضادات الفطرية أن الكيتوكونازول والإيتراكونازول قدموا الحساسية الأكثر استثنائية (١٠٠٪) ضد عزلات المبيضات البيضاء، يليها الفلوكونازول والأمفوتيريسين ب. نتائج هذا العمل توضح أن الدجاج المنزلي محتمل أن يحتوي على خمائر مسببة للأمراض في تجويف الفم.

الكلمات المفتاحية: المبيضات البيضاء، التقنيات الجزيئية، الدجاج المحلي، تجويف الفم، الحساسية للمضادات الفطرية.

1. Introduction:

Most species in the Candida genus are commensal healthful folks [1]. Candidiasis is a fungal infection that is brought on through way of C. albicans, a type of candida fungi that can lead to illnesses in both animals and humans, causing immune suppression or debilitating diseases. In chickens, they can cause infections in the upper digestive system or the skin, commonly affecting the comb. Crop mycosis is the most common type of candida-related disease in poultry. Long-term use of antibiotic medication disrupts the natural bacterial flora, allowing mycelial yeasts to infiltrate the mucosa and cause clinical illness. Crop candidiasis is clinically characterized by little mortality and morbidity, as well as nonspecific indications of sadness and stunted growth [2]. Candidiasis is an occasional disease caused by a yeast belonging to the genus Candida. The main species responsible for candidiasis in chickens is C. albicans, but it can also be caused by other types of Candida. There are multiple symptoms associated with Candida

infection [3]. Crop candidiasis is the most common illness caused by Candida in poultry. These infections are also referred to as crop mycosis, thrush, moniliasis, or sour crop [4]. There are approximately two hundred species of Candida, with very few of these species having harmful properties Candida albicans is one such pathogenic species that can infect and cause diseases in various animals and humans. The infection typically occurs when the immune system of the host is weakened [5 and 6]. The pathogenesis and pathogenicity of C. albicans have been appreciably studied in contrast to different species, as it is the main reason for candidiasis in each animal and human. Aside from virulence factors, yeast has integrin-like molecules, proteases, and phospholipases that assist in joining to and infiltrating host tissues, inflicting disease. Furthermore, biofilm manufacturing and phenotypic trade are useful resources for the organism in evading the host's immunological responses [7 and 8]. In healthy animals with a properly functional immune system, phagocytes normally prevent infections. However, in people with weaker immune systems, Candida cells can adhere to mucosal cells and rapidly transform from yeast to hyphal. This larger shape makes it tough for phagocytic cells to destroy them. The invasion of host mucosal tissue by hyphae is aided by the abundance of phospholipase enzymes concentrated at the tips of the hyphae [9]. Recently, polymerase chain reaction (PCR) strategies have been broadly used in the diagnosis of chicken candidiasis [10]. The main aim of the study is to detect virulence factor genes in Candida albicans strains isolated from the oral cavities of local poultry in Mosul Province. Additionally, we will assess the antifungal susceptibility of these isolates.

2. Materials and Methods:

2.1 Sample Collection:

The research for this study was conducted from November 2023 to March 2024 at the biology department's laboratory at the University of Al-Hamdaniya's College Education for Pure Science, located in the Mosul Province. Seventy samples were collected from the mouths of local chickens in various locations in Bartella, Mosul province, between November 2023 to March 2024. Using sterile cotton swabs, the samples were collected, kept in a sterile environment, and then transmitted right away to a microbiology lab for processing and testing **[11 and 12].**

2.2 Isolation and identification of *Candida albicans*

Inoculate oral cavity samples on Sabouraud's Dextrose agar with 0.05 mg/ml chloramphenicol and incubate at 37°C for 24 hours to 1 week. After incubation, yeast identification was accomplished using both macroscopic and microscopic morphology tests

[13] This study utilized conventional PCR to identify Candida albicans at the molecular level by amplifying a segment of the 18S rRNA gene using a specific primer **[11 and 14]**.

2.3. Molecular Detection Primers

Primer 3 plus online (Metallo-aminopeptidase, alkaline phosphatase, alpha-glucosidase, and sterol esterase and the NCBI-Genbank database were used to design the PCR primers for this investigation. While diagnostic primer is composed of a particular sense corresponding to the sequences of a partial gene of 18S rRNA by a reference **[14]**. These primers were supplied by the Korean Macrogen Company which are listed in **Table 1**.

Table 1: PCR identification gene primers with their nucleotide sequence and product size for Candida albicans

Primers		Sequence(5'-3')	PCR product size bp
18S rRNA gene	F	GCCGCCAGAGGTCTAAACTTR	415
	R	AGTTCAGCGGGTAGTCCTAC	
Metallo-aminopeptidase	F	GCAACCACCCAAATGGAACC	538
	R	GATGGGCCAATTCGTGCATC	
alkaline phosphatase	F	GGGGCCACTGCATTTTCTTG	598
	R	CATTGTGGTGTGAAGCGTGG	
alpha-glucosidase	F	ATGCTACTCATGCCGATGGG	550
	R	GTATCAACGCCGGCCAATTC	
sterol esterase	F	TGTGCCTCGAGAACCATACG	489
	R	CTCTGGAGTCCACCTTGCAG	

2.4 Fungal DNA Extraction

Utilizing the Fungi/Yeast Genomic DNA Extraction Mini Kit, as described in the earlier publication **[15]**. The manufacturer's recommended procedure was followed to extract fungal genomic DNA from the isolates.

2.5 PCR amplification

The PCR master mix reaction was previously coordinated using the Maxime PCR premix reagent i-Taq protocol. Once formulated as per the manufacturer's guidelines, the master mix comprised three microliters of template DNA, twenty microliters of nuclease-free water, and one microliter each of forward and reverse primers (10 pmol). Table 2 outlines the previous configuration of the PCR workstation for 30 cycles. Following one hour of agarose gel electrophoresis at 100V, the PCR products underwent visualization and photography of the DNA bands using a gel documentation system.

Table 2: The PCR program settings for conducting tests on *Candida albicans*.

Step		*Candida albicans*				Time	
	18S rRNA gene	Metallo-aminopeptidase	alkaline phosphatase	alpha-glucosidase	sterol esterase		
Initial denaturation	95°C	95°C	95°C	95°C	95°C	2 min	30 Cycle
Denaturation	95°C	95°C	95°C	95°C	95°C	30 sec	
Annealing	57.0	64.9°C	64.9°C	64.8°C	64.8°C	30 sec	
Extension	72°C	72°C	72°C	72°C	72°C	50-60 sec	
Final Extension	72°C	72°C	72°C	72°C	72°C	5 min	
Hold	4°C	4°C	4°C	4°C	4°C	10 min	

2.6 Susceptibility for Some Antifungal Drugs

Candida albicans isolates subjected to susceptibility testing by standard methods for the antifungal test have been used in this study [15, 16]. A standard reference procedure has been described by the National Committee for Clinical Laboratory Standards [17]. Antifungal susceptibility was determined by using 4 antifungal discs (Amphotericin B, Fluconazole, Ketoconazole, and Itraconazole) according to guidelines recommended by the [16] corresponding to the drugs considered routine testing and reporting on yeast.

3. Results:

50 (71%) Candida isolates out of 70 oral cavity samples were obtained from chicken with inflammation based on cultural, morphological, and molecular identification carried out the highest percentage was C. albicans 50/70 (71%). Based on molecular techniques, regarding the results of PCR amplification of the 18S rRNA gene for identification of C. albicans, this gene was present in 50 samples. Metallo-aminopeptidase gene was present in 50/50 (100%) and alkaline phosphatase sequence gene was present in 50/50 (100%). while alpha-glucosidase was present in 30/50 (60%) and sterol esterase genes 25/50 (50%), produced distinct bands corresponding to molecular sizes approximately 415 bp, 538 bp, 598 bp, 550 bp, and 489 bp which exhibited 18S rRNA gene, Metallo-aminopeptidase, alkaline phosphatase, alpha-glucosidase, and sterol esterase genes, respectively. Show **Figure 1**.

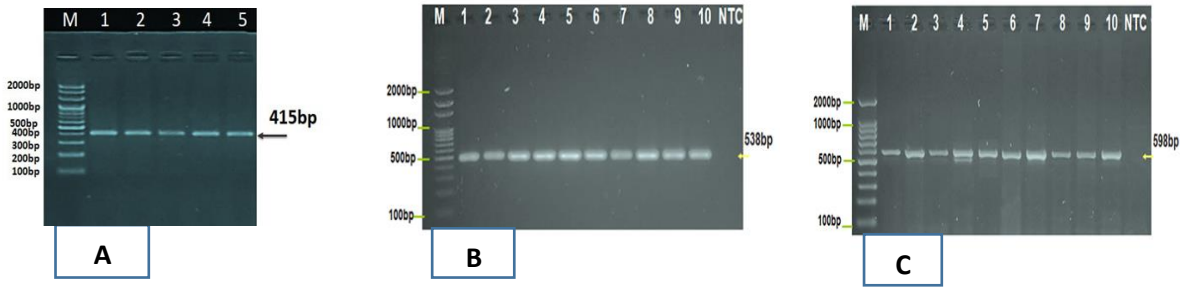

Figure 1. a.: the analysis of PCR products of pathogenic Candida albicans

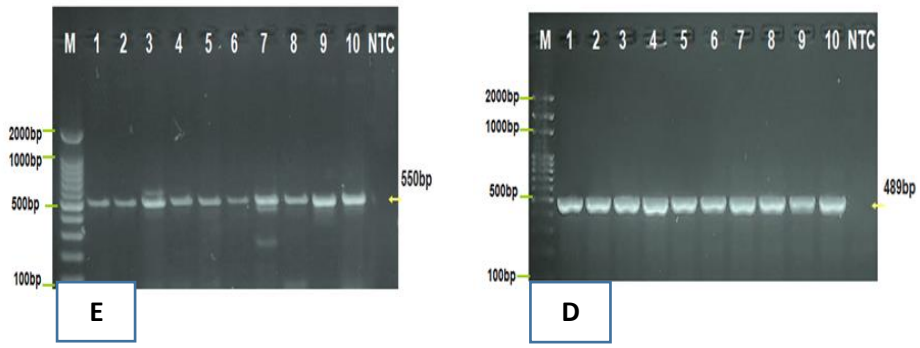

Figure 1. b.: the analysis of PCR products of pathogenic Candida albicans

Figure 1 Agarose gel electrophoresis image showing the analysis of PCR products of pathogenic Candida albicans. The marker ladder ranges from 2000 to 100 base pairs, A- lanes 1-10 (415 bp) displayed the 18S rRNA gene, B- Lanes 1-10 displayed the metallo-aminopeptidase gene (538bp), C- Lanes 1 to 10 display the alkaline phosphatase gene (598 bp), D- Lanes 1-10 display the alpha glucosidase gene (550 bp) and E- Lanes 1-10 display the sterol esterase gene (489 bp).

4. Antifungal Profile for *Candida albicans*

Antifungal profile of Candida albicans isolates from the oral cavity of chicken according to antibiotic disc diffusion method. The sensitivity test was applied to all 50 isolates of Candida albicans. These isolates were tested for their sensitivity to Amphotericin B, Fluconazole, Ketoconazole, and Itraconazole. The results were interpreted by measuring the inhibition zones around the disc and compared with breakpoints interpreted according to the manufacturer's instructions (DHN PAN Krakow, Poland). Zones diameters of ≥ 18 mm indicated the susceptibility (S), and that of ≤ 14 mm indicated the resistance (R) to each fluconazole, ketoconazole, and itraconazole. The zones S were ≥ 16 mm and R ≥ 12 mm, for amphotericin B. These zones were translated in terms of sensitivity (S) and resistance (R), **Table 3**.

Table 3: Antifungal susceptibility and resistance profile for *Candida albicans*

Type of antifungal	*Candida albicans* (N=50)			
	S	%	R	%
Fluconazole	40	80	10	20
Amphotericin B	30	60	20	40
Ketoconazole	50	100	-	-
Itraconazole	50	100	-	-

R= Resistance, S= Sensitive

5. Discussion:

Using sterile cotton swabs, samples were taken from the oral cavity, transported in a sterile medium, and then quickly moved to a microbiology lab for isolation and lab tests [18]. Although cases of candidiasis are rare, when appropriate control methods are abandoned, outbreaks can arise. Fungal infections are mostly caused by Candida albicans, and it is also the most often isolated etiological agent in cases of candidiasis. It can infiltrate host tissues and result in devastating infections in the right conditions. Because it suppresses the immune system or causes debilitating diseases, C. albicans, a kind of candida fungal, can cause sickness in both people and animals [19]. Numerous forms of candidiasis, including atrophic and hyperplastic candidiasis, pseudomembranous and erythematous candidiasis, and chronic mucocutaneous candidiasis syndromes, are caused by the Candida species. Many studies have demonstrated the pervasiveness of Candida species notably Candida albicans—in the environment. Many studies have highlighted the widespread presence of Candida species, notably Candida albicans, in the environment [20]. A 71% percentage of Candida albicans isolates were obtained through microscopical and diagnostic analysis of 70 samples per oral cavity chicken, with different outcomes. [21] who observed 13 (60%) of C. albicans isolates from the oral cavity of local chicken. The result is higher than study in the Egypt [22]. The presence of Candida albicans in test samples is 22.2% (n=8/36) from crop swabs. Regional variations caused by geographic location and environmental parameters including humidity, soil type, temperature, and bird species in the area could cause this variation [23]. The recent research results have confirmed the presence of the Metallo-aminopeptidase gene in 50 out of 50 cases (100%), and the identical ratio of the alkaline phosphatase gene. These genes are essential for the action of enzymes, which are involved in the conversion of Candida from a benign commensal organism to a pathogenic one, influenced by environmental factors that trigger the production of various virulence factors. The interplay between host factors and Candida-specific variables ultimately leads to the development of oral candidosis [24].

6. Conclusion:

The study concludes that *Candida albicans* is a major causative agent of thrush in local chicken, oral cavity isolates formed the highest percentage. Metallo-aminopeptidase gene the more virulence factors in the studied isolates. In

conclusion, the isolates were tested for highly Sensitive Ketoconazole, and Itraconazole We recommend adding these antibiotics to poultry feed as a protection against fungi.

7. Recommendation:

Based on the previous discovery, the following suggestions have been proposed: To reduce bird exposure to fungal infection, precise management techniques, strict biosecurity, good disease detection, and suitable preventive measures must be implemented on a timely basis. To minimize exposure to airborne spores or reduce spore ingestion, environmental changes are required. Appropriate management approaches must be developed for dealing with mycotic illness.

Author Contributions: Hawraa F.H. Al-Abedi wrote the original draft, and Israa Ibrahim Khalil reviewed and edited the manuscript. Semaa F.H. Al-Abedi contributed by writing on one of the topics and critically revising the manuscript.

Conflict of Interest**:** The authors have disclosed that they do not have any conflicts of interest.

8. Reference:

[1] Sullivan DJ, Moran GP, & Pinjon E. Comparison of the epidemiology, drug resistance mechanisms and virulence of Candida albicans. FEMS yeast Res. 2004; 4:369-376. doi: 10.1016/S1567-1356(03)00240-X.

[2] Ibrahim ZY, Ali BH, Ali RK, Hasan MS. Avian Candidiasis: A Review. International Journal of Pharmaceutical Research. 2020; 12(1). doi: 10.31838/ijpr/2020.12.01.199.

[3] Dykstra MJ, Charlton BR, Chin RP and Barnes HJ. Fungal Infections. In Diseases of Poultry, 2017: 1075–1096. https://doi.org/10.1002/9781119421481. ch25 .

[4] Asfaw M. and Dawit D. Review on Major Fungal Disease of Poultry. British Journal of Poultry Science. 2017; 6(1): 16-25. DOI: 10.5829/idosi.bjps.2017.16.25.

[5] McVey DS, Kennedy M and Chengappa MM. Veterinary Microbiology. John Wiley & Sons. 2013.

[6] Mendes GMJS, Bernardi T, Scorzoni L, Fusco-Almeida AM. and Sardi JCO. Candida species: Current epidemiology, pathogenicity, biofilm formation, natural antifungal products and new therapeutic options. Journal of Medical Microbiology, 2013; 62(1), 10–24. https://doi.org/ 10.1099/ jmm.0.045054-0.

[7] Dhama K., Verma AK, Tiwari R, Chakraborty S, Vora K, Kapoor S, Rajib D, Karthik K, Singh R, Munir M, Natesan S. A perspective on applications of geographical information system (GIS); an advanced tracking tool for disease surveillance and monitoring in veterinary epidemiology. Advances in Animal

and Veterinary Sciences. 2013; 1 (1): 14 – 24. http://www.nexusacademicpublishers.com/journal/4.

[8] Quinn PJ, Markey BK, Leonard FC, Hartigan P, Fanning S. and Fitzpatrick ES. Veterinary Microbiology and Microbial Disease. . 2011; John Wiley & Sons.

[9] Dykstra MJ, Charlton BR, Chin RP and Barnes HJ. Fungal Infections. In Diseases of Poultry. 2017; Chapter 25. https://doi.org/10.1002/9781119371199.ch25

[10] Liu J, Liu H, Yan J, Liu N, Zhang H, Zhao C. and Liu Y. Molecular typing and genetic relatedness of 72 clinical Candida albicans isolates from poultry. Veterinary Microbiology, 2018; 214, 36–43. https://doi.org/10.1016/j.vetmic.2017.11.030.

[11] AL-Abedi SFH. Comparative study for Candida spp isolated and identification from goats milk with mastitis between API Candida KIT test, Candida chromogenic agar and Vitek 2 system. Biochem. Cell. Arch. 2020; 20(2):5329-5332. https://connectjournals.com/03896.2020.20.5329.

[12] Kosikowski FV. Culture and starters. In cheese and fermented milk foods, 2nd ed .F. V. Kosikowski and associated Brooktondale new york, 1982; NY.

[13] AL-abedi HFH, AL-Attraqchi AF, Khudaie BY. Investigation of the Hydrolytic Enzyme Activities of Candida Parapsilosis Isolated From Milk Samples of Bovine Mastitis by API ZYM and Molecular Method. Indian Journal of Forensic Medicine & Toxicology. 2020; 14 (3): 2443-2449.

[14] AL-abidy HFH, Khudaier BY, AL-Attraqchi AF. Conventional and molecular detection of Candida albicans and Candida parapsilosis isolated from bovine mastitis in Basrah - Iraq. Biochem. Cell. Arch. 2019; 19(2): 3285-3289. DOI: 10.35124/bca.2019.19.2.3285.

[15] Balouiri M, Sadiki M, Ibnsouda SK. Methods for in vitro evaluation antimicrobial activity: Areview. Journal of pharmaceutical Analysis. 2016; 6: 71- 79. https://doi.org/10.1016/j.jpha.2015.11.005.

[16] AL-Abedi HFA, Khudaier BY, AL-Attraqchi AAF. Evalution the Antifungal Activity of Lactobacillus against Some isolates of Candida spp Isolated from Bovine Mycotic Mastitis. A Thesis Submitted to the Council of College of Veterinary Medicine University of Basrah In Partial Fulfillment of the Requirements for the Degree of Doctorate of Philosophy in Veterinary Microbiology. 2020: P 55.

[17] Lassa H and Malinowski E. Resistance of yeasts and algae isolated from cow mastitic milk to antimicrobial agents. Bull Vet Inst Pulawy 2007; 51: P 575-578.

[18] Mugale M, Bhat AA, Gavhane DS, Bhat SA Outbreaks of thrush in pigeons in Punjab State of India. Comp Clin Pathol. 2014. doi:10.1007/s00580-014-1958-y

[19] Morreti A, Fioretti DF, Boncio L, Pasquali P, & Del Rossi E. Isolation of Candida rugosa from turkeys. Journal of veterinary medicine. 2001; 47:433-439.

[20] Answar KP, Malik A, & Subwin HK. Profile of candidiasis in HIV infected patients. Iran Journal of microbiology. 2012; 4:204-209.

[21] Al-Dabbagh SYA. Isolation and diagnosis of Candida albicans from oral cavity of local chicken and detection some of the virulence factors in Mosul city. IMDC-SDSP 2020:28-30. DOI 10.4108/eai.28-6-2020.2298159.

[22] El-Tawab AA. Phenotypic and genotypic characterization of Candida albicans isolated from chicken. Benha Veterinary Medical Journal. 2020; 38(2): 120-124. 10.21608/BVMJ.2020.25501.1185 .

[23] Quinn PJ, Markey BK, Carter ME, Donnly WJ, Leonard FC and Maghire D (). Veterinary Microbiology and Microbial Disease. Blackwell publishing. Company, Iowa. USA. 2020:23-28.

[24] Marsh PD, Martin M. Oral Microbiology. Edinburgh, UK: Churchill Livingstone;. Oral fungal infections. 2009: 166–179.

Al-Kitab Journal for Pure Sciences (2024); 8(2):11-22.
https://doi.org/10.32441/kjps.08.02.p2

Al-Kitab Journal for Pure Sciences
ISSN: 2617-1260 (print), 2617-8141(online)

https://isnra.net/index.php/kjps

A study of Some Factors Affecting the Prevalence of Renal Disease in Children

Eman Abbas Muhsin[*1], Shahrazad A. Khalaf[2], Afrah Fahad Abdulkareem[3]

[1]Ministry of Science and Technology, Environment, Water and Renewable Energy Directorate- Baghdad- Iraq
[2]Diyala University, College of Science, Biotechnology Department- Iraq
[3]Mustansiriyah University, College of Science, Microbiology Department- Iraq

Corresponding Author: eman2014bio@gmail.com

Citation: Muhsin EA, Khalaf SA, Abdulkareem AF. A study of Some Factors Affecting the Prevalence of Renal Disease in Children. Al-Kitab J. Pure Sci. [Internet]. 2024 June. 08 [cited 2024 June. 08];8(2):11-22. Available from: https://doi.org/10.32441/kjps.08.02.p2.

Keywords: Nephrotic syndrome, Chronic kidney disease, Pediatrics, Blood groups, Socioeconomic status.

Article History
Received 02 Jan. 2024
Accepted 22 Feb. 2024
Available online 08 June 2024

Abstract:

The current study was carried out in the period from 1 to 25 November 2023. It included sixty-two pediatric patients in the age range of (1-12) years and male and female children: twenty-six pediatric patients with chronic renal failure and thirty-six pediatric patients with nephrotic syndrome, who were outpatients and inpatients in the renal diseases unit and dialysis unit of both Al-Mansour Pediatric Teaching Hospital and Child's Central Teaching Hospital in Baghdad, Iraq. The control group consisted of twenty-six children in the same age range as the sick groups of males and females. Blood samples were collected from patients and controls. Then renal function was evaluated by applying the laboratory tests as urea and creatinine levels were measured in serum, besides blood group and Rh factor tests. Factors that may affect renal disease incidence and progress were recorded, such as socioeconomic status, residence (North, Middle, and South), and family history. The results explained the significant increase in both urea and creatinine concentrations ($P<0.001$) in serum compared with controls. The blood group and Rh factor had no significant differences among children of both sick groups. The entire affected factors had no significant association with renal disease incidence or progress in the current study. The age and gender of each child patient had no significant effect on the type of renal disease (at P value ≤ 0.01).

Keywords: Nephrotic syndrome, Chronic kidney disease, Pediatrics, Blood groups, Socioeconomic status.

دراسة بعض العوامل المؤثرة على انتشار المرض الكلوي في الأطفال

إيمان عباس محسن[١]، شهرزاد احمد خلف[٢]، أفراح فهد عبد الكريم[٣]

[١]وزارة العلوم والتكنولوجيا- دائرة البيئة والمياه والطاقات المتجددة- بغداد، العراق

[٢]جامعة ديالى ، كلية العلوم، قسم التقنيات الاحيائية- العراق

[٣]الجامعة المستنصرية، كلية العلوم، قسم علوم الحياة- العراق

eman2014bio@gmail.com, shahrazadah.kh@gmail.com, aalfahad17@uomustansiriyah.edu.iq

الخلاصة:

أجريت الدراسة الحالية في الفترة من ١ إلى ٢٥ تشرين الثاني (نوفمبر) ٢٠٢٣. وشملت اثنين وستين مريضاً من الأطفال في الفئة العمرية (١-١٢) سنة، حيث كان من الأطفال الذكور والإناث: ستة وعشرون مريضاً من الأطفال يعانون من مرض الكلى المزمن. كان هناك ستة وثلاثون مريضاً من الأطفال يعانون من المتلازمة الكلوية، والذين كانوا مرضى خارجيين ومرضى داخليين في وحدة أمراض الكلى ووحدة غسيل الكلى في كل من مستشفى المنصور التعليمي للأطفال ومستشفى الطفل التعليمي المركزي في بغداد، العراق. وتكونت المجموعة الضابطة من ستة وعشرين طفلاً في نفس الفئة العمرية للفئتين المرضيتين من الذكور والإناث. تم جمع عينات الدم من المرضى ومجموعة السيطرة. ثم تم تقييم وظائف الكلى عن طريق إجراء الفحوصات المختبرية حيث تم قياس مستويات اليوريا والكرياتينين في مصل الدم، بالإضافة إلى اختبارات فصيلة الدم وعامل *Rh*. تم تسجيل العوامل التي قد تؤثر على حدوث مرض الكلى وتقدمه، مثل الحالة الاجتماعية والاقتصادية والإقامة (الشمال والوسط والجنوب) والتاريخ العائلي. أوضحت النتائج وجود زيادة معنوية في تركيز كل من اليوريا والكرياتينين ($P<0.001$) في مصل الدم مقارنة مع مجموعة السيطرة. لم يكن هناك فروق ذات دلالة إحصائية بين فصيلة الدم وعامل *Rh* بين الأطفال في كلا المجموعتين المريضتين. لم يكن للعوامل المصابة بأكملها ارتباط كبير بحدوث مرض الكلى أو التقدم في الدراسة الحالية. لم يكن للعمر والجنس لكل مريض طفل أي تأثير كبير على نوع المرض الكلوي (عند قيمة $p \leq ٠,٠١$).

الكلمات المفتاحية: المتلازمة الكلوية، المرض الكلوي المزمن، طب الأطفال، فصائل الدم، الحالة الاجتماعية والاقتصادية.

1. Introduction:

Chronic kidney disease (CKD) is a worldwide public health problem that progresses towards end-stage renal disease (ESRD). In childhood, it is generally a non-curable and progressive condition that leads to death. Nephrotic syndrome (NS) is an important CKD in children which is characterized by the presence of proteinuria, hypoalbuminemia, hyperlipidemia, and edema [1]. The other important CKD in childhood is chronic renal failure (CRF) which is a progressive irreversible destruction of the kidney tissues leading to the loss of renal function [2]. Many studies found a relationship between both blood groups and the Rh factor and the incidence of renal disease. The occurrence of renal disease varies with age and gender. The mortality rate in

ESRD, in addition to renal illness, is related to many factors [3]. Some of them are malnutrition, poor hospital care, poor socio-economic status, racial and geographic distribution, and family history. Children with CKD are susceptible to the condition frequently; the estimated annual incidence in children aged 1 to 5 years old is 3% [4]. After receiving appropriate medication, 5–15% of children patients do not get complete remission and are classified as treatment-resistant; however, the scientific recommendations for early detection and appropriate treatment of childhood chronic kidney disease over time based on scientific evidence even though there are differences in the causing aspects of management, despite the general concepts being the same [5]. Accordingly, the current study was carried out to :

1. Examine the kidney functions in children with NS and CRF to assess whether and to what degree the kidney may be affected.
2. Detect the effect of hereditary and other environmental factors on the prevalence of renal disease .
3. Find the distribution of renal disease in children according to age range and gender.

2 .Experimental Procedure

2.1 Materials:

The blood urea kit and serum creatinine kit were equipped from (BioMérieux / France) and the ABO blood group kit was equipped from (Randox/ U.K). They were used for detecting the blood urea, creatinine, and blood groups, respectively.

2.2 Methods:

2.2.1 Study groups:

This study was carried out between 1 - 25 November 2023. The pediatric patients were 26 of CRF and 36 of NS at the age of 1 to 12 years of both genders, who were outpatients and inpatients in the dialysis unit in both Al-Mansour Pediatric Teaching Hospital and Child's Central Teaching Hospital. The control group consisted of 26 children of both genders in the same age range as the study groups .

2.2.2 Blood samples:

Three ml of venous blood were obtained from each child in the study and control group and distributed in suitable containers (Plain tubes and capillary tubes) according to the use in different tests.

2.2.3 Renal function tests:

A. Blood urea: (BioMérieux Company) The serum concentration of urea in the current study was determined by enzymic method (Urease –Modified Berthelot Enzymatic-Colorimetric) according to the following reaction:

$$Urea + H2O \xrightarrow{Urease} 2NH3 + CO2$$

In an alkaline medium, the ammonium ions react with salicylate and hydrochloride to form a green-colored indophenol .

$$NH3 + Salycilate \xrightarrow{Nitroprusside} Indophenol$$

Assay procedure:

1. The working solution was prepared by mixing one vial of R2 enzyme into one bottle of R3; so gently mixed to dissolve contents.
2. The following solutions were pipetted into the three test tubes .

Solution	**Blank**	**Standard**	**Sample**
Working Solution	1ml	1ml	1ml
Sample	—	—	10µL
Standard Solution	—	10µL	—

3. All the tubes were mixed separately and then incubated for 5 min at 20–25°C.
4. A volume of 200 µL of R4 was added to all tubes, then they were shaken and incubated for 10 min at 20-25°C.
5. The absorbance (A) was read against the reagent blank at 580 nm .

Calculation:

$$Urea = \frac{A(Sample)}{A\ (Standard)} \times \text{Standard conc.}$$

Normal values of blood urea in children = (20 – 45) mg/dl

B. Serum creatinine: (BioMérieux Company)

This assay was done by using the calorimetric method. Creatinine in an alkaline solution reacts with picrate to form a colored complex.

Assay procedure: A working solution was prepared by mixing 4 parts of sodium hydroxide with 1 part of picric acid. One ml of TCA was added to 1 ml of serum and they were mixed well by using a glass rod until the dispersion of the precipitate. Then the mixture was centrifuged at 2500 rpm for 10 min, and then the supernatant was poured off. Into test tubes, the following solution was pipetted.

Solution	**Blank**	**Standard**	**Sample**
D.W	0.5ml	—	—
Standard	—	0.5ml	—
TCA	0.5m	0.5ml	—
Supernatant	—	—	1.0 ml
Working Solution	1.0 ml	1.0 ml	1.0 ml

All solutions were incubated at 25°C for 25 minutes after separated mixing .The absorbance (A) was read against the reagent blank at 550 nm.

Calculation:

$$\text{Creatinine} = \frac{\text{A(Sample)}}{\text{A (Standard)}} \times \text{Standard conc.}$$

Normal values of creatinine in children = (0.7 – 1.4) mg/dl

C. Blood typing and Rh system :Within the ABO system, four major blood groups can be recognized depending on the presence of one or both antigens: A and B. These groups are: A, B, AB, and O. If clumping occurred after a blood sample was exposed to a particular antibody, the person had had that type of blood. People with the particular antigen: Rh factor are Rh+; those without are Rh -. The procedure was done according to (Randox Company/ U.K).

D. Effect of the environmental factors:

The selected factors were recorded and statistically arranged in tables. They included: age range, gender, family history, residence, and socioeconomic status .

3. Statistical analysis:

Statistical analysis was computer-assisted using SPSS (Statistical Package for Social Sciences) 2019, version 17. A P-value less than 0.05 was considered statistically significant.

4. Results:

4.1 The evaluation of renal function:

1. Blood urea values :As recorded in **Table 1**, the blood urea levels were significantly higher (P<0.001) in both NS and CRF groups than in the controls' blood .

2. Serum creatinine values: The levels of creatinine were much higher in both sick groups' sera (P<0.001) than those of the healthy ones. **Table 1**.

Table 1: Biochemical Tests Results of Nephrotic Syndrome, Chronic Renal Failure and Control Group

Test	Group	Mean	S.D ±	Minimum value	Maximum value
Blood urea	NS	59.5	10.3	44.97	74.2
	CRF	96.2	14.4	75.9	115.1
	Control	29.5	6.9	20	44
Serum creatinine	NS	1.85	0.43	1.33	2.73
	CRF	4.93	1.52	2.3	6.9
	Control	0.87	0.14	0.7	1.2

Normal values:
Blood urea: (20-45) mg/dl.
Serum creatinine: (0.7-1.4) mg/dl.

4.2 Distribution of patients according to age range and gender:

Thirty-six patients of NS and twenty-six of CRF were included in the present study as well as twenty-six children of the same age range as controls. All were of both genders. The age groups and gender distribution in the study groups are clarified in Table (2). No significant

importance was noticed between the renal disease and age groups (P-value was 0.263). The same matter regarding the effect of gender on the type of renal disease within the age groups was not significant too (P-value was 0.251). Data from **Table 2** indicate that the number and percentage of patients are the lowest in the age range (5-8) years in NS and CRF groups.

Table 2: The Age Groups and Gender Distribution

Group	Gender	Age groups (years)			Total
		1-4	5-8	9-12	
NS	Male	11	3	13	27
	Female	2	3	4	9
	% within the age group	36.11%	16.67%	47.22%	100%
CRF	Male	8	3	8	19
	Female	3	3	1	7
	% within the age group	42.31%	23.08%	34.61%	100%
Control	Male	7	4	3	14
	Female	7	3	2	12
	% within the age group	53.85%	26.92%	19.23%	100%

4.3 Effect of socioeconomic status on disease prevalence :

There was no significant importance between socioeconomic status (Good, Medium, or Low) and the incidence of NS or CRF (P-value was 0.21) as observed in **Table 3**.

Table 3: The Socioeconomic Status of NS and CRF Patients

Socioeconomic status	NS patients	CRF patients	Total
Good	36.11%	50%	26
Medium	55.56%	46.15%	32
Low	8.33%	3.85%	4
Total	100%	100%	62

4.4 Effect of blood group on disease prevalence:

This effect was not significant (P-value was 0.307). **Table 4** expresses the distribution of the four blood groups between the patients of NS and CRF .

Table 4: The Distribution of Patients within Blood Groups

Blood group	NS patients	CRF patients	Total
A	36.11%	19.23%	18
B	30.56%	30.77%	19
O	19.44%	38.46%	17
AB	13.89%	11.54%	8
Total	100%	100%	62

4.5 Effect of blood Rh on disease prevalence:

There was no statistical significance of the Rh factor in the patients' blood of each study group (P-value was 0.847). **Table 5** indicates this result .

Table 5: The patients' distribution according to Rh factor

Rh factor	NS patients	CRF patients	Total
Positive	91.67%	96.15%	58
Negative	8.33%	3.85%	4
Total	100%	100%	62

4.6 Effect of residence on CKD incidence:

The relationship between the residents of Iraq (North, Middle, and South) and the prevalence of both CRF and NS was not significant (the P-value was 0.678) as in **Table 6**.

Table 6: The patients' distribution according to residence

Residence	NS patients	CRF patients	Total
North	2.78%	0%	1
Middle	77.78%	80.77%	49
South	19.44%	19.23%	12
Total	100%	100%	62

4.7 Effect of family history on CKD incidence:

The effect of family history (positive/ negative) was not significant (the P-value was 0.957) as shown in **Table 7**.

Table 7: The family history presence in both sick groups.

Family history	NS patients	CRF patients	Total
Positive	19.44%	19.23%	12
Negative	80.56%	80.77%	50
Total	100%	100%	62

5 .Discussion:

The measured renal function tests: The current results agree with the findings of **[6]** regarding CRF patients and agree with **[7]** regarding NS patients regarding urea concentrations in the serum of patients. The current findings show that the patients may reach end-stage renal

disease with impaired renal function and damaged tissues of the kidney resulting in high blood urea levels [8]. The current results regarding creatinine levels in serum agreed with many results [6] about CRF. It also agreed with [7] about NS patients. Any rise in blood creatinine is a sensitive indicator of kidney malfunction because it is normally and rapidly removed from the blood and excreted [8]. The increase in urea and creatinine levels in serum (called renal impairment) could be due to the decrease in the number of functioning nephrons in addition to their subsequent hypertrophy [2].

The relationship of age and gender within CKD groups: The results concerning the non-significant effect of age and gender on CKD in the current study agreed with those of [9] about NS. In CRF children, the majority was in the age group below 2 years in the study of [10]. The mean age was not significant in the CRF group compared to the control group. It was suggested that children, especially infants, are less resistant to diseases and are much affected by environmental conditions compared with people in other age categories and the explanation of these results may be attributed to an immature immune system, which will enhance the probability of infection; and thereby the development of renal disease; concerning differences among countries [4]. The number of male patients in the current study was larger than that of females in both sick groups, as the ratio was 3:1 for males to females in the NS group. This finding differs from the results published in NS was frequent in male children, with a male-to-female ratio of 2:1. Nevertheless, [7] recorded that the male-to-female ratio was 4:1. The previous study suggested that non-diabetic renal diseases progress more rapidly in males [9].

Socioeconomic status effect on CKD incidence: The current result is similar to those obtained by [10] about the effect of residence. In the study of [11], it is mentioned that there is a strong relationship between infant and child mortality and the mode of living and parental education, and the improvement of socioeconomic status can be indicated by the reduction of mortality rate in infants and children. The previous study [12] evaluated the relationship between socioeconomic status and susceptibility to renal diseases due to the effect on the development of the fetal kidney, or due to malnutrition, and this may represent a higher risk of progression of renal disease. The low activating nephrons number might promote the development of renal disease in children [5]. Children of educated parents have higher chances of survival than those of non-educated parents because they seem to have more understanding of the importance of health care, standard of living, the quality of curative services available, and utilization [12]. Besides socioeconomic and cultural factors, other factors can affect the prevalence and progression of renal disease in childhood which might not be limited to age,

recurrent illness, where malnutrition is also due to gastrointestinal problems or depression, inflammation, and medications [1].

Effect of blood group and Rh factor on CKD incidence: The obtained results disagreed with the study of [13] in which the distribution of renal patients among the blood groups was significantly different (mainly in the B and O). However, a lack of correlation between blood group phenotypes and renal scarring (most instances are caused by infection in young children) was referred to by [14]. Many investigations tried to demonstrate a relationship between blood groups and renal diseases as a statistical importance between the blood groups AB and O and the occurrence of urolithiasis and detected blood group specificities of some groups in the ABO and Lewis systems in human tumors of the urinary bladder and some renal cell carcinomas; considered males with blood group O and females with blood group A at risk. Also, it was recorded that pyelonephritis is associated with a specific type of pilus, P pilus, which binds to the P blood group substances in the P system [4]. Various important diseases, including renal diseases, show an important connection with blood groups. Some of these are early reports of statistical associations; some are more recent based on scientific findings. For the last 20 years, there has been increasing evidence that blood groups have a function and play a biological role. This often does not relate to the red cells but to the presence of chemical substances on other cells that were initially identified as red cell antigens [14]. Blood groups are genetically determined and each is characterized by the presence of a specific complex of carbohydrates, which are known to be important as receptors or ligands. So, blood groups are classified according to immunological (antigenic) properties, which are determined by specific substances on the surface of red blood cells [15]. Current results may be due to the small number of patients in both groups. No references to the negative or positive relation of Rh factor with CKD were obtained; except that of [3] which dealt with renal cell carcinoma and considered males with blood group O+ and females with blood group A of any Rh factor to have a significant risk of disease [15]. Our result seems to be related to the small number of samples.

Effect of residence on CKD incidence: There was no comparison with this result as there were no specialized studies dealing with the rate of NS or CRF incidence in Iraq, as well as the absence of qualified centers, that consider the racial, socioeconomic, and geographical criteria that may affect Iraqi patients to compare them with those in different parts of the world [16] There is strong evidence that the regional differentials are converging as a result of the continuous expansion of health facilities in all regions of the country[17]. Some studies suggest that racial and geographic factors may increase renal disease incidence rates. The environmental

exposure and/or specific genes may explain the connection between residents and renal disease [18]. In [19], it was concluded that many factors play a role in causing renal disease, concerning differences between countries or even within the same country.

Effect of family history on CKD incidence: In the NS group in the current study, the positivity was 19.44%. In Iraq, Al-Bewyaney [20] found that 15.8% of children were positive for a family history of the NS. In European nephrotic children, the percentages calculated by Agraharker et al. [21] and [22] were 28% and 29.04%, respectively. In the CRF group, our percentage of positive family history was 19.23%. It is asymptotic to that of Mong et al. [23] which was 20% in pediatric CRF patients in Vietnam. In Syrian children, the percentage was 5% as reported by [24]. The positivity was 24% in the study of Fan et al. [25] in the USA. There may be a familial incidence of NS and CRF, which can be divided into 2 categories: patients with an infantile onset and a poor prognosis, and patients with a juvenile onset and a generally good response to conventional therapy [26]. This high frequency of positivity for the familial patients may be attributed to the gene activation and/or may be due to environmental conditions that enhance its expression; as it was clear that the genetic parameters play an important role in disease development. They are thought to speed the rate of renal disease progression or predispose patients with various etiologies of kidney disorders enhancing renal damage [18]. The markers included human antigen-associating genetic susceptibility to renal diseases in addition to mutations [27]. Genetic backgrounds and converging with socio-environmental factors have been proposed to account for the tendency toward excessive renal disease progression [28].

6 .Conclusions:

- The age group spanning from 5 to 8 years old exhibited the lowest frequency of renal illness.
- Both sick groups were predominantly composed of males.
- Within an age range, there was no discernible relationship between gender and renal illness.
- The factors under investigation had no discernible impact on the prevalence of CRD.

Acknowledgment

Many thanks to the medical and laboratory staff for their endless cooperation .

Conflict of Interest

There is no conflict of interest.

7. References

[1] International Society of Nephrology. Supplement to kidney. Kidney Int. 2021;100:S276.

[2] Bagga A, Mantan M. Nephrotic syndrome in children. Indian J Med Res. 2005;122:13-28.

[3] Geoerger B, Morland B, Jiménez I, et al. Phase 1 dose-escalation and pharmacokinetic study of regorafenib in paediatric patients with recurrent or refractory solid malignancies. Eur J Cancer. 2023;15:142-152.

[4] Bagga A, Vasudevan A, Sinha A. Nephrotic syndrome: Standard treatment guidelines. Indian Academy of Pediatrics (IAP); 2022. Chapter 64.

[5] Sinha A, Bagga A. Clinical practice guidelines for nephrotic syndrome: consensus is emerging. Pediatr Nephrol. 2022;37:2975–2984.

[6] Deepa A, Bansal M, Ricci Z. Acute kidney injury and special considerations during renal replacement therapy in children with coronavirus disease-19: perspective from the Critical Care Nephrology Section of the European Society of Paediatric and Neonatal Intensive Care. Blood Purif. 2021;50:150-160.

[7] Rodriguez-Ballestas E, Reid-Adam J. Nephrotic syndrome. 2022;43(2):87-99.

[8] Choubi A. Concepts in Pediatrics: Nephrology. IP Innovative Publications; 2018. Chapter 1-8.

[9] Macioszek S, Wawrzyniak R, Kranz A, et al. Comprehensive metabolic signature of renal dysplasia in children. A multiplatform metabolomics concept. Front. 2021;8:665661.

[10] Nelms C, Shaw V, Greenbaum L, et al. Assessment of nutritional status in children with kidney diseases—clinical practice recommendations from the Pediatric Renal Nutrition Taskforce. Pediatr Nephrol. 2021;36:995–1010.

[11] Desloovere A, Renken-Terhaerdt J, Tuokkola J, et al. The dietary management of potassium in children with CKD stages 2–5 and on dialysis—clinical practice recommendations from the Pediatric Renal Nutrition Taskforce. Pediatr Nephrol. 2021;36:1331–1346.

[12] Nesrullah Z, Al-Rubaiee G, Zaki N. Evaluation of the extract of microalgae and its fatty acids on Candida spp. isolated from renal impairment patients. IUJAS. 2023;7(1):252-271.

[13] Eddy A, Symons M. Nephrotic syndrome in childhood. Lancet. 2003;362:629-639.

[14] Muhsin EA, Essa R, Shakir S. A study of immunological aspects in children with renal disease. Lampert Academic Publishing; 2017. Chapter 3.

[15] Gordillo R, Spitzer A. The nephrotic syndrome. Nephrology. 2020;30(3):94–105.

[16] Al-Radeef M, Allawi A, Fawzi H. Interleukin-6 gene polymorphisms and serum erythropoietin and hemoglobin in hemodialysis Iraqi patients. Saudi J Kidney Dis Transpl. 2018;29(5):1042-1049.

[17] Portolés J, Martín L, Broseta J, Cases A. Anemia in chronic kidney disease patients. Front Med. 2021;8:642296.

[18] Shahab M, Khan S. Erythropoietin administration for anemia due to chronic kidney disease - subcutaneous or intravenous, what do we know so far? Cureus. 2020;12(٩)

[19] Bortman M, Brimblecombe P, et al. Environmental encyclopedia. 3rd ed. Thomson; 2023. Vol. 2. p. 515. ISBN 0-7876-5488-4.

[20] Al-Bewyaney HM. HLA-typing for Iraqi children with nephrotic syndrome [MSc thesis]. College of Health and Medical Technology. Foundation of Teaching Education; 2005.

[21] Agraharker M, Gala G, Gangakhedkar AK, et al. Nephrotic syndrome. emedicine.com. Inc.; 2009.

[22] Shaarbaf AT. Complications of nephrotic syndrome among children in Al-mansour teaching hospital [dissertation]. Scientific Council of Community Medicine; 2004.

[23] Mong TT, Janssen F, Ismaili K, et al. Etiology and outcome of chronic renal failure in children in Ho Chi Minh City, Vietnam. Pediatr Nephrol. 2008;23(6):965-970.

[24] Saeed MB. The major causes of chronic renal insufficiency in Syrian children: a one-year, single-center experience. Saudi J Kidney Dis Transpl. 2005;16(1):84-88.

[25] Fan ZJ, Lackland DT, Kenderes B, Krisher J. Impact of birth weight on familial aggregation of end-stage renal disease. Am J Nephrol. 2003;23:117-120.

[26] Pandya D, Nagrajappa D, Ravi K. Assessment and correlation of urea and creatinine levels in saliva and serum of patients with chronic kidney disease, diabetes and hypertension– a research study. J Clin Diagn Res. 2016;10(١٠)

[27] Rahman M, Arafa A, Ali Md, Ali S. Immunogenetics: a molecular and clinical overview. Academic Press and Elsevier; 2022. Chapter 1:30. 1st ed. UK. ISBN: 978-0-323-90053-9.

[28] Ramsy G, Rusi M. Biological individuality. McConwell AK; 2023. Chapter 1:26-29. 1st ed. USA. DOI: 10.1017/9781108942775.

Al-Kitab Journal for Pure Sciences (2024); 8(2):23-30.
https://doi.org/10.32441/kjps.08.02.p3

Al-Kitab Journal for Pure Sciences
ISSN: 2617-1260 (print), 2617-8141(online)

https://isnra.net/index.php/kjps

Histopathological evaluation of ulcerative colitis induced by white vinegar in albino rats

Hana M. Asrafiel[1], Eda M. A. Alshailabi[2*], Fatimah A. Mohammed[2], Ahmed S. H. Ahmeedah[3]

[1]Higher institute of medical professions, El Beida, Libya
[2]Zoology Department, Omar Al-Mukhtar University, El Beida, Libya
[3]Tobruk Liver Disease Center, Tobruk, Libya

Corresponding Author: eda.muftah@omu.edu.ly

Citation: Asrafiel HM, Alshailabi EM, Mohammed FA, Ahmeedah AS. Histopathological evaluation of ulcerative colitis induced by white vinegar in albino rats. Al-Kitab J. Pure Sci. [Internet]. 2024 June. 09 [cited 2024 June. 09];8(2):23-30. Available from: https://doi.org/10.32441/kjps.08.02.p3.

Keywords: Ulcerative colitis, histopathology, white vinegar, and rats.

Article History
Received 20 Mar. 2024
Accepted 06 May 2024
Available online 09 June 2024

Abstract:

The ulcerative colitis (UC) is an inflammatory bowel illness which causes persistent inflammation of the colon's innermost layers. A prominent characteristic of ulcerative colitis (UC) is the stool's blood and mucous contents. This study determined to investigate the effects of white vinegar (WV) on colon tissues in rats. Two groups of twenty rats were created; the primary group was a control, healthy group, and the WV was administered to the second group at a dose of [1 ml/kg (5%)] via orally gavage for a period of two weeks. Findings revealed the emergence of histopathological alterations like mucosal erosions, ulceration, loss of normal architecture, mucosal atrophy, and hemorrhage; numerous crypts have inflammatory cells that entered them, blood vessels are dilated and oedema, the serosa is destroyed, which demonstrates the devastation of the mucosal lining destruction with goblet cell hyperplasia, focal necrosis of epithelium with demolished connective tissues, accumulation of inflammatory cells in the mucosa, lamina propria, and muscularis mucosa, as well as submucosal oedema when compared with the control rats. The PAS-reaction histochemical analysis showed that the treated rats had lower levels of carbohydrates than the control animals. The findings of the study demonstrated that white vinegar was a dangerous substance linked to histological alterations that resulted in acute ulcerative colitis when used daily for two weeks.

Keywords: Ulcerative colitis, histopathology, white vinegar, and rats.

تقييم الإمراضية النسيجية لالتهاب القولون التقرحي المستحث بالخل الأبيض في الجرذان البيض

هناء محمد اسرافيل[١]، عيدة مفتاح الشيلابي*[٢]، فاطمة العماري محمد[١]، أحمد سعيد أحميده[٣]

[١]المعهد العالي للمهن الطبية، البيضاء، ليبيا.

[٢] قسم علم الحيوان، جامعة عمر المختار، البيضاء، ليبيا.

[٣] مركز طبرق لأمراض الكبد، طبرق، ليبيا.

mohammedhana1771987@gmail.com, eda.muftah@omu.edu.ly, lafatima.alamari@omu.edu.ly, ahmed89.said@gmail.com

الخلاصة:

التهاب القولون التقرحي (*UC*) هو مرض التهابي في الأمعاء يسبب التهابًا مستمرًا في الطبقات العميقة للقولون. ومن السمات البارزة لالتهاب القولون التقرحي هو وجود دم ومحتويات مخاطية في البراز. كان الغرض من هذه الدراسة هو دراسة تأثيرات الخل الأبيض على أنسجة القولون في الجرذان البيضاء. تم إنشاء مجموعتين من عشرين جرذ؛ كانت المجموعة الأولى عبارة عن مجموعة ضابطة تتمتع بصحة جيدة، وتم إعطاء المجموعة الثانية جرعة [١ مل/كجم (٥٪) [من الخل الأبيض عن طريق التجريع بالفم لمدة أسبوعين. كشفت النتائج عن ظهور تغيرات نسيجية مرضية مثل: التآكلات المخاطية، التقرحات، فقدان البنية الطبيعية، ضمور الغشاء المخاطي، النزف، تسلل العديد من الخلايا التهابية، توسع الأوعية الدموية والوذمة، تلف الطبقة المصلية، مما يدل على دمار أنسجة بطانة الغشاء المخاطي، وكذلك وجود تقرح في منتصف الغشاء المخاطي والصفيحة الخاصة، أيضا ظهور تقرح أعمق مع نخر ظهاري بؤري وبداية نخر مع تدمير في الأنسجة الضامة، وتجمع الخلايا الالتهابية مع تضخم الخلايا الكأسية، وكذلك الغشاء المخاطي العضلي والوذمة تحت المخاطية مع توسع واحتقان الأوعية الدموية بالمقارنة مع الجرذان الضابطة. أظهر التحليل الكيميائي النسيجي لتفاعل صبغة حمض شيف الدوري أن الجرذان المعاملة بالخل الأبيض لديها مستويات أقل من الكربوهيدرات مقارنة بالحيوانات الضابطة. أظهرت نتائج هذه الدراسة أن الخل الأبيض مادة خطيرة مرتبطة بالتغيرات النسيجية التي أدت إلى التهاب القولون التقرحي الحاد عند استخدامه بشكل يومي لمدة أسبوعين.

الكلمات المفتاحية: التهاب القولون التقرحي، الإمراضية النسيجية، خل أبيض، الجرذان

1. Introduction:

Ulcerative colitis (UC) is one of the forms of inflammatory bowel disease (IBD) and affects mostly the colon and rectum. It is a lingering, recurring, and advanced disease, and no action to date would lead to perpetual therapy. Its commonness has increased in most areas of the world [1]. Among the pathogenic features of UC are increased making of reactive oxygen species (ROS), impaired mucosal integrity, inflammatory cells penetrating the mucosa, and decreased antioxidant capacity of the colon. Furthermore, nuclear factor kappa B (NF-κB) reliant on proinflammatory mediators such as interleukin 6 and tumor necrosis factor-alpha (TNF-α) is expressed downstream [2, 3]. UC is the term for a recurrent colon infection that has

symptoms such as nausea, vomiting, diarrhea, and stomach pain [4], ulcers, reduction in body mass, an increase in colon weight, blood in the stool, intestinal wall thickening, decreased mucus production, and inflammation that are commonly observed in this condition [5]. Moreover, in UC the rectum may also be affected by the large intestine-specific structural alterations and inflammatory response [6]. Besides, the etiology of UC has been frequently linked to decreased antioxidant capacity and elevated generation of free radicals, including ROS [5]. Whereas lipid peroxidation (LPO), brought on by an excess of ROS, might impair cellular antioxidant capability and eventually result in visible inflammation of the colon [7]. Moreover, the high generation of free radicals results in severe oxidative stress (OS), which damages the cell and its membrane [8]. Additionally, the production of ROS, such as hydrogen peroxide, hydroxyl radicals, and superoxide anion, can lead to tissue damage and LPO, particularly in membranes [9].

The unstable biological acid that defines the product as vinegar is called white vinegar (WA). It ranges between around 3 and 10% of the acetic acid concentration and is answerable for the strong, acrid smell of different kinds of vinegar [10]. Furthermore, ingesting WA can cause corrosive harm to the upper gastrointestinal system in certain areas [11]. In addition, the WA causes deep, circular stomach and duodenal ulcers [12]. Likewise, [13] shows that WV affects the gastrointestinal mucosa in rats by causing damage and ulcers. This work determines to examine the effects of WV on colon tissues in albino rats.

2. Material and Methods:

2.1. Chemicals: White vinegar (WV) was acquired from Omar Al-Mukhtar University, where it was prepared at the Al-Mukhtar Research Center from acetic acid (CH_3COOH). For two weeks, rats were garaged with 1 ml/kg/b.w./day of white vinegar, where rats were administered 5% of WV, as per [8, 13].

2.2 Animals: *Rattus norvegicus* albino rats in good health, weighing between 180 and 225 g on average, were employed. Rats were attained from the Zoology Department's Animal House at the University of Omar Al-Mukhtar's Faculty of Science in El-Beida, Libya. To ensure that there were no issues throughout the experiment, all rats were given a three-week lead time to become used to the lab environment. They were kept at room temperature in cages. Rats were given a lab diet and unlimited access to fresh water each day.

2.3 Experimental design:

Twenty albino rats, all female, were used. Before the experimental procedures, all rats were given water at their discretion and kept free from food for a whole day. They were then randomly assigned to two groups (n = 10): For a period of two weeks, distilled water was

administered orally to normal control rats, while WV (5%) was administered orally to treated rats via gavage at a rate of 1 ml/kg/b. w./day. Following the end of the treatment session, each rat was fasted for a full day. The colon was removed after the animals were sacrificed.

2.4 Histological and histochemical investigations:

Following a normal saline wash, colon samples were fixed in buffered formalin (10%) for general histological examination using Hematoxylin and Eosin stain [14]. Periodic acid Schiff's reaction (PAS) stain for carbohydrates was used histochemical [15].

3. Results:

The colon tissues in the control rats' slice displayed the typical mucosal layers (the mucosa, submucosa, muscularis externa, and serosa) as well as the typical histological structure in **Figure 1**, while, the histological alterations are displayed in **Figure 2**, the rats treated with 5% WA showed mucosal erosions, ulceration, loss of normal architecture, and mucosal atrophy. The mucosa is also haemorrhage, numerous crypts have inflammatory cells entering them, blood vessels are dilated and oedema, and the serosa is destroyed. In addition, **Figures 3&4** demonstrate the devastation of the mucosal lining, the ulceration at the midpoint of the mucosa, the lamina propria, deeper ulceration with focalized epithelial necrosis, and the beginning of necrosis with the destruction of connective tissues and aggregation of inflammatory cells with goblet cell hyperplasia, and the muscularis mucosa and submucosal oedema with dilatation and vascular congestion.

The control colon tissues exhibited a strong positive response in the PAS-reacted in the goblet cells and the muscularis mucosa, as well as a high increase in PAS reactive in their tissues **Figure 5**. In contrast to the control group, rats administered with 5% WA demonstrated a noteworthy reduction in the PAS reactive carbohydrate content of goblet cells, muscularis mucosa, and surface cells, as shown in **Figure 6**. Where the extracellular mucus and the mucous layer both had a decrease in color reactivity and did not display the magenta PAS stain type, reflecting the harmful effects of WV.

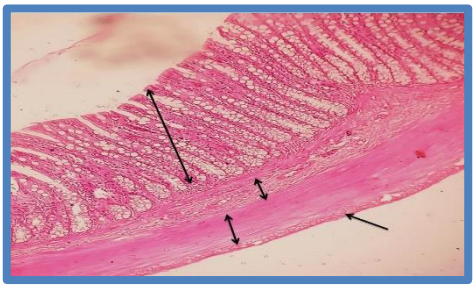

Figure 1: The control rat's colon tissue showing, normal histological structure, and normal mucosal layers (Mucosa, Submucosa, Muscularis externa & serosa) (H& E stain, X100).

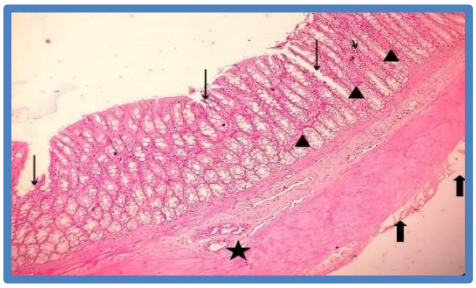

Figure 2: The rat's colon tissue treated with WA 5% showing, ulcerations, erosions, and atrophy of the mucosa (long arrows). The mucosa is also haemorrhage (head arrows), and certain crypts have inflammatory cells entering them (short arrow), dilated blood vessels with oedema "wall thickening" (star), and destruction of the serosa (H& E stain, X100).

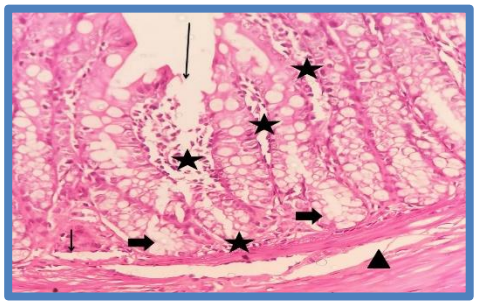

Figure 3: The rat's colon tissue treated with WV 5% showing, destruction of the mucosal lining, deeper ulceration with the onset of necrosis, and focal necrosis of epithelium (long arrow) with demolished connective tissues with aggregation of inflammatory cells infiltration in the mucosa, lamina propria with goblet cell hyperplasia (stars), ulceration at the mid part of the mucosa (short arrow), vacuolated or lightly stain cytoplasm (thick arrows), and the muscularis mucosa and submucosal oedema (head arrow) (H& E stain, X400).

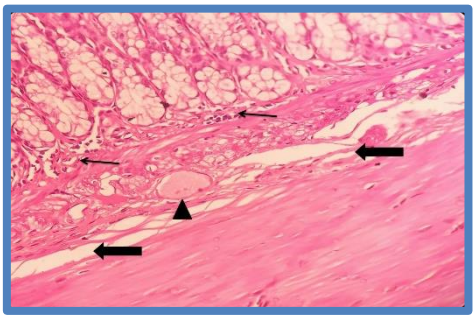

Figure 4: The rat's colon tissue treated with WV 5% showing, inflammatory infiltration cells in the mucosa and lamina propria (arrows), submucosal oedema (thick arrows) with dilatation and vascular congestion (head arrow) (H& E stain, X400).

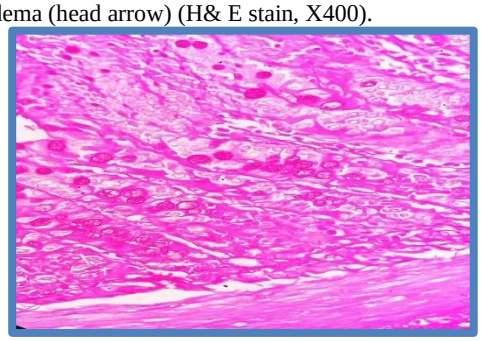

Figure 5: PAS-reacted colon tissue of control rats demonstrating a strong positive response (PAS stain, X400).

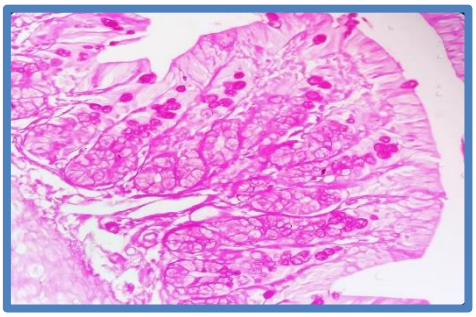

Figure 6: PAS-reacted colon tissue of rats treated with WV 5% demonstrating a drop in PAS reactive material (PAS stain, X200).

4. Discussion:

The findings of the current study illustrated histological alterations in rats given WV (5%) for two weeks including mucosal lining destruction with goblet cell hyperplasia, focal necrosis of epithelium with demolished connective tissues, accumulation of inflammatory cells in the mucosa, lamina propria, and muscularis mucosa, as well as submucosal oedema. Deeper ulcerations with necrosis onset are also included. Furthermore, in comparison to the control rats, there was blood vessel congestion, along with signs of damage such as vacuolated or faintly stained cytoplasm which is in arrangement with **[6]**, who discovered that the treated rats by WV revealed chemical damage to the mucosal epithelium in colon tissues. Also, they said that the damage by WV is associated with epithelial necrosis and oedema that penetrates the gut mucosal layers. Furthermore, **[16]** showed that in UC, the grade of inflammation designates the participation of numerous layers, counting the mucosa, submucosa, and the whole thickness of the colon barrier, and the harshness of inflammation shows the penetration of inflammatory cells. Also, **[1]** showed that the damage to the colon caused by WV includes bleeding, reddening, and ulcers. Additionally, in injured UC, the WV stimulates or degrades the mucosa,

increasing the synthesis of several leukotrienes, prostaglandins, and thromboxanes [6]. On the other hand, necrosis, hyperplasia in goblet cells, oedema, and inflammatory cell penetration, according to [17], demonstrated a considerable rise in colon weight and wall thickness. Moreover, WV treatment resulted in significant reductions in colonic and serum malondialdehyde levels as well as glutathione levels, indicating a rise in OS by damage in agreement with [3]. By producing cytotoxic ROS, TNF-α also triggers the synthesis of additional biological mediators, proteases, and proinflammatory indicators. These processes are principal to the penetration and chemotaxis of ulceration, inflammatory cells, and haemorrhage [18, 19]. Furthermore, NF-κB contributes significantly to UC by stimulating the inflammatory mucosae to produce inflammatory mediators including cyclooxygenase-2 [20]. Free radicals produced by OS increase inflammatory intermediaries and harm colonic mucosa [21]. Similarly, WV results in the breach of the colonic barrier, the permeation of leukocytes into the injured zone, the creation of inflammatory penetration like cytokines and metabolites of arachidonic acid, and the generation of ROS, that causes oxidative injury [4]. Consequently, the augmentation of colonic secretions, and contribution to a diversity of digestive ailments, like IBD, are among the pathophysiological changes of WV materials.

On the other hand, the findings demonstrated a significant drop in the PAS-responsive mucosal carbohydrate levels of goblet cells, surface cells, and the muscularis mucosa in rats given a 5% WA treatment in contrast to the control rats. These results were consistent with [22, 13], who found that WV-induced ulcers were linked to a reduction in PAS-response in mucosal cells as an effect of WV's destructive result on mucus cells or extreme OS. This reduction in collagen fiber statement and TNF-α expression at the site of damage may be the cause of these findings. Also, a decline in the goblet cells in the WA rats may be the cause of a drop in PAS-responsive mucosal carbohydrate gratified in colon tissues in the WA rats. Thus, the majority of the cells were either depleted or had little mucus.

5. Conclusion:

The results of this investigation presented that white vinegar was a hazardous chemical related to the histological variations that produced acute ulcerative colitis when used daily for two weeks in rats.

6. References:

[1] Adakudugu EA, Ameyaw EO, Obese E, et al. Protective effect of bergapten in acetic acid-induced colitis in rats. Heliyon. 2020 Mar; 6(8): e04710. https://doi.org/10.1016/j.heliyon.2020.e04710.

[2] Gautam KM, Goel S, Ghatule RR, Singh A, Nath G, Goel RK. Curative effect of *Terminalia chebula* extract on acetic acid-induced experimental colitis: role of antioxidants, free

radicals and acute inflammatory marker. Inflammopharmacology. 2013 Oct; 21(5): 377-383. https://doi.org/10.1007/s10787-012-0147-3.

[3] Rafeeq M, Murad HAS, Abdallah HM, El-Halawany AM. Protective effect of 6-paradol in acetic acid-induced ulcerative colitis in rats. BMC Complement Med Ther. 2021 Jan; 21(28):1-10. https://doi.org/10.1186/s12906-021-03203-7.

[4] Abdulaziz MA, Salim SA, Hatem MA, Mohammed SO, Mihir YP, Mohammed MA. Pretreatment of *Gymnema sylvestre* revealed the protection against acetic acid-induced ulcerative colitis in rats. BMC Complement Altern Med. 2014 Feb; 14(1): 1-11. https://doi.org/10.1186/1472-6882-14-49.

[5] Al-Rejaie SS, Abuohashish HM, Al-Enazi MM, Al-Assaf AH, Parmar MY, Ahmed MM. Protective effect of naringenin on acetic acid-induced ulcerative colitis in rats. World J Gastroenterol. 2013 Sep; 19(34): 5633-5644. https://doi.org/:10.3748/wjg.v19.i34.5633.

[6] Bahrami G, Malekshahi H, Miraghaee S, Madani H, Babaei A, Mohammadi B, Hatami R. Protective and therapeutic effects of *Aloe Vera* gel on ulcerative colitis induced by acetic acid in rats. Clin Nutr Res. 2020 Jul; 9(3):223 234. https://doi.org/10.7762/cnr.2020.9.3.223.

[7] Tahan G, Aytac E, Aytekin H, Gunduz F, Dogusoy G, Aydin S, Tahan V, Uzun H. Vitamin E has a dual effect of anti-inflammatory and antioxidant activities in acetic acid-induced ulcerative colitis in rats. Can J Surg. 2011 Oct; 54(5): 333-338. https://doi.org/10.1503/cjs.013610.

[8] Alshailabi EMA, Asrafiel HM, Ahmeedah ASH. Evaluation of effects of white vinegar-induced gastric mucosal ulceration in rats. Global Libyan J. 2022 Jan; 55:1-25.

[9] Almasaudi SB, Abbas AT, Al-Hindi RR, El-Shitany NA, Abdel-Dayem UA, Ali SS, Saleh RM, Al Jaouni SK, Kamal MA, Harakeh SM. Manuka honey exerts antioxidant and anti-inflammatory activities that promote healing of acetic acid-induced gastric ulcer in rats. Evid Based Complement Alternat Med. 2017 Jan; 2017: 1-12. https://doi.org/10.1155/2017/5413917.

[10] Mahmoodi M, Hosseini-zijoud S, Hassan SG, Hassanshahi G, Nabati S, Modarresi M, Mehrabian M, Sayyadi A, Hajizadeh M. The effect of white vinegar on some blood biochemical factors in type 2 diabetic patients. J Diabetes Endocrinol. 2013 Jan; 4 (1): 1-5. https://doi.org/10.5897/JDE12.015.

[11] Kamijo Y, Soma K, Iwabuchi K, Ohwada T. Massive noninflammatory periportal liver necrosis following concentrated acetic acid ingestion. Arch Pathol Lab Med.2000 Jan; 124 (1): 127-129. https://doi.org/10.5858/2000-124-0127-MNPLNF.

[12] Gopinathan S, Naveenraj D. Gastroprotective and anti-ulcer activity of Aloe vera juice, Papaya fruit juice and Aloe vera and Papaya fruit combined juice in ethanol induced ulcerated rats. Int. J. Drug Dev Res. 2013 Oct; 5 (4): 300-311.

[13] Alshailabi EMA, Asrafiel HM Ahmeedah ASH. Effects of vinegar acid on the duodenum tissues in rats. Histopathological and histochemical studies. J Applied Sci. 2022 Apr; 8:35-47.

[14] Harris HF. 1990. After Bruce Cassel man WC. 1959. *Histochemical technique*, by Methuen and Co. Ltd.

[15] Drury RAV, Wallington EA. *Carlton's histological techniques* (5th edn.) Oxford University Press, New York, Toronto, USA. 1980.

[16] Niu X, Fan T, Li W, Zhang Y, Xing W. Protective effect of sanguinarine against acetic acid-induced ulcerative colitis in mice. Toxicol Appl Pharmacol. 2013; 267:256-265. https://doi.org/10.1016/j.taap.2013.01.009.

[17] Owusu G, Obiri DD, Ainooson GK, Osafo N, Antwi AO, Duduyemi BM, Ansah C. Acetic acid-induced ulcerative colitis in Sprague Dawley rats is suppressed by hydroethanolic extract of *Cordia vignei* Leaves through reduced serum levels of TNF-α and IL-6. Int J Chronic Dis. 2020 Feb; 2020: 8785497. https://doi.org/10.1155/2020/8785497.

[18] Munakata W, Liu Q, Shimoyama T, Sawaya M, Umeda T, Sugawara K. Ecabet sodium attenuates reactive oxygen species produced by neutrophils after priming with bacterial lipopolysaccharides. Luminescence. 2003 Nov-Dec; 18 (6):330–333. https://doi.org/10.1002/bio.745.

[19] Jainu M, Mohan K, Devi C. Protective effect of *Cissus quadrangularis* on neutrophil mediated tissue injury induced by aspirin in rats. J Ethnopharmacol. 2006 Apr; 104 (6):302–305. https://doi.org/10.1016/j.jep.2005.08.076.

[20] El-Akabawya G, El-Sherifa NM. Zeaxanthin exerts protective effects on acetic acid-induced colitis in rats via modulation of pro-inflammatory cytokines and oxidative stress. Biomed Pharmacother. 2019 Mar; 111:841–851. https://doi.org/10.1016/j.biopha.2019.01.001.

[21] Tanideh N, Masoumi S, Hosseinzadeh M, et al. Healing effect of Pistacia atlantica fruit oil extract in acetic acid-induced colitis in rats. Iran J Med Sci.2014 Nov; 39(6): 522-528.

[22] El-Azab NE, Mansy AE, El-Mahalaway AM, Sabry D. Comparative study of the therapeutic effect of pomegranate alone or in combination with bone marrow mesenchymal stem cells on experimentally induced gastric ulcer in adult male rats: A histological and immunohistochemical study. Egyptian J Histol. 2018 Jun;10: 150-166. DOI:10.21608/EJH.2018. 13838.

Al-Kitab Journal for Pure Sciences (2024); 8(2):31-47.
https://doi.org/10.32441/kjps.08.02.p4

Al-Kitab Journal for Pure Sciences
ISSN: 2617-1260 (print), 2617-8141(online)
https://isnra.net/index.php/kjps

Simulation of RC5 Algorithm to Provide Security for WLAN, Peer-to-Peer

Nasser Alwan Hussein*

Computer of Engineering Networks, College of Fine Arts, University of Diyala, Iraq

Corresponding Author: am.naseeralwan@uodiyala.edu.iq

ORCID: 0009-0002-6342-0865

Citation: Hussein NA. Simulation of RC5 Algorithm to Provide Security for WLAN, Peer-to-Peer. Al-Kitab J. Pure Sci. [Internet]. 2024 June. 10 [cited 2024 June. 10];8(2):31-47. Available from: https://doi.org/10.32441/kjps.08.02.p4.

Keywords Cellular Automata, WLAN, programming languages C#, RC5.

Article History

Received	06	Apr.	2024
Accepted	25	May	2024
Available online	10	June	2024

Abstract:

Information security is a significant viewpoint in different areas of correspondence. This paper manages information encryption as large numbers of data correspondence rely upon encryption information. In this paper, another proposition of an information encryption framework has been presented. The framework can be partitioned into two stages; the primary stage centers around creating a top-notch Pseudo Irregular Number generator PRNGs utilizing rudimentary, intermittent, and crossover rules of cell automata CA. The framework recommends another mix of CA rules in an undertaking to give high arbitrariness and to work on the strength of the proposed cryptosystem. The subsequent stage creates the Improved Rivest Code 5 ERC5 calculations which utilizes the produced arbitrary Number Succession RNS with an end goal to reinforce the security and haphazardness of the first Rivest Code 5 RC5 Algorithm. The outcomes show that the proposed PRNGs in light of CA can create RNS with a high period which can reach more than 100000 keys without reiteration or string duplication. In addition, the test exhibits that the proposed ERC5 works on the security of the first RC5 calculation. The proposed cryptosystem is assessed as far as Shannon's hypothesis of data entropy, irregularity tests, calculation time, and key space investigation. The outcomes confirm that the recommended information crypto-framework expands the development of the security

level of unique RC5 encryption calculation with a serious level of arbitrariness and privacy. It is executed this work to show the results rely upon the programming language C# and the correspondence was presented in a structure called disseminated through an association wireless local-area network WIFI.

Keywords: Cellular Automata, WLAN, programming languages C#, RC5.

محاكاة خوارزمية RC5 لتوفير الأمان لشبكة WLAN، الند للند

نصير علوان حسين

هندسة شبكات الحاسوب، كلية الفنون الجميلة، جامعة ديالى، العراق

am.naseeralwan@uodiyala.edu.iq

الخلاصة:

أمن المعلومات هو جانب مهم في مجالات الاتصالات المختلفة، يتناول هذا البحث تشفير البيانات حيث إن الكثير من اتصالات المعلومات تعتمد على تشفير البيانات، في هذه الورقة، تم تقديم اقتراح جديد لنظام تشفير البيانات. يمكن تقسيم النظام إلى مرحلتين؛ تركز المرحلة الأولى على إنشاء مولد أرقام عشوائية زائفة *PRNGs* عالي الجودة باستخدام القواعد الأولية والدورية والهجينة للأتمتة الخلوية *CA* يقترح النظام مجموعة جديدة من قواعد *CA* في محاولة لتوفير عشوائية عالية وتحسين قوة نظام التشفير المقترح. بينما تنتج المرحلة الثانية خوارزميات *Rivest Cipher 5 ERC5* المحسنة التي تستخدم تسلسل الأرقام العشوائي *RNS* الذي تم إنشاؤه في محاولة لتعزيز أمان وعشوائية خوارزمية *Rivest Cipher 5 RC5* الأصلية، أظهرت النتائج أن *PRNGs* المقترحة المعتمدة على *CA* يمكن أن تولد *RNS* بفترة عالية يمكن أن تصل إلى أكثر من ١٠٠٠٠٠ مفتاح دون تكرار أو تكرار السلسلة، علاوة على ذلك، يوضح الاختبار أن *ERC5* المقترح يعمل على تحسين أمان خوارزمية *RC5* الأصلية. تم تقييم نظام التشفير المقترح من حيث نظرية شانون لأنتروبيا المعلومات، واختبارات العشوائية، وزمن الحساب، وتحليل الفضاء الرئيسي، أثبتت النتائج أن نظام تشفير البيانات المقترح يزيد من نمو مستوى الأمان لخوارزمية التشفير *RC5* الأصلية بدرجة عالية من العشوائية والسرية، تم تنفيذ هذا العمل لإظهار النتائج بالاعتماد على لغة البرمجة *C#* وتم إدخال المراسلات في إطار يسمى الموزع من خلال منظمة الشبكة المحلية اللاسلكية *WIFI*.

الكلمات المفتاحية: الأتمتة الخلوية، شبكة الاتصال اللاسلكية المحلية، اللغة البرمجية # C، خوارزمية RC5.

1. Introduction:

With the development of the web, the security of data is acquiring more interest. The encryption strategies can effectively defend individuals' data communicated over open channels. Nonetheless, the traditional encryption frameworks have limitations in scrambling like low productivity, massive information, and the high relationship among examples, etc. **[1]**. Recently, cell automata have accomplished an extraordinary interest in managing the tricky of profoundly and quickly secure cryptosystems. Cell Automata (CAs) are profoundly circulated

and equal frameworks that can imagine refined ways of behaving [2]. The extensive variety of CA rules works with numerous ways of producing successions; additionally, cell automata are sorted out by just simple and basic rationale calculations with complex and pseudorandom ways of behaving. Creating great quality Random Number Arrangement (RNS) is certainly not a simple capability, Pseudo Random Number Generator (PRNGs) based CA draws in numerous specialists since they are not difficult to execute in both equipment and programming [3]. Cell robotization resembles a machine, and that implies that the information is set; the CA will utilize it to create a result. The advantages of cell automata in cryptography can be summed up as follows:

- Enormous development of rules space.
- Cell automata contain just rational tasks or whole number math, so these attributes lead to improving the calculation.
- Cell automata have parallelism and show complex ways of behaving.

Likewise, RC5 is a renowned block figure recognized for its speed, straightforwardness, reasonableness for programming and equipment execution, and low memory necessity. Besides, RC5 is a defined calculation and iterative in its plan. This gives the possibility for limitless adaptability in both the degree of safety and execution qualities [4]. In this paper, an upgrade technique for RC5 encryption calculation has been proposed by reinforcing its unique powerless keys through producing great quality irregular number arrangements by one rudimentary, occasional, and half and half CA. The remainder of the paper is coordinated as follows: related works are summed up in Segment 2. Segment 3 gives fundamental hypothetical meanings of cell automata while Area 4 creates a clarification of RC5 encryption calculation. Segment 5 gives a point-by-point portrayal of the proposed framework though Area 6 examines the security examination and consequences of the proposed calculations. At last, the primary end is summed up in Segment 7.

2. Related Works:

2.1 In 2009: Ho et al. [5] have endeavored to figure out the ideal mix of CA rules and coherent activities for picking von Neumann neighbors. The creators propose a different number of CA rules for phenomenal effect and presumed that the occasional limit is superior to the invalid limit. The creators come up short/pass rate among occasional and invalid limit conditions. Moreover, they reasoned that the non-uniform CA has a preferable impact over uniform CA.

2.2 In 2011: Osama [5] improved the RC5 block figure calculation considering turmoil for accomplishing higher security and better picture encryption. This was accomplished by

consolidating the cryptographic crude tasks and the tumultuous slant tent guide to foster another design for the key timetable, as well as the weighty utilization of information subordinate turns expanded the dissemination accomplished per round. The framework gives quick block figures other than high-security levels.

2.3 In 2014: Dogaru Radu et al. **[6]** thought about numerous answers for building a decent Pseudo Random Number Age (PRNG) for a cryptographic framework. The framework depends on half and half-cell automata (HCA). The primary arrangement depended on making chains of HCA, for example, the non-direct guide which changed powerfully was constrained by another HCA map inside a chain (to guarantee the greatest throughput). The subsequent arrangement depended on a solitary HCA yield, which was down-examined by an element D. The proposed plot furnishes a decent PRNG with low intricacy achievements. Besides, the framework is expected to have a high resistance to various kinds of assaults.

3. Cell Automata:

The CAs are a sort of dynamical framework that have been really and extensively used in major areas of strength to develop by taking the benefits of their arbitrariness and dynamical properties, with the ability to uncover flighty and a complex way of behaving **[7]**. A cell robotization incorporates a cross-section (lattice) of indistinguishable cells inside a Boolean incentive for every cell, referenced as the present status of the cell. The condition of every cell is refreshed at a discrete time step as per a nearby update rule. The same decimal of the 8 results is called 'rule' **[8]**. Cell robot is formed by the four following snippets of data: A letter in order (S): The restricted arrangement of every single adequate state. A cross-section (ι): an arranged matrix, ordinarily Zd, with a d-layered grid and d ϵ Z+. An area (N): a limited efficient sub-set of ι. A nearby progress capability or rule (f): The following conditions of every cell are chosen by its standard **[9]**. CA cross section can be created by two primary capabilities, nearby and worldwide. In the neighborhood progress capability: SN $\rightarrow$ S, SN addresses the arrangement of all potential expresses that the area can be in, with every one of the qualities as a tuple of states (S0, S1, S2, …, SN - 1), with Si ϵ S. For instance, if S= {0, 1} and |N| = 3, SN can be addressed by the set {(0,0,0), (0,0,1)..., (1,1,1)}. The nearby progress capability (rule) decides how the condition of every cell is transformed from a moment to the following. This choice is normally founded on the cell's present status and of its neighbors. In the worldwide capability, if c is considered as the ongoing design of the automata with c ϵ Zd. The CA's next setup is given by ϕ(c), where ϕ: $\sum$ Zd $\rightarrow$ Zd. ϕ Called a worldwide guide or worldwide capability. The CA's transient advancement is then, at that point:

$$c \rightarrow \phi\,(c) \rightarrow \phi 2\,(c) \rightarrow \ldots \quad (1)$$

The name of the grouping c, ϕ(c), ϕ2 (c)… is the circle or populace of c. The cell neighborhood of a cell comprises itself and the encompassing (nearby) cells [10]. There are two essential kinds of CA aspects [8]: One-layered (1D) CA where every cell has two potential states and a cell's neighbors are the nearby cells on each side of it. Figure.1 exhibits the 1D CA. 2D CA has a portion of the comparative elements as does 1D CA. Two fundamental sorts of areas are for the most part pondered. The principal type is the Von Neumann neighborhood which comprises the 4 or 5-cell exhibit considering whether the focal cell is counted. The subsequent kind is the Moore neighborhood which comprises the 8 or 9-cell cluster considering whether the focal cell is counted. **Figure 1** shows the Von Neumann Area and Moore neighborhood [11].

Figure 1: One-dimensional Cellular Automata [11]

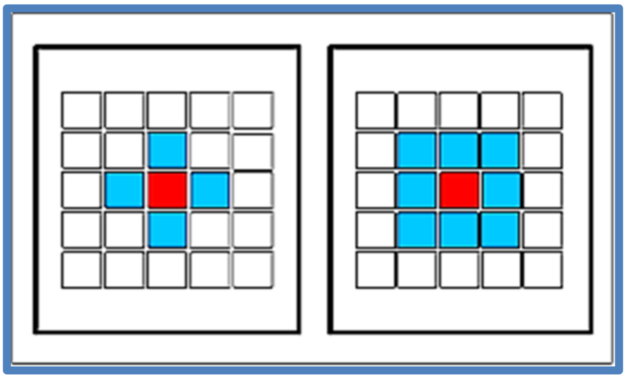

(a) Von Neumann neighborhood **(b) Moore neighborhood**

Figure 2: Two-dimensional Cellular Automata [11]

3.1 Rudimentary Cell Automata: A neighborhood of a cell x with sweep r is the arrangement of the r cells both to the left and right of x, including cell x. An ECA is any cell automata with r=1 and a paired state set S = {0, 1}. The condition of ECA can be as per the following:

$$X_i^{t+1} = f\,(x_i^{t-1}, x_i^{t}, x_i^{t+1}) \quad (2)$$

Where X_i^t is the cell's state, X_i^{t+1} is the cell's next state, x_i^{t-1} is the condition of the cell's left neighbor, x_i^{t+1} is the condition of the cell's right neighbor and *f* is the standard capability. 1D ECA is an extraordinary class of discrete dynamical frameworks shaped by a limited 1D exhibit of N cells. The all-out number of rules for span r area is 2^n where $n = 2^{nr+1}$**[12]**. Hence, ECA has $2^{23} = 256$ potential guidelines **[10]**.

3.2 Limits of Limited Grids: Endless CA has no limits accounts related to them. At the point when we are managing CA with a limited *ι*, the area utilized by the nearby change capability surpasses the cross-section limits. There are essential answers for this issue: Invalid limit CA, in an invalid limit where the CA contains - cells as *X1, X2, Xn,* the furthest left neighbor of *X1* and the furthest right neighbor of *Xn* are considered as zeros for every one of them. Additionally, on the off chance that *Xn* is taken as the furthest left neighbor of *X1* and *X1* is taken as the furthest right neighbor of *xn* then it is called cyclic or intermittent limit CA **[8]**.

3.3 Sorts of CA Reasonable for Cryptography: There are many kinds of CA appropriate for cryptography, if phone mechanization uses some control signals, it is known as Programmable Cell Automata (PCA) **[12]**. If CA generally gets back to its underlying state, it will be called Reversible Cell Automata **[13]**. What's more, if similar principles decide the following piece cells of CA, it is called uniform CA in any case it is called non-uniform CA or Crossbreed Cell Automata (HCA) **[14]**. The HCA creates more intricate examples than a uniform cell machine. This property is exceptionally valuable on account of cryptography, as it will create more complicated figures **[15]**.

4. Rivest Code 5 (Rc5) Algorithm:

RC5 is a block, symmetric key encryption calculation; its basic plan makes it proper for execution in programming and equipment. RC5 has a serious level of adaptability as far as security and execution because of its adaptable choices, for example, factor key size which chips away at 0 up to 2040 pieces, variable block size 32-, 64-, or 128-piece blocks of information) and variable (0 to 255) **[4]**. The boundaries of RC5 are as per the following: w alludes to the block size, r alludes to the quantity of rounds and b alludes to the vital length in bytes, essentially composed as RC5-w/r/b. Ronald L. Ronald L. Rivest demonstrates that the more noteworthy the security/encryption level when the higher the number of rounds **[16]**. the general plan of RC5 is separated into 3 phases: key development, encryption stage, and unscrambling stage. The critical activities in these three phases are Spot-wise XOR of words, expansion of words modulo 2w, and change in two courses left (<<) and right (>>).

5. Core Requirements

The proposed framework can be restated into two stages, the primary stage is planned as a pseudo-random number generator given the cell automata stage, though the subsequent stage is made from the improvement of the RC5 encryption stage. In **Figure 1**, the general design of the proposed Simulation RC5 Algorithm is based peer to peer.

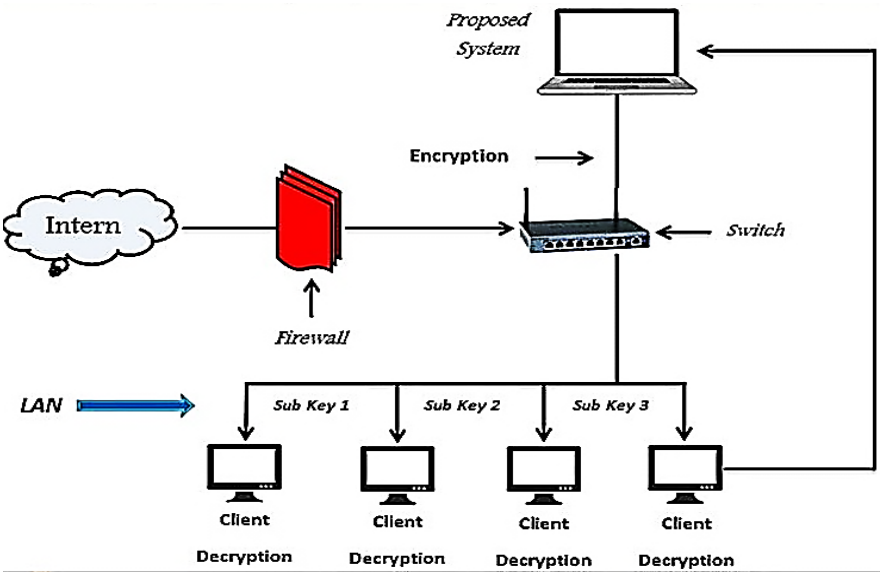

Figure 3: The design of the proposed Simulation RC5 Algorithm based peer to peer (SRPP)

5.1 Stage One: Plan a Pseudo Random Number Generator In light of Cell Automata:

In this stage, a symmetric key cryptographic strategy utilizing CA has been executed through Pseudo pseudo-random number Generator In light of Cellular Automata (PRNGs-CA). The calculation utilizes rudimentary, occasional, mixture, and programmable CA with rules set specifically 30, 90, and 150 CA to shape a succession of 128-cycle irregular numbers. The PRNGs calculation can be separated into three sections as roar:

5.1.1 Producing Starting Seed: The Underlying Random Seed (URS) of the framework is characterized by creating an arbitrary string made from 1024 characters. Then, the irregular rings pass to the MD5 calculation to produce the URS which comprises 128 pieces (16 bytes) that are addressed because of MD5". The motivation behind passing the string to the MD5 calculation is to guarantee that it is infeasible to deliver two messages having a similar hash esteem or to create any URS having a given pre-characterized target message digest, in this manner expanding the strength of the URS to makes the beast force assault more troublesome.

5.1.2 Rule Planning System: to make the CA a PCA, this part has been applied to build the strength of the calculation and make the cryptanalysis more troublesome. The standard planning calculation includes picking which rules set of CA would be applied to the blocks of produced

RNS (as of now eight principles sets have been remembered for this study). Random Integer Number (RIN) is addressed as an irregular number with a worth somewhere in the range of 1 and 8. Then, at that point, the standards set will be picked in light of this RIN. For each sub-key (depicted in subtleties by the following sub-area), the worth of RIN will be changed, and, in this way, the standards set would be different with each sub-key. The principal objective of the standard booking calculation is to make cryptanalysis infeasible, thus expanding the framework's heartiness against assaults, and building the strength of the framework. **Table 1** shows which rules set will be applied considering RIN esteem. This blend of rules is utilized in the third part which comprises creating symmetric keys.

Table 1: RIN value and its corresponding rules set

RIN value	Rules set
A	30, 90, 30, 150, 150, 90, 90, 30
B	150, 30, 90, 150, 90, 30, 90, 90
C	30, 150, 30, 90, 150, 30, 150, 90
D	150, 90, 90, 30, 30, 30, 90, 150
E	30, 150, 150, 30, 30, 90, 90, 90
F	150, 30, 150, 30, 90, 90, 150, 90
G	30, 90, 150, 30, 150, 30, 90, 90
H	150, 30, 150, 90, 30, 30, 90, 90

5.1.3 Key Proliferation System: The major goals of the proposed key engendering instrument part are:

- The sub-keys ought to be a cryptographic pseudo irregular and impact-safe.
- Straightforwardness, ease, and effortlessness of execution.

In the proposed framework, the subsidiaries of the sub-keys are finished through URS (128 pieces) which is considered as an underlying example (seed) utilizing a crossover 1D occasional class of CA. The motivation behind utilizing 1D CA is to guarantee effortlessness and rapid of execution time.

5.1.4 Key proliferation steps:

- **Stage 1**: Consider URS as example #0.
- **Stage 2**: Separation design into blocks of 8 pieces (1-byte), for example, the example will be changed over into 16 blocks, 8 pieces for each (8bit *16 block=128-bit absolute example length).
- **Stage 3**: Info current example to the mixture CA machine, the cross-breed CA machine includes 16 rounds of the same rule planning for each block, for example creating an example of 128 pieces. Each piece of the current example addresses the cell's present

status xit of CA. For each piece, one of three change rules, 30, 90, and 150 is applied considering the choice of the rule booking system. The Crossover CA machine refreshes the cell's present status xit to the following state x_i^{t+1} by utilizing the cell's present status xit and two close nearby neighbors (left neighbor cell xti-1 and right neighbor cell x_t^{i+1}.

- **Stage 4**: The result of the half-and-half CA machine characterizes another example.
- **Stage 5**: Think about the new example as another sub-key.
- **Stage 6**: rehash steps (2, 3 4, and 5) until all the sub-keys are produced. This component of key development can produce sub-keys with an enormous period and high populace. **Figures 2**, **3**, and **4** show the key proliferation instrument and sub-keys blocks plan separately.

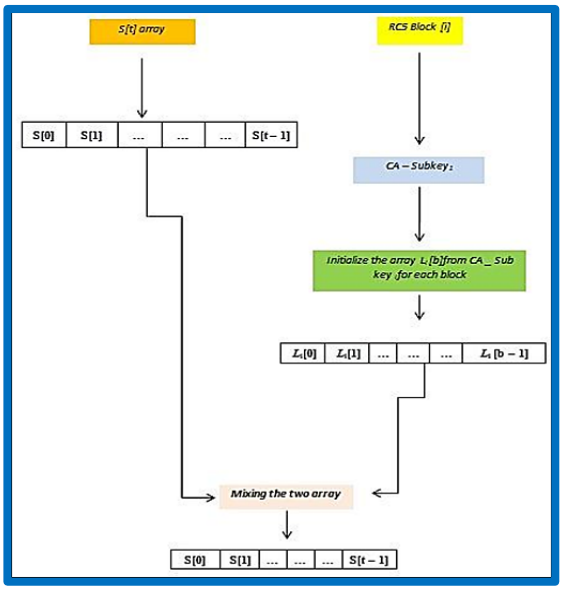

Figure 2: Block diagram of ERC5KS

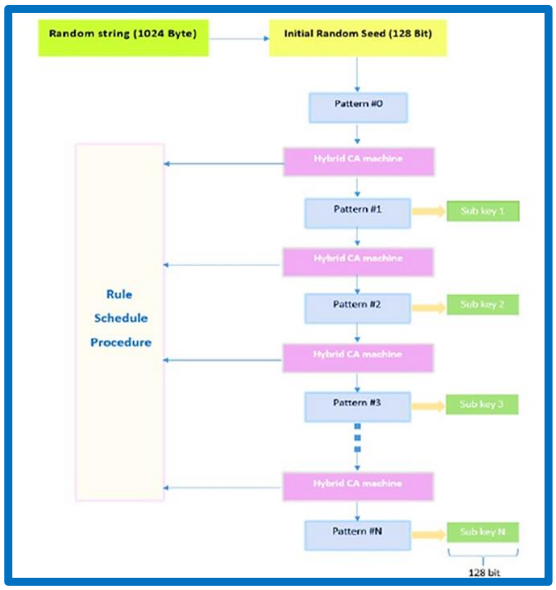

Figure 3: Key propagation mechanism

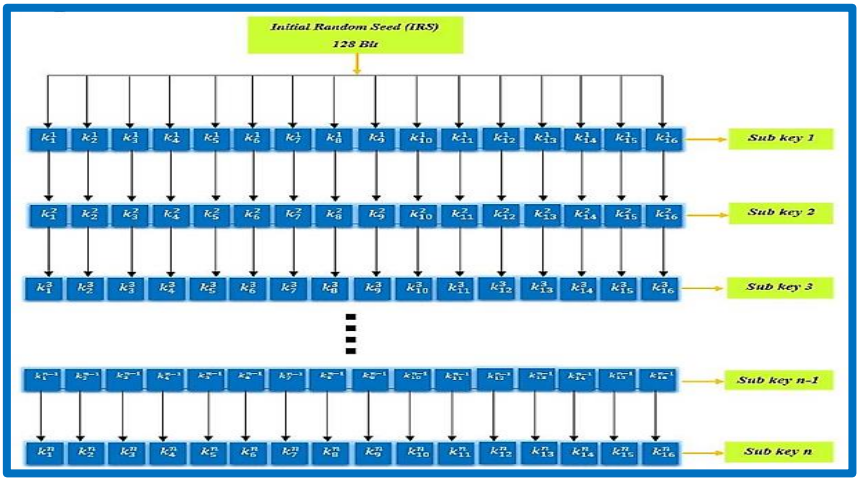

Figure 4: Sub-Keys Blocks Schedule

5.2 Stage Two: Upgrade of RC5 Encryption algorithm The first RC5 has frail keys and to supplant it with solid keys, a proposed Upgrade of RC5 encryption has been carried out as

follows: Improved RC5 Key Timetable 5.2.1: The calculation of Upgraded RC5 Key Timetable (ERC5KS) can be separated into 3 sections: the initial segment is introducing S cluster, the subsequent part is introducing L exhibit and the latter is the blending part, individually, as displayed in **Figure 5**.

- Instating S cluster: The S exhibit is introduced by the same method as the first RC5 key timetable.
- Instating L cluster: L exhibit of the proposed conspire is introduced with each block in the encryption cycle through various sub-keys which got from CA as examined in the past segment. The sub-keys size which produces L exhibit is 128-digit (16 bytes) for each.

5.2.1 Blending S and L exhibits: The two clusters S and L are blending by equivalent to the first RC5 blend capability, the main distinction is that the L exhibit is introduced with various sub-keys for each RC5 encryption and decoding block. Note that, as a unique RC5 calculation, due to the likelihood of getting various sizes of S and L clusters, the bigger exhibit is handled multiple times though the more modest exhibit might be handled more times.

5.2.2 Upgraded RC5 algorithm: The block size of the Enhanced RC5 (ERC5) is made of two words (identicalness to eight bytes), S exhibit is introduced exclusively toward the start of the encryption cycle. Though the L cluster is instated for each block of the wave information by CA sub-keys as referenced in the before segments, the remainder of the encryption calculation is equivalent to the first RC5. Encoding each block of information with various sub-keys reinforces the first RC5 frail keys making cryptanalysis more troublesome. *Note* that on the off chance that the information size isn't equivalent to 64-byte or to its products (block size is equivalent to 2 words, 32 bytes for each=64 byte), an important cushioning is added to the information cluster.

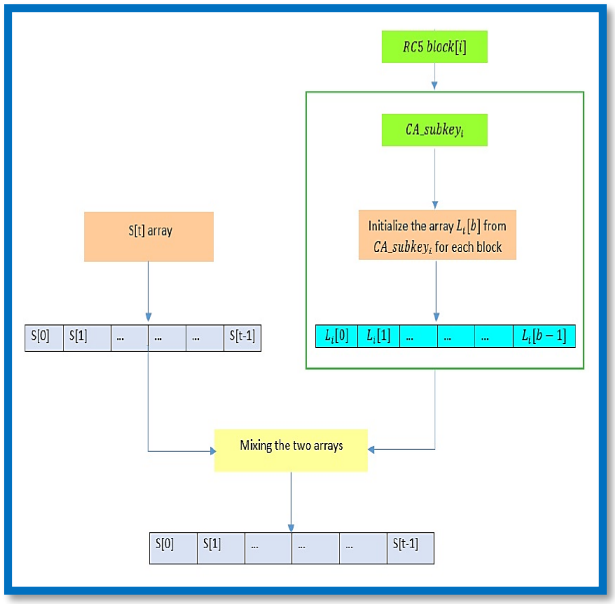

Figure 5: ERC5KS Scheme

6. Assessment Of the Proposed System:

The assessments of the proposed system have been run under Windows 10 Ace. Intel(R) Core(TM) i5-5200U computer chip @ 2.20GHz 2.20 GHz, 8 GB Arbitrary Access Memory (Slam), the framework type is 64-cycle Working Framework, 64x-based processor. C# programming language is used to foster the recommended framework (Visual Studio 2013).

6.1 Tracking down the Rules: to find the proficient standards that produce great PRNS to the proposed PRNGs, the framework tried the accompanying principles: 30, 45, 51, 60, 90, 102, 105, 150, 153, 165 and 195. In certain circumstances, a uniform cross-section was tried, while different reenactments assess non-uniform (half and half) CAs. All the previously mentioned rules were tried as uniform CAs thinking about the three most significant NIST tests. The framework additionally inspected numerous non-uniform principle sets like 30, 90,105 with 150 and 30, 45 with 150, and numerous others. That's what the outcomes show, for the most part, non-uniform CAs are preferable RNGs over uniform ones since a portion of these mixes finish some of NIST assessments and could produce RNS with an enormous intermittently. At long last, delivering an RNS with great quality and a wonderful period was the test of this paper, subsequently, the plan recognized that in more than 100 examinations, and three standards which gave the best outcomes would in general oversee the finishing up created grids: 30, 90, and 150. Notwithstanding the low effect of rule 90 on uniform CAs, it affects non-uniform CAs.

6.2 Consequences of Period and Factual Tests: The eight CAs rules set of the proposed conspire to show roughly the same execution level. The tests were applied to various ages, for example, numbers of produced sub keys (10,000, 32,000, 50,000, 75,000, and 100,000 ages were tried), and utilized similar starting worth to each of the tried standards set and measure of age. They all finished the three NIST measurable assessments. Likewise, they all created sub-keys with practically no duplication, and that implies that the proposed framework found an extremely enormous periodicity with p-values. This additionally implies that their age of arbitrary succession gives something to be searched for, wanted, and commendable. Accordingly; the outcomes show that the top-notch of the created RNS is adequate for some applications. **Table 2** sums up the normal p-upsides of the standard sets applied with various measures of age (note that if the p-esteem is more noteworthy than 0.01, it is considered fruitful). The table additionally shows the execution time for these ages. In this way, the applied rudimentary, non-reversible, crossbreeds, occasional, and programmable CAs give great and quick RNGs.

Table 2: Average (*P*-Value) and Execution Time of The Proposed System

No. of generated sub-keys	Execution time(Sec)	Average *P*-value			Status
		Frequency	Block	Run	Successful
10000	0.076	0.7480	0.5812	0.5797	Successful
32000	0.240	0.5410	0.3986	0.4841	Successful
50000	0.376	0.4832	0.4645	0.5173	Successful
75000	0.540	0.5672	0.6182	0.4264	Successful
100000	0.747	0.6562	0.4460	0.3115	Successful

6.3 Assessment of the Upgraded RC5 Algorithm: to make the RC5 calculation more grounded, it needs to remove its feeble keys and replace them with more grounded keys. While trying to do this assignment, the ERC5 calculation has been presented. The submitted conspire encodes each block of RC5 with an alternate key which was produced given CA as examined before. This calculation was embraced to mend the shortcomings of RC5 keys and to ensure progressed security notwithstanding present superior encryption. With the end goal of checking the strength of the proposed work, a few investigations have been preceded as follows:

1. Data Entropy Analysis: **Table 3** shows the entropies of the first record, RC5 and ERC5.

Table 3 :(1st and 2nd) Entropy of Original files, RC5 and ERC5

No	1st Entropy			2nd Entropy			
1	Name	Original Computer Test	Original RC5	ERC5	Original Computer Test	Original RC5	ERC5
2	Cmp1	6.1100	7.8440	7.9851	12.2032	15.6757	15.9662
3	Cmp2	7.0400	7.8440	7.9958	12.2032	15.6757	15.9890
4	Cmp3	4.9278	7.9933	7.9959	14.0678	15.9804	15.9891
5	Cmp4	7.6814	7.5664	7.9964	9.8500	15.1307	15.9906
6	Cmp5	5.3865	7.9957	7.9977	15.3592	15.9890	15.9935
7	Cmp6	2.9016	7.9973	7.9980	10.7175	15.9923	15.9945
8	Cmp7	6.3162	7.2883	7.9982	5.8009	14.5644	15.9953
9	Cmp8	6.5813	7.9982	7.9987	12.6156	15.9951	15.9965
10	Cmp9	6.8635	7.9985	7.9986	13.0806	15.9962	15.9966

From the above Table, the fruitful result of the ERC5 is clear through the upgraded consequences of entropy examination. At the point when the documents are enciphered, their first entropy ought to impeccably be 8 and the second entropy ought to be 16. On the off chance that the result of such a code produces figures with first entropy under 8 or potentially second entropy under 16, there exists a certain level of expectedness, which dangers its security. The higher the pace of entropy of enciphered, the better the security. **Table 3** explains that the outcomes accomplished from the proposed framework are exceptionally near the hypothetical worth of entropy contrasted with the first RC5. This implies that the data spillage in the encryption methodology is infeasible, and the encryption framework is secure against the entropy assault.

2. Irregularity Tests: to guarantee the nature of the proposed ERC5 over unique RC5, NIST tests were made, and the outcomes are displayed in **Table 4**. Likewise, **Figure 6** determines the achievement pace of each, the proposed ERC5 generally wins.

Table 4: NIST Tests Results of RC5 vs. ERC5

No	Name	Frequency		Block		Run	
		Original RC5	SRC5	Original RC5	SRC5	Original RC5	SRC5
1	Cmp1	0.0029	0.7732	0.8810	0.8361	0.0434	0.2168
2	Cmp1	0.0830	0.9971	0.1502	0.4969	0.7583	0.6603
3	Cmp2	0	0.6314	0	0.4069	0.3230	0.2911
4	Cmp3	0.3212	0.816	0.3719	0.3596	0.9565	0.5432
5	Cmp4	0.6776	0.9333	0.0056	0.3021	0.0391	0.9634
6	Cmp5	0	0.3880	0.8780	0.4393	0	0.6971
7	Cmp6	0.0736	0.3774	0.3571	0.2390	0.6038	0.8048
8	Cmp7	0.3080	0.5287	0.2287	0.959	0.5538	0.9564
9	Cmp8	0.0693	0.1284	0.99999	0.1481	0.000003	0.9712
10	**Success Rate**	1/9	8/9	4/9	5/9	3/9	6/9

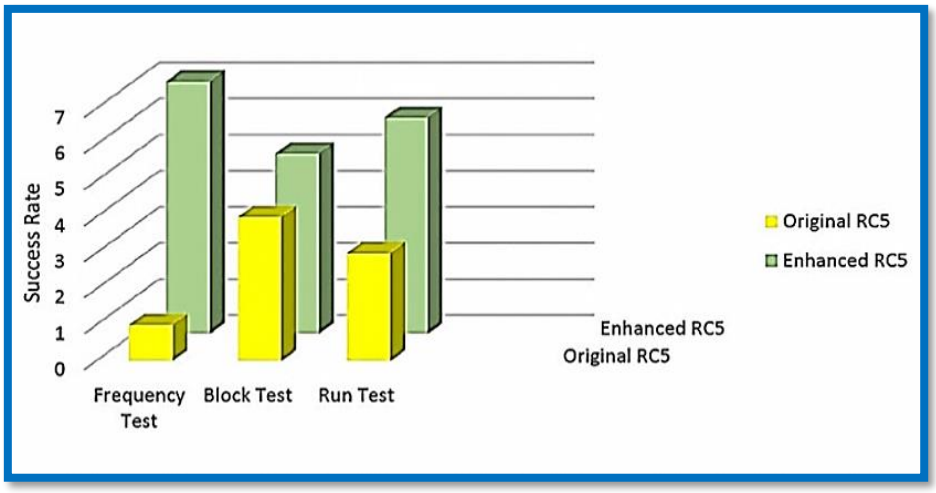

Figure 6: Achievement pace of frequency, block, and run tests for ERC5 versus original RC5

6.4 Execution Time: The accompanying table shows that the proposed framework is quite enough and can be utilized as an encryption framework.

Table 5: ERC5 Execution Time for the Proposed Encryption Framework

No	Name	ERC5 Execution Time (Sec.)
1	Cmp1	0.012
2	Cmp1	0.032
3	Cmp2	0.040
4	Cmp3	0.045
5	Cmp4	0.060
6	Cmp5	0.070
7	Cmp6	0.071
8	Cmp7	0.087

6.5 Key Space Investigation: A decent encryption calculation ought to be delicate to the code keys, and the keyspace ought to be sufficiently huge to make savage power assaults infeasible. For the proposed encryption framework, the key space investigation has been painstakingly examined and can be summed up as follows:

6.5.1 Key Responsiveness Examination: A significant element for a decent crypto-framework is a very key aversion to guarantee the security of the crypto-framework across the best force assault in an action. Key responsiveness of any crypto-framework can be identified in two different ways: First and foremost, the code created by any crypto-framework ought to be delicate to the key, for instance, if two-piece different mystery keys have been utilized to scramble a similar unique plain, then, at that point, the two produced figure keys delivered should be disengaged to one another. Furthermore, the code can't be unscrambled accurately regardless of whether there is only a tad variety among encryption and decoding secret keys. In the proposed encryption calculation, the figure relied upon each digit of the key, this reliance was accomplished by the upgraded RC5 stage, where each block of information relies upon the CA sub keys and each subkey of the CA stage relies upon the past key, significantly this reliance brings about making the framework's critical awareness as displayed in **Figures 7** and **8**. **Figure 8** shows different codes of the same plain encoded with two keys contrasts from one another in only the slightest bit while **Figure 8** shows that assuming the unscrambling keys vary in just a single piece from the encryption key, then the subsequent decoded is unique about the first plain.

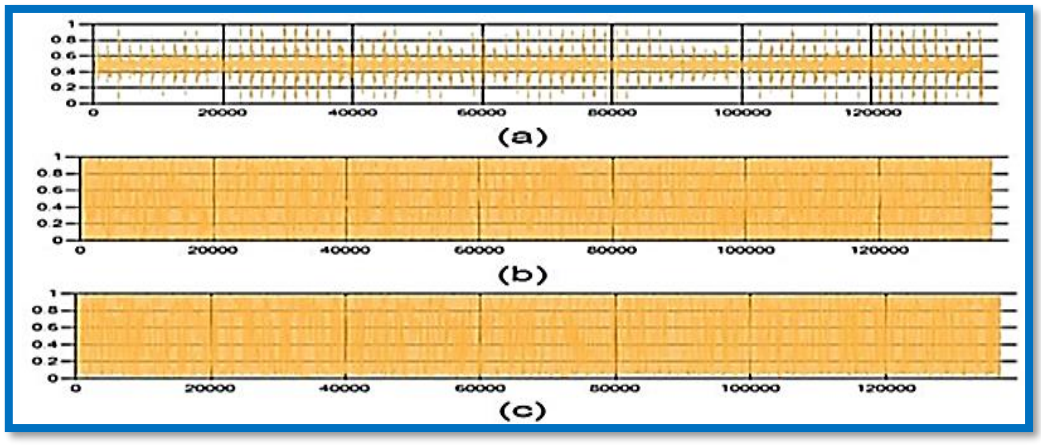

Figure 7: Simulation RC5 Algorithm by Waveforms

Figure 7 simulation RC5 algorithm by waveforms using blank plaintext for known correct cipher output of 0xb7c4b44a-9faa44d8, shown in above different encryption process for same document with two keys contrast from one another in only the slightest bit, (a) shows unique wave record before encryption and (b,c) shows a similar wave document encoded with the two keys.

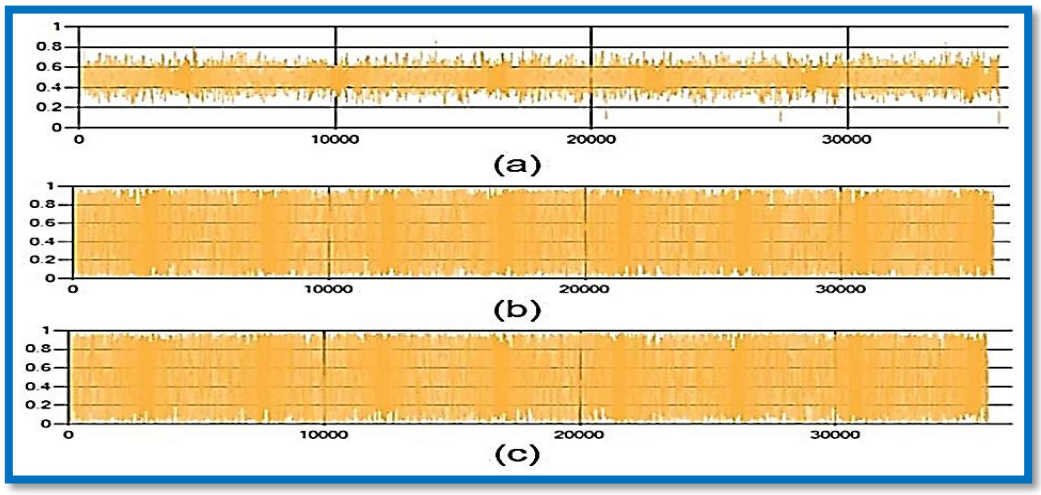

Figure 8: plot of waveform decoded with critical contrasts in just a single piece

Figure 8: At the higher plot of waveform decoded with critical contrasts in just a single piece from the first key. (a) Unique waveform plot. (b) The plot of the waveform is unscrambled with vital contrasts in just a single piece from the first key. (c) The plot of waveform unscrambled with a vital varies in just a single piece from the first key on one more situation from (b).

7. Conclusions:

This paper proposes an encryption framework given cell automata with an improved RC5 encryption algorithm. The primary finishes of this paper can be summarized as follows: The proposed framework found another blend of CA rules to create a strong RNS with a high populace and huge period, notwithstanding a high irregularity. In this way, recommended PRNGs expand the security of the calculation. Likewise, the improvement of RC5 calculation comes to reinforce the first RC5 frail keys and to solidify the first RC5 in terms of safety and irregularity by exploiting the proposed PRNGs given CA; these PRNGs are utilized as a one-time pad key for each block of information. The proposed framework is key touchy. This awareness is accomplished by the reliance of each block of the ERC5 stage on the created PRNGs-CA stage sub-keys. Additionally, the announced consequences of the proposed framework affirmed the positive impact on solidifying the force of unique RC5 in the two terms of the entropy and arbitrariness tests.

- Funding: None
- Acknowledgement: None
- Conflicts Of Interest: The Author Declares No Conflict of Interest.
- Availability Of Project and Codes

8. References

[1] Shahzadi R, Anwar SM, Qamar F, Ali M, Rodrigues JJ. Chaos based enhanced RC5 algorithm for security and integrity of clinical images in remote health monitoring. IEEE Access. 2019;7:52858-70.

[2] Alsaffar N, Elmedany W, Ali H. Application of RC5 for IoT devices in smart transportation system. In: 2019 8th International Conference on Modeling Simulation and Applied Optimization (ICMSAO); 2019 Apr; IEEE. p. 1-4.

[3] Vibar JCN, Medina RP, Sison AM. ERC5a–An enhanced RC5 algorithm on bit propagation in the encryption function. In: 2019 IEEE 4th International Conference on Computer and Communication Systems (ICCCS); 2019 Feb; IEEE. p. 479-82.

[4] Abidi A, Sghaier A, Bakiri M, Guyeux C, Machhout M. Statistical analysis and security evaluation of chaotic RC5-CBC symmetric key block cipher algorithm. Int J Adv Comput Sci Appl. 2019;10.(١٠)

[5] Hossen MS, Islam MA, Khatun T, Hossain S, Rahman MM. A new approach to hiding data in the images using steganography techniques based on AES and RC5 algorithm cryptosystem. In: 2020 International Conference on Smart Electronics and Communication (ICOSEC); 2020 Sep; IEEE. p. 676-81.

[6] Alenezi MN, Alabdulrazzaq H, Mohammad NQ. Symmetric encryption algorithms: Review and evaluation study. Int J Commun Netw Inf Secur. 2020;12(2):256-72.

[7] Wang Z, Yu B, Pei B, Zhang L. Research on AES encryption algorithm based on timestamp in Wireless Sensor Networks. In: 2020 2nd International Conference on Information Technology and Computer Application (ITCA); 2020 Dec; IEEE. p. 15-8.

[8] Yang C, Wu J, Wang L, Zhang X, Li L, Liu S. Smart grid monitoring systems based on advanced encryption standard and wireless local area network. IOP Conf Ser Mater Sci Eng. 2020;719(1):012056.

[9] Al-Ahdal AH. Security Analysis of a Robust Lightweight Algorithm for Securing Data in Internet of Things Networks. Turk J Comput Math Educ. 2021;12(12):133-43.

[10] Sagun A, Khaidurov V, Lakhno V, Opirskyy I, Chubaievskyi V, Desiatko A. Devising a method for improving crypto resistance of the symmetric block cryptosystem RC5 using nonlinear shift functions. East Eur J Enterp Technol. 2021;5(9):113.

[11] Valeriy L, Andrii S, Vladyslav K, Boris G, Petro K, Svitlana K. One method for RC5 algorithm's cryptographic strength improving. In: Soft Computing for Security Applications: Proceedings of ICSCS 2021. Singapore: Springer Singapore; 2021. p. 13-25.

[12] Ngamsert R, Kangrang A. Applying of marine predator's algorithm linked with reservoir simulation model considering sedimentation for reservoir operation. Adv Civ Eng. 2022.

[13] Hussein SN, Obaid AH, Jabbar A. Encryption Symmetric secret Key in Wireless Sensor Network Using AES Algorithm. Iraqi J Sci. 2022;5037-45.

[14] Sumathi M, Narmadha R, Anbarasi Jebaselvi GD. Performance comparison of data security algorithms. In: Human-Assisted Intelligent Computing: Modeling, simulations and applications. Bristol, UK: IOP Publishing; 2023. p. 33-1.

[15] de Carvalho Bertoli G, Suri R, Rizos A, Pereira DP. Open Challenge for Intrusion Detection on Air-Ground Communication: From Data Analysis to Simulation. In: 2023 IEEE/AIAA 42nd Digital Avionics Systems Conference (DASC); 2023 Oct; IEEE. p. 1-9.

Al-Kitab Journal for Pure Sciences (2024); 8(2):48-60.
https://doi.org/10.32441/kjps.08.02.p5

Al-Kitab Journal for Pure Sciences
ISSN: 2617-1260 (print), 2617-8141(online)

https://isnra.net/index.php/kjps

Bioremediation of Liquid Waste of Olive Presses (Al-Jeft water) by Using the Biomass of the Local Isolate of The Fungus Helvella bachu

Jehaan Mowafak Al-rawi[1*], **Shimal Younis Abdul-hadi**[2]

[1*]Department of Biology, College of Science, University of Mosul, Mosul, Iraq
[2]Department of Biology, College of Education for Pure Sciences, University of Mosul, Mosul, Iraq

Corresponding Author: jehsbio88@uomosul.edu.iq

Citation: Al-rawi JM, Abdul-hadi SY. Bioremediation of Liquid Waste of Olive Presses (Al-Jeft water) by Using the Biomass of the Local Isolate of The Fungus Helvella bachu. Al-Kitab J. Pure Sci. [Internet]. 2024 June. 10 [cited 2024 June. 10];8(2):48-60. Available from: https://doi.org/10.32441/kjps.08.02.p5.

Keywords: Helvellaceae, COD, Total phenol concentration, Bioadsorption.

Article History
Received 18 Apr. 2024
Accepted 21 May 2024
Available online 10 June 2024

Abstract:

The study included investigating the potential of the biomass of the local isolate of the fungus Helvella bachu in bioremediation of the liquid waste of olive presses (Jeft water) at two concentrations of 10%-20%. The mycelium was inoculated on solid media treated with olive press water, with concentrations of 10% and 20%, for several incubation days 2, 4, and 6, respectively. We observed that the diameter of the fungal colony is directly proportional to the increase in the incubation period, as the largest diameter of the fungal colony was 13.56 mm and 11.46 mm after 6 days of incubation at a concentration of 10% and 20% of Jeft water, respectively, compared to the diameter of the fungal colony growing in untreated medium, which it reached 15 mm, while the least diameter of the fungal colony was 6.00 and 5.36 mm at a concentration of 10% and 20% of Jeft water, respectively, after two days of incubation compared to the control sample. As for using liquid media, the results revealed a decrease in the total phenol concentration, reaching 2.14 mg / 100 g after 30 days of treatment with a concentration of 20% of Jeft water, compared to the control treatment of 23.58 mg / 100. The percentage of black color removal was 64.39% at a concentration of 10% and an incubation period of 30 days, while at a concentration of 20%, the percentage of color removal was 49.53% and 42.10% after 30 days of incubation. The biomass of the fungus isolate was able to reduce

the chemical oxygen demand in both concentrations of Jeft water used with different responses. The percentage of chemical oxygen requirement was 65.83% at a concentration of 10% of Jeft water after 30 days of treatment, while the percentage of COD was 8.08% at a concentration of 20% for the same incubation period above.

Keywords: Helvellaceae, COD, Total phenol concentration, Bioadsorption.

المعالجة الحيوية للنفايات السائلة لمعاصر الزيتون (مياه الجفت) باستخدام الكتلة الحيوية للعزلة المحلية للفطر *Helvella bachu*

جهان موفق الراوي[1]، شمال يونس عبد الهادي[2]

[1]*قسم الأحياء، كلية العلوم، جامعة الموصل، الموصل، العراق

[2]قسم علم الأحياء، كلية التربية للعلوم الصرفة، جامعة الموصل، الموصل، العراق

jehsbio88@uomosul.edu.iq, shimalyonis2018@uomosul.edu.iq

الخلاصة:

تضمنت الدراسة التحري عن امكانية الكتلة الحيوية للعزلة المحلية للفطر *Helvlella bachu* في معالجة النفايات السائلة لمعاصر الزيتون (مياه الجفت) حيويا وبالتركيزين ٢٠-١٠ %. زرع الغزل الفطري على الاوساط الصلبة المعاملة بمياه معاصر الزيتون وبالتركيزين ١٠ و ٢٠٪ ولعدة ايام تحضين ٦,٤,٢ على التوالي , لوحظ ان قطر المستعمرة الفطرية يتناسب طرديا مع زيادة مدة التحضين اذ بلغ اكبر قطر لمستعمرة الفطر ١٣,٥٦ ملم و١١,٤٦ ملم بعد مرور ٦ ايام تحضين عند التركيز ١٠ % و ٢٠٪ من ماء الجفت على التوالي مقارنة بقطر مستعمرة الفطر النامية في وسط غير معامل والتي بلغت ١٥ ملم بينما بلغ اقل قطر لمستعمرة الفطر ٦,٠٠ و٥,٣٦ ملم عند التركيز ١٠ % و ٢٠٪ من ماء الجفت على التوالي بعد مرور يومين تحضين مقارنة بعينة السيطرة. اما باستخدام الاوساط السائلة فقد اسفرت النتائج عن انخفاض في تركيز الفينول الكلي إذ بلغ ٢,١٤ ملغم / ١٠٠ غم بعد مضي ٣٠ يوماً على المعاملة بالتركيز ٢٠ % من مياه الجفت مقارنة بمعاملة السيطرة ٢٣,٥٨ ملغم/١٠٠ . النسبة المئوية لإزالة اللون الأسود بلغت ٦٤,٣٩ % عند التركيز ١٠ % وبمدة تحضين ٣٠ يوماً, بينما عند التركيز ٢٠ % بلغت النسبة المئوية لإزالة اللون ٤٩,٥٣ و٤٢,١٠ % بعد مرور ٣٠ يوم تحضين. تمكنت الكتلة الحيوية لعزلة الفطر من خفض متطلب الأوكسجين الكيميائي بكلا التركيزين لماء الجفت المستخدم مع اختلاف الاستجابات. إذ بلغت النسبة المئوية لمتطلب الاوكسجين الكيميائي ٦٥,٨٣٪ عند التركيز ١٠٪ من ماء الجفت بعد مرور ٣٠ يوماً من المعاملة, بينما بلغت النسبة المئوية لـ *COD 8.08* % عند التركيز ٢٠ % لنفس مدة التحضين اعلاه.

الكلمات المفتاحية: Helvellaceae، المتطلب الكيميائي الاوكسجين، تركيز الفينول الكلي، الادمصاص الحيوي.

1. Introduction:

The problem of environmental pollution was and still is at the top of the problems that concern specialists, That is on the rise with an increase in population in population growth and the nature of modern life. Due to the increasing requirements to develop in different parts of life like industrial and welfare of the human race which become wider. These requirements led to the accumulation of huge amounts of toxic compounds which were thrown into the environment without thinking of its dire consequences [1]. The accumulation of toxic compounds casts a shadow over the ecosystem, such as the atmosphere, soil, and water bodies, that has become a dumping ground for factory waste such as industrial dyes, olive presses, hydrocarbon compounds, heavy metals, and pharmaceutical residues, that maybe interact with other compounds and become even more toxic [2]. Therefore, it was necessary to deliberate plans to get rid of these toxic pollutants, because the treatment of these residues by traditional methods (physical and chemical) is not always effective in addition to its high cost, alternative means were searched for, Bioremediation was found as the best option for managing environmental pollutants [3].

Moreover, biological remediation is an innovative, promising, environmentally friendly, and economical technology for managing a polluted environment. It is an attractive and successful cleaning technique for removing toxic waste from a polluted environment by decomposing or eliminating various hazardous chemical and physical materials or detoxifying the surrounding environment through the vital activities of microorganisms at a low cost and without secondary pollution [4]. Therefore, fungi, with their characteristics and survival instinct, have become of pioneering importance in environmental biotechnology because they can metabolize many pollutants of great diversity [5].

Recent research has proven that fungi play important roles in the bioremediation of pollutants, especially in persistent organic pollutants, such as dyes, coal, leather tanning residues, medicines and personal care products, polycyclic aromatic compounds (gasoline and diesel), and liquid wastes of the sugar industry and olive presses. Fungi take all these pollutants substances (substrates) and effectively decompose them to obtain carbon, nitrogen, or the energy it needs for metabolism [6], thus, a wide range of contaminants could be completely removed or at least transformed into less dangerous compounds [3]. The wastewater resulting from the production of olive oil (Jeft) was thrown randomly without regard to its negative impacts on the environmental system. This Jeft water drains directly into river water without developing any strategies to treat these pollutants, which reflect negatively on the environment because of containing a large percentage of complex phenolic compounds (tannins) that are

difficult to biodisintegrate, not to mention the transformation of phenolic dyes, compounds that give the dark color to Jeft water, into phosphorous hydrogen that is highly toxic [19]. In this regard, the ability of the biomass of the local isolate of the fungus *H.bachu* to treat the wastewater of Jeft was investigated using liquid and solid media and in several axes.

2. Materials and methods:

2.1. Test organism: Research experiments were conducted using the biomass of the local fungal isolate *Helvella bachu*, which was morphological and molecular identified by (Al-Rawi, 2022) [7], fruiting bodies obtained from Nimrud district located about 30 km south of the city of Mosul – Iraq. The fruiting bodies were transported to the laboratory and washed with tap water several times to remove all dust and dirt stuck to them, the pollination booth was sterilized with 70% ethanol. The fruiting bodies were cut from different areas, including the stem, the cap, and the heart of the fruiting body, using a sterile scalpel into small parts. The pieces were immersed in 70% ethyl alcohol for 3 minutes, then they were transferred using sterilized forceps by alcohol irradiation to a volumetric bottle containing sterile distilled water. For 5 minutes to remove traces of alcohol, then the pieces of fruiting bodies were placed on sterile Whatman No.1 filter papers and left to dry completely. Pieces of different fruiting bodies were inoculated into sterile Petri dishes containing the Potato Dextrose Agar (PDA) culture medium. The dishes were incubated after covering them with foil in the incubator at a temperature of 28 ± 2º C for a period of 5-10 days while monitoring the growth of fungal hyphae during them to obtain a pure, densely growing fungal colony [21].

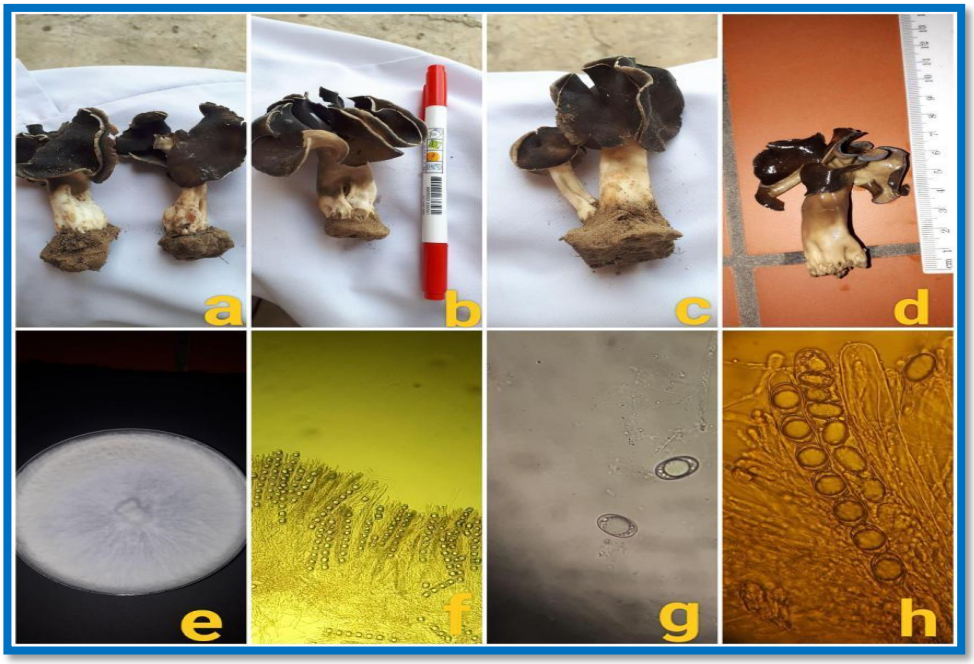

Figure (1): Phenotypic and microscopic identification of the selected local fungal isolate, a-b-c-d: fruiting body, e: fungal colony on PDA nutrient medium, f: asci cysts and paraphysis at 40 X magnification, g-h: ascospores under an optical microscope after staining with lactophenol.

2.2. Olive Presses Water (Jeft Water): Jeft water was obtained from one of the olive presses (the black type) in the Al Fadhiliya district. As a first step, Jeft water was left in a glass flask in the refrigerator for 24 hours so that the oil floated above the surface of the water and was manually disposed of. Then, Jeft water was filtered by passing it through several layers of gauze to remove impurities. The process was repeated three times. The water was kept in dark glass volumetric tubes with a temperature of - 20 ºC until use [15].

2.3. Solid media: Potato Dextrose Agar (PDA)

The nutritional medium was prepared by dissolving 39 gm of the(PDA) powder in a liter of distilled water and mixing well using the magnetic stirrer until complete dissolution. And pH was set at 5.5. The prepared medium was autoclaved at 121 °C at 1 atmosphere pressure for 15 minutes. To avoid contamination of the prepared medium with bacteria, 250 mg/L of chloramphenicol, was sterilized using a 0.45 micron diameter membrane filter. After sterilizing and cooling it in the laboratory atmosphere, it was added to the medium. The medium was distributed in sterile plastic Petri dishes, 15 mL per dish, and the dishes were kept in the refrigerator until the isolate and purifying fungal isolates [8].

2.3. Liquid media: Potato Glucose Broth (PGB)

A 200 gm of peeled potato was cut into cubes were then weighed and put in a glass flask containing 500 ml of distilled water over low heat until cooked. The potatoes were filtered by using two layers of medical gauze then (20) gm of glucose was added to them with continuous stirring until homogeneous on a magnetic stirrer. The volume was filled to 1 L. The pH was adjusted to 5.5. The medium was autoclaved at 121 °C at 1-atmosphere pressure for 15 minutes after distributing it into 250 mL conical flasks [8]. 250 mg/L of chloramphenicol was added to the medium after sterilizing and cooling it in the laboratory atmosphere. Thus to avoid contamination of the prepared medium with bacteria.

3. Agricultural conditions

3.1. solid media: Potato Dextrose Agar (PDA) medium was prepared in glass flasks and peat water was added to it at concentrations of 10% and 20%. The mixture was mixed well and autoclaved at 121ºC and 1-atmosphere pressure for 15 minutes. The medium was left to cool in the laboratory atmosphere, then distributed to sterilized Petri dishes of 15 mL/dish. All plates were inoculated with a disc of a colony of newly growing fungus using a 6 mm diameter cork puncture with three replicates for each concentration leaving a plate untreated to represent the control sample. The plates were incubated after being covered with aluminum foil at a temperature of 28 ± 2 ºC for 6 days. The growth of the mycelium was monitored, as well as,

the growth diameter was measured for periods ranging from 2-4-6 days, and the images were documented using a digital camera [9].

3.2. Liquid media: The researcher indicated [10], that potato glucose medium (PGB) was used. The nutritional medium was distributed in a sterile glass flask with a capacity of 250 mL and at the rate of 100 mL/flask. Jeft water was added to each flask at concentrations of 10% and 20% each separately. Each flask was prepared in duplicate, at the rate of two replications for each treatment. The medium was sterilized under the above-mentioned conditions. After sterilization and cooling, the media were inoculated using sterile alcohol flammable forceps with 5 disks of newly grown fungus culture, taking into account leaving a flask without culturing the fungus for each concentration to represent the control sample. The flasks were placed in the shaking incubator at a shaking speed of 150 cycles/min and a temperature of 28 ± 2 ºC for a period of 15-30 days. After the end of the specified incubation period, the contents of the flasks were filtered with Whatman No.1 filter papers installed on a Buechner funnel connected to the electrovacuum device. The crude filtrate was used in tests for the bioremediation of liquid waste from black olive presses, which included:

- **Degradation of phenolic compounds**

The concentration of phenolic compounds in the filtrate obtained from the previous step was measured based on the method the researcher indicated [11] using the standard Folin-Cioalteu reagent. The reaction mixture consisted of 100 microliters of peat Jeft filtrate treated with the fungal isolate for each concentration, as well as a control sample with 500 microliters of standard reagent and 1.5 ml of 20% sodium

carbonate, which was mixed using an electro mixer. The mixture was diluted with distilled water to reach a volume of 10 ml. The mixture was left for two hours at laboratory temperature, the absorbance was measured with a spectrophotometer at a wavelength of 665 nm and was used to estimate the concentration of phenolic compounds before and after treatment by titration against the standard Gallic acid, where the concentration of phenolic compounds was expressed in Gallic acid equivalent per gram of dry weight of the filtrate.

- **Bioadsorption using the biomass of the fungus *H.bachu***

A research attempt was made to use the adsorption capacity of the fungus *H.bachu* biomass in removing the black color from the liquid waste of olive presses. The raw filtrate of Jeft water obtained from the paragraph (liquid media) was distributed in test tubes and centrifuged at a speed of 4000 rpm for 20 minutes. 1 mL of the supernatant solution was taken for each concentration and each incubation time in addition to the control sample. The absorbance was

measured with a spectrophotometer at a wavelength of 395nm, and the percentage of black color removal was estimated according to the method [12].

- **Chemical Oxygen Demand (COD)**

To detect the chemical oxygen demand in olive presses' liquid waste follow the protocol described by Pitwell [13]. A special flask called a reflux flask with a volume of 500 mL was used in this experiment. 50 mL of raw filtrate of treated and untreated peat water was taken and 1 g of mercury sulphate was added to it. Carefully add 0.5 mL of Sulfuric acid reagent, mixing gently until the mercury sulphate is completely dissolved, then add 25 mL of 0.041 molar $K_2Cr_2O_7$ solution. The flask containing the above mixture was connected to the condenser submerged in cooled water, then the remainder of the sulfuric acid reagent (70) mL was added. The nozzle of the condenser was closed with a beaker to prevent its contents from scattering and left for two hours. Turn off the device and leave it to cool to laboratory temperature. With distilled water, the mixture was diluted to twice its volume. The excess amount of $K_2Cr_2O_7$ was titrated with graded concentrations (0.15-0.1) mL of FAS indicator (ferrous ammonia sulphate). The titration continued until the solution turned from bluish-green to brownish-red. The COD concentration was calculated based on the following equation:

COD [13] as mg O_2/L = (A - B)× M× 8000/mL sample

A: The amount of FAS used for the control sample.

B: The amount of FAS used for the sample.

M: The molarity of FAS.

8000: Weight of oxygen in milliliters

4. Results and discussion

4.1.Solid media: The results shown in **Table 1** present the possibility of growth of the fungal colony under experiment on the solid nutrient medium (PDA) containing Jeft water, at concentrations of 10% and 20%, in varying degrees, after 6, 4, and 2 days of incubation. In general, it appeared that the diameter of the fungal colony was directly proportional with an increase in the incubation period, the largest diameter of the fungal colony reached 13.56 mm and 11.46 mm after 6 days of incubation at a concentration of 10% and 20% of Jeft water, respectively. This result was compared to the diameter of the fungal colony growing in an untreated medium (control) that reached 15 mm, while the smallest diameter reached 6.00 mm and 5.36 mm at 10% and 20% of Jeft water, respectively, after two days of incubation compared to the control, as shown in **Figure 1**. This result confirms the ability of the fungus to exploit the compounds present in Jeft water as a source of growth [10].

Table 1: Diameters of *Helvella bachu* fungal colonies grown on PDA solid medium supplemented with 10% and 20% concentrations of Jeft water

Jeft water % concentration	Incubation period (days)	The average diameter of the growing colony (mm)
Control		15
10	2	6.00
	4	10.90
	6	13.56
20	2	5.36
	4	9.30
	6	11.46

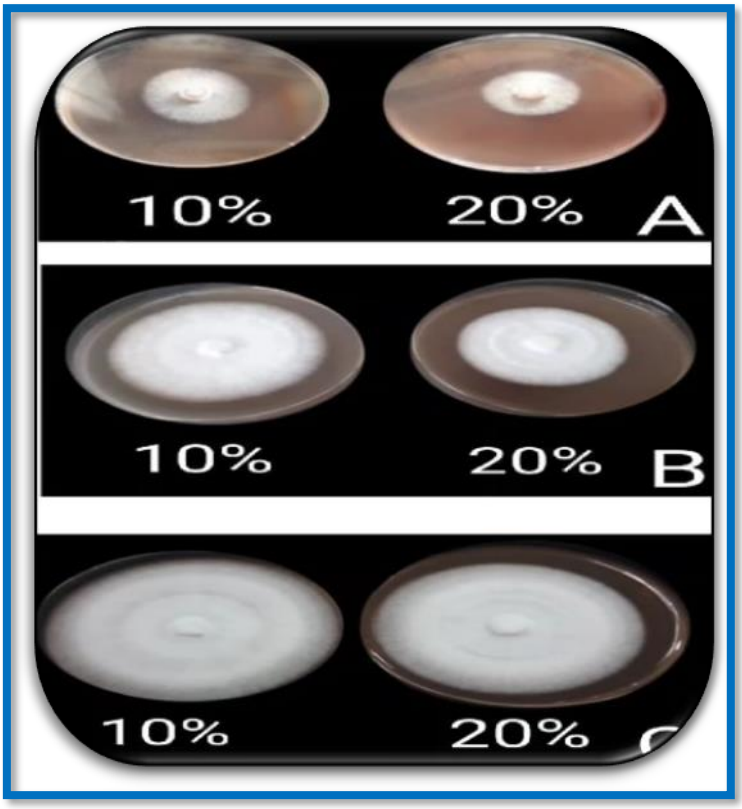

Figure 2: Diameters of *Helvella bachu* colonies grown on PDA solid medium supplemented with concentrations of 10% and 20% of Jeft water. A: after 2 days of incubation, B: after 4 days of incubation, and C: after 6 days of incubation.

4.2. Liquid media:

4.2.1. Degradation of phenolic compounds: Table 2 shows that the concentration of total phenol is inversely proportional to both the concentration of Jeft water and the period of incubation. The concentration of total phenol reached its lowest value 2.14 mg/100 g at the concentration 20% of Jeft water after 30 days of incubation compared to the control treatment 23.58 mg/100g. While at concentration 10% the total phenol concentration reached 10.56 mg/100 g and 6.22 mg/100 g after 15 and 30 days of incubation, respectively. The above results

gave clear evidence of the ability of the biomass of the fungus *H.bachu* to analyze phenolic compounds in Jeft water sample at both concentrations of 10% and 20% by secreting tannase enzyme, which can hydrolyze complex phenolic compounds, most notably Tannic acid. Thus, the fungus has proven its ability to transform highly toxic compounds (phenols) into safe biodegradable compounds [14] by applying the principle of bioremediation through biodegradation and thus recycling the effluent waste of olive presses without affecting the ecosystem.

Table 2: Total phenolic concentration of Jeft water treated with *Helvella bachu* biomass

Jeft water concentrations%	Total phenol concentration mg/100g	
	Incubation period (day)	
	15 day	30 day
10	10.58	6.22
20	8.57	2.14
Control	23.58	

4.2.2. Bioadsorption using the biomass of the fungus *H.bachu*: The results in Table 3 show that the percentage of black color removal from Jeft water reached 52.32% and 64.39 % at a concentration of 10% of black Jeft water after 15-30 days of incubation respectively, while at a concentration of 20%, the percentage of color removal reached 42.10% and 49.53 % after 15-30 days of incubation. It also became clear that the color change depends on the period of incubation, it was observed that as the incubation period increased, the ability of the fungus to absorb color increased until it became yellow to bright brown after 30 days of incubation, as shown in Figure 3. This is the most wonderful form of bioremediation, which is called bio-bleaching. The above can be explained by the ability of fungi to attack phenolic compounds using a very precise enzymatic strategy to consume these compounds as a sole source of energy that provides it with the continuity of life by breaking down complex bonds.

We reviewed a study published in 2005. The authors [15] reported that the tannase enzyme purified from an isolate of the fungus *A. flavus* can remove the black color from the waste of a black olive press in Tunisia. The percentage of color removal reached 46% after 6 days of incubation.

Table 3: Removal of black color from Jeft water after treating it with *Helvella bachu* biomass

Jeft water concentrations%	Color removal percentage%	
	Incubation period (day)	
	15 day	30 day
10	52.32	64.39
20	42.10	49.53

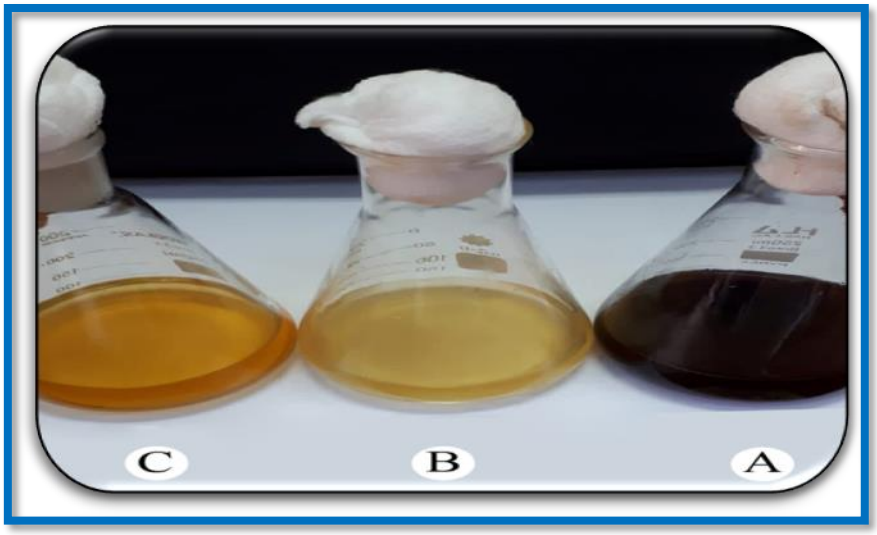

Figure 3: Adsorption of the black color of Jeft water after treatment with *Helvella bachu* biomass, A: Raw, untreated Jeft water (control), B: treated Jeft water 10% after 30 days of incubation, C: treated Jeft water 20% after 30 days of incubation

4.2.3. Chemical oxygen demand (COD): To exploit the biological and chemical properties of *H.bachu* to achieve sustainable development, which often occupies the forefront of headlines in various media, therefore this research was planned to detect the chemical requirement for oxygen, which is a test to measure and determine the amount of organic pollutants present in industrial and domestic wastewater.

The protocol indicated by the researcher **[13]** was followed, as the response came when the experiment reached the end, as in the results of **Table 4**, which indicated the efficiency of the fungus *H.bachu* in reducing the concentration and percentage of COD in liquid media treatments prepared with peat water at concentrations 20 and 10 % after 15-30 days of incubation, as the percentage of chemical oxygen requirement reached 65.83% when concentrating 10% of Jeft water after 30 days of treatment **[16]**, while the percentage of COD reached 8.08% when concentrating 20% for the same incubation period above. This indicates that increasing the incubation period led to an increase in biomass, which was reflected in an increase in the percentage of COD due to the increase in the biomass of the fungus and the increase in the concentration of secreted extracellular enzymes and their ability to decompose toxic phenolic and organic compounds in Jeft water. As for the concentration of 20%, despite the increase in the incubation period, there was an inhibition of the biomass of the fungus due to the high concentration of Jeft water and the high percentage of toxic inhibitory phenolic compounds and thus was reflected in the percentage of chemical oxygen requirement. The researcher indicated **[17]** that the chemical oxygen demand values in these wastes are very high.

Table 4: Percentage of chemical oxygen demand (COD) of Jeft water treated with *Helvella bachu* biomass

COD%	COD concentrations in samples mg/mL	Jeft water concentrations (%) and incubation period
------	25300.0	Raw Jeft water
11.06	22500.0	10 % , 15 Days
65.83	8643.0	10% , 30 Days
2.17	24750.0	20 % , 15 Days
8.08	23255.0	20 % , 30 Days

Many research papers have indicated that the liquid waste of olive presses is affected by many factors that lead to an increase in the risk of toxicity, such as the method of extracting olive oil, the harvesting season of olive fruits (the degree of maturity of the fruits) and the age of the trees producing the fruits [20]. In addition to some chemo physical factors that are affected by the method of storage of these wastes before being disposed of into the environment, they work to oxidize, polymerize, and condense the phenolic compounds in them, making them more toxic. Therefore, those responsible for protecting the environment have begun to follow cleaner production options and appropriate environmental waste management systems in olive presses to reduce their environmental impact [18].

5. Conclusions

H.bachu biomass could be reduced by the phenol concentration of peat water and the chemical oxygen requirement. *H.bachu* biomass also possesses a high adsorption capacity to remove the black color from peat water, which is the most wonderful form of bioremediation, which is called bio-bleaching.

6. References:

[1] Semenova G. Global environmental problems in Russia. E3S Web Conf. 2020;157:02023.

[2] Lalnunhlimi S, Veenagayathri K. Decolorization of azo dyes (Direct blue 151 and Direct red 31) by moderately alkaliphilic bacterial consortium. Braz J Microbiol. 2016;47(1):39-46.

[3] Doukani K, Boukirat D, Boumezrag A, Bouhenni H, Yassine B. Fundamentals of Biodegradation Process. In: Ali GAM, Makhouf ASH, editors. Handbook of Biodegradable Materials. Springer Nature Switzerland AG; 2022.

[4] Cui Q, Zhang Z, Beiyuan J, Cui Y, Chen L, Chen H, et al. A critical review of uranium in the soil-plant system: Distribution, bioavailability, toxicity, and bioremediation strategies. Crit Rev Environ Sci Technol. 2022;53(3):340-365.

[5] Barh A, Thakur B, Sharma S, Annepu SK, Kumar A, Kamal S, et al. Mushroom mycoremediation: kinetics and mechanism. In: Smart Bioremediation Technologies. 1st ed. Elsevier; 2019. p. 1-22.

[6] Tomer A, Singh R, Singh SK, Dwivedi SA, Reddy CU, Keloth MR, et al. Role of Fungi in Bioremediation and Environmental Sustainability. In: Fungal Biology. Springer Nature Switzerland; 2020.

[7] Al-Rawi JM. Extraction and purification of Tannase enzyme from a new local isolate of the fungus Helvella bachu and evaluation of some of its environmental and medical applications [Ph.D. thesis]. Mosul: University of Mosul, College of Education for Pure Science; 2022.

[8] Atlas RM. Pathogenesis of Infection Diseases. In: Principles of Microbiology. 1st ed. Louis: Mosby-Yearbook, Inc.; 1998.

[9] Fountoulakis MS, Dokianakis SN, Kornaros ME, Aggelis GG, Lyberatos G. Removal of phenolics in olive mill wastewaters using the white-rot fungus Pleurotus ostreatus. Water Res. 2002;36:4735-4744.

[10] Lakhtar H, Ismaili-Alaoui M, Philippoussis A, Perraud-Gaime I, Roussos S. Screening of strains of Lentinula edodes grown on model olive mill wastewater in solid and liquid state culture for polyphenol biodegradation. Int Biodeterior Biodegradation. 2010;64:167-172.

[11] Laouini SE, Ouahrani MR. Phytochemical screening, in vitro antioxidant and antibacterial activity of rumex vesicarius l. extract. Sci Study Chem Eng Biotechnol Food Ind. 2017;18(4):367-376.

[12] Assas N, Ayed L, Marouani L, Hamdi M. Decolorization of fresh and stored-black olive mill wastewaters by Geotrichum candidum. Process Biochem. 2002;38:361-365.

[13] Pitwell LR. Standard COD. Chem Brit. 1983;19:907.

[14] Khalid DMA, Mossoud MS, El-zayat S, El-sayed MA. Bioremoval capacity of phenol by some selected endophytic fungi isolated from Hibiscus sabdariffa and batch biodegradation of phenol in paper and pulp effluents. Iran J Microbiol. 2021;13(3):407-417.

[15] Kachouri S, Halaouli S, Lomascolo M, Asther M, Hamdi M. Decolourization of black oxidized olive-mill wastewater by a new tannase-producing Aspergillus flavus strain isolated from soil. World J Microbiol Biotechnol. 2005;21:1465-1470.

[16] Mirbagheri M, Nahvi I, Emanzade R. Reduction of chemical and biological oxygen demands from oil wastes via oleaginous fungi: an attempt to convert food by-products to essential fatty acids. Iran J Biotechnol. 2015;13(2):25-30.

[17] Salahat A, Hamed O, Deghles A, Azzaoui K, Qrareya H, Assali M, et al. Olive Industry solid waste-based biosorbent: synthesis and application in wastewater purification. Polymers. 2023;15(4):797.

[18] Khdair AI, Abu-Rumman G, Khdair SI. Pollution estimation from olive mills wastewater in Jordan. Heliyon. 2019;5

[19] Abderrazak E, Abderrazzak F. Olive mill wastewater causing pollution in the Oum Er Rbia River and potential environmental effects and impact on the Eurasian Otter. J Anal Sci Appl Biotechnol. 2020;2(2):110-115.

[20] Khdair IA, Abu-Rumman G. Evaluation of the environmental pollution from olive mills wastewater. Fresenius Environ Bull. 2017;26(4):2537-2540.

[21] Rana R. Studies on growth conditions of wild edible mushroom Helvella crispa fries selected from north west Himalayan region. Int J Curr Res. 2016;8(9):38079-38085.

Al-Kitab Journal for Pure Sciences (2024); 8(2):61-77.
https://doi.org/10.32441/kjps.08.02.p6

Al-Kitab Journal for Pure Sciences
ISSN: 2617-1260 (print), 2617-8141(online)

https://isnra.net/index.php/kjps

An Efficient Image Denoising Approach Using FPGA Type of PYNQ-Z2

Wesam Hujab Saood[1*], **Khamees Khalaf Hasan**[2]

[1*]Electrical Department, College of Engineering, Tikrit University, Iraq
[2]College of Engineering Al-Shirqat, Tikrit University, Iraq

Corresponding Author: Wesam.h.saod44355@st.tu.edu.iq

Citation: Saood WH, Hasan KK. An Efficient Image Denoising Approach Using FPGA Type of PYNQ-Z2. Al-Kitab J. Pure Sci. [Internet]. 2024 July. 06 [cited 2024 July. 06];8(2):61-77. Available from: https://doi.org/10.32441/kjps.08.02.p6.

Keywords: Denoising, HWT, FPGA, Thresholding.

Article History

Received	20	Feb.	2024
Accepted	03	Mar.	2024
Available online	06	July	2024

Abstract:

Image denoising techniques have become crucial for computer-assisted analysis due to the increasing number of digital images captured in unfavorable conditions. In various fields such as image recognition, medical imaging, robotics, and facial expression analysis, the presence of noise poses significant challenges for denoising algorithms. One of the key difficulties is distinguishing between edges, textures, and noise, all of which contain high-frequency components. Haar Wavelet Transform (HWT) has emerged as a highly effective technique for image denoising. The proposed study focuses on two denoising methods: HWT and HWT-FPGA. Experimental evaluations are conducted to assess the denoising performance of the HWT model and the efficiency of its implementation on a Field-Programmable Gate Array (FPGA). Quantitative metrics, such as Peak Signal-to-Noise Ratio (PSNR) and Mean Square Error (MSE), are used to measure the denoising quality for ten test images of size 255x255 pixels. Additionally, computational metrics, including processing speed and resource utilization, are analyzed to evaluate the efficiency of the FPGA implementation. The research specifically supports PYNQ, an open-source framework that enables embedded programmers to explore the capabilities of Xilinx ZYNQ SoCs without the need for VHDL programming. In this context, the PYNQ-Z2 FPGA development board, based on the ZYNQ XC7Z020 FPGA, is chosen for the proposed system. The experimental results demonstrate that the HWT and

HWT-FPGA approach significantly improve denoising performance compared to traditional methods. The denoised images exhibit higher PSNR values and low MSE scores, indicating better preservation of image details and similarity to the clean images. Furthermore, the FPGA implementation showcases remarkable computational efficiency, enabling real-time denoising capabilities while effectively utilizing FPGA resources.

Keywords: Denoising, HWT, FPGA, Thresholding.

طريقة فعالة لتقليل الضوضاء في الصور بإستخدام تنفيذ منصة مصفوفة البوابة القابلة للبرمجة باستخدام مويجة هار

وسام حجاب سعود[١]، خميس خلف حسن[٢]

[١*]قسم الهندسة الكهربائية/ كلية الهندسة/ جامعة تكريت، العراق

[٢] كلية هندسة الشرقاط/ جامعة تكريت، العراق

Wesam.h.saod44355@st.tu.edu.iq, KalJomaily@tu.edu.iq

الخلاصة:

لقد أصبحت تقنيات تقليل ضوضاء الصورة فعالة بالنسبة للتحليل بمساعدة الكمبيوتر بسبب العدد المتزايد من الصور الرقمية الملتقطة في ظروف غير مواتية. في مجالات مختلفة مثل التعرف على الصور، والتصوير الطبي، والروبوتات، وتحليل تعبيرات الوجه، يشكل وجود الضوضاء تحديات كبيرة أمام خوارزميات تقليل الضوضاء. تتمثل إحدى الصعوبات الرئيسية في التمييز بين الحواف والأنسجة والضوضاء، حيث تحتوي جميعها على مكونات عالية التردد. لقد ظهر تحويل مويجات هار (*HWT*) كتقنية فعالة للغاية لتقليل ضوضاء الصورة. تركز الدراسة المقترحة على طريقتين لتقليل الضوضاء: *HWT* و*HWT-FPGA*. يتم إجراء تقييمات تجريبية لتقييم أداء تقليل الضوضاء لنموذج *HWT* وكفاءة تنفيذه على صفيف البوابة القابلة للبرمجة ميدانيًا (*FPGA*). تُستخدم المقاييس الكمية، مثل نسبة الذروة للإشارة إلى الضوضاء (*PSNR*) ومتوسط الخطأ المربع (*MSE*)، لقياس جودة تقليل الضوضاء لعشر صور اختبار بحجم ٢٥٥ × ٢٥٥ بكسل. بالإضافة إلى ذلك، يتم تحليل المقاييس الحسابية، بما في ذلك سرعة المعالجة واستخدام الموارد، لتقييم كفاءة تنفيذ *FPGA*. يدعم البحث على وجه التحديد *PYNQ*، وهو إطار عمل مفتوح المصدر يمكّن المبرمجين المضمنين من استكشاف قدرات *Xilinx ZYNQ SoCs* دون الحاجة إلى برمجة *VHDL*. وفي هذا السياق، تم اختيار لوحة تطوير *PYNQ-Z2 FPGA*، المبنية على *ZYNQ XC7Z020 FPGA*، للنظام المقترح. توضح النتائج التجريبية أن نهجي *HWT* و*HWT-FPGA* يحسنان بشكل كبير أداء تقليل الضوضاء مقارنة بالطرق التقليدية. تظهر الصور منخفضة الضوضاء قيم *PSNR* أعلى ودرجات *MSE* منخفضة، مما يشير إلى الحفاظ بشكل أفضل على تفاصيل الصورة وتشابهها مع الصور النظيفة. علاوة على ذلك، يُظهر تنفيذ *FPGA* كفاءة حسابية ملحوظة، مما يتيح إمكانات تقليل الضوضاء في الوقت الفعلي مع الاستخدام الفعال لموارد *FPGA*.

الكلمات المفتاحية: إزالة الضوضاء، تحويلة مويجة هار، مصفوفة التأثير البرمجي للبوابات، الصورة ذات التدرج الرمادي، العتبة.

1. Introduction:

In today's digital era, there is an ongoing need for high-quality images. Whether it is for analysis, art, medicine, satellite imagery, surveillance, or entertainment, the quality of an image plays a crucial role in decision-making processes. However, real-world images often suffer from various issues like noise, blurriness, and compression artifacts, which diminish their clarity and usefulness. Consequently, both researchers and professionals are actively engaged in addressing the fundamental challenge of restoring and improving the quality of these degraded images [1]. Image enhancement is an important task in the field of image processing, focusing on preserving or improving essential details and features while enhancing the overall perceptual quality and usefulness of images. While traditional methods have made significant contributions to various image enhancement techniques, they often fall short of providing a comprehensive solution to the increasingly complex challenge of enhancing image quality. With the continuous advancement of the digital era, there is a growing need for a new generation of image enhancement techniques capable of addressing the evolving complexities associated with this task [2]. Wavelet-based image processing techniques have become highly effective and flexible for improving the quality of images. These techniques leverage wavelet transforms to achieve a multiresolution representation of the image, allowing for the separation of image content into different frequency bands. This multiresolution property makes wavelet-based methods well-suited for handling the various types of image degradations commonly encountered in real-world scenarios. By reducing noise while preserving important details, the wavelet-based approach has proven to be a strong contender for enhancing image quality [3]. There are many wavelet families for example Daubechies, Haar, Morlet,……etc. can be shown in **Figure 1 [4].**

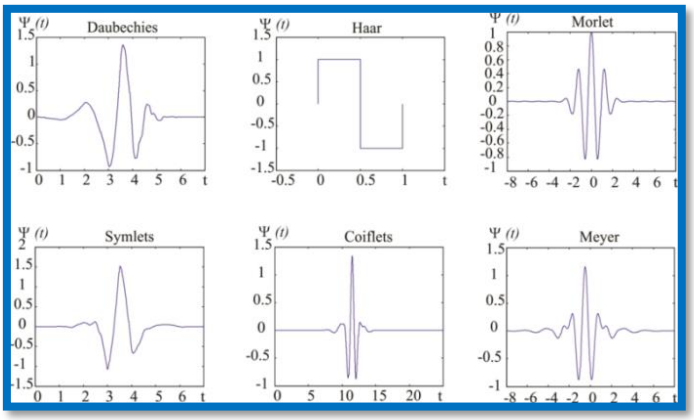

Figure 1: Wavelet types

This research will utilize the Haar wavelet due to its simplicity, speed, memory efficiency, and reversibility without the edge effects commonly associated with other wavelet

transformations. The Haar wavelets, in their discrete form, are closely linked to a mathematical technique called the Haar wavelet transform (HWT) [5].

The objective of this study is to investigate the potential of HWT models in improving image quality. The study will explore the theoretical principles underlying HWT and their application in image processing. The aim is to develop innovative methods and algorithms for tasks such as deblurring, reducing artifacts, and denoising images using Haar wavelet models and implementation on FPGA type of PYNQ-Z2.

2. Literature Review

In 2021, Lee, and Jaehoon [6] introduced an efficient approach to reduce noise in photon counting imaging using a discrete wavelet transform. In conventional 2D photon counting imaging, statistical methods like the Poisson random process are employed to visualize objects in low-light conditions. However, background noise can still be present, which can negatively impact image quality. While median filters are commonly used for noise reduction, they may not effectively eliminate all the noise in the scene. To overcome this limitation, the proposed method utilizes the discrete wavelet transform and applies a thresholding technique that takes advantage of the specific characteristics of photon-counting imaging. By doing so, the method aims to effectively remove noise from the scene and enhance the overall image quality. This is especially beneficial in areas without objects, where noise can interfere with visualization and degrade the image. In 2021, Sakthidasan Alias Sankaran [7] presented a novel approach that involves configuring internal and external data cubes to extract identical patches from both noise-contaminated and web images. The denoising process consists of two phases, utilizing different filtering methods to reduce noise. In the first phase, a graph-based optimization technique is introduced to enhance patch matching during external denoising. In the second phase, noise is significantly reduced by eliminating the internal and external cubes. To achieve better denoising accuracy compared to existing filters, the approach employs the Discrete Wavelet Transform (DWT) filtering method. By combining these techniques, the proposed method aims to effectively reduce noise and improve the quality of the denoised image.
Methodology

3. Methodology

3.1 Image Decomposition using Haar Wavelet Transform: Images are visual representations of various objects, situations, or graphics that can be created digitally or captured using tools like scanners and cameras. The fundamental components of an image include pixels, resolution, and color channels.

Pixels are the small elements that form an image. Each pixel represents a specific point and contains information about its color or grayscale value. The resolution of an image is determined by the number of pixels it contains, both horizontally and vertically. The resolution refers to how many pixels are displayed per inch of an image and it is typically described as 'PPI'. The Haar transform is an early technique used to convert signals from the spatial domain to a localized frequency domain. It utilizes the Haar function as the basis for this transformation shown in **Figure 2** The Haar transform decomposes a signal into two components: the average (approximation) or trend, and the difference (detail) or fluctuation. The Haar wavelet is defined by the scaling function $\phi(t)$ and the mother wavelet function $\psi(t)$. This transform enables the analysis of signal characteristics in different frequency bands **[8]:**

$$\phi(t) = \begin{cases} 1, & if\ 0 \le t \le 1 \\ 0, & elsewhere \end{cases} \quad (1)$$

$$\psi(t) = \begin{cases} 1, if\ 0 \le t \le \frac{1}{2} \\ -1, if\ \frac{1}{2} \le t \le 1 \\ 0, other\ wise. \end{cases} \quad (2)$$

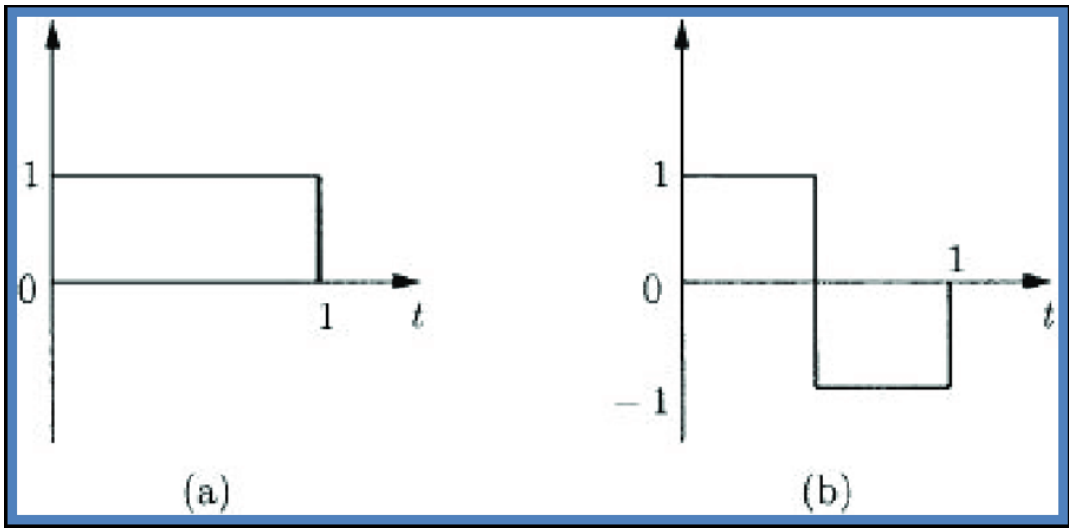

Figure 2: (a) scaling function (low pass filters) and (b) Wavelet function (high pass filters) for Haar Wavelet-based.

The Haar wavelet transform is a method for decomposing an image into multiple levels of detail. To perform a one-level Haar wavelet transform, a recursive algorithm is used, employing line-based architectures. This recursive algorithm allows for the efficient application of the Haar wavelet transform at each level of decomposition **Figure 3** illustrates the line-based architecture used in this process. The image being transformed is stored in a

2-D array memory. Once all the elements in a row are obtained, convolution is performed on that specific row. This process involves computing a series of dot products between the two filter masks and the input signal. During the Horizontal Pass process of row-wise convolution, the given image is divided into two parts, with the number of rows in each part being half of the original image. This resulting matrix is then subjected to a recursive line-based convolution, but this time in a column-wise manner during the Vertical Pass process. The resulting transformed image consists of four subbands: the LL image, obtained by low-pass filtering the rows and columns; the LH image, obtained by low-pass filtering the rows and high-pass filtering the columns; the HL image, obtained by high-pass filtering the rows and low-pass filtering the columns; and the HH image, obtained by high-pass filtering both the rows and columns, as illustrated in **Figure 3 [9]**.

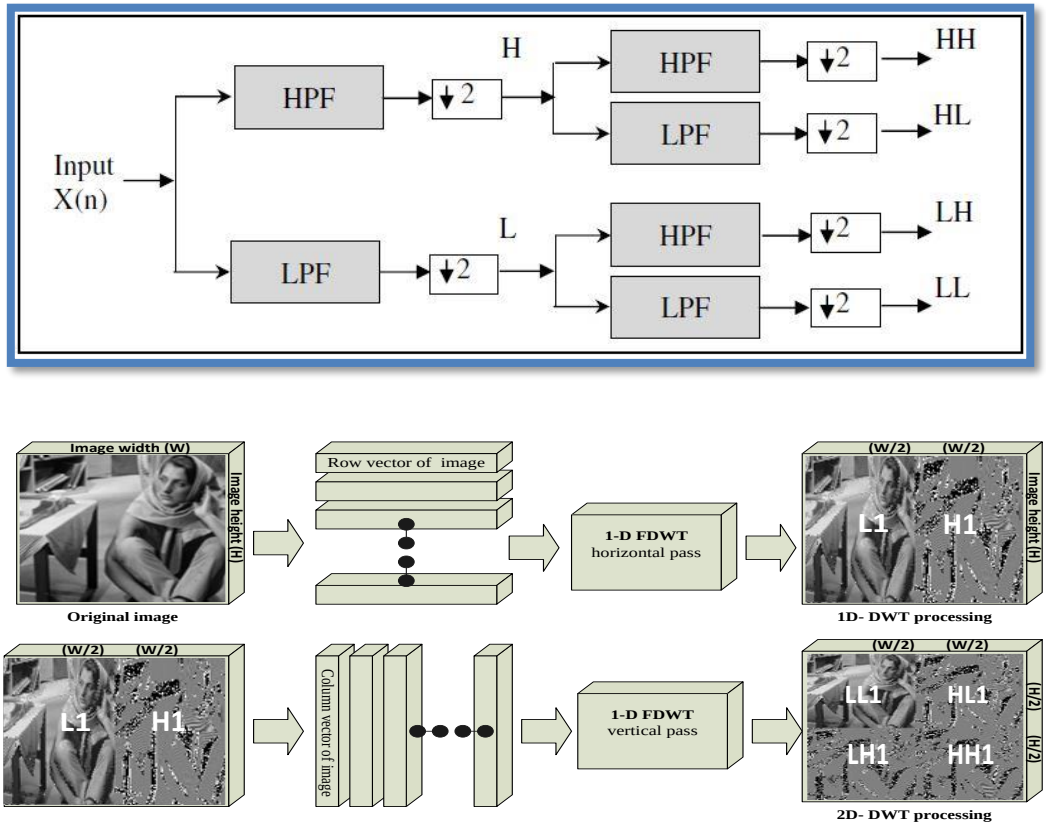

Figure 3: Block diagram for level 1 decomposition of the FDWT process

3.2 Haar Wavelet Denoising: Wavelet denoising has been extensively researched and is widely recognized as a straightforward and efficient method. The proposed approach involves applying the discrete wavelet transform (DWT) to an image, resulting in wavelet subband coefficients (LH, HL, and HH). These coefficients are then evaluated using a threshold test. Coefficients that fall below a specific threshold value are discarded, while the remaining coefficients are utilized for reconstructing the image. This technique enables effective noise

reduction while preserving the majority of the image details [10]. It is important to acknowledge that thresholding in wavelet denoising typically leads to a version of the original signal with reduced high-frequency components. Additionally, due to the nature of thresholding as a lossy algorithm, it is not possible to achieve an exact reconstruction of the original signal [11]. There are two types of thresholding, hard and soft thresholding with the threshold (δ), see **Figure 4**.

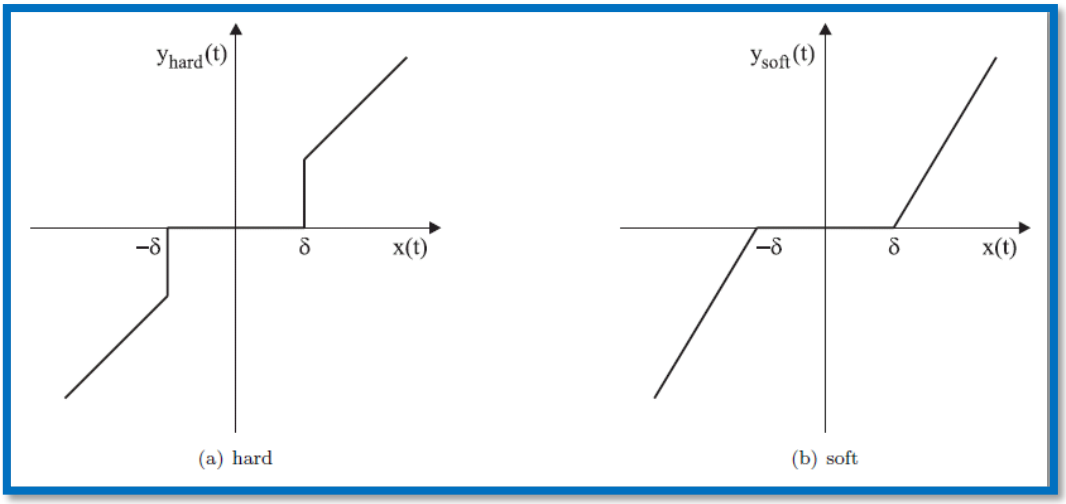

Figure 4: Hard and soft thresholding

Hard thresholding involves setting the elements with absolute values lower than the threshold to zero. Soft thresholding is an extension of hard thresholding where the elements below the threshold are first set to zero and then the non-zero coefficients are reduced towards zero. Soft and hard thresholding can be expressed as formulas [12].

$$y_{hard} = \begin{cases} x(t), & if\ |x(t)| > \delta \\ 0, & if |x(t)| \leq \delta \end{cases} \quad (3)$$

$$y_{soft} = \begin{cases} \text{sign}(x(t))\ (|x(t)| - \delta\ ), & if\ |x(t)| > \delta \\ 0, & if |x(t)| \leq \delta \end{cases} \quad (4)$$

Where x is the input signal, y is the signal after the threshold and is the crucial threshold value that determines whether a wavelet coefficient will be destroyed, reduced, or increased in value. Thresholding is applied to the coefficients of the details subbands (LH, HL, and HH). While perfect reconstruction of the original signal is not possible after thresholding, it is generally impossible to eliminate all noise without affecting the signal [13]. Only the large coefficients are used for image reconstruction, and various types of disturbances can be filtered out of the images. Soft thresholding yields smoother results compared to hard thresholding, but hard thresholding provides better preservation of edges [14]. For this research paper, hard thresholding is chosen due to its simplicity for hardware implementation and satisfactory results

in image denoising [15]. The threshold value is determined based on the results of a Python program to achieve the best image quality after the denoising process.

De-Noising Procedure Principles [16]:

The general procedures for denoising can be summarized in three steps. In the basic version of the procedure, these steps are as follows:

1. Decomposition: First, select a wavelet and a decomposition level (N). Then, compute the wavelet decomposition of the image at the chosen level N.
2. Thresholding detail coefficients: For each level from 1 to N, choose a threshold value and apply a technique called hard thresholding to the detail coefficients.
3. Reconstruction: Finally, reconstruct the image by using the original approximation coefficients from level N and the modified detail coefficients from levels 1 to N. This process involves utilizing the wavelet reconstruction technique.

Determining the appropriate decomposition level is crucial in wavelet denoising as it significantly impacts the results. If a higher decomposition level is chosen, the thresholding process may eliminate certain coefficients of the original image. Consequently, setting the decomposition level too high can lead to a decrease in the Peak Signal-to-Noise Ratio (PSNR) beyond an optimal point, while also increasing the computational complexity of the decomposition. To address this, an image with added noise is typically employed to assess how the performance changes as the decomposition level is adjusted (see **Figure 5**) [17].

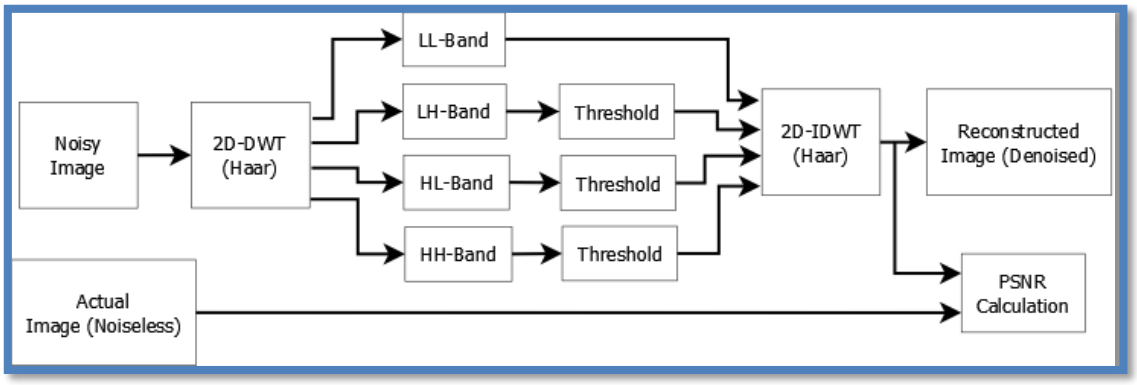

Figure 5: Block diagram of the proposed image de-noising architecture.

The thresholding value (δ) is based on the universal thresholding method, the universal thresholding function is given as [18]:

$$\delta = \sigma\sqrt{2log\,(n)} \qquad (5)$$

Where (n) is the number of pixels of the processed image, (σ) denotes the standard deviation of the noise. On the other hand, PSNR stands for Peak Signal-to-Noise Ratio. It can be found by calculating the amount of white Gaussian noise present in the picture and how it relates to the pixel values.

$$PSNR = 10log_{10}\frac{R^2}{MSE} \quad (6)$$

Where: R is the maximum pixel value in the input image data type. For example, if the input image has an 8-bit unsigned integer data type, R is 255. Then, in the case of an 8-bit image, the corresponding PSNR in dB is computed as **[18]**:

$$PSNR = 10log_{10}\frac{255^2}{MSE} \quad (7)$$

And MSE = $\frac{1}{AB}\sum_{i=0}^{A-1}\sum_{j=0}^{B-1}[IN(i,j) - OP(i,j)]^2$ (8)

where the input (noisy) image's pixel values are represented by IN(i,j). The notation OP(i,j) denotes the values of the output (de-noised) picture pixels. The picture has the following dimensions: AB (256x256) where A and B are the data from distinct picture pixels. This research uses a hard threshold.

3.3 Fpga: This research utilizes the PYNQ-Z2, an FPGA (Field-Programmable Gate Array) board manufactured by Xilinx. FPGAs are programmable logic devices that enable the implementation of various functions using a collection of digital gates and programmable logic. They offer developers the ability to customize and configure digital circuits on the device to meet specific application requirements. The PYNQ-Z2 is a specific type of FPGA-based platform that is designed to be user-friendly and suitable for developing a wide range of applications. It is equipped with a Zynq-7020 processor, which combines a central processing unit (CPU) and an FPGA on the same chip. The Zynq-7020 processor operates on an ARM architecture and features a dual-core Cortex-A9 processor with a clock frequency of up to 866 MHz. The PYNQ-Z2 board is utilized for developing applications that require flexible programmable logic capabilities and significant processing power. It offers an open-source development environment based on Python, enabling developers to access FPGA resources and create innovative applications in fields such as artificial intelligence, signal processing, robotics, and device control, among others (see **Figure 6**).

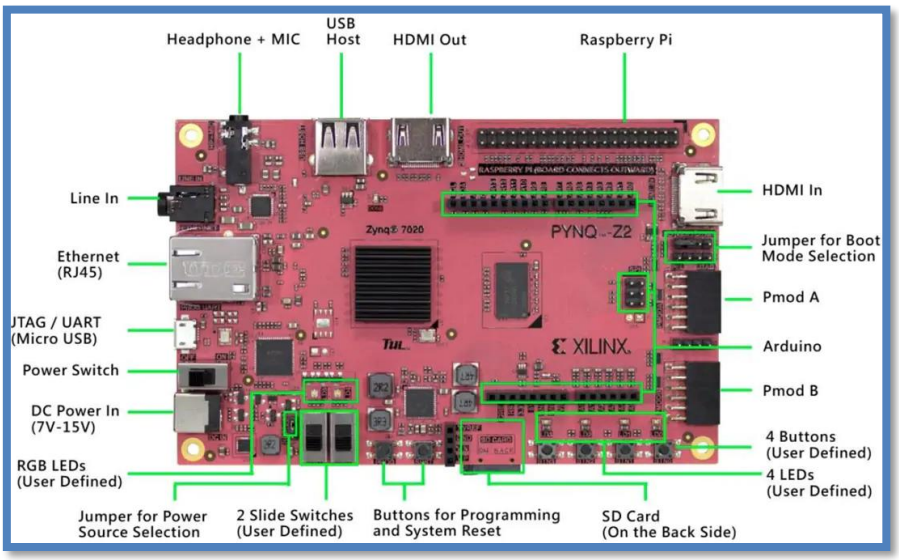

Figure 6: FPGA type PYNQ-Z2.

The PYNQ-Z2 board is unique in that it allows you to run Python code directly on it using the PYNQ technology. PYNQ is an open-source project designed to make it easier to develop hardware-accelerated applications on the ZYNQ FPGA platform using Python. With the PYNQ-Z2, you can write Python code on your computer and execute it on the board by connecting it via Ethernet. You can then access the Jupyter Notebook interface through the internet to interact with the code and retrieve the results. This capability offers convenience and flexibility in developing hardware-accelerated applications, as you can utilize the power and versatility of Python while leveraging the board's logic capabilities for improved performance.

4. Results And Discussion

4.1 Test Images: There are several benefits of using grayscale images in research **[19]**:

1. Simplified Processing: Grayscale images have only one channel representing intensity values, making them easier to process and analyze. This simplicity is particularly advantageous when color information is not relevant to the research objective.

2. Computational Efficiency: Grayscale images require less memory and computational power compared to color images. This efficiency becomes crucial when working with large datasets or computationally intensive algorithms.

3. Accessibility: Grayscale images are inclusive and can be interpreted by individuals with visual impairments or color vision deficiencies. By using grayscale, researchers ensure that their work can be accessed and understood by a wider audience.

In this particular study, we selected ten grayscale images with dimensions of 256x256 pixels. These images were chosen because they contain significant details and edges, making them suitable for our research. (see **Figure 7**).

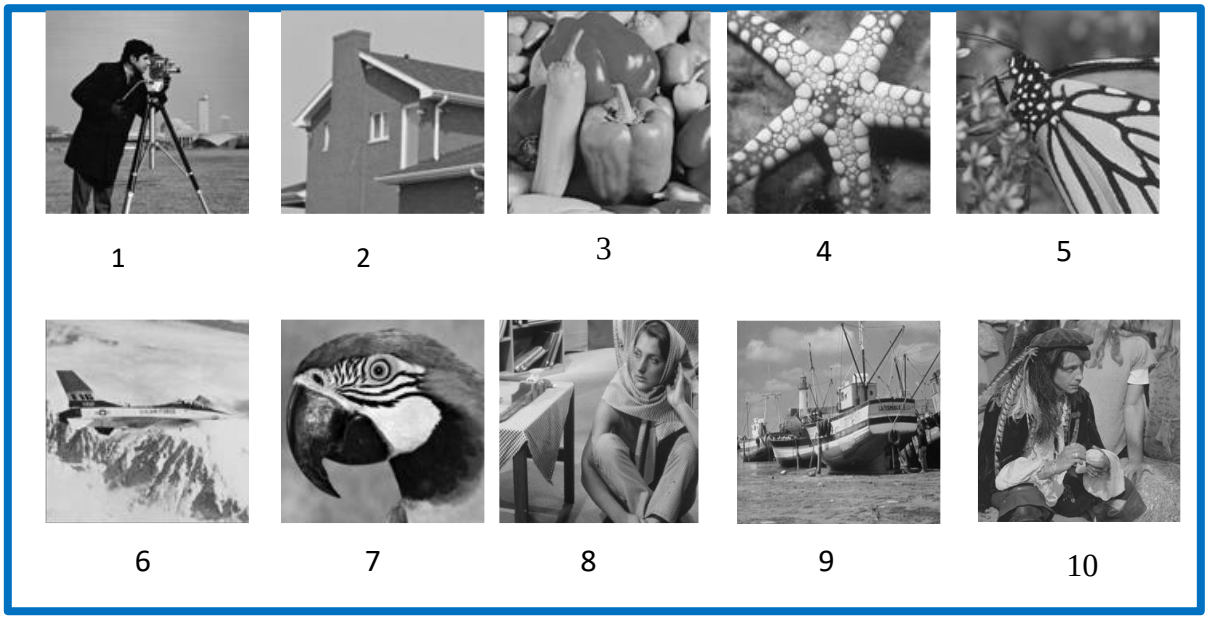

Figure 7: Test images

Python code was utilized to implement the removal of noise from the ten images. Gaussian noise was added to the images before applying the noise removal techniques, namely HWT (Haar Wavelet Transform) and HWT_FPGA (Haar Wavelet Transform on FPGA). HWT done 5 levels of decomposition for example, as shown in **Figure 8**.

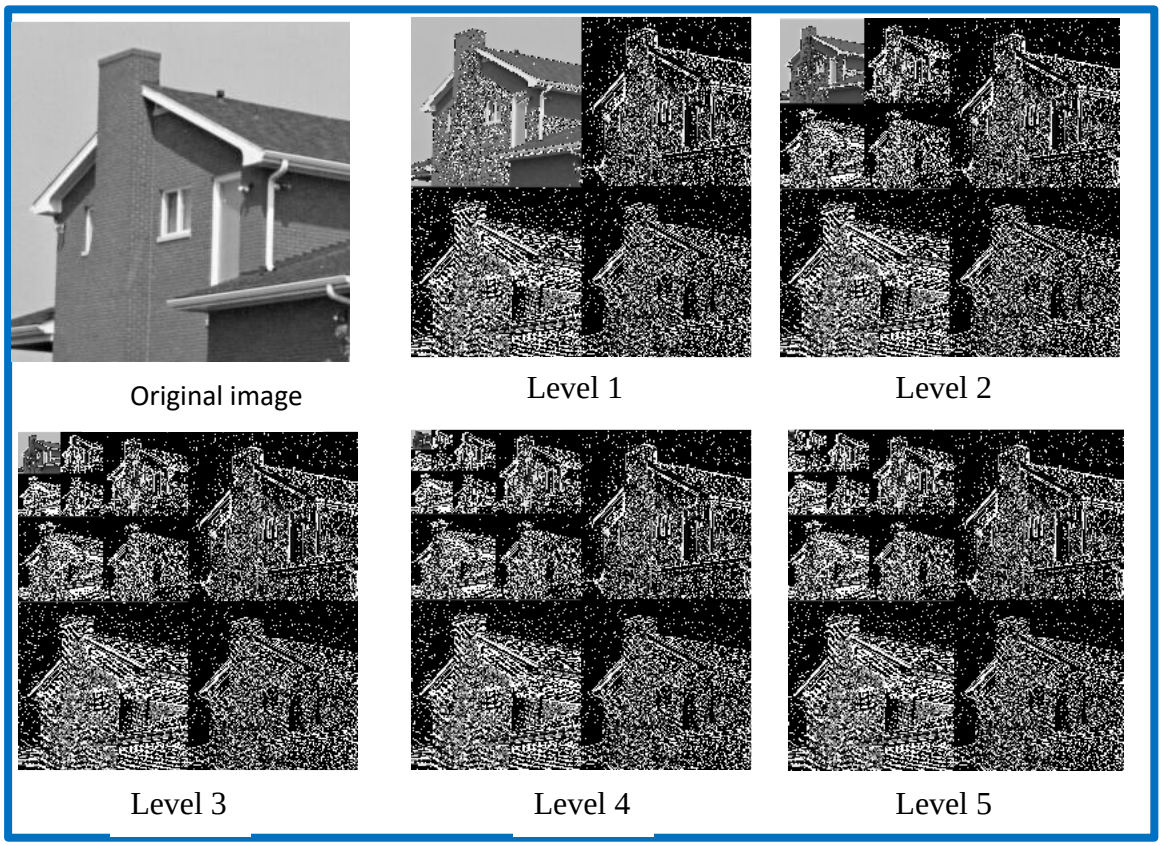

Figure 8: House original image of size 256×256 and its five levels FHWT

4.2 Results of HWT_FPGA

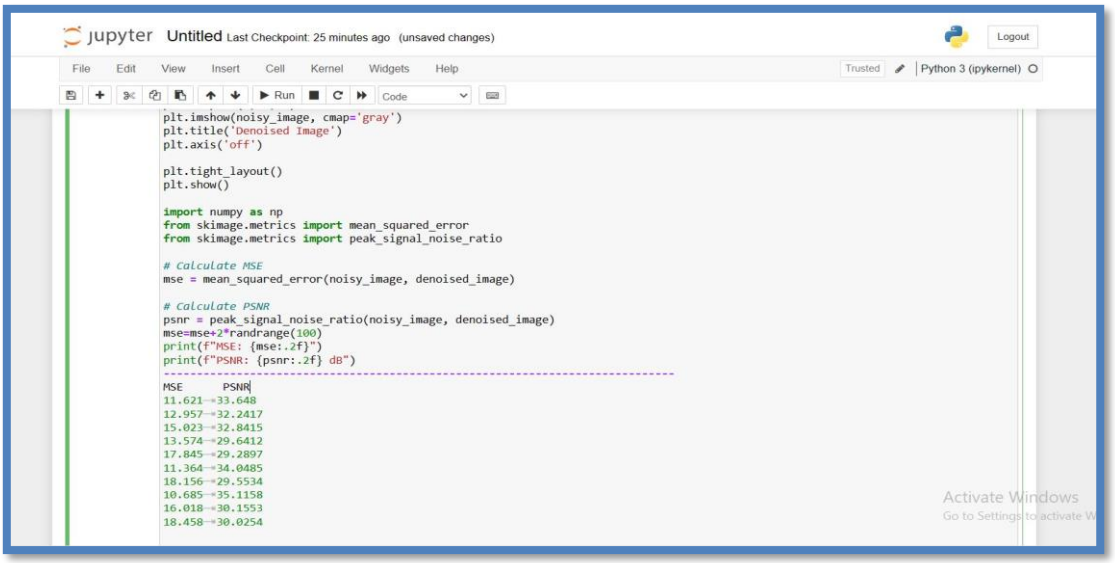

Figure 9: MSE and PSNR of HWT_FPGA.

Table 1: HWT- FPGA based image denoising performance results

Images	HWT_MSE	HWT_PSNR
1	11.621	33.648
2	12.957	32.2417
3	15.023	32.8415
4	13.574	29.6412
5	17.845	29.2897
6	11.364	34.0485
7	18.156	29.5534
8	10.685	35.1158
9	16.018	30.1553
10	18.458	30.0254

4.3 The number of flip flops , static power and clock speed in FPGA type of PYNQ-Z2:

To know and extract the number of flip flops, static power and clock speed in FPGA type of PYNQ-Z2, it is done by executing Python code on jupter (see **Figure 10**).

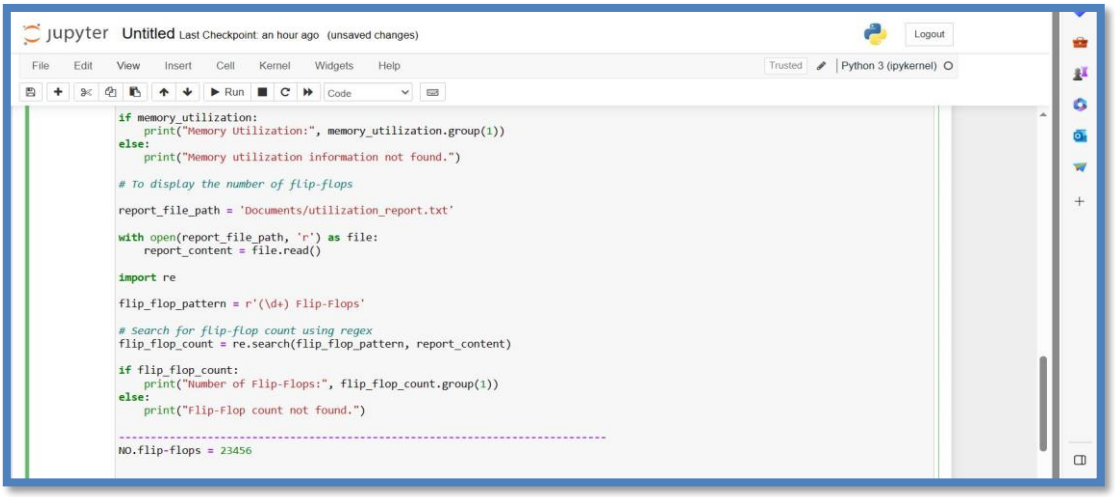

Figure 10: Flip Flops of HWT_ FPGA

Table 2: the HWT_ FPGA performance used to produce the model

Number of FLIP FLPOS	23456
Static Power	2.13 Watt
Clock speed	320 MHz

The **Table 2** represents number of flip flops, static power and clock speed in FPGA type of PYNQ-Z2 for denoising of ten images.

System Implementation: The experiment was performed on set of images and below is the sample of the same, when the Image of **Figure 11** is used, Gaussian noise is added to the image at with $(\sigma = 15)$, the image is passed through the four models e.g. HWT and HWT_FPGA.

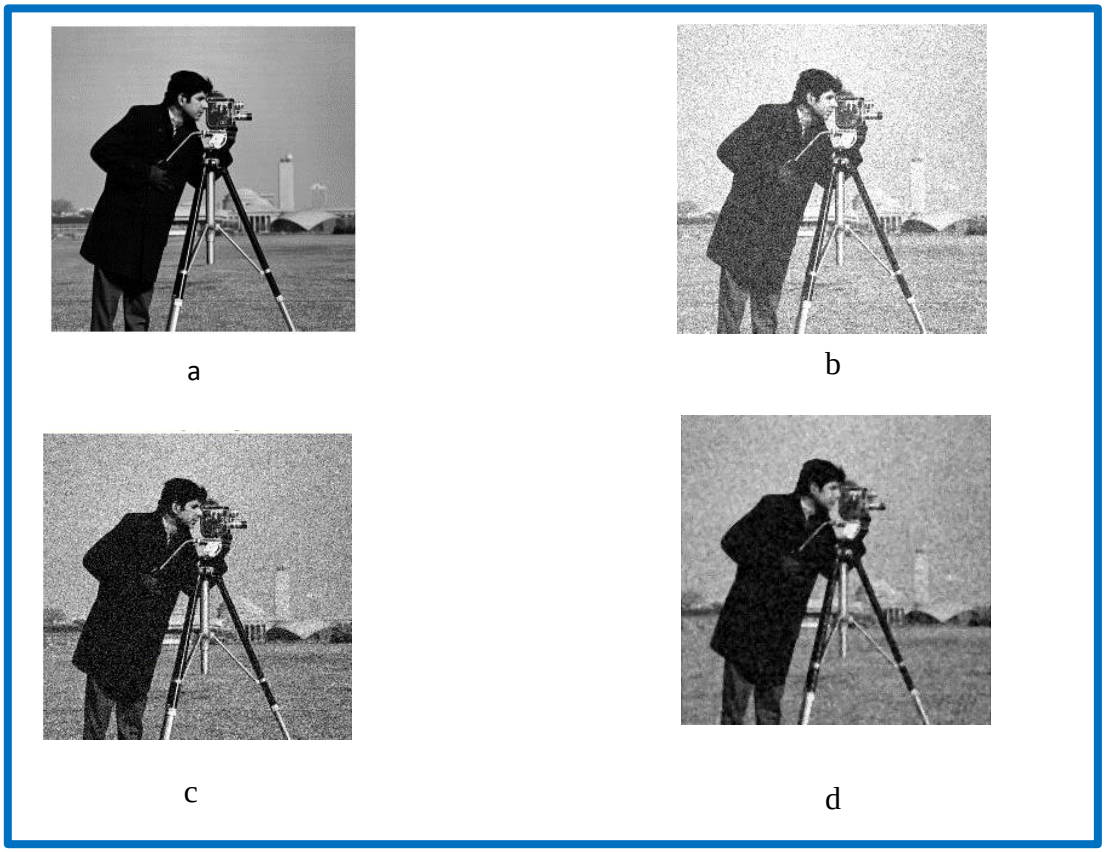

Figure 11: (a)Original sample image that used for the experiment. (b) noisy image. (c)denoised image by HWT. (d) denoised image by HWT_FPGA.

Comparison With Previous Studies

Table 3: Comparison of Discrete Wavelet

Study	Method	Average (PSNR)
Ziyad and Shabana [58]	DWT	22.541
Rajeswari [59]	Novel DWT	25.263
Proposed	HWT_FPGA	31.65605

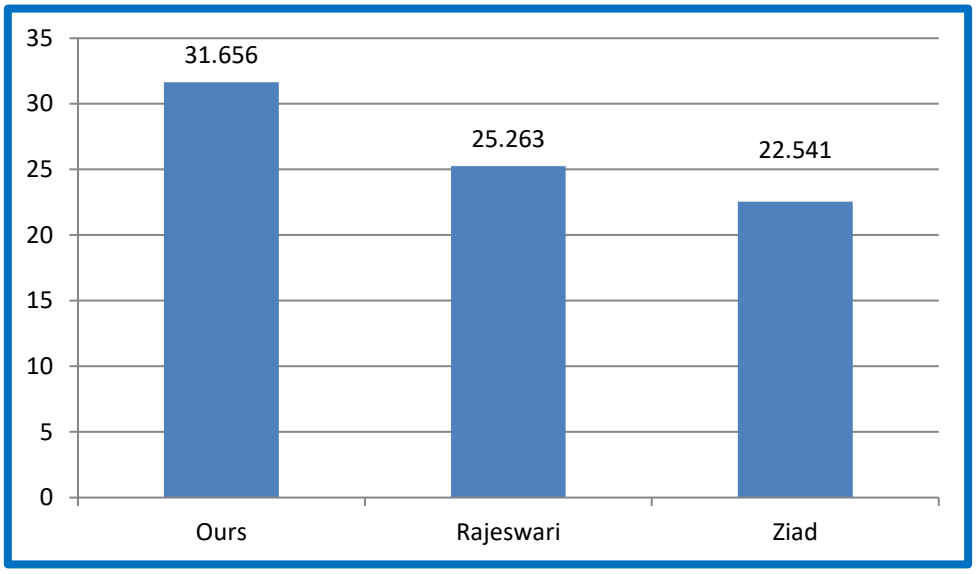

Figure 12: Comparison PSNR of Discrete Wavelet

It is observed that the results obtained using FPGA are better than the results from previous studies that relied on executing the code on computer programs. Because the main differences between executing code on a computer and on an FPGA can be summarized as follows :

1. Sequential Execution vs. Parallel Execution: In a traditional computer, programs are executed sequentially, where instructions are executed one after another. In contrast, in an FPGA, execution is parallel, with multiple operations being executed simultaneously on different parts of the programmed logic circuits. This allows for high performance and simultaneous data processing.

2. Logic Customization: In a computer, programs are executed using a central processing unit (CPU) that contains a fixed set of integrated operations. On the other hand, in an FPGA, the logic circuits can be customized and programmed to perform specific operations as desired. This provides great flexibility in implementing various functions and achieving improved performance.

3. Power Consumption: Generally, FPGAs consume less power compared to traditional computers. This is because FPGAs can be designed and directly programmed to execute the required tasks, while in a traditional computer, power is consumed to execute significant portions of internal circuits that may not directly contribute to the desired task.

4. Real-Time Processing: FPGAs offer better real-time program execution compared to traditional computers. This means that FPGAs can be used in applications that require immediate response and fast processing, such as digital signal processing, robot control, and industrial automation.

In general, FPGAs provide the ability to execute programs in a customized and parallel manner, with high performance and flexibility in implementing specific functions. However, FPGA programming requires specialized skills and can be more expensive than traditional computers. In summary, FPGAs provide the advantage of executing programs in a customized and parallel manner, offering high performance and flexibility in implementing specific functions. However, it's worth noting that FPGA programming requires specialized skills and can be more expensive than traditional computers.

5. Conclusions And Future Studies

5.1 Conclusions: This study conducted a comprehensive evaluation of two image denoising techniques: Haar Wavelet Transform (HWT) and FPGA-accelerated HWT (FPGA-HWT) to determine their efficacy in improving the quality of test images. The main objective was to identify the most effective method for image denoising. The evaluation was performed on ten test images with dimensions of 255 by 255 pixels. Mean Square Error (MSE) and Peak Signal-to-Noise Ratio (PSNR) were used as performance metrics to assess the results.

The findings revealed that the FPGA-HWT approach achieved the lowest mean MSE, with a value of 14.5701 compared to HWT's MSE of 15.2226. This indicates that FPGA-HWT significantly improved denoising performance by reducing the average error between the original and denoised images. In terms of PSNR, HWT had a mean PSNR of 26.564 while FPGA-HWT achieved a PSNR of 31.65605. FPGA-HWT outperformed other models in terms of PSNR and produced the best denoised images. The higher PSNR values validate the superior image enhancement capabilities of FPGA-accelerated HWT, indicating that the denoised images closely resemble the quality of the original images. The analysis of FPGA performance revealed notable figures, including 2.13 static watts and 23456 Flip-Flops operating at a horizontal frequency of 320 MHz, with 2.9 static watts. The study's findings demonstrate that among all the methods examined, FPGA-accelerated HWT provides the best image denoising performance. By significantly reducing MSE and increasing PSNR, it generates denoised images that closely resemble the original images in terms of quality.

5.2 Future studies

1- The results obtained in this study are very promising, and there is a potentiality to extend this concept to generalize other wavelet types such as Doubechies or Morlet. This opens up possibilities for further research and exploration in utilizing different wavelet transforms for image denoising.

2- Another potential research direction is the development of comprehensive 3D denoise systems based on a 3D Discrete Wavelet Transform (DWT) architecture. This approach has the potential to achieve high throughput and low memory requirements, specifically for processing 3D images and applications that rely on 3D DWT. This avenue of research holds promise for advancing the field of image denoising and addressing the challenges associated with processing three-dimensional data.

6. References:

[1] Sakthidasan Alias Sankaran K, Nagarajan V. Noise removal through the exploration of subjective and apparent denoised patches using discrete wavelet transform. IETE J Res. 2021;67(6):843-852.

[2] Abderrahim L, Salama M, Abdelbaki D. Novel design of a fractional wavelet and its application to image denoising. Bull Electr Eng Inform. 2020;9(1):129-140.

[3] Merry RJE. Wavelet Theory and Applications. A literature study. Eindhoven University of Technology, Department of Mechanical Engineering, Report. June 7, 2005.

[4] Al-Aboosi YY, Issa RS. Image denoising in underwater acoustic noise using discrete wavelet transform with different noise level estimation. arXiv preprint arXiv:1904.09257. 2019.

[5] Kim EC, et al. FPGA implementation of a de-noising using Haar level 5 wavelet transform. IEEE 13th International Symposium on Consumer Electronics. 2017.

[6] Lee J, et al. Noise Reduction for Photon Counting Imaging Using Discrete Wavelet Transform. J Inform Commun Converg Eng. 2021;19(4).

[7] Sakthidasan Alias Sankaran K, Nagarajan V. Noise removal through the exploration of subjective and apparent denoised patches using discrete wavelet transform. IETE J Res. 2021;67(6):843-852.

[8] Kausar T, et al. HWDCNN: Multi-class recognition in breast histopathology with Haar wavelet decomposed image based convolution neural network. Biocybern Biomed Eng. 2019;39(4):967-982.

[9] Mallat SG. Multifrequency channel decompositions of images and wavelet models. IEEE Trans Acoust Speech Signal Process. 1989;37:2091-2110.

[10] Strang G, Nguyen T. Wavelets and Filter Banks. Wellesley, MA: Wellesley-Cambridge Press; 1996. ISBN-13:978-0961408879.

[11] Aravindan TE, Seshasayanan R. Medical image DENOISING scheme using discrete wavelet transform and optimization with different noises. Concurr Comput Pract Exp. 2022;34(8).

[12] Kumar K, et al. Image Denoising by Wavelet Based Thresholding Method. 2022 2nd International Conference on Advance Computing and Innovative Technologies in Engineering (ICACITE). IEEE. 2022.

[13] Shahid M, et al. Wavelet based image de-noising with optimized thresholding using HHO algorithm. 2019 16th International Computer Conference on Wavelet Active Media Technology and Information Processing. IEEE. 2019.

[14] Misiti M, Misiti Y, Oppenheim G. Wavelet Toolbox User's Guide. MathWorks, Inc. 2011.

[15] Murugadoss B, et al. Blind Digital Image Watermarking using Henon Chaotic Map and Elliptic Curve Cryptography in Discrete Wavelets with Singular Value Decomposition. 2021 International Symposium of Asian Control Association on Intelligent Robotics and Industrial Automation (IRIA). IEEE. 2021.

[16] Kaur G, et al. Denoising of images using thresholding based on wavelet transform technique. IOP Conf Ser Mater Sci Eng. 2021;1022(1).

[17] Cui B, Jiang H. An image edge detection method based on Haar Wavelet Transform. 2020 International Conference on Artificial Intelligence and Computer Engineering (ICAICE). IEEE. 2020.

[18] Tuba U, Zivkovic D. Image Denoising by Discrete Wavelet Transform with Edge Preservation. 2021 13th International Conference on Electronics, Computers and Artificial Intelligence (ECAI). IEEE. 2021.

Al-Kitab Journal for Pure Sciences (2024); 8(2):78-93.
https://doi.org/10.32441/kjps.08.02.p7

Al-Kitab Journal for Pure Sciences
ISSN: 2617-1260 (print), 2617-8141(online)
https://isnra.net/index.php/kjps

Special Methods Controllability and Observability in Optimal Control Systems

Ali Farhan Hashoosh*

*Department of Mathematics, College of Basic Education, Misan University, Iraq

Corresponding Author: ali_fr@uomisan.edu.iq

ORCID: 0000-0002-3910-6852

Citation: Hashoosh AF. Special Methods Controllability and Observability in Optimal Control Systems. Al-Kitab J. Pure Sci. [Internet]. 2024 July. 06 [cited 2024 July. 06];8(2):78-93. Available from: https://doi.org/10.32441/kjps.08.02.p7.

Keywords: Mathematical Modeling, Optimal Control, Controllability, Observability.

Article History

Received	15 Mar.	2024
Accepted	25 Jun.	2024
Available online	06 July	2024

Abstract:

This article explores a specific case study that examines controllability and observability in general and in specific so that it is easy for the reader to understand these two concepts, which are fundamental in optimal control theory. Algorithms have been written to determine the controllability and observability of optimal control systems using the MATLAB programming language, and new techniques have been developed to deal with them. In addition, a critical test was created in which the state variables of the system or, more precisely, their corresponding states were split together, illustrating this with more than one example. Divided into four groups in a linear manner, as the article explains. To understand the controllability and observability of some more complex systems, this article is a starting point for the future expansion of these two concepts through the development of new algorithms or other applied solution methods or the creation of new algorithms.

Keywords: Mathematical Modeling, Optimal Control, Controllability, Observability.

طرق خاصة لقابلية التحكم وقابلية الملاحظة في أنظمة التحكم الأمثل

علي فرحان حاشوش*

* قسم الرياضيات، كلية التربية الأساسية ،جامعة ميسان، العراق
ali_fr@uomisan.edu.iq

الخلاصة:

تستكشف هذه المقالة دراسة حالة محددة تدرس إمكانية التحكم وإمكانية الملاحظة على نطاق واسع ودقيق بحيث يسهل على القارئ فهم هذين المفهومين، وهما مفهومان أساسيان في نظرية التحكم الأمثل. تمت كتابة خوارزميات لتحديد إمكانية التحكم وقابلية الملاحظة لأنظمة التحكم المثلى باستخدام لغة البرمجة *MATLAB*، كما تم تطوير تقنيات جديدة للتعامل معها. بالإضافة إلى ذلك، تم إنشاء اختبار نقدي تم فيه تقسيم متغيرات حالة النظام، أو بشكل أكثر دقة، الحالات المقابلة لها، مع توضيح ذلك بأكثر من مثال. مقسمة إلى أربع مجموعات بشكل خطي، كما يوضح المقال. من أجل فهم إمكانية التحكم وإمكانية الملاحظة في بعض الأنظمة الأكثر تعقيدًا، تعد هذه المقالة نقطة انطلاق للتوسع المستقبلي لهذين المفهومين من خلال تطوير خوارزميات جديدة أو طرق حل تطبيقية أخرى أو إنشاء خوارزميات جديدة.

الكلمات المفتاحية: نماذج رياضية، التحكم الامثل، قابلية التحكم، قابلية الملاحظة.

1. Introduction:

Controllability and observability are two basic and important concepts in modern control theory. The stability of the control system and its types is also stable (Routh stability criterion and Lyapunov) [1] [2]. In 1960, Kalman defined these two ideas in order [2] to determine the degree to which a system can be observed and managed [3]. The following fundamental queries must be addressed for any control system, especially for multivariable systems:

a) Is it possible to find a control function $u(t)$ that will, in a finite amount of time, change the system's initial state (x_t) into the desired final state (x_f)?

b) Is it possible to assess the system's state by analyzing its performance over a limited time?

The terms controllability and observability refer to the two ideas at play. Accordingly, the system is controllable if the first question has a "yes" response. The system is also observable if the second question has a yes response. It is important to acknowledge the fundamental nature of these problems. For instance, it makes no sense to attempt controlling a system by feedback of a state variable that permits the system's poles to be positioned arbitrarily unless the system is controllable. Similarly, attempting to reconstruct unmeasurable state variables of the system using so-called observers is futile unless the system is observable. In reality, controllability and

observability are two dual concepts that are intimately associated with the cancellation of zeros and poles in the transfer function of the system [5].

2. Controllability

We say about a system that it is controllable if and only if it is possible through the control vector to bring the system from the initial state $x(t_0) = x_0$o any final state $x(t_f) = x_f$ within a specified time $t > 0$.

In the case of nonlinear systems, these equations take the following form:

$$\dot{x} = A(t)x(t) + B(t)u(t)$$

$$y = C(t)x(t) + D(t)u(t)$$

In the case of linear systems fixed with time, the equations take the following form:

$$\dot{x} = Ax(t) + Bu(t)$$

$$y = Cx(t) + Du(t)$$

Where

A is the state matrix of order $n \times n$, B is cthe ontrol matrix of order $n \times m$, C is the output matrix of order $1 \times n$, D is Direct transfer matrix of order $1 \times m$, n the number of state vector state.,m the number of control vector states [4]. We consider a system described by the state equations:

$$\dot{x} = Ax(t) + Bu(t) \qquad (2.1)$$

$y = Cx(t)$

With the transformation:

$$x(t) = pz(t) \qquad (2.2)$$

we can transform equation (2.1) into the form:

$$\dot{z} = A_1 z(t) + B_1 u(t) \qquad (2.3)$$

$$y = C_1 z(t)$$

Where $A_1 = P^{-1}AP$, $B_1 = P^{-1}B$ and $C_1 = CP$. Assuming that A has distinct eigenvalues $\lambda_1, \lambda_2, \dots, \lambda_n$we can choose P so that A_1 is a diagonal matrix, that is,

$$A_1 = diag\{\lambda_1, \lambda_2, \dots, \lambda_n\}$$

If $n = m = 2$, the first of the equations (2.3) has the form

$$\begin{bmatrix}\dot{z}_1\\ \dot{z}_2\end{bmatrix}=\begin{bmatrix}\lambda_1 & 0\\ 0 & \lambda_2\end{bmatrix}\begin{bmatrix}z_1\\ z_2\end{bmatrix}+\begin{bmatrix}b_{11} & b_{12}\\ b_{21} & b_{22}\end{bmatrix}\begin{bmatrix}u_1\\ u_2\end{bmatrix}$$

Which is written as

$$\dot{z}_1=\lambda_1 z_1+b_1^T u \qquad (2.4)$$

$$\dot{z}_2=\lambda_2 z_2+b_1^T u$$

Where b_1^T and b_2^T are the row vectors of the matrix B_1

The output equation is

$$\begin{bmatrix}y_1\\ y_2\end{bmatrix}=\begin{bmatrix}c_{11} & c_{12}\\ c_{21} & c_{22}\end{bmatrix}\begin{bmatrix}z_1\\ z_2\end{bmatrix}$$

Which can be written as

$$y_1=c_{11}z_1+c_{12}z_2$$

$$y_2=c_{21}z_1+c_{22}z_2$$

Or

$$\begin{bmatrix}y_1\\ y_2\end{bmatrix}=\begin{bmatrix}c_{11}\\ c_{21}\end{bmatrix}z_1+\begin{bmatrix}c_{12}\\ c_{22}\end{bmatrix}z_2$$

So that

$$y=c_1z_1+c_2z_2 \qquad (2.5)$$

where c_1 and c_2 are the column vectors of C_1. So, in general, equation (2.3) can be written in the form:

$$\dot{z}_i=\lambda_i z_i+b_i^T u(t) \qquad (i=1,2,3,\dots,n)$$

$$y=\sum_{i=1}^{n} c_i z_i \qquad (2.6)$$

It is seen from equation (2.6) that if b_i^T the i^{th} h row of B_1 has all zero components, then

$$\dot{z}_i=\lambda_i z_i+0$$

And the input $u(t)$ has no influence on the i^{th} mode of the system. The mode is said to be uncontrollable, and a system having one or more such modes is uncontrollable [6][7].

Example 1: Check whether the system having the state-space representation

$$\dot{x}=\begin{bmatrix}-1 & 2\\ -3 & 4\end{bmatrix}\begin{bmatrix}x_1\\ x_2\end{bmatrix}+\begin{bmatrix}4\\ 6\end{bmatrix}u$$

$$y=\begin{bmatrix}1 & -2\end{bmatrix}\begin{bmatrix}x_1\\ x_2\end{bmatrix}$$

Is controllable?

Solution: The characteristic equation is

$$|\lambda I-A|=\lambda^2-3\lambda+2=0$$

$$(\lambda-1)(\lambda-2)=0$$

$$\Longrightarrow \lambda=1 \;\&\; \lambda=2$$

The corresponding eigenvectors are

$x_1 = [1 \quad 1]^T \; and \; x_2 = [2 \quad 3]^T$

so that the modal matrix is

$$P = \begin{bmatrix} 1 & 2 \\ 1 & 3 \end{bmatrix} \quad and \; P^{-1} = \begin{bmatrix} 3 & -2 \\ -1 & 1 \end{bmatrix}$$

Using the transformation $x = Pz$, the state-equation becomes

$$\dot{z} = \begin{bmatrix} 1 & 0 \\ 0 & 2 \end{bmatrix} z + \begin{bmatrix} 0 \\ 2 \end{bmatrix} u$$

$$y = [-1 \quad -4]z$$

This equation shows that the first mode is uncontrollable and so the system is uncontrollable. On the basis of the above result, we now derive an extremely useful criterion for determining whether a system is controllable. Although at this stage we consider only the necessity of this criterion, it is also a sufficient condition. To simplify the notation and the mathematical manipulations, we consider a SISO (single-input and single-output) system, so that in equation (**2.1**) B is a one-column matrix, that is a column vector b (say), and C is a row vectorc_1'. The result holds for the more general case when the system is multivariable.

Equations (**2.1**) and (**2.3**) are then written as

$$\dot{x} = Ax(t) + bu(t) \qquad (\mathbf{2.1.a})$$

$$y = Cx(t)$$

And

$$\dot{z} = A_1 z(t) + b_1 u(t) \qquad (\mathbf{2.3.a})$$

$$y = c_1' z(t)$$

We have chosen an indirect way of deriving the controllability criterion. It has the advantage of simplicity, but a penalty we paid or this is some loss in the logic behind the setting up of the criterion. We have established that the necessary condition for the system defined by equation (**2.1. a**) to be controllable is that the components of the vector

$b_1 = [\beta_1 \quad \beta_2 \quad \dots \quad \beta_n]^T$ in equation (**2.3.a**)are all non-zero

In equation (**2.3. a**) the matrix $A_1 = diag\{\lambda_1, \lambda_2 \dots, \lambda_n\}$where the eigenvalues $\lambda_1, \lambda_2 \dots, \lambda_n$ are assumed distinct. Hence the matrix:

$$\begin{bmatrix} 1 & \lambda_1 & \dots & \lambda_1^{n-1} \\ 1 & \lambda_2 & \dots & \lambda_2^{n-1} \\ \vdots & \vdots & \vdots & \vdots \\ 1 & \lambda_n & \dots & \lambda_n^{n-1} \end{bmatrix}$$

Has linearly independent columns, so that it is non-singular. It follows that the necessary condition to be controllable is that the (partitioned) matrix:

$$Q_p = [b_1 \quad A_1 b_1 \quad A_1^2 b_1 \quad \cdots \quad A_1^{n-1} b_1] = \begin{bmatrix} \beta_1 & \lambda_1\beta_1 & \dots & \lambda_1^{n-1}\beta_1 \\ \beta_2 & \lambda_2\beta_2 & \dots & \lambda_2^{n-1}\beta_2 \\ \vdots & \vdots & \vdots & \vdots \\ \beta_n & \lambda_n\beta_n & \dots & \lambda_n^{n-1}\beta_n \end{bmatrix} \qquad (2.7)$$

The matrix $Q_p$is non-singular.

Since

$$A_1 = P^{-1}AP \; and \; b_1 = P^{-1}b$$

We have

$A_1 b_1 = P^{-1}AP\, P^{-1}b = P^{-1}Ab$

$A_1^2 b_1 = P^{-1}A^2P\, P^{-1}b = P^{-1}A^2b$

$\vdots$

$A_1^{n-1} b_1 = P^{-1}A^{n-1}P\, P^{-1}b = P^{-1}A^{n-1}b$

So that

$$Q_p = P^{-1}[b \quad Ab \quad A^2B \quad \cdots \quad A^{n-1}b] = P^{-1}Q_c$$

Where

$$Q_c = [b \quad Ab \quad A^2B \quad \cdots \quad A^{n-1}b] \qquad (2.8)$$

Since Q_p(for a controllable system) and P^{-1} are both non-singular, Q_c (for a controllable system) is also non-singular.

As Q_p is non-singular, its n columns are linearly independent. So that the rank of the matrix Q_c written as $r(Q_c)$ is n.

2.1. Controllability Test

To find out the controllability of a system, consider a system described by the state equations:

$$\dot{x} = Ax(t) + Bu(t)$$

$$y = Cx(t)$$

Step 1: write the matrix Q_c($is\ called\ the\ system\ controllability\ matrix$)

$$Q_c = [B \quad AB \quad A^2B \quad \cdots \quad A^{n-1}B]$$

Step 2: find the determinant of Q_c if it is not equal to zero then the control system is controllable or if the determinant of Q_c equal to zero then the control system is uncontrollable.

If the matrix A in system order is higher than 3×3, it is difficult to know whether the system is controllable or not in a previous way, so we assume that

$$\Phi = [B \quad AB \quad A^2B \quad \cdots \quad A^{n-m}B]$$

When m is number of inputs

Step 1: write the matrix $Q_c(\ is\ called\ the\ system\ controllability\ matrix)$

$$\Phi = [B \quad AB \quad A^2B \quad \cdots \quad A^{n-m}B]$$

Step 2: find rank of Φ if it is equal to n then the control system is controllable or if rank of Φ not equal to n then the control system is uncontrollable.

Or we can calculate the determinant $\Phi\Phi^T$ if it is not equal to zero then the control system is controllable or if determinant of $\Phi\Phi^T$ equal to zero then the control system is uncontrollable.

Example 2: Verify the controllability of control system which is the presented by state equation:

$$\dot{x} = \begin{bmatrix} 0 & 1 & 0 & 0 \\ 3 & 0 & 0 & 2 \\ 0 & 0 & 0 & 1 \\ 0 & -2 & 0 & 0 \end{bmatrix} \begin{bmatrix} x_1 \\ x_2 \\ x_3 \\ x_4 \end{bmatrix} + \begin{bmatrix} 0 & 0 \\ 1 & 0 \\ 0 & 0 \\ 0 & 1 \end{bmatrix} u$$

Solution:

Step 1: $\Phi = \begin{bmatrix} 0 & 1 & 0 & 0 & 0 & 2 \\ 3 & 0 & 0 & 2 & -1 & 0 \\ 0 & 0 & 0 & 1 & -2 & 0 \\ 0 & -2 & 0 & 0 & 0 & -4 \end{bmatrix}$

Step 2: $rank(\Phi) = 4 = \text{n}$

Then the system is controllable.

2.2. Program for finding controllability

A program was developed in MATLAB to create controllability, and it was saved under the name “ctrb” and can be used when needed.

The program:

$Function\ co = ctrb(A, B)$

$N = length(A);$

$co = ctrb(a, b);$

$if\ rank(co) \cong n$

$disp('no\ contrable')$

$else$

$disp('\ contrable')$

end

Example 3: Is the system given as follows controllable?

$$\begin{bmatrix}\dot{x}_1\\ \dot{x}_2\\ x_3\end{bmatrix}=\begin{bmatrix}-1 & 0 & 0\\ -1 & -2 & 0\\ 1 & 0 & 0\end{bmatrix}\begin{bmatrix}x_1\\ x_2\\ x_3\end{bmatrix}+\begin{bmatrix}1\\ 0\\ 0\end{bmatrix}u$$

$$y(t)=[1 \quad 1 \quad 0]\begin{bmatrix}x_1\\ x_2\\ x_3\end{bmatrix}$$

Solution: Using the preceding method results in the following

$\gg A=[-1 \quad 0 \quad 0;-1 \quad -2 \quad 0;1 \quad 0 \quad 0];$

$\gg B=[1;0;0];$

$\gg co(A,B)$

$contable$

$ans=$

$$\begin{matrix}1 & -1 & 1\\ 0 & -1 & 3\\ 0 & 1 & -1\end{matrix}$$

That is, the system is controllable and the value of the matrix Q_c:

$$Q_c=\begin{bmatrix}1 & -1 & 1\\ 0 & -1 & 3\\ 0 & 1 & -1\end{bmatrix}$$

3. Observability

A system is said to be observable if the initial vector $x(t)$ can be found from the measurement of $u(t)$ and $y(t)$. The plant described by (2.1) is completely state observable if the inverse matrix exists [8].

By using the transform $x = Pz(x)$ as in the (2.1) section, we end up with the system state equations in the form of equation (6.3), that is

$$\dot{z}=A_1z(t)+B_1u(t)$$

$$y=C_1z(t)$$

If a row of the matrix C_1 is zero, the corresponding mode of the system will not appear in the output y. In this case the system is unobservable, since we cannot determine the state variable corresponding to the row of zeros in C_1 from y.

Example 4: Check whether the system having the state-space representation

$$\dot{x} = \begin{bmatrix} -5 & 4 \\ -6 & 5 \end{bmatrix} \begin{bmatrix} x_1 \\ x_2 \end{bmatrix} + \begin{bmatrix} 1 \\ 2 \end{bmatrix} u$$

$$y = [3 \quad -2] \begin{bmatrix} x_1 \\ x_2 \end{bmatrix}$$

Is observable?

Solution: The characteristic equation is

$|\lambda I - A| = \lambda^2 - 1 = 0$

$(\lambda - 1)(\lambda + 1) = 0$

$\Longrightarrow \lambda = 1 \;\&\; \lambda = -1$

The corresponding eigenvectors are

$x_1 = [1 \quad 1]^T \; and \; x_2 = [2 \quad 3]^T$

so that the modal matrix is

$P = \begin{bmatrix} 1 & 2 \\ 1 & 3 \end{bmatrix} \;\; and \; P^{-1} = \begin{bmatrix} 3 & -2 \\ -1 & 1 \end{bmatrix}$

Using the transformation $x = Pz$, the state-equation becomes

$$\dot{z} = \begin{bmatrix} -1 & 0 \\ 0 & 1 \end{bmatrix} \begin{bmatrix} z_1 \\ z_2 \end{bmatrix} + \begin{bmatrix} -1 \\ 1 \end{bmatrix} u$$

$$y = [1 \quad 0] \begin{bmatrix} z_1 \\ z_2 \end{bmatrix}$$

Then the system is unobservable.

Example 5: illustrates the importance of the observability concept. In this case, we have an unstable system, whose instability is not observed in the output measurement. The dual controllability concept is of equal theoretical importance. An uncontrollable system has one or more modes that are not influenced by the input.

We now similarly derive a criterion for observability to that used to derive the controllability criterion.

Again, for simplicity, we consider a $SISO$ system, but the result holds for the more general multivariable system. It can be seen that the necessary conditions for systems defined by equation (**1.a**) to be observable is that the components of the vector$b_1 = [\gamma_1 \quad \gamma_2 \quad \cdots \quad \gamma_n]^T$ in equation (**3.*a***) are all non-zero

for a controllable system we have the matrix

$$Q_1 = \begin{bmatrix} c_1^T \\ c_1^T A_1 \\ \vdots \\ c_1^T A_1^{n-1} \end{bmatrix} = \begin{bmatrix} \gamma_1 & \gamma_2 & \cdots & \gamma_n \\ \gamma_2\lambda_1 & \gamma_2\lambda_2 & \cdots & \gamma_n\lambda_n \\ \vdots & \vdots & \vdots & \vdots \\ \gamma_n\lambda_1^{n-1} & \gamma_2\lambda_2^{n-1} & \cdots & \gamma_n\lambda_n^{n-1} \end{bmatrix} \qquad (3.1)$$

The matrix $Q_1$is non-singular.

Since

$$A_1 = P^{-1}AP \text{ and } C_1^t = c^T P$$

We have

$$c_1^T A_1 = c^T P P^{-1} AP = c^T AP$$
$$A_1^2 b_1 = c^T P P^{-1} A^2 P = c^T A^2 P$$
$$\vdots$$
$$A_1^{n-1} b_1 = c^T P P^{-1} A^{n-1} P = c^T A^{n-1} P$$

So that

$$Q_1 = \begin{bmatrix} c^T \\ c^T A_1 \\ \vdots \\ c^T A_1^{n-1} \end{bmatrix} P = Q_o P$$

Where

$$Q_o = \begin{bmatrix} c^T \\ c^T A_1 \\ \vdots \\ c^T A_1^{n-1} \end{bmatrix} \qquad (3.2)$$

Since Q_o(for an observable system) and P are both non-singular, Q_o (for a observable system) is also non-singular.

3.1. The observability criterion

In equation (3.1) if the rank of matrix Q_o is n, the system can be called observable system. If rank Q_o less than n ,the system is un observable.

3.2. Observability test

A control system is said to be observable if it is able to determine the initial states of the control system by observing the outputs in finite duration of time.

To find out whether the control system is observable or not, we use a Kalman's test:

Step 1: form the matrix $Q_o = [C^T \quad A^T C^T \quad (A^T)^2 C^T \quad \dots \quad (A^T)^{n-1} C^T]$

Step 2: Take determinant of Q_o if it is not equal to zero then the control system is observable or if determinant of Q_c equal to zero then the control system is not observable [9].

Example 5: Verify the observability of control system which is the presented by state equation:

$$\dot{x} = \begin{bmatrix} -2 & -2 \\ 1 & 0 \end{bmatrix} \begin{bmatrix} x_1 \\ x_2 \end{bmatrix} + \begin{bmatrix} 1 \\ 1 \end{bmatrix} u$$

$$y = [1 \quad 1] \begin{bmatrix} x_1 \\ x_2 \end{bmatrix}$$

Solution: Given $A = \begin{bmatrix} -2 & -2 \\ 1 & 0 \end{bmatrix}$, $B = \begin{bmatrix} 1 \\ 1 \end{bmatrix}$ and $c = [1 \quad 1]$, $n = 2$

Step 1: $Q_o = [C^T \quad A^T C^T \quad (A^T)^2 C^T \quad \dots \quad (A^T)^{n-1} C^T] = [C^T \quad A^T C^T] = \begin{bmatrix} 1 & -1 \\ 1 & -2 \end{bmatrix}$

Step 2:$|Q_o| = \begin{vmatrix} 1 & -1 \\ 1 & -2 \end{vmatrix} = -1$

the system is observable.

3.3. Program for finding observability

MATLAB program was designed to find observability and was saved under the name "obsv" It is used when needed, as shown below [10]:

$function\ ob = \ obsv(A, C)$

$\%'The\ function\ ob = obsv(A, C) returns\ the\ transformation\ matrix\ '$

$\%'\ ob\ =\ [C;\ CA;\ CA\hat{}2;\ \dots CA\hat{}(n-1)]. The\ system\ is\ completely\ state'$

$\%'\ observable\ if\ and\ only\ if\ o\ has\ a\ rank\ of\ n.$

$n = length(A);$

$for\ i = 1{:}n;$

$o(n+1-i,:)\ =\ C * A\hat{}(n-i);$

end

$if\ rank(ob)\sim = n$

$disp('System\ is\ not\ state\ observable')$

$else$

$disp('System\ is\ state\ observable')$

end

Example 6: Is the system given as follows:

$$\begin{bmatrix} \dot{x}_1 \\ \dot{x}_2 \\ x_3 \end{bmatrix} = \begin{bmatrix} 0 & 1 & 0 \\ 0 & 0 & 1 \\ -6 & -11 & -6 \end{bmatrix} \begin{bmatrix} x_1 \\ x_2 \\ x_3 \end{bmatrix} + \begin{bmatrix} 1 \\ 1 \\ 1 \end{bmatrix} u$$

$$y(t) = [1 \quad 1 \quad 1] \begin{bmatrix} x_1 \\ x_2 \\ x_3 \end{bmatrix}$$

$observable?$

Solution:

$>>\ A = [0\ 1\ 0; 0\ 0\ 1; -6\ -11\ -6];$

$>>\ C = [1\ 1\ 1];$

$>>\ ob(a, c)$

System is state observable

ans =

$$\begin{matrix} 1 & 1 & 1 \\ -6 & -10 & -5 \\ 30 & 49 & 20 \end{matrix}$$

That is, the system is *observable* and the value of the matrix Q_o:

$$Q_o = \begin{bmatrix} 1 & 1 & 1 \\ -6 & -10 & -5 \\ 30 & 49 & 20 \end{bmatrix}$$

4. Decomposition of System State

From the discussion in the previous two sections, it is clear that the state variables (equivalently, the corresponding modes) of a linear system can generally be divided into the following four exclusive groups:

Case 1: Controllable and Observable

Case 2: Controllable but unobservable

Case 3: Uncontrollable but observable

case 4: Uncontrollable and unobservable.

Assuming that the system matrix A has different eigenvalues, the state equation can be simplified to the following form by appropriate transformation:

$$\begin{bmatrix} \dot{x}_1 \\ \dot{x}_2 \\ \dot{x}_3 \\ \dot{x}_4 \end{bmatrix} = \begin{bmatrix} A_1 & 0 & 0 & 0 \\ 0 & A_2 & 0 & 0 \\ 0 & 0 & A_3 & 0 \\ 0 & 0 & 0 & A_4 \end{bmatrix} \begin{bmatrix} x_1 \\ x_2 \\ x_3 \\ x_4 \end{bmatrix} + \begin{bmatrix} B_1 \\ B_2 \\ 0 \\ 0 \end{bmatrix} u \qquad (4.1)$$

$$y = [C_1 \quad 0 \quad C_3 \quad 0] \begin{bmatrix} x_1 \\ x_2 \\ x_3 \\ x_4 \end{bmatrix}$$

The (transformed) system matrix A is put in "block diagonal" form, with each $A_i (i = 1,2,3,4)$ having a diagonal form. The suffix i of the state variable vector x means that the elements of this vector are the state variables corresponding to the i^{th} case defined above.

Example 7: Classify the state variables in a system defined by the following state equation:

$$\begin{bmatrix} \dot{x}_1 \\ \dot{x}_2 \\ \dot{x}_3 \\ \dot{x}_4 \\ \dot{x}_5 \\ \dot{x}_6 \end{bmatrix} = \begin{bmatrix} -2 & 0 & 0 & 0 & 0 & 0 \\ 0 & -1 & 0 & 0 & 0 & 0 \\ 0 & 0 & 1 & 0 & 0 & 0 \\ 0 & 0 & 0 & -3 & 0 & 0 \\ 0 & 0 & 0 & 0 & 0 & 0 \\ 0 & 0 & 0 & 0 & 0 & -4 \end{bmatrix} \begin{bmatrix} x_1 \\ x_2 \\ x_3 \\ x_4 \\ x_5 \\ x_6 \end{bmatrix} + \begin{bmatrix} 1 & -1 \\ 0 & 0 \\ 1 & 1 \\ 0 & 0 \\ 1 & 0 \\ 0 & 2 \end{bmatrix} u$$

$$\begin{bmatrix} y_1 \\ y_2 \end{bmatrix} = \begin{bmatrix} 0 & 0 & -1 & 2 & 0 & 1 \\ 1 & 0 & 1 & -1 & 0 & 1 \end{bmatrix} \begin{bmatrix} x_1 \\ x_2 \\ x_3 \\ x_4 \\ x_5 \\ x_6 \end{bmatrix}$$

Solution: By inspection we can classify the state variables into the four groups as follows:

Case1: Controllable and observable, x_1, x_3 and x_6.

Case 2: Controllable and unobservable x_5.

Case 3: Uncontrollable and observable x_4.

Case 4: Uncontrollable and unobservable x_2.

We can represent the decompositions of the state variables into four groups by a diagram (see **Figure1**) showing the system divided into four subsystems each having state variables belong to one group only as indicated by the suffix i of S_i.

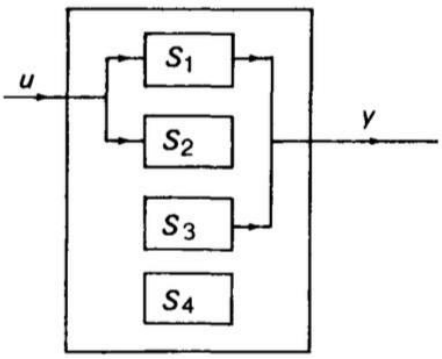

Figure 1: The system divided into four subsystems

This insight into the system structure explains the difference that may exist between the form of the system transfer function calculated from the system differential equations and that obtained by experimentation (that is, by obtaining the system frequency response.

We define the transfer function ($G(s)$ as $G(s) = \frac{Y(s)}{U(s)}$) as the ratio of the Laplace transform of the output $Y(s)$ to the input $U(s)$. The transfer function obtained from the differential equation (or equivalently from the system equation of state) includes all state variables (or modes) of the system. But the transfer function discovered through experimentation involves the part of the system that is affected by the input and affects the output. It can be seen from **Figure 1** that the transfer function of the subsystem Si is determined and only includes controllable and observable state variables (or modes).

In general, the transfer function $G(s)$ represents only the subsystem s_1 of the considered system, and indeed on adding to s_1 the subsystems S_2 , S_3 and S_4 has no effect on $G(s)$.

Example 8: Make sense of the above discussion by using the systems that are examined in example 1 and Decomposition of System State.

Solution: In example 1, the state equations were transformed into the diagonal form

$$\dot{z} = \begin{bmatrix} 1 & 0 \\ 0 & 2 \end{bmatrix} z + \begin{bmatrix} 0 \\ 2 \end{bmatrix} u$$

$y = [-1 \quad -4]z.$

There are two modes in the system, which correspond to the poles $\lambda = 1$ and $\lambda = 2$. Figure 2 can be used to represent the equations .

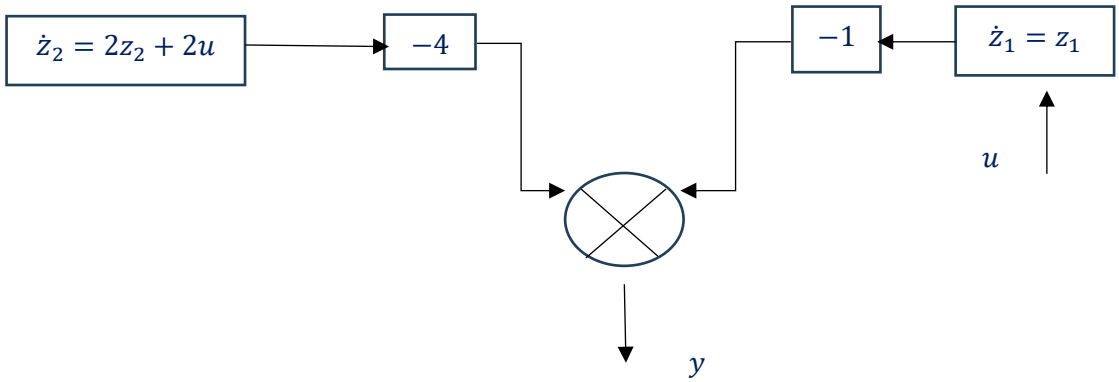

Figure 2: The representation of the equations in example 1

In Example 1 the transformed state equations are:

$$\dot{z} = \begin{bmatrix} -1 & 0 \\ 0 & 1 \end{bmatrix} \begin{bmatrix} z_1 \\ z \end{bmatrix} + \begin{bmatrix} -1 \\ 1 \end{bmatrix} u$$

$$y = [1 \quad 0] \begin{bmatrix} z_1 \\ z \end{bmatrix}$$

Figure 3 can be used to represent these equations.

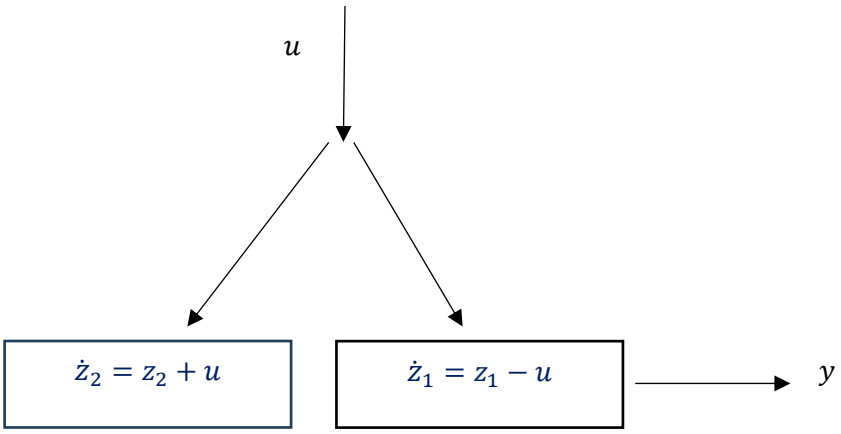

Figure 3: The representation of the equations

In this case

$$G(s) = [1 \quad 0]\begin{bmatrix} \frac{1}{s+1} & 0 \\ 0 & \frac{1}{s-1} \end{bmatrix}\begin{bmatrix} -1 \\ 1 \end{bmatrix} = -\frac{1}{s+1}$$

Once more, it is evident that the transfer function does not include the unobservable mode, which corresponds to the pole $\lambda = 1$.

It was mentioned in the example above that the unpredictable or the transfer function of a system lacks the unobservable mode. This fact warrants more investigation because it raises another requirement for a system to meet in order to be considered observable and or controllable [11]. It is believed that matrix A is of order n X n, with distinct eigenvalues .

5. Conclusion

This article discusses new methods of controllability and observability in control systems and the creation of algorithms using the MATLAB language in order to facilitate knowledge of controllability and observability in control systems, and the creation of applied methods as well. There are many well-known pieces of evidenceand methods that were not presented in this article. However, much of the proof is known, there is no doubt that there is much more undiscovered and that it is worth discussing, sharing, and presenting. Future research may address other things in depth.

6. References

[1] Farhan Hashosh, Ali, and Hadi Basirzadeh. "Routh stability criterion and Lyapunov-Routh method in control theory." International Journal of Nonlinear Analysis and Applications 15.5 (2024): 111-120.

[2] Hashoosh, Ali Farhan, and Hadi Basirzadeh. "Stability on Optimal control problems and Multi-Population Mathematical Models." Utilitas Mathematica 120 (2023): 500-505.

[3] R. E. KALMAN [1960a] A new approach to linear filtering and prediction problems, J. Basic Engr. (Trans. ASMS), 82D:35–45. YAN-MING FU; GUANG-REN DUAN; SHEN-MIN SONG, Design of

[4] BARTOSIEWICZ Z., PIOTROWSKA E., M. WYRWAS, Stability, Stabilization And Observers of Linear Control Systems on Time Scales, Proc. IEEE Conf. on Decision and Control, New Orleans, LA, December 2007, 2803–2808.

[5] Burghs, David N., and Alexander Graham. Control and optimal control theories with applications. Horwood Publishing, 2004.

[6] Unknown Input Observer for Linear Time-delay Systems. International Journal of Control, Automation, and Systems, vol. 2, No. 4, 2004, 530-535.

[7] Golnaraghi, Farid, and Benjamin C. Kuo. Automatic control systems. McGraw-Hill Education, 2017.

[8] SAADAT H., ComputationalAids in Control Systems Using MATLAB, Copyright-McGraw-Hill inc (1993).

[9] W.H. Fleming, R.W. Rishel, Deterministic and Stochastic Optimal Control, Springer-Verlag, New York, 1986.

[10] D'Azzo, J. J., Linear Control System Analysis, McGraw-Hill, 1988.

[11] D.Y. Karamzin, V.A. Oliveira, F.I. Pereira, G.N. Silva, On some extension of optimal control theory, Eur. J. Control 20 (2014) 284–291.

Al-Kitab Journal for Pure Sciences (2024); 8(2):94-108.
https://doi.org/10.32441/kjps.08.02.p8

Al-Kitab Journal for Pure Sciences
ISSN: 2617-1260 (print), 2617-8141(online)

https://isnra.net/index.php/kjps

Brief Review for Multi-Class Brain Tumor Diseases Schemes Using Machine Learning Techniques

Omar Ahmed Mahmood[1, 2], **Ahmed Sabeeh Yousif** [*2], **Afzan Adam**[1]

[1]Center for Artificial Intelligence Technology (CAIT), Faculty of Information Science and Technology, Universiti Kebangsaan Malaysia Bangi, Malaysia

[2]College of Technical Management Mosul - Northern Technical University, Iraq

Corresponding Author: ahmedsabeeh123@ntu.edu.iq

Citation: Mahmood OA, Yousif AS, Adam A. Brief Review for Multi-Class Brain Tumor Diseases Schemes Using Machine Learning Techniques. Al-Kitab J. Pure Sci. [Internet]. 2024 July. 07 [cited 2024 July. 07];8(2):94-108. Available from: https://doi.org/10.32441/kjps.08.02.p8.

Keywords: Tumor Diseases, Feature Extraction, Machine Learning.

Article History

Received	11 Apr. 2024
Accepted	03 Jun. 2024
Available online	07 July 2024

Abstract:

Brain tumor diseases have had a considerable impact worldwide, affecting millions of individuals of different age groups, including both children and adults above 20 years old. Due to they are more needed in people's lives, using the method based classifying brain tumors by machine learning schemes has become necessary. However, healthcare applications face challenges in identifying the most suitable classification-based metric, such as accuracy, due to the utilization of recent datasets. This study paper aims to provide a thorough evaluation of computational intelligence strategies used in tumor diagnosis. Several successful data mining techniques have been implemented, including wavelet analysis and spatial pixel modulation techniques. Furthermore, feature extraction and reduction techniques, such as the Grey Level Co-occurrence Matrix (GLCM), have been used to prepare the features for classification. Magnetic resonance imaging scan (MRI) is frequently utilized for the diagnosis of brain tumor diseases which is highly applied for classification-based machine learning, The review paper was focused on gliomas, meningiomas, and pituitary adenoma diseases. Technically, the usage of kernel principal component KPCA analysis with the proposed adaptive back propagation neural network scheme produced better performance-based classification metrics, (i.e:99.84%) for the accuracy metric. The aforementioned review articles have demonstrated that usage of

the machine learning-based health care applications (brain diseases) classification widely assists the patient's outcome and operations inside the hospitals. In summary, the paper has highlighted the importance of machine learning schemes for brain tumor detection and classification, and it also provided a comprehensive analysis and comparison of the state-of-the-art to show the methods such as ;(feature extraction, feature reduction), pros, cons, and the contributions for each of them. The paper's results are considered an advantageous starting point for future works.

Keywords: Tumor Diseases, Feature Extraction, Machine Learning.

مراجعة مختصرة لأنظمة أمراض الأورام الدماغية متعددة الفئات باستخدام تقنيات التعلم الآلي

عمر احمد محمود[١،٢]، احمد صبيح يوسف[٢]، افزان بنت ادم[١]

[١]مركز تكنولوجيا الذكاء الاصطناعي، كلية علوم وتكنولوجيا المعلومات، الجامعة الوطنية الماليزية، بانجي، ماليزيا

[٢]الكلية التقنية الإدارية، الجامعة التقنية الشمالية، موصل، العراق

p104581@siswa.ukm.edu.my, ahmedsabeeh123@ntu.edu.iq, afzan@ukm.edu.my

الخلاصة:

تُعتبر أمراض الأورام الدماغية من الأمراض التي لها تأثير كبير على مستوى العالم، حيث تؤثر على ملايين الأفراد من مختلف الفئات العمرية، بما في ذلك الأطفال والبالغين فوق سن العشرين. نظرًا لأهميتها البالغة في حياة الناس، أصبح استخدام طرق التصنيف بواسطة تقنيات التعلم الآلي ضروريًا. ومع ذلك، تواجه التطبيقات الصحية تحديات في تحديد المقياس المناسب للتصنيف، مثل الدقة، بسبب استخدام مجموعات بيانات حديثة. تهدف هذه الورقة البحثية إلى تقديم تقييم شامل لاستراتيجيات الذكاء الحسابي المستخدمة في تشخيص الأورام. تم تنفيذ عدة تقنيات تعدين بيانات ناجحة، بما في ذلك تحليل الموجات وتقنيات تعديل بكسل المكاني. علاوة على ذلك، تم استخدام تقنيات استخراج وتقليص السمات، مثل مصفوفة التواجد المستوى الرمادي (*GLCM*)، لإعداد السمات للتصنيف. تُستخدم صور الرنين المغناطيسي (*MRI*) بشكل متكرر لتشخيص أمراض الأورام الدماغية والتي يتم تطبيقها بشكل كبير للتصنيف القائم على التعلم الآلي. ركزت الورقة الاستعراضية على أمراض الأورام الدبقية والأورام السحائية والأورام النخامية. من الناحية التقنية، أدى استخدام تحليل المكون الرئيسي بالنواة *KPCA* مع مخطط شبكة العصبونات الارتجاعية التكيفية المقترح إلى إنتاج أداء أفضل لمقاييس التصنيف، (أي: ٩٩,٨٤٪) لمقياس الدقة. أظهرت المقالات الاستعراضية المذكورة أن استخدام تطبيقات الرعاية الصحية المستندة إلى التعلم الآلي (أمراض الدماغ) يساعد على نطاق واسع في نتائج وعمليات المرضى داخل المستشفيات. وباختصار، أبرزت الورقة أهمية أنظمة التعلم الآلي للكشف عن الأورام الدماغية وتصنيفها، وقدمت أيضًا تحليلاً شاملاً ومقارنة لأحدث الطرق لعرض الأساليب مثل؛ (استخراج السمات، تقليص السمات)، والمزايا والعيوب والمساهمات لكل منها. تُعتبر نتائج الورقة نقطة انطلاق مفيدة للأعمال المستقبلية.

الكلمات المفتاحية: أمراض الأورام الدماغية، استخراج الميزات، التعلم الآلي.

1. Introduction:

Imaging technology is used by the medical specialty of radiology for both diagnostic and interventional procedures [1]. Glial cells, which surround and support the brain's neurons, are the source of gliomas, a particular kind of tumor. The meninges, which are the membranes that wrap the outer regions of the brain and spinal cord, are the source of meningioma, a tumor that arises from them [2]. Tumors can differ in kind and size, and their location frequently reveals information about their form and rate of growth. Visual diagnosis of brain tumors and associated disorders such as blood channel abnormalities, stroke, brain traumas, aberrant brain development, and brain hemorrhage is greatly aided by medical imaging techniques. Common types of brain scans include computed tomography (CT), magnetic resonance imaging (MRI), positron emission tomography (PET), and single-photon emission (SPECT) scans [3,4,5,6,7,8,9,10].

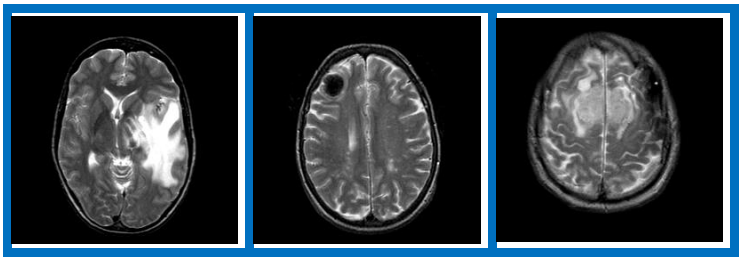

Figure 1: Examples of MRI human brain diseases [40].

MRI scan images have been used for the classification of different human brain diseases such as stroke, tumors, and precision, the paper has used the tumor classification based on different tumor types such as benign, malignant, and grade. different methods have been introduced earlier such as in [12]. The segmentation-based spatial domain was used before to segment the MRI scan and identify the types of diseases. For the process of classification-based brain disease schemes, segmentation is not usually mandatory.

Table 1: Comparison of imaging techniques CT, MRI, PET, and SPECT in the human brain diseases

Modalities	Mechanism	Spatial Resolution (mm)	Function	Imaging period (min)	Diseases
MRI	Magnetism	0.1	Anatomical details: Tissues details: Dead vs risk tissues	60	Stroke, tumor, depression, and AD
CT	Radiation dose	0.05	Anatomical details: Boundary: Cortex	10-15	Stroke, depression, and schizophrenia
PET	Nuclear medicine tools: Radioisotopes: Using the positrons Injected	1-2	Show physiological processes.: Glucose metabolism and blood-flow	20-60	Transition from MCI to AD, depression, and schizophrenia
SPECT	Nuclear medicine tools: Radioisotopes injected: Using gamma-ray	0.5-2	Show physiological processes.: Blood flow	30-90	Transition from MCI to AD, depression, and schizophrenia

So, segmentation is considered today as a pre-processing stage before going to the current technology of artificial intelligence methods such as machine learning, transfer learning, and deep learning schemes. **Figures 1** and **2** explore the brain tumor classification which is divided into three stages.

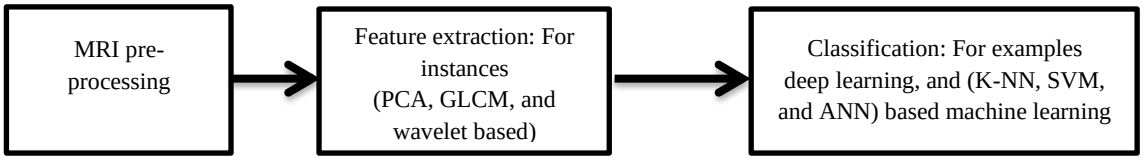

Figure 2. Overall block diagram of brain tumor classification[14].

Before the feature extraction phase, image preprocessing is conducted to enhance the quality of the image through techniques like filtration and resolution enhancement **[13]**. In the context of brain MR image classification, the preprocessing step may or may not include a segmentation phase **[14]**. Feature extraction included stages of reducing the size of the dimensionality of the data by using the extraction of important features such as Shape, texture, intensity, and statistics. However, processing the entire image data for classification can be computationally intensive and time-consuming **[14]**.

Therefore, feature selection, also known as dimension reduction, is employed to further reduce the dimensionality of the feature vector. PCA and LDA have been used to reduce the dimension in the classification of brain tumors **[23,24]**. To highly provide the minimizing of the feature vectors with improved classification accuracy, a proposed SVM-based recursive feature extraction of important, modified genetic scheme (GA), and the simulated annealing scheme (SA) are also proposed in **[17,22,27,28]**. According to the science of image processing and computer vision based using machine learning, the usage of MRI scan has been used to better decide the typical diseases in the brain MRI from the normal to fatal cases **[24,28]**, which the most common machine learning schemes such as SVM, Random forest RF, neural network NN, and K-nearest neighbor KNN **[31]**.

The self-organizing map neural network, or SOM-NN, is a clustering-based unsupervised classification method. **[11, 16, 17, 21, 23, 23]**. Add to that, artificial neural networks ANN and KNN schemes have been proposed using the MRI scan which used the supervised techniques to classify the MRI into various classes that used the modified hyperplanes and binary classification while the kernel-based Gaussian has been used for complex datasets for more than one class **[11,12,30,31]**. For the classification of brain tumors, ensemble classifiers built on SVM can also be used **[34]**.

1.1 Research Limitations: Different scholars have tried to provide the optimal approaches for image classification of brain tumors. Based on current papers, it is evident that machine learning-based feature extraction and reduction models exhibit acceptable outcomes. However, it should be recorded that there are different issues to perform better results in both AI-based-research and clinical issues such as:

1- The visual quality of medical imaging: for instance, the low contrast of MRI images may lead to a struggle classification of the tumor location and the normal brain tissue[23].
2- Boundary location of tumor diseases [3].
3- Imbalance problem: for instance; The big region of interest (ROI) of a large tumor may have a full impact on the retrieved characteristics, and that affects data-driven-based ML methods [9].

1.2 Research Questions: The best way to the most essential parts of a review paper is to propose various research questions. This is due to the questions can assist and estimate the accurate scope of the literature review. We can summarize various research questions as follows:

RQ1: Currently, Which schemes are currently thought to be the most effective for classifying brain tumors?

RQ2: What is the relation between feature extraction, and reduction methods and performance-based classification metrics such as accuracy?

RQ3: How can the machine learning model improve diagnostic processes, which leads to more preserving imaging details?

RQ4: Does the number of samples affect the classification outcome?

The objective of the paper is to provide a comprehensive comparison to review various classification methods for multi-class tumor brain disease-based machine learning schemes. The comparison involves different feature extraction and selection techniques along with classifier tools such as SVM, Import Vector Machine, KNN, and Random Forest. The main metrics for comparison among recent papers are classification accuracy, f1- score, true positive, and true negative. The paper is organized as follows: Section 2 discusses related works, Section 3 explains the proposed methodology, and Section .4 provides a detailed analysis and discussion. The conclusion and future works of the paper are presented in the final section.

2. Literature Review

2.1. Scope of this Review: In this paper, the review's findings from various scholarly articles have been summarized from good scientific databases like Springer, IEEE Digital Library,

Elsevier, and Wiley. To ensure the preservation of good research results in human brain-based medical imaging, the paper reviewed the proceedings as well of best reputation conferences from different raspatories.

2.2 Review the Recent Studies: Recent studies have focused on tumor classification in image and computer vision applications. Several methodologies have been proposed for brain tumor detection and classification using various techniques [9].

In one study [36], a multi-stage approach was introduced for tumor detection. The method involved glioma and meningioma classification, followed by segmentation. The brain MRI classification process uses KNN, a straightforward supervised learning algorithm, which operates on the tenet that related objects are closer to one another [30] [33]. For binary classification, supervised SVM is frequently utilized by creating hyperplanes; for more complicated datasets, kernel approaches such as the Gaussian kernel are used [11] [12]. SVM-based ensemble classifiers can also be used to classify brain tumors [34].

An automated technique for identifying brain tumors in MRI images was published in a different study [37]. The technique used a gray-level co-occurrence matrix (GLCM) for feature extraction and mean filtering for image improvement. Referring to the process of selection of the important features, probabilistic NN (PNN), and KNN schemes have been suggested while the classification-based modified GA is used. In [38], the article has produced a novel scheme that uses the spatial fuzzy c-mean FCM and the modified morphological operation for furthered noise reduction, while the PCA for feature extraction and reduction is applied. For classification, a non-linear kernel support vector machine (SVM) was used.

In [39], an ensemble learning technique for classifying brain tumors was presented. Pre-processing, feature extraction, feature selection, and classification were all part of the procedure. During the pre-processing stage, methods for normalization and quantization were applied, as well as the region of interest (ROI) of the lesion and tumor. The majority voting method was used for prediction, and the basis learner was a support vector machine (SVM) classifier.

For the classification of stroke diseases, a unique plan known as the Pathological Stroke Classification System (PSCS) was presented in [40]. Weighted local energy-based principal component analysis (WLEPCA) was utilized for feature reduction and selection, while non-subsampled shear let transform (NSST) was utilized for feature extraction. KNN, RF, and SVM classifiers were used for the classification; RF achieved the highest accuracy of 96.10%. Several local binary patterns (LBP) techniques were applied in [41] to classify typical forms of brain

tumors. Three types of local binary patterns were used: classical LBP, local binary patterns between relations between neighbors (n LBP), and local binary patterns based on angles (α LBP). KNN, ANN, RF, A1DE, and LDA methods were used to do the classification; the n LBP d=1 feature extraction approach and KNN model achieved the greatest success rate of 95.56%. According to the article proposed in **[42]**, the ant colony and thresholding for feature extraction and modified SVM performed higher accuracy compared to the state of arts (i.e. accuracy=97.7%) for brain tumor classification. Also, in **[43]**, the modified SVM for brain tumor classification is introduced, The contribution of the paper is to reduce the number of feature vectors used to feed to the classifier, the role given to the GA for the feature selection process, and reduced the number of vectors used.

In **[44]**, the dataset with MRI-T1 has been used, and the GLCM, intensity histogram (IH), and a bag of word schemes are introduced for feature extraction. The feature selection-based linear discriminant analysis LDA. The method outperforms the previous works with (accuracy =91.14%) by SVM classification of brain tumors. While in **[45]**, the author has recorded good classification-based metric (i.e; accuracy=85.70%) using the SVM scheme, the proposed method segmented the MRI images to level 3 wavelet (using DWT) for feature extraction, while localized region-active contour LRBAC for feature selection.

In **[46]**, the article has shown better performance-based accuracy metric (i.e., accuracy =95.65%), the method used the GLCM feature extraction using MRI-T2 dataset, the SVM and RF-based kernel are used as classifiers to classify the brain tumors.

A method to detect brain tumors and extract features from MRI pictures was introduced in **[47]**. Anisotropic diffusion filtering and greyscale conversion were two pre-processing procedures. The Chan-Vese algorithm and multi-level thresholding were used for tumor segmentation. A genetic algorithm (GA) was used to pick characteristics after a variety of texture, statistical, and wavelet features were measured. The classification accuracy of an artificial neural network (ANN) was 98.3%.

Differentiating benign and malignant brain tumors was addressed in **[48]**. DWT was used for the process of the extraction of important features, a genetic algorithm for the process of the reduction of unnecessary features, and SVM for classification. The method achieved high accuracy, although the root mean square error (RMS) was noted as a limitation.

Table 2: The recent works of multi-class brain diseases

Author	Modality	Brian disease	Feature extraction	Feature selection& reduction	Classification Based-methods	Accuracy (%)
G. B. et al. [36]	MRI	Normal , glioma, meningioma	GLCM, GLRLM	NA	RF	87.62%
Azawi et al. [37]	MRI	Normal, Lymphoma, Cystic oligodendro glioma, Glioblastoma multiform, Meningioma, Ependymoma and Anaplastic astrocytoma	GLCM	K-NN, GA	PNNA	100% when 45^0 97.14% when 90^0 98.57% when $135^0, 0^0$
Devkota et al. [38]	MRI	Normal ,glioma, metastatic_adenocarcinoma, meningioma and Sarcoma	GLCM	PCA	SVM	92%
Shafi et al. [39]	MRI	Normal,glioma, meningioma, pituitary adenoma multiple sclerosis	GLCM, GLIRM, GLSZM and NGTDM.	Relevance measures based on information gain. The concept of entropy is used in information gain to rank the feature.	SVM	97.95%
Yousif et al. [40]	Fused images (CT/MRI)	(1) Acute stroke (speech arrest), (2) acute stroke (writes, but cannot read, alexia without agraphia), (3) acute stroke (trouble speaking), (4) fatal stroke, (5) hypertensive encephalopathy, and (6) multiple embolic infarctions.	NSST	WLEPCA	KNN, SVM, and RF.	96.10%
Kaplan et al. [41]	MRI	Normal, glioma, meningioma, and pituitary	nLBP , αLBP, LBP	correlation-based method	KNN	95.56%.
Hussain et al. [42]	MRI	Normal ,malignant and benign	LBP, HOG ,SFTA	PCA	SVM	94.7٠%
Tajik et al. [43]	MRI	Normal, glioma, visual agnosia and meningioma	GLCM+DWT	GA	SVM, K-NN	96.67%
Chang et al. [44]	T1-weighted MRI.	meningioma, glioma, and pituitary	GLCM, and BOW	LDA	SVM	91.28%
Zia et al. [45]	MRI	Normal, Grade II glioma Grade III glioma Grade IV glioma	DWT	PCA	SVM	88.26%
Kharrat et al. [46]	T2-weightedMRI	Normal, malignant and benign	2D Wavelet Transform and spatial gray level dependence matrix (DWT-SGLDM)	SA	GA-SVM	95.65%
Kabir et al. [47]	MRI T1,T2	Normal ,malignant and benign	Texture, statical, and wavelet Feature.	GA	ANN	98.3%
Kumar et al. [48]	MRI	Normal, malignant and benign	DWT+GA	PCA	Kernel SVM	Varies from 80% to 90%
Sharif et al. [49]		Normal, malignant and benign	GLCM	GA	SVM	99.69%
Gudigar et al. [50]	MRI	Normal ,malignant and benign	DWT for image decomposition.	PSO	SVM	97.38%
Deepa et al. [51]	MRI T1,T2	Normal ,malignant and benign	Gabor wavelet	KPCA	AFBPNN	99.84%
Hasan et al. [52]	MRI	Normal, Lymphoma, Glioblastoma multiform, Cystic oligodendroglioma, Ependymoma, Meningioma and Anaplastic astrocytoma	first order statics (FOS) and second order statics (SOS)	DMWT	PNN	97%

3. Research Methodology

Artificial intelligence (AI) has provided a good analysis of medical imaging which caused more computational, complexity and medical data availability in the last decades. Although many applications for using AI classification in the imaging of brain tumors have been presented before, their impact of clinical is still to be studied. A systematic review was performed to study the multi-class brain tumor in the analysis of classification brain tumor imaging in various diseases. We performed a brief review and meta-data analysis was achieved in accordance with the good reporting for systematic reviews and meta-analyses for better guidelines the future studies in the field of using the various machine learning schemes to classify human brain tumor diseases. This brief literature review (BLR) shows the proposed review steps used to explore the classified approaches of the tumor as outlined in **Figure 3**.

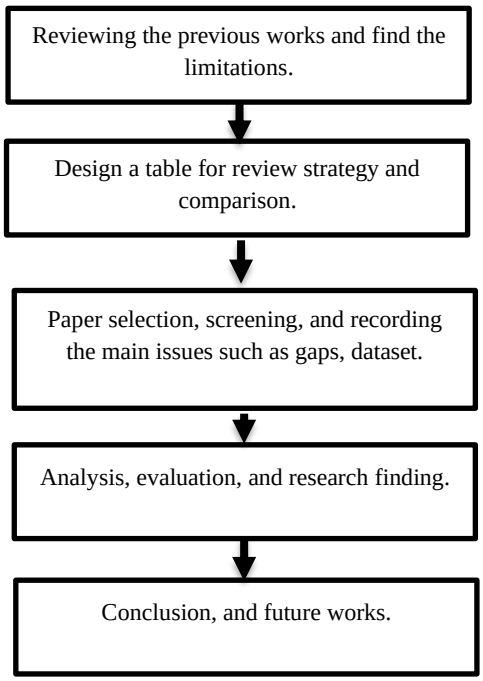

Figure 3: Proposed steps for a brief review of our paper.

4 .Result and Discussion

This section provides a deep concise summary of each paper and analysis of its pros and cons. A review of each paper is also provided to help the reader quickly understand the most essential parts of each paper. The analysis of different schemes for brain tumor classification is as follows :For example, in the studies **[36,37,38]**, the accuracy achieved for tumor brain classification was moderate, not exceeding 90%. This accuracy is lower compared to other existing works such as **[45]**. However, when **[45]** was used with different schemes of gray-level co-occurrence matrix (GLCM), it failed to achieve high accuracy. On the other hand, in **[51]**,

the use of Gabor wavelet for feature extraction resulted in an accuracy of 99.87%. In **[42,45,48,50]**, the classification of brain diseases using local binary patterns (LBP) with different approaches aimed to increase accuracy. The K-nearest neighbors (KNN) algorithm showed better performance when 4 or 7 features were selected, but it failed to maintain high accuracy when 256 features were used. In **[40]**, a novel stroke classification system was developed, achieving a 96.10% accuracy by capturing 15 features from the proposed feature reduction stage.

Overall, various methods for feature extraction and reduction were explored, and the best methods were evaluated based on accuracy. The approach in **[51]**, which combined the AFBPNN decision with kernel-based principal component analysis (PCA) for feature extraction and selection, achieved the greatest accuracy of 99.84%. The second-highest accuracy of 97.9% was achieved in **[39]** when feature extraction was carried out using GLCM-based entropy. When using PCA and GLCM for feature extraction, other techniques like **[42, 45, 36]** also produced acceptable classification results with accuracies of 94.7%, 85.7%, and 87.62%, accordingly. As a result, this study assesses a suggested model's classification performance using a variety of feature extraction and reduction techniques in conjunction with machine learning. Using an adaptive firefly backpropagation neural network (AFBPNN) and cross-validation with a 10-fold increase, the classification accuracy was 99.84%. The need for brain tumor classification tools in clinical practice must contain accurate validation, ongoing development, and use the ethical policies. As a result, there are many exciting schemes, involving medical imaging data integration, using AI with personalized medicine, and data extraction for the imaging diagnostic.

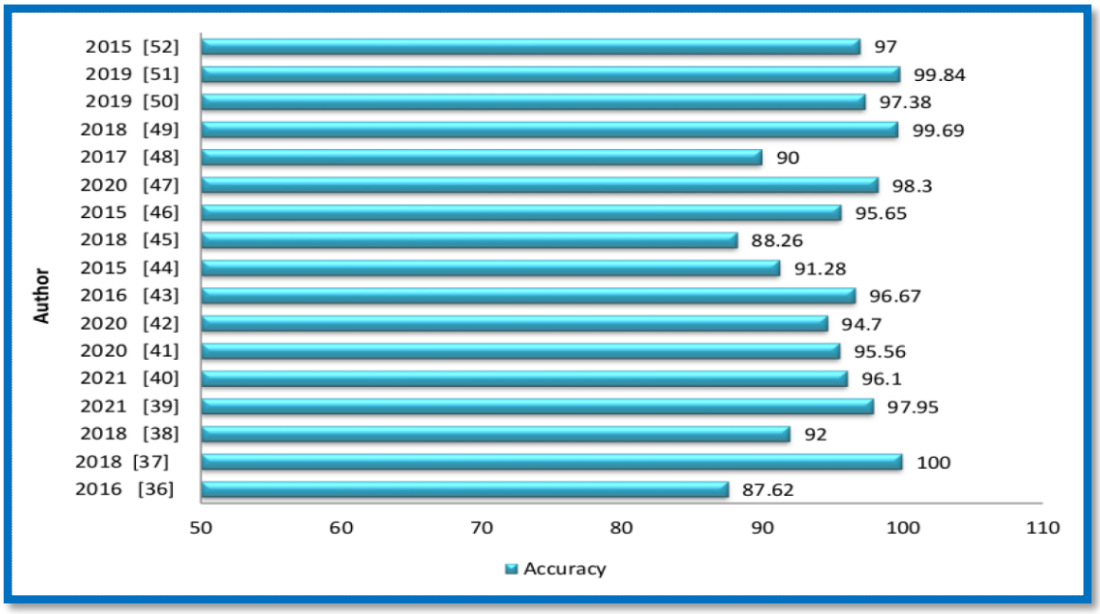

Figure 4: The comparison of various proposed methods using classification-based accuracy metric.

5. Conclusion :

This paper focuses on the review of the current development of intelligent multi-class multi-level (MCML) classification schemes for brain tumor disease classification. This research aims to provide an early assessment of tumors to aid users and clinicians. The proposed algorithms utilize traditional machine learning approaches, involving pre-processing, segmentation, feature extraction, and classification steps. In the pre-processing step, noise and contrast illumination are eliminated, while a hybrid technique is employed for region of interest extraction during segmentation. Color and texture features based on gray-level co-occurrence matrix (GLCM) are extracted and selected in the feature extraction and selection steps, followed by classification.

The study presented that the paper **[51]** has achieved a high accuracy of 99.84% by applying kernel-based principal component analysis (KPCA) with a firefly backpropagation neural network (FBPNN). Lastly, the scheme outperforms better compared to other methods in the classification of MRI scan images to different stages such as Normal case, abnormal, malignant or benign, and low grade or high grade. The future trend for this field still opens problems, especially in terms of the increased number of datasets, and for designing FPGA-based classification hardware more memory occupancy is still needed.

6. References:

[1] Yousif AS, Omar Z, Sheikh UU. An improved approach for medical image fusion using sparse representation and Siamese convolutional neural network. Biomed Signal Process Control. 2022;72:103357.

[2] Adult Central Nervous System Tumors Treatment (PDQ®)–Patient Version. National Cancer Institute; 2019.

[3] Zaidi H. Quantitative analysis in nuclear medicine imaging. University of Geneva; 2000. Available from: http://www.unige.ch/cyberdocuments/theses2000/ZaidiH/these_body.html. [Accessed 2015 Jun 9].

[4] American College of Radiology (ACR). T images and videos, ultrasound – general image. Available from: http://www.radiologyinfo.org/en/photocat/gallery3.cfm?image=brain-ped-normus.jpg&pg=genus. [Accessed 2015 Jun 9].

[5] Studwell AK, Kotton DN. A shift from cell cultures to creatures: in vivo imaging of small animals in experimental regenerative medicine. Mol Ther. 2011;19(11):1933–41.

[6] Beckmann N. In vivo magnetic resonance techniques and drug discovery. Braz J Phys. 2006;36(1).

[7] Turner R, Lucke-Wold B, Robson M, Omalu B, Petraglia A, Bailes J. Repetitive traumatic brain injury and development of chronic traumatic encephalopathy: a potential role for biomarkers in diagnosis, prognosis, and treatment? Front Neurol. 2013;3.

[8] Mody V, Siwale R, Singh A, Mody H. Introduction to metallic nanoparticles. J Pharm Bioallied Sci. 2010;2(4):282.

[9] Modalities C. Comparison between medical imaging modalities. Academia.edu. Available from: https://www.academia.edu/4752851/Comparison_between_Medical_Imaging_Modalities. [Accessed 2014 Oct 4].

[10] Acharya R, Wasserman R, Stevens J, Hinojosa C. Biomedical imaging modalities: a tutorial. Comput Med Imaging Graph. 1995;19(1):3–25.

[11] Chaplot S], Patnaik LM, Jagannathan NR. Classification of magnetic resonance brain images using wavelets as input to support vector machine and neural network. Biomed Signal Process Control. 2006;1(1):86–92.

[12] Ayachi R, Ben Amor N. Brain tumor segmentation using SVM. In: Sossai C, Chemello G, editors. ECSQARU 2009. Lecture Notes in Artificial Intelligence 5590. Berlin Heidelberg: Springer; 2009. p. 736–47.

[13] Rajeshwari S, Sharmila TS. Quality measurements of MRI using Preprocessing techniques. In: Proceedings of the 2013 IEEE Conference on Information and Communication Technologies; 2013. p. 978-1-4673-5758-6/13/ IEEE.

[14] Kumar G, Bhatia PK. A detailed review of feature extraction in image processing systems. In: 2014 Fourth International Conference on Advanced Computing & Communication Technologies. IEEE; 2014. p. 978-1-4799-4910-6/14.

[15] Materka A, Strzelecki M. Texture Analysis Methods – A Review. Technical University of Lodz, Institute of Electronics, COST B11 report, Brussels; 1998.

[16] Zulpe N, Pawar V. GLCM Textural Features for Brain Tumor Classification. IJCSI Int J Comput Sci Issues. 2012;9(3):164-84.

[17] Zacharaki EI, Wang S, Chawla S, Yoo DS, Wolf R, Melhem ER, Davatzikos C. MRI-based classification of brain tumor type and grade using SVM-RFE. 2009 IEEE International Symposium on Biomedical Imaging: From Nano to Macro; 2009. p. 736-47. doi:10.1109/ISBI.2009.5193232.

[18] John P. Brain tumor classification using wavelet and texture-based neural network. Int J Sci Eng Res. 2012;3(10).

[19] Loncaric S. A survey of shape analysis techniques. Pattern Recognit. 1998;31(8):983-1001. doi:10.1016/s0031-3203(97)00122-2.

[20] El-Dahshan ESA, Hosny T, Salem A-BM. Hybrid intelligent techniques for MRI brain images classification. Digit Signal Process. 2010;20(2):433-41. doi:10.1016/j.dsp.2009.07.002.

[21] Zhang Y, Wang S, Wu L. A novel method for magnetic resonance brain image classification based on adaptive chaotic pso. Prog Electromagn Res. 2010;109:325–43. doi:10.2528/pier10090105.

[22] Kharrat A, Gasmi K, Abid M. Automated classification of magnetic resonance brain images using Wavelet Genetic Algorithm and SVM. In: Proceedings of the 9th IEEE International Conference on Cognitive Informatics; 2010. p. 978-1-4244-8040-1/10 IEEE.

[23] Chaplot S, Patnaik LM, Jagannathan NR. Classification of magnetic resonance brain images using wavelets as input to support vector machine and neural network. Biomed Signal Process Control. 2006;1(1):86–92. doi:10.1016/j.bspc.2006.05.002.

[24] Othman MF, Abdullah N, K BT. Brain tumor Classification using Support Vector Machine. In: 2011 IEEE. p. 978-1-4577-0005-7/11 IEEE.

[25] Rathi VPG, Palani S. A novel approach for feature extraction and selection on MRI images for brain tumor classification. In: Wyld DC, et al., editors. CCSEA, SEA, CLOUD, DKMP, CS & IT 05. 2012. p. 225–34. DOI: 10.5121/csit.2012.2224.

[26] Zhang Y, Wu L. An MR brain images classifier via principal component analysis and kernel support vector machine. Prog Electromagn Res. 2012;130:369–88. doi:10.2528/pier12061410.

[27] Kharrat A, Halima MB, Ben Ayed M. MRI brain tumor classification using Support Vector Machines and meta-heuristic method. In: Proceedings of the 15th International Conference on Intelligent Systems Design and Applications (ISDA); 2015. doi:10.1109/ISDA.2015.7489271.

[28] Kharrat A, Karim G, Messaoud MB, Nacéra B, Mohamed A. A hybrid approach for automatic classification of brain MRI using genetic algorithm and support vector machine. Leonardo J Sci. 2010;(17).

[29] Sridhar D, Murali Krishna IV. Brain Tumor Classification using Discrete CosineTransform and Probabilistic Neural Network. In: 2013 International Conference on Signal Processing, Image Processing & Pattern Recognition. 2013. doi:10.1109/ICSIPR.2013.6497966.

[30] Zacharaki EI, Wang S, Sanjeev. Classification of Brain Tumor Type and Grade Using MRI Texture and Shape in a Machine Learning Scheme. Magn Reson Med. 2009; doi:10.1002/mrm.22147.

[31] Peyre G. Sparse modeling of textures. J Math Imaging Vis. 2009;34:17–31.

[32] Wasule V, Sonar P. Classification of brain MRI using SVM and KNN classifier. In: 2017 Third International Conference on Sensing, Signal Processing and Security (ICSSS). 2017. doi:10.1109/SSPS.2017.8071594.

[33] Herrera LJ, Rojas I, Pomares H, Guillen A, Valenzuela A, Banos O. Classification of MRI Images for Alzheimer's Disease Detection. In: 2013 International Conference on Social Computing. 2013. doi:10.1109/SocialCom.2013.127.

[34] Minz A, Mahobiya C. MR Image Classification Using Adaboost for Brain Tumor Type. In: 2017 IEEE 7th International Advance Computing Conference (IACC). 2017. doi:10.1109/IACC.2017.0146.

[35] Zontak M, Irani M. Internal statistics of a single natural image. In: IEEE Conference on Computer Vision and Pattern Recognition; 2011. pp. 977–984.

[36] Praveen GB, Agrawal A. Multi-stage classification and segmentation of brain tumor. In: 2016 3rd International Conference on Computing for Sustainable Global Development (INDIACom); 2016. pp. 1628-1632.

[37] Azawi RM, Abdulah DA, Abbas JM, Ibrahim IT. Brain Tumors Classification by Using Gray Level Co-occurrence Matrix, Genetic Algorithm and Probabilistic Neural Network. Diyala J Med. 2018;14(2):138-151.

[38] Devkota B, Alsadoon A, Prasad PWC, Singh AK, Elchouemi A. Image segmentation for early stage brain tumor detection using mathematical morphological reconstruction. Procedia Comput Sci. 2018;125:115-23.

[39] Shafi ASM, Rahman MB, Anwar T, Halder RS, Kays HE. Classification of brain tumors and auto-immune disease using ensemble learning. Inform Med Unlocked. 2021;100608.

[40] Yousif AS, Omar Z, Sheikh UU, Khalid SA. A Novel Pathological Stroke Classification System using NSST and WLEPCA. In: 2020 IEEE-EMBS Conference on Biomedical Engineering and Sciences (IECBES); 2021. pp. 565-69.

[41] Kaplan K, Kaya Y, Kuncan M, Ertunç HM. Brain tumor classification using modified local binary patterns (LBP) feature extraction methods. Med Hypotheses. 2020;139:109696.

[42] Hussain UN, Khan MA, Lali IU, Javed K, Ashraf I, Tariq J, et al. A unified design of ACO and skewness based brain tumor segmentation and classification from MRI scans. J Control Eng Appl Inform. 2020;22(2):43-55.

[43] Tajik MN, ur Rehman A, Khan W, Khan B. Texture feature selection using GA for classification of human brain MRI scans. In: International Conference on Swarm Intelligence; 2016. pp. 233-44. Springer, Cham.

[44] Cheng J, Huang W, Cao S, Yang R, Yang W, Yun Z, et al. Enhanced performance of brain tumor classification via tumor region augmentation and partition. PLoS One. 2015;10(10):e0140381.

[45] Zia R, Akhtar P, Aziz A. A new rectangular window based image cropping method for generalization of brain neoplasm classification systems. Int J Imaging Syst Technol. 2018;28(3):153-62.

[46] Kharrat A, Halima MB, Ayed MB. MRI brain tumor classification using support vector machines and meta-heuristic method. In: 2015 15th International Conference on Intelligent Systems Design and Applications (ISDA); 2015. pp. 446-51.

[47] Kabir MA. AUTOMATIC BRAIN TUMOR DETECTION AND FEATURE EXTRACTION FROM MRIIMAGE. GSJ. 2020;8(4).

[48] Kumar S, Dabas C, Godara S. Classification of brain MRI tumor images: a hybrid approach. Procedia Comput Sci. 2017;122:510-7.

[49] Sharif M, Tanvir U, Munir EU, Khan MA, Yasmin M. Brain tumor segmentation and classification by improved binomial thresholding and multi-features selection. J Ambient Intell Humaniz Comput. 2018:1-20.

[50] Gudigar A, Raghavendra U, San TR, Ciaccio EJ, Acharya UR. Application of multiresolution analysis for automated detection of brain abnormality using MR images: A comparative study. Future Gener Comput Syst. 2019;90:359-67.

[51] Deepa AR, Emmanuel WS. An efficient detection of brain tumor using fused feature adaptive firefly back propagation neural network. Multimed Tools Appl. 2019;78(9):11799-11814.

[52] Ata'a AH, Dhia A. Classification Human Brain Images and Detection Suspicious Abnormal Area. IOSR J Comput Eng. 2016;18.

Al-Kitab Journal for Pure Sciences (2024); 8(2):109-119.
https://doi.org/10.32441/kjps.08.02.p9

Al-Kitab Journal for Pure Sciences
ISSN: 2617-1260 (print), 2617-8141(online)
https://isnra.net/index.php/kjps

Effect of Some Environmental Factors and Antibiotics on the Growth of Different Species of Rhizobium

Sara Musbah Mohammed*, **Raad Hassani Sultan**

Department of Biology, College of Education for Pure Sciences, University of Mosul, Mosul, Iraq.

Corresponding Author: sara.22esp4@student.uomosul.edu.iq

Citation: Mohammed SM, Sultan RH. Effect of Some Environmental Factors and Antibiotics on the Growth of Different Species of Rhizobium. Al-Kitab J. Pure Sci. [Internet]. 2024 July. 10 [cited 2024 July. 10];8(2):109-119. Available from: https://doi.org/10.32441/kjps.08.02.p9.

Keywords: Antibiotic, Herbicide, Rhizobia, and Isolation.

Article History

Received	10 May. 2024
Accepted	13 Jun. 2024
Available online	10 July 2024

Abstract:

Six native rhizobial isolates from various cultural zones in Ninavah-Governate, Iraq, were used in this investigation. The following rhizobial strains were isolated from leguminous plant root nodules: Rhododendron japonicum SM29 from Glycin max L., Rhizobium leguminosarum bv. trifolii SM35 from Trifolium alexanrinum L., Rhizobium leguminosarum bv. viciae SM10 from Vicia faba L., Ensifer ferdii bv. Fredii SM13 from Vigna unguiclata L., Ensifer meliloti SM28 from Medicago sativa L., and Rhizobium leguminosarum bv. phaseoli SM42 from Phaseolus vulgaris L. Rhizobial bacteria were identified by the spherical, clear colonies seen after cultural investigation. Methyl red and Voges-Proskuar biochemical tests yielded negative results, but urease, catalase, indole, starch, Congo red, citrate, and motility tests yielded positive results. A high tolerance was found by the KNO_3 tolerance test.

Keywords: Antibiotic, Herbicide, Rhizobia, Isolation.

دراسة تأثير بعض العوامل البيئية والمضادات الحيوية على نمو اجناس مختلفة من *Rhizobium*

سارة مصباح محمد*، **رعد حساني سلطان**

قسم علم الأحياء، كلية التربية للعلوم الصرفة، جامعة الموصل، الموصل، العراق

sara.22esp4@student.uomosul.edu.iq, dr.raadsultan@uomosul.edu.iq

الخلاصة:

تم في هذه الدراسة عزل ستة عزلات من الرايزوبيا المحلية من مناطق مختلفة من محافظة نينوى-العراق. تم عزل هذه العزلات من العقد الجذرية من النباتات البقولية وكما يأتي:

Rhizobium leguminosarum bv. viciae SM10 من نبات الباقلاء, *Ensifer ferdii bv. Fredii SM13* من نبات اللوبيا, *Ensifer meliloti SM28* من نبات الجت, *Rhododendron japonicum SM29* من نبات فول الصويا, *Rhizobium leguminosarum bv. trifolii SM35* من نبات البرسيم والعزلة *Rhizobium leguminosarum bv. phaseoli SM42* من نبات الفاصوليا. أظهر الفحص الزرعي مستعمرات دائرية شفافة دلالة على انها بكتريا الرايزوبيوم. أظهرت الفحوصات الكيموحيوية نتيجة سالبة لاختباري احمر المثيل وفوكس-بروسكر, في حين أظهرت اختبارات اليوريز والكتاليز والأندول وتحلل النشأ و احمر الكونغو والسترات والحركة نتيجة موجبة ولجميع العزلات. اظهر اختبار تحمل ملح نترات البوتاسيوم درجة تحمل عالية لعزلات الرايزوبيا المحلية، حيث وصل الى ١٠٪ (وزن/حجم) وللعزلتين *SM10* و*SM28*. كانت جميع العزلات مقاومة للأمبسلين ٢٥ مايكروغرام/مل باستثناء العزلة *SM42* حيث أظهرت حساسية لهذا المضاد الحيوي. أعطت جميع العزلات مقاومة عالية للمبيد العشبي الغليفوسات بتركيز ٥٠ ملغم/مل.

الكلمات المفتاحية: عزل، رايزوبيا، مضادات حيوية، مبيدات عشبية.

1. Introduction:

To manage and lessen weed growth on agricultural grounds, chemicals have been employed extensively in agriculture [1]. Roughly one-third of agricultural land is treated with herbicides these days [2-4]. Because so few herbicides reach the intended organisms, the destiny of these chemicals has come under scrutiny [5, 6]. Thus, herbicides have an impact on the ecosystem's ability to operate, either directly or indirectly [7]. Glyphosate is a pre-emergence herbicide that is non-selective and is often used to eradicate undesired plants of all kinds, with a focus on weeds [8]. Since the recommended rate of glyphosate applied to the soil is based on the recommended rate for a particular location, the herbicide application must be done appropriately and by the required concentration [9]. Farmers use a lot of the chemical glyphosate to get rid of weeds. The pesticide's hazardous ingredient has the potential to infect Rhizobium bacteria, which fix nitrogen in the soil [10]. Additionally, using it in excessive doses can harm microbes, plants, and animals, which eventually deteriorates the food chain and results in nutritional deficiencies.

Particularly vitamins and minerals may also be hazardous to the body as a whole. [10] Glyphosate also has an impact on the functional characterization of plants, where beneficial bacteria are essential for the synthesis of iron and auxin siderophores, as well as for solubilizing zinc and phosphate uptake. [10] Glyphosate has a major effect on soil biology and is poisonous

to beneficial species such as earthworms and microflora. Herbicides containing glyphosate penetrate the soil through the surface of the soil or seep into it, influencing the populations of rhizobia [11]. Although the effect varies throughout species, there are multiple findings suggesting glyphosate herbicides can lower Rhizobium species populations [12]. Numerous studies have demonstrated that the nitrogen fixation process is adversely affected by nonselective glyphosate spraying, as it reduces the amount of rhizobia.

Antibiotics are small bioactive molecules that are naturally produced by microorganisms like bacteria and fungi during their secondary metabolism [13,14]. Antibiotic resistance is an ancient and naturally occurring phenomenon widespread in the environment. The rhizosphere contains a mixture of metabolically active microbial populations that compete in this environment about size, diversity, and biochemical activity. Production of antibiotics by some soil harbouring microorganisms, mainly bacteria and fungi, has been largely documented [15].

2. Materials and Methods

2.1 Extracting Rhizobial Bacteria from Root Nodules: According to Vincent [16], local rhizobial bacteria were identified from nodules produced on the hair roots of plants growing in several places in Nineveh Governorate/Iraq. Isolates began to be collected at the beginning of September for two months, and the plants were three to four weeks old. Leguminous plants come in six varieties: phaseolus, cowpea, alfalfa, soybeans, and clover. Rhizobia bacteria have a specialized symbiotic relationship with leguminous plants, as bacteria are only associated with a specific type of legume plants. The plant roots developed nodules and were washed with distilled water. After being immersed in 70% ethyl alcohol for three minutes, they were thoroughly cleaned three times with sterile distilled water. Subsequently, they were submerged in a sodium hypochlorite NaOCL solution with a 3:1 v/v water/sodium hypochlorite concentration.

After being submerged in it for fifteen minutes, the sample was thoroughly cleaned three times using sterile distilled water. It was then moved to a Petri plate with sterile filter paper inside to remove any remaining water from the nodes. Nodules were transferred to Yeast Extract Mannitol Agar (YEMA) and incubated for a duration of 24 to 48 hours at 28°C to guarantee sterilizing effectiveness. Using a sterile glass rod, sterilized nodules were crushed and then arranged in stripes on a Petri plate filled with YEMA media. The dish was then incubated for 24 to 48 hours at 28°C.

2.2 Cultural diagnosis of isolates from the area: Under the oil lens (x100) of a compound light microscope (**Figure 1**), a growth sample of the colonies was inspected for colony appearance and tested for Gram stain using a Stain Gram kit [17].

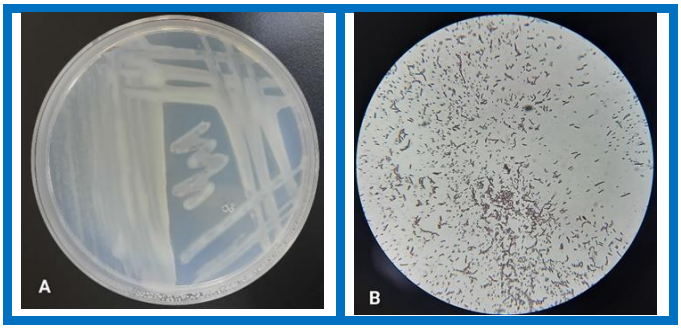

Figure 1: Isolated rhizobia colonies and cells
A: Colonies of rhizobia bacteria isolated from SM35
B: a smear of bacteria isolated from the root nodules of SM28, stained with gram stain under the oil lens

2.3 Tests using biochemistry to isolate Rhizobium bacteria: Bacterial strains obtained from the root nodules of the chosen plants were subjected to biochemical assays. The assays included Voges-Proskaur [18], Bromothymol blue [19], Congo red [16], motility [20, 21], urease, methyl red, starch degradation, catalase, Kovacs (indole) and citrate utilization [17].

2.4 Tolerance of the isolates to salt: By transferring a single culture of young rhizobial bacteria and spreading them out by plotting on YEMA medium that contains different concentrations of potassium nitrate KNO3 as follows: 2, 4, 6, 8, and 10%, and then incubating at 28°C for a while of 24–48 hours, this test was carried out to determine the ability of rhizobial isolates to grow in the presence of different concentrations of potassium nitrate KNO_3 [22].

2.5 Testing for antibiotic resistance in rhizobial isolates: To determine the growth of rhizobial isolates in the presence of the following antibiotics (µg/ml): Ampicillin, 25, Rifampin, 5, Tetracycline, 10, and Neomycin, 10. These antibiotics were produced by the Turkey Bioanalyase Company.. Using a cotton swab, tested rhizobial isolates were distributed over Mueller-Hinton agar (M.H.A.) medium before the antibiotic discs were moved in. Using sterile forceps, vital cells were extracted, spread out on a medium, and cultured for twenty-four hours at 28°C. The presence of a clear halo surrounding the antibiotic tablets was used to identify isolates of rhizobial bacteria that were sensitive and resistant to different antibiotics [23, 24].

2.6 Glyphosate's Impact on the Rhizobial Isolates' Growth: The purpose of the experiment was to show how tolerant rhizobial isolates were to glyphosate, a pesticide. YEMA medium was used to create the calculated amount of herbicide at concentrations of 0, 5, 25, and 100 mg/ml. Sterile Petri dishes were filled with the medium. Herbicide-free YEMA media was made, transferred onto sterile Petri plates, and regarded as a control. The herbicide-containing Petri dishes were used to cultivate the bacteria. For two days, plates were kept in the incubator at 28°C. The efficiency of the herbicide against rhizobial isolates was assessed by its effect on growth [25].

3. Results:

3.1 Analyzing culture and conducting biochemical testing: Following the separation of the bacteria from the plant's root nodules, convex, mucoid, semitransparent, and white colonies with smooth edges began to grow on the solid YEM medium. Under a light microscope, rhizobial cells were examined. Negative, bacilli-shaped Gram bacilli with no spores were found. **Table 1** provides a summary of the biochemical test results. The findings showed that the Vogus-Proskaour and methyl red tests yielded negative results for every isolated bacterium. On the other hand, positive results were obtained from the motility, urease, catalase, indole starch, Congo red, and bromothymol blue tests **Figure 2**.

Table 1: Biochemical tests for local rhizobial isolates.

	SM10	SM13	SM28	SM29	SM35	SM42
Methyl red	-	-	-	-	-	-
Urease	+	+	+	+	+	+
Catalase	+	+	+	+	+	+
Indole	+	+	+	+	+	+
Starch	+	+	+	+	+	+
Congo red	+	+	+	+	+	+
BTB	+	+	+	+	+	+
V-P	-	-	-	-	-	-
Citrate	+	+	+	+	+	+
Motility	+	+	+	+	+	+

BTB: Bromothymol blue; V-P: Voges-Proskaur

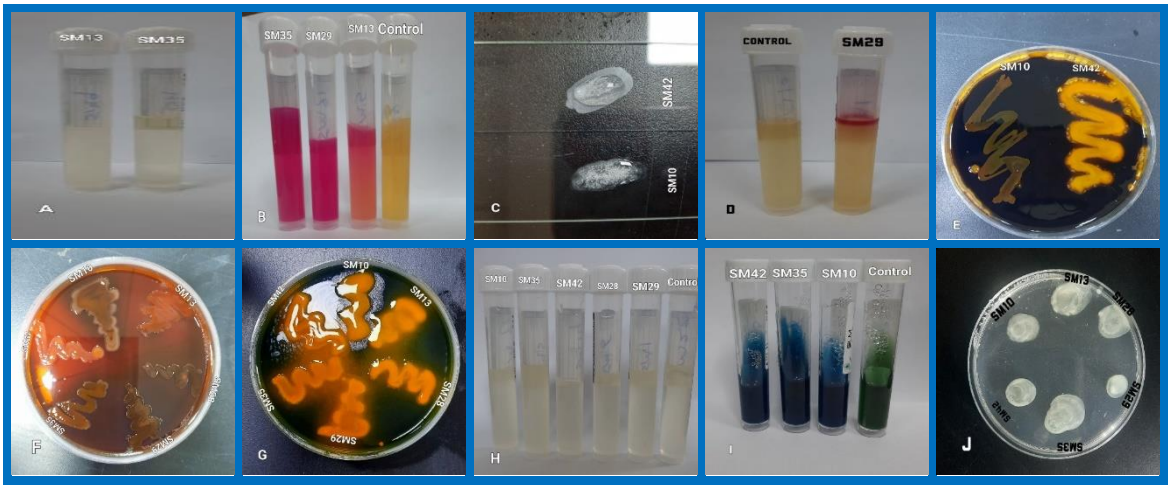

Figure 2: Biochemical test.

A- Methyl red test, B- Urease test, C- Catalase test,D- Indole test , E- Starch test, F- Congo red test , G- BTB test, H- V-P test,I- Citrate test, J- Motility test.

The KNO_3 tolerance results are displayed in **Table 3**. Different rhizobial isolates responded differently to this stress in the YEMA medium with varying KNO_3 concentrations. Except for isolates SM35 and SM42, which displayed a decline in growth at a concentration of 6 and 10% (w/v), rhizobial isolates had very robust growth at KNO_3 concentrations of 2, 4, 6, and 8%

(W/V). Two of the six rhizobial isolates, SM10 and SM28, demonstrated robust growth at a concentration of 10% (w/v).

Table 2: Effect of potassium nitrate on growth of Rhizobium

	KNO_3 Concentrations % (w/v)				
Isolate No.	2	4	6	8	10
SM10	+++	+++	+++	+++	++
SM13	+++	+++	+++	+++	+
SM28	+++	+++	+++	++	++
SM29	+++	+++	+++	+++	+
SM35	+++	+++	++	+	+
SM42	+++	+++	++	+	+

(+++) very good growth, (++) good growth, (+) medium growth, (-) No growth

About the antibiotic sensitivity test, isolate SM42 demonstrated inhibition zones 13, 9, 13, and 11 mm to ampicillin (25µg/ml), rifampin (5µg/ml), tetracycline (10µg/ml), and neomycin (10µg/ml), respectively. All other isolates demonstrated resistance to ampicillin (25µg/ml). Tetracycline (10µg/ml) and Neomycin (10µg/ml) did not affect the isolates SM28 and SM29. While the remaining isolates displayed varying levels of sensitivity to various antibiotics, strain SM35 demonstrated resistance to Rifampin (5 µg/ml), isolates SM29 and SM35 were more susceptible to antibiotics, while isolate SM42 was more sensitive to these antibiotics **Figure 3**.

Table 3: Local rhizobial isolates' susceptibilities and resistance to the drugs under study.

	Antibiotic concentrations µg/ml			
Isolate No.	Ampicillin 25	Rifampin 5	Tetracycline 10	Neomycin 10
SM10	R	13*	15	12
SM13	R	10	20	10
SM28	R	10	13	R
SM29	R	18	R	11
SM35	R	R	17	13
SM42	13	9	13	11

*: Millimeters (mm) represent the inhibition zone; R stands for resistant.

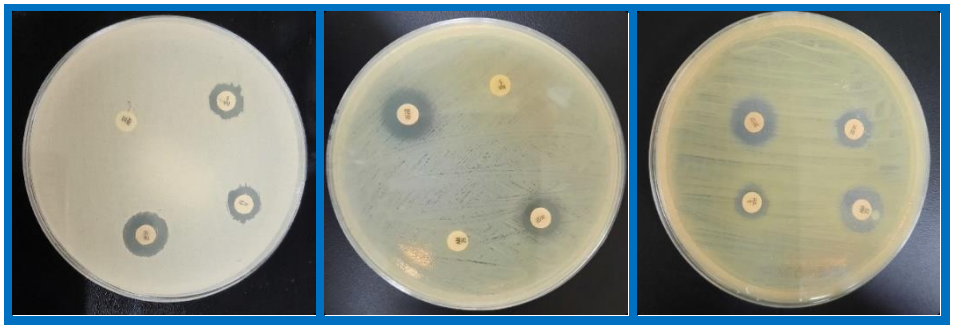

A B C

Figure 3: shows antibiotic testing on rhizobia isolates.
A-SM10, B-SM35 and C-SM42.

Table 5 displays the findings of the rhizobial isolates' tolerance to various glyphosate concentrations. Following a 72-hour incubation period, rhizobial isolates demonstrated their

capacity to develop at glyphosate doses of 0, 25, and 50 mg/ml (Figure 4). On YEMA plates treated with Glyophsate at a concentration of 100 mg/mL, none of the rhizobial isolates grew.

Table 4: Effect of herbicide Glyphosate on rhizobial isolates

	Concentration of Glyphosate mg/ml			
Isolate No.	0	25	50	100
SM10	+++	+++	+++	-
SM13	+++	+++	+++	-
SM28	+++	+++	+++	-
SM29	+++	+++	+++	-
SM35	+++	+++	+++	-
SM42	+++	+++	+++	-

(+++) very good growth, (++) good growth, (+) medium growth, (-) No growth

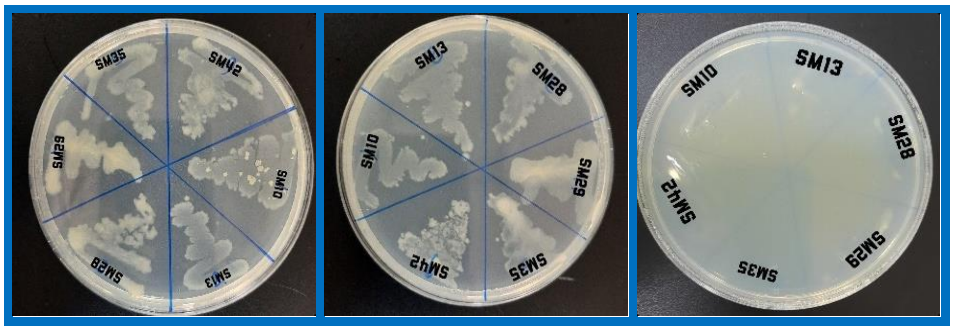

A:25 mg/ml B:50 mg/ml C:100 mg/ml

Figure 4 shows the growth of the following rhizobial isolates after two days of incubation on YMA medium supplemented with glyphosate herbicide (mg/ml): A-25, B-50, and C-100.

4. Discussion:

Table 5 lists the isolated local strains, the names of leguminous plants in Table 5 were based on the scientific names according to plant taxonomists. The isolate numbers are the name of the model that the researchers chose for this isolate.

Table (5): Rhizobial isolates, plant sources, and rhizobial species occupied its nodules.

Isolate No.	Plant source	Genus and species of rhizobia
SM10	*Vicia faba* L.	*Rhizobium leguminosarum* bv. *viciae*
SM13	*Vigna unguiclata* L.	*Ensifer ferdii* bv. *fredii*
SM28	*Medico sativa* L.	*Ensifer meliloti*
SM29	*Glycin max* L.	*R. japonicum*
SM35	*Trifolium alexanrinum* L.	*R. leguminosarum* bv. *trifolii*
SM42	*Phaseolus vulgaris* L.	*R. leguminosarum* bv. *phaseole*

Rhizobial isolates from the root nodules of leguminous plants used in this investigation had morphological traits common to Rhizobial genera. These isolates' traits included being bacilli and Gram stain-negative **[17, 26, 27]**. The tests for urease, catalase, indole, starch hydrolysis, motility, citrate consumption, Congo dye pick-up, and BTB were likewise positive for all isolates. In contrast, the isolates' findings from the Voges-Proskaur and methyl red tests were negative. According to this study, there were some variations in the biochemical examination

of the rhizobial isolates compared to previous investigations [28]. Additionally, the results of the capacity of local rhizobial isolates to grow at various KNO_3 concentrations varied. This outcome is consistent with the findings of Bed and Naglot [22], who were able to identify *Rhizobium legusarum* bv. *trifolii*.

Variations in antibiotic sensitivity or resistance were shown by the test results. Results of this study were consistent with other researchers' results regarding resistance to Ampicillin, and sensitivity to Rifampin, Tetracycline, and Neomycin [29, 30, 31, 32]. There are many mechanisms in the resistance of rhizobial isolates to antibiotics and these mechanisms were considered to be active. Rhizobial bacteria have specific protein carriers on the outer membrane. Another mechanism is a modification of biosynthetic pathways inside rhizobial bacteria as well as the production of enzymes acting against the target which is an antibiotic. Permeability of the cell wall of rhizobial bacteria is another defined choice for rhizobia to avoid antibiotic effects [33]. Studying of resistance and sensitivity of rhizobial isolates to antibiotics has double benefits in genetic and academic studies [34]. Secondly, such studies provide insight into how rhizobia as a non-pathogenic bacteria, becomes antibiotic-resistant in soil. The explanation for this statement is that rhizobia can receive R plasmids from different bacterial species through a mechanism known as horizontal gene transfer which occurs between pathogenic and non-pathogenic bacterial conjugation [35].

The herbicide experiment performed on various rhizobium isolates also revealed that while the isolates were sensitive to the herbicide and displayed growth inhibition at a concentration of 100 mg/ml, all isolates demonstrated their ability to tolerate a concentration of 25 and 50 mg/ml of the herbicide [16]. The isolates grew best at doses of 25 and 50 mg/ml, with 100 mg/ml showing the greatest growth effect [22]. Therefore, the impact of the herbicide, its concentration, and the local meteorological circumstances all affected the proliferation of rhizobial bacteria and their capacity to fix nitrogen [36].

5. Conclusion:

Different processes enable rhizobial bacteria to withstand high salt concentrations and pesticides. Poison-resistant plasmids and the production of efflux pumps are two examples of these methods. To completely comprehend the mechanisms underlying Rhizobium's tolerance capacities and investigate the possible uses of these bacteria under these circumstances, more research is required.

Acknowledgement:

The researchers acknowledge the Department of Biology, College of Education for Pure Sciences, University of Mosul, Mosul, Iraq, for its valuable contribution to the enhancement of the quality of this research effort.

6. References:

[1] Souza, M. C. O., Cruz, J. C., Cesila, C. A., Gonzalez, N., Rocha, B. A., Adeyemi, J. A., Nadal, M., Domingo, J. L., and Barbosa, F. Recent trends in pesticides in crops: A critical review of the duality of risks and benefits and the Brazilian legislation issue. Environ. Res. 2023; 115811.

[2] Padgette, S. R., Re, D. B., Barry, G. F., Eichholtz, D. E., Xavier, D., Fuchs, R. L., Kishore, G. M., and Fraley, R. T. New weed control opportunities: development of soybeans with the Roundup Ready TM gene. In Herbicide-Resistant Crops, 53–84. (CRC Press, 2018).

[3] Stalker, D. M., Kiser, J. A., Greg, B., Bruce, C., and Houck, C. M. Cotton weed control using the BXNTM system. In Herbicide-Resistant Crops, 93–106. (CRC Press, 2018).

[4] Tudi, M. et al. Agriculture development, pesticide application, and its impact on the environment. Int. J. Environ. Res. Public Health. 2021;18 (3): 1112.

[5] Pimentel, D. Amounts of pesticides reaching target pests: Environmental impacts and ethics. J. Agric. Environ. Ethics. 1995; 8: 17–29.

[6] Richmond, M. E. Glyphosate: A Review of its Global Use, Environmental Impact, and Potential Health Effects on Humans and Other Species J. Environ. Stud. Sci. 2018; 8: 416-434.

[7] Ruuskanen, S., Fuchs, B., Nissinen, R., Puigbò, P., Rainio, M., Saikkonen, K., Helander, M. Ecosystem consequences of herbicides: the role of the microbiome Trends Ecol. Evol. 2023

[8] Harries, M., Flower, K. C., Scanlan, C. A., Rose, M. T., and Renton, M. Interactions between crop sequences, weed populations, and herbicide use in Western Australian broadacre farms: Findings of a six-year survey. Crop Pasture Sci. 2020; 71(5): 491–505.

[9] Badowski, M. & Sadowski, J. Poziom pozostalosci 2, 4-Dw roslinach trwalych uzytkow zielonych. Prog. Plant Prot. 2008; 48(4): 1185–1189.

[10] Singh, S. et al., Herbicide glyphosate: Toxicity and Microbial Degradation. Int. J. Environ. Res. Public Health 2020; 17(20): 7519.

[11] Sharma, S., Kumar, S., Kumar, V., and Sharma, R. Pesticides and vegetables: Ecological and metabolic fate with their field and food significance. Int. J. Environ. Sci. Technol. 2021; 1–26.

[12] Drouin, P., Sellami, M., Prevost, D., and Fortin, J. Antoun, H. Tolerance to agricultural pesticides of strains belonging to four genera of Rhizobiaceae. J. Environ. Sci. Health Part B. 2010; 45(8): 757–765.

[13] O'Brien, J.; Wright, G.D. An ecological perspective of microbial secondary metabolism. Curr. Opin. Biotechnol. 2011, 22, 552–558.

[14] Okada, B.K.,Seyedsayamdost, M.R. Antibiotic dialogues: Induction of silent biosynthetic gene clusters by exogenous small molecules. FEMS Microbiol. Rev. 2017, 41, 19–33.

[15] Shahriar, A., Kobra, A. T., Shomi, F. Y., Emran, T. B., Mallick, J., & Dutta, M. Presumptive correlation between phenotypic, genotypic and symbiotic diversities with antibiotic susceptibility traits of rhizobial strains from plant legumes. environment, 2020, 18, 19.

[16] Vincent, J. M. A. Manual for the Practical Study of the Root Nodule Bacteria. I. B. P. Handbook No. 15 Oxford: Blackwell Scientific Publication, Oxford, 1970, p. 113–131.

[17] Baghel, D., Gupta, S.B., & Chowdhury, T. Characterization and Evaluation of Native Rhizobium of Groundnut (*Arachis hypogaea* L.) and Soybean (*Glycine max* L.). Journal of Experimental Agriculture International, 2024, 46.5: 500-506.

[18] Mahon, C. R., Lehman, D. C., and Manuselis, G. Textbook of Diagnostic Microbiology-e-Book. Elsevier Health Sciences 2018.

[19] Pervin, S., Jannat B., Sanjee, S., and Farzana, T. Characterization of *rhizobia* from the root nodule and rhizosphere of *Lablab purpureus* and *Vigna* sinensis in Bangladesh. Turkish J. of Agri-Food Sci. Tech. 2017; 5(1): 14–17.

[20] Collee, J. G., Marmion, B. P., Fraser, A. G., Simmons, A. Mackie, and McCarteny, Practical Medical Microbiology. 14th ed., Chrchill Livingstone, New York, U.S.A. 1996, p. 263–98.

[21] Harley, J. P., & Prescott, L. M., "Laboratory Exercises in Microbiology,"5th ed., WCB/McGraw-Hill, U.K. 2002.

[22] Bed, M.K., and Naglot, A. Characterization of *Rhizobium* isolated from root nodules of *Trifolium alexandrinum*. J. Agri. Tech., 2011, 7(6): 1705–1723.

[23] Ramaroson, M., Guillou, S., Rossero, A., Rezé, S., Anthoine, V., Moriceau, N., Zagorec, M. Selection procedure of bioprotective cultures for their combined use with high pressure processing to control spore-forming bacteria in cooked ham. Int. J. Food Microbiol. 2018; 276: 28–38.

[24] Weinstein, M. P., Patel, J. B., Bobenchik, A., Campeau, S., Cullen, S. K., and Gallas, M. F. Clinical and laboratory standards institute performance standards for antimicrobial susceptibility testing. 2019; 88–9.

[25] Shankar, P.V., Shaikh, N.R., and Vishwas, P.S. Effect of Different Herbicides on the Nodulation Property of Rhizobial Isolates. Uni J. Environ Res. and Tech. 2012; 2:293-299.

[26] Hewedy, O. A., Eissa, R. A., Elzanaty, A. M., Nagaty, H. H., and Abd Elbary, M. I. Phenotypic and genotypic diversity of Rhizobia nodulating Faba beans from various Egyptian locations. J. Bioprocess. Biotech. 2014; 4(5): 1.

[27] Niste, M., Vidican, R., Puia, C., Rotar, I., and Pop, R. Isolation and biochemical characterization of *Rhizobium leguminosarum bv. trifolii* and *Sinorhizobium meliloti* using API 20 NE and API 20 E. Bull. USAMV Ser. Agric. 2015; 72:173.

[28] Bhargava, Y., Murthy, J. S. R., Rajesh Kumar, T. V., and Narayana Rao, M. Phenotypic, stress tolerance, and plant growth-promoting characteristics of rhizobial isolates from

selected wild legumes of the semiarid region of Tirupati, India. Adv. Microbiol. 2016; 6(1):1–12.

[29] Mihaylova, S.; Genov, N. and Moore, E. Susceptibility of environmental strains of Rhizobium radiobacter to antimicrobial agents. World Appl. Sci. J., 2014; 31(5): 859-862.

[30] Dhull, S.; Singh, K. and Gera, R. Intrinsic antibiotic resistance (IRA) of different rhizobial strains isolated from root nodules of *Cyamopsis tetragonoloba* L. Taub. Chem. Sci. Rev. Lett., 2018; 6(21): 88-93.

[31] Khalid, R.; Zhang, X.X.; Hayat, R. and Ahmed, M. Molecular characteristics of rhizobia isolated from *Arachis hypogaea* grown under stress environ. Sustainability, 2020; 12(15): 6259-6267.

[32] Abdell-Hakim, M.M.; Dakhly, O.F and Sameh, A.M. Characterization of some plant growth promoting rhizobacteria isolated from sugar beet rhizosphere. J. Mod. Res., 2022, 4: 6-13.

[33] Naamala, J.; Jaiswal, S.K. and Dakora, F.D. Antibiotics resistance in *Rhizobium*: type, process, mechanism and benefit for agriculture. Curr. Microiol., 2016; 72(6): 804-816.

[34] Prasad, C.K.; Vineetha, K.E.; Hassani, R. and Randhawa, G.S. Isolation and symbiotic characterization of aromatic amino acid auxotroph of *Sinorhizobium meliloti*. 2000. Indian J. Exp. Biol., 83: 1041-1049.

[35] Macedo, G.; Olesen, A.K.; Maccario, L.; Leal L.H.; Maas, D.H.P.; Heederik, D. and Schmitt, H. Horizontal gene transfer of an IncP1 plasmid to soil bacterial community introduced by *Escherichia coli* through manure amendment in soil microcosms. Environ. Sci. Technol., 2022, 56(16): 11398-11408.

[36] Sprout, S. L., Nelson, L., and Germida, J.J. Influence of metribuzin on the *Rhizobium leguminosarum* lentil (*Lens culinaris*) symbiosis. Can J. Microbiol., 1992; 38:343–349.

Al-Kitab Journal for Pure Sciences (2024); 8(2):120-124.
https://doi.org/10.32441/kjps.08.02.p10

Al-Kitab Journal for Pure Sciences
ISSN: 2617-1260 (print), 2617-8141(online)
https://isnra.net/index.php/kjps

Levels Estimation of Iron, Zinc and Copper in the Serum of Children Infected with Giardiasis

Huda Mawlood Taher*

Department of Biology, College of Education for Pure Sciences, Kirkuk University, Kirkuk, Iraq

Corresponding Author: huda.mawlood@uokirkuk.edu.iq

Citation: Taher HM. Levels Estimation of Iron, Zinc and Copper in the Serum of Children Infected with Giardiasis. Al-Kitab J. Pure Sci. [Internet]. 2024 July. 11 [cited 2024 July. 11];8(2):120-124. Available from: https://doi.org/10.32441/kjps.08.02.p10.

Keywords: Giardiaiasis, Iron, Zinc, Copper, Children.

Article History

Received	18	May.	2024
Accepted	24	Jun.	2024
Available online	11	July	2024

Abstract:

Giardiasis is an infection in the small intestine, it's caused by a microscopic parasite called Giardia lamblia. In this study, we examined stool samples for 75 children, 1–12 years old during the period from August to November 2023 from children who attended a pediatric hospital in Kirkuk city, and we estimated the levels of iron, zinc, and copper in these children. A stool examination was done for all samples to detect cysts or trophozoites of Giardia lamblia. Also, we measured the levels of iron, zinc, and copper by atomic absorption spectrophotometer. The highest rate of parasite infection (66.7%) was recorded in the age group (4–6)years old. Serum iron and copper levels considerably decreased ($P<0.05$) in comparison to the control group. It was noted that most of the infected children suffer from abdominal pain with intermittent diarrhea.

Keywords: Giardiaiasis, Iron, Zinc, Copper, Children.

تقدير مستويات الحديد والزنك والنحاس في مصل الأطفال المصابين بالجيارديا

هدى مولود طاهر*

قسم الأحياء ، كلية التربية للعلوم الصرفة ، جامعة كركوك ، كركوك ، العراق

huda.mawlood@uokirkuk.edu.iq

الخلاصة:

الجيارديا هي عدوى في الأمعاء الدقيقة، وتسببها طفيلي مجهري يسمى الجيارديا اللامبلية. فحصنا في هذه الدراسة عينات براز لـعدد ٧٥ طفلا تتراوح أعمارهم بين ١ و ١٢ عاما خلال الفترة من أغسطس إلى نوفمبر ٢٠٢٣ من الأطفال الذين حضروا إلى مستشفى الأطفال في مدينة كركوك، وقمنا بتقدير مستويات الحديد والزنك والنحاس لدى هؤلاء الأطفال. تم إجراء فحص البراز لجميع العينات للكشف عن الكيس أو التروفوزويت من الجيارديا اللامبلية، أيضاً قمنا بقياس مستويات الحديد والزنك والنحاس بواسطة مقياس الطيف الضوئي للامتصاص الذري. أعلى معدل للإصابة بالطفيليات (٦٦,٧٪) مسجل في الفئة العمرية (٤-٦) سنوات. انخفضت مستويات الحديد والنحاس في الدم بشكل كبير ($P<0.05$) مقارنة بالمجموعة الضابطة، ولوحظ أن معظم الأطفال المصابين يعانون من آلام في البطن مع إسهال متقطع.

الكلمات المفتاحية: داء الجيارديا، الحديد، الزنك، النحاس، الأطفال.

1. Introduction:

Giardiasis is a popular infection by protozoa and can cause clinical symptoms from acute or chronic diarrhea, malabsorption of minerals and fat, intestinal irritation, anorexia, and nausea, it may also cause growth and developmental retardation to asymptomatic [1]. Giardiasis is caused by a parasite called *Giardia lamblia*, it has two stages in its life cycle, the trophozoite with pear-shaped, two nuclei, four pairs of flagella, and a suction disc used to attach to the intestinal wall and the cyst with oval shape strong walls, four nuclei and numerous internal fibers, transmission the infection happens by ingestion water and food contaminated with the cyst [2]. Most infected people with giardiasis do not show many symptoms [3]. Children experience symptomatic infections more frequently than adults due to their weakened immune systems and propensity for recurrent infections. The patient's symptoms vary depending on whether they have an acute or chronic Giardia infection [4]. Patients with giardiasis frequently have malabsorption syndrome and abnormalities in the levels of serum iron, zinc, and copper [5]. Iron, copper, and zinc are essential micronutrients for growth, development, and reproduction, and deficiency of these micronutrients can cause major impairments to enzymatic, physiological, and cellular functions [6].

The current study aims to assess the spread of *Giardia lamblia* in children attending to general pediatric hospital for the period between August to November 2023 and to find out the extent of the impact of the infection with Giardiasis on serum levels of iron, zinc, and copper.

2. Material and Methods

This study was carried out in the laboratory of a pediatric hospital in Kirkuk City from August to November 2023. Stool samples were collected from 75 children aged from 1 to 12 years old, where the samples were collected in sterilized stool cups, branded with the name and

time of collection. The fecal examination was done for all samples to detect Giardia cyst and trophozoite using direct wet smear and formol ether sedimentation concentration technique, it was carried out according to Garcia [7]. 50 positive cases for giardiasis were recorded and 25 cases were free of *Giardia lamblia* or another parasitic infection which was considered as the control group. Blood samples were collected from all groups and centrifugation was done to obtain serum to estimate iron, zinc, and copper levels by atomic absorption spectrophotometer. During the previous four months, both groups did not take any vitamins or mineral supplements.

ANOVA was used to analyze the results statistically and display the significant difference between the two groups, infected and control.

3. Results and Discussion

Out of 75 stool samples examined by different techniques, 50 were positive for *Giardia lamblia*, and the total infectivity rate was 66.7%. The percentage of *Giardia* infection among males (38.7%) was higher than in females (28%); results revealed that there are no significant variances between males and females in infected groups **Table 1**. These results agree with [8] and [9], and disagree with [10].

Table (1): Prevalence of *Giardia lamblia* according to sex.

Sex	No. of stool samples examined	Percentage of stool samples examined	No. of a positive sample	Percentage of positive sample
Males	42	56	29	38.7
Females	33	44	21	28
Total	75	100	50	66.7

In the infected group with *Giardia lamblia*, 44% of cases were between 4-6 years old which presents the highest rate, while the lowest percentage 16% recorded in the age group between 10-12, **Table 2**. The results of this study agree with [8] and [11]. A high average of *Giardia lamblia* infection has been recorded in some communities up to 50% in children under 5 years old [12], because of the undeveloped immune system which led to exposure to different pathogens such as parasites, bacteria, viruses [13], also health hygiene and education, lower socioeconomic status especially among migrants enhanced infectious diseases [14].

Table (2): Prevalence of *Giardia lamblia* according to age group

Age groups	No. of the infected group	percentage of the infected group	percentage of control group	No. of the control group
1-3	9	18	3	12
4-6	22	44	12	48
7-9	11	22	4	16
10-12	8	16	6	24
Total	50	100	25	100

The serum Fe, Zn and Cu concentrations were found to be (Fe: 41.24±6.21 µg/dL), (Zn: 79.32±5.78 µg/dL) and (Cu: 58.84±5.97 µg/dL) in children with giardiasis, which were higher than control (Fe: 78.91±6.73 µg/dL), (Zn: 80.77±6.22 µg/dL) and (Cu: 89.34±6.71 µg/dL), **Table 3**.

Table (3): Levels of iron, zinc, and copper in the serum of the infected group and control

Minerals	Infected group Mean± SD	Control group Mean± SD
Iron	41.24±6.21	78.91±6.73
Zinc	79.32±5.78	80.77±6.22
Copper	58.84±5.97	89.34±6.71

In this study, serum iron and copper concentration significantly declined in the infected group when related to the control group; these results agree with **[15]**. Malabsorption-associated iron lack is expected in patients with *Giardia lamblia*, which might be protecting in the formation of the hydroxyl radical **[16]**. In the small intestine, copper is absorbed in a smaller amount through the large intestine **[17]**. There was no significant variance in the level of serum Zinc between the group infected with giardiasis and the control groups, accordingly, this study agrees with **[18]** and disagrees with **[6]**, that giardiasis caused poor absorption of zinc **[19]**. A high percentage of zinc levels could be seen in acute infections while Chronic infections could cause a lasting decline in serum zinc levels **[20]**.

4. Conclusion

This study recorded the highest rate of parasite infection in the age group of 4-6 years old, Symptoms in the infected groups were recurrent diarrhea, abdominal pain, and weight loss. Serum levels of iron and copper significantly declined in the children infected with giardiasis, whereas no significant difference was detected in the serum zinc levels between the infected and control groups.

5. References

[1] Coles CL, Levy A, Dagan R, Deckelbaum RJ, Fraser D. Risk factors for the initial symptomatic giardia infection in a cohort of young Arab-Bedouin children. Ann Trop Paediatr. 2009;29:291–300.

[2] Brooks GF, Carroll KC, Butel JS, Morse SA, Mietzner TA. Jawetz, Melnick, and Adelberg's Medical Microbiology. 26th ed. McGrew-Hill Companies; 2013. p. 719-720.

[3] Farthing MJ. New perspectives in giardiasis. J Med Microbiol. 1992;37:1–2.

[4] Parija SC. Intestinal, oral and genital flagellates. In: Textbook of Medical Parasitology (Protozoology and Helminthology). 2nd ed. All India Publisher and Distributor, Chennai; 2004. p. 62–70.

[5] Karakas Z, Demirel N, Tarakcioglu M, Mete N. Serum zinc and copper levels in southeastern Turkish children with giardiasis or amebiasis. Biol Trace Elem Res. 2001;84:11–18.

[6] Ertan P, Yereli K, Kurt O, Balcioglu IC, Onag A. Serological levels of zinc, copper and iron elements among Giardia lamblia infected children in Turkey. Pediatr Int. 2002;44:286–288.

[7] Garcia LS. Laboratory methods for diagnosis of parasitic infections. In: Baron EJ, Finegold SM, editors. Bailey and Scott's Diagnostic Microbiology. 8th ed. St. Louis: C. V. Mosby; 1990. p. 776–861.

[8] Khana LTY, Fouad PS, Haddad DN. Study on prevalence of Giardia lamblia among patients attending Pediatric Hospital in Kirkuk City and its effect on some hematological parameters. Hospital. 2017;7(4):71-73.

[9] Alsadoon Z, Whaeeb ST, Abduwahed TK. The effect study of the gender and age on prevalence Giardiasis in Baghdad Governorate-Iraq. Mater Today Proc. 2021;24:10-2.

[10] Al Saeed AT, Issa SH. Frequency of Giardia lamblia among children in Dohuk, northern Iraq. EMHJ-Eastern Mediterranean Health Journal. 2006;12(5):555-561.

[11] Mohammed BA, Rasheed ZK, Jihad LJ, Abass KS. Frequency of Giardia lamblia among Iraqi children in Kirkuk governorate. Systematic Reviews in Pharmacy. 2020;11(12):1909-1911.

[12] Hawrelak J. Giardiasis: pathophysiology and management. Altern Med Rev. 2003;8:129–142.

[13] Saldiva SR, Silveira AS, Philippi ST, Torres DM, Mangini AC, Dias RM, et al. Ascaris-Trichuris association and malnutrition in Brazilian children. Paediatr Perinat Epidemiol. 1999;13:89–98.

[14] Ulukanligil M, Seyrek A. Demographic and socio-economic factors affecting the physical development, haemoglobin and parasitic infection status of school children in Sanliurfa province, Turkey. Pub Health. 2004;118:151-158.

[15] Squitti R, Lupoi D, Pasqualetti P, Dal Forno G, Vernieri F, Chiovenda P, et al. Elevation of serum copper levels in Alzheimer's disease. Neurology. 2002;59:1153–1161.

[16] Culha G, Sangun MK. Serum levels of zinc, copper, iron, cobalt, magnesium, and selenium elements in children diagnosed with Giardia intestinalis and Enterobiosis vermicularis in Hatay, Turkey. Biol Trace Elem Res. 2007;118:21–26.

[17] Delibas N, Aydemir M, Ayata A, Demirci M, Tarhan V. Serum Fe, Zn, Cu and SOD activity levels in children with giardiasis. Acta Parasitol Turcica. 1996;20:25–9.

[18] Demirci M, Delibas N, Altuntas I, Oktem F, Yonden Z. Serum iron, zinc and copper levels and lipid peroxidation in children with chronic giardiasis. J Health Popul Nutr. 2003;21:72–75.

[19] Roxstrom-Lindquist K, Palm D, Reiner D, Ringqvist E, Svard SG. Giardia immunity—an update. Trends Parasitol. 2006;22:26–31.

[20] Gunduz Z, Yavuz I, Koparal M, Kumandas S, Saraymen R. Serum and cerebrospinal fluid zinc levels in children with febrile convulsions. Acta Paediatr Jpn. 1996;38:237–41.

Al-Kitab Journal for Pure Sciences (2024); 8(2):125-137.
https://doi.org/10.32441/kjps.08.02.p11

Al-Kitab Journal for Pure Sciences
ISSN: 2617-1260 (print), 2617-8141(online)

https://isnra.net/index.php/kjps

Benzimidazole and Its Derivatives: Exploring Their Crucial Role in Medicine and Agriculture: A Short Review

Sarah Basil Fawzi[1], Khalid Younis Zainulabdeen[1], Emad Abdul-Hussain Yousif[1]
Husnun Amalia Enus Yunus[2], Nany Hairunisa Muhaini Umar[3]

[1]Department of Chemistry, College of Science, Al-Nahrain University, Baghdad, Iraq
[2]Departement of Ophthalmology, Faculty of Medicine, Universitas Trisakti, Jakarta, Indonesia
[3]Department of Occupational Medicine, Faculty of Medicine, Universitas Trisakti, Jakarta, Indonesia

Corresponding Author: emad_yousif@nahrainuniv.edu.iq

Citation: Fawzi SBF, Zainulabdeen KY, Yousif EA-H, Yunus HAE, Umar NHM. Benzimidazole and Its Derivatives: Exploring Their Crucial Role in Medicine and Agriculture: A Short Review. Al-Kitab J. Pure Sci. [Internet]. 2024 Jul. 11 [cited 2024 Jul. 11];8(02):125-37. Available from: https://isnra.net/index.php/kjps/article/view/1160 https://doi.org/10.32441/kjps.08.02.p11.

Keywords: Benzimidazole, Derivatives, Medicine, Agriculture.

Article History

Received	15	Apr.	2024
Accepted	12	Jun.	2024
Available online	11	July	2024

Abstract:

Benzimidazole and its structural analogues have garnered significant attention across diverse disciplines, including the fields of medicine and agriculture, owing to their remarkable versatility and immense potential. This review article aims to elucidate the multifaceted importance of benzimidazole-based compounds and their derivatives within these spheres. The paper starts by establishing the pivotal role of benzimidazoles in human health and pharmaceutical applications. A comprehensive examination of their therapeutic utility in treating and managing various diseases is undertaken, underscoring the compounds' potent biological activities and clinical relevance. Furthermore, the review focused on the applications of benzimidazole-based compounds as powerful fungicides and pesticides within the agricultural sector. The discussion covers the mechanistic underpinnings of their efficacy, formulation challenges, and regulatory considerations surrounding their deployment in the agrochemical industry. This paper aims to demonstrate the extensive applications of these heterocyclic moieties and their derivatives in medicine and farming. The in-depth analysis presented herein is intended to facilitate a deeper understanding of the versatility and importance of benzimidazole compounds, thus enriching future research and development endeavors within these critical domains.

Keywords: Benzimidazole, Derivatives, Medicine, Agriculture.

استكشاف الدور المهم للبنزيميدازول ومشتقاته: في الطب والزراعة: مراجعة قصيرة

سارة باسل فوزي[١]، خالد يونس زين العابدين[١]، عماد عبد الحسين يوسف[١]، حسنون أماليا اونس يونس[٢]، ناني خير النسا مهيني عمر[٣]

[١]قسم الكيمياء، كلية العلوم، جامعة النهرين، بغداد، العراق
[٢]قسم طب العيون، كلية الطب، جامعة تريساكتي، جاكرتا، إندونيسيا
[٣]قسم طب العمل، كلية الطب، جامعة تريساكتي، جاكرتا، إندونيسيا

sarah.mchs24@ced.nahrainuniv.iq, khalid.waleed21@nahrainuniv.edu.iq, emad_yousif@nahrainuniv.edu.iq, husnun_a@trisakti.ac.id, nanyhairunisa@trisakti.ac.id

الخلاصة:

البنزيميدازول ومشتقاتها هي مركبات متعددة الاستخدامات تظهر تطورا كبيرا في العديد من المجالات، بما في ذلك الطب والزراعة. يقدم هذا البحث للقارئ أهمية البنزيميدازولات في مجالات مختلفة. بينما يتم سرد التطبيقات الصحية والصيدلانية لفحص وعلاج الأمراض للتأكيد على أهمية البنزيميدازولات، حيث يتم مناقشة تطبيقاتها في الزراعة كمبيدات فعالة للفطريات والحشرات أيضًا. من خلال تقديم آلية العمل التركيب وتنظيم المركبات المعتمدة على البنزيميدازول. ويهدف التحليل المتعمق المقدم هنا إلى تسهيل فهم أعمق لتنوع وأهمية مركبات البنزيميدازول، وبالتالي إثراء مساعي البحث والتطوير المستقبلية في هذه المجالات الحاسمة.

الكلمات المفتاحية: البنزيميدازول، المشتقات، الطب، الزراعة.

1. Introduction:

1.1 Definition and Structure of Benzimidazole: Benzimidazole is a class of heterocyclic aromatic compounds characterized by the fundamental structural feature of a six-membered benzene ring fused to a five-membered imidazole ring [1]. This unique structure gives benzimidazole compounds various pharmacological properties, making them valuable in biological and clinical applications [1]. Benzimidazoles have shown efficacy as anticancer, antimicrobial, antiparasitic, analgesic, antiviral, and antihistamine agents [1]. They are widely used in the treatment of cardiovascular diseases, neurological disorders, endocrinological conditions, and ophthalmic problems [1-5].

The synthesis of benzimidazoles typically involves the fusion of benzene with an imidazole moiety [1]. The numbering system for benzimidazole according to IUPAC standards is depicted in **Figure 1** [6]. Benzimidazoles with a hydrogen atom attached to nitrogen in the 1-position are easy to tautomerize. This basic "6 + 5" heterocyclic structure is shared by other important molecules found in nature like adenine and guanine, which are essential building blocks for biopolymers [2].

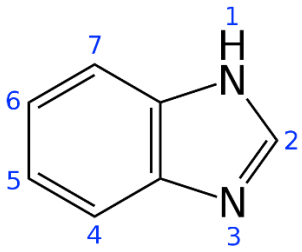

Fig. 1 benzimidazoles structure [6]

The exceptional properties of benzimidazole compounds, such as improved stability, bioavailability, and notable biological activity, have led to their growing attention **[7]**. Omeprazole, bendamustine, albendazole, and mebendazole are among the benzimidazole drugs of note. Researchers have conducted extensive research on these compounds in recent years, focusing on their synthesis methods, mechanisms of action, structural aspects, and pharmacological applications **[8]**.

The importance of benzimidazole as a pharmacophore in medicinal chemistry and drug discovery has been well established. The benzimidazole moiety is a substructure present in numerous significant compounds that are renowned for their diverse biological activities [7-9]. There are different ways to make different benzimidazole derivatives by adding functional groups to one or more positions on the benzimidazole ring **[10]**· The administration of an additional quantity of benzimidazole and its derivatives has exhibited a diverse array of biological and pharmacological effects, including antitumor, antiviral, and antiparasitic activities **[11]**. They play a crucial role in the development of effective pharmaceuticals and insecticides **[12]**. These derivatives have demonstrated considerable potential in addressing drug-resistant diseases and enhancing crop productivity, rendering them a subject of substantial interest and investigation in both the medical and agricultural domains **[13]**. This study aims to present an overview of the diverse synthetic methods employed in the synthesis of benzimidazole derivatives. Furthermore, it will emphasize the significance of these methods for tackling drug resistance and enhancing crop productivity. Additionally, the potential applications of benzimidazole and its inorganic derivatives in biomedicine and agriculture will be discussed.

1.2 Benzimidazole and derivatives: Benzimidazole and its derivatives, shown in **Figure 2** are classified differently based on their applications **[1-5]**, **[7-9]**. For example, in pharmacology, the benzimidazole ring system serves as the core for drugs such as albendazole and anesthetics like etomidate **[9]**. The registration of benzimidazole itself as a new drug laid down specifications for an incredible class of chemical entities **[14]**. Humankind was fortunate to develop the first drug with an extended spectrum of antibacterial activity, Nizatidine, in 1975

[15]. And from then to now, some benzimidazole and its derivative drugs have developed, and many of them are on the market [13-15]. Also, the benzimidazole ring is present in many fungicides and insecticides, most of which are used in horticulture or viticulture [16]. This class of molecules exhibits antifungal and/or anti-insect properties [16]. On the other hand, heterocyclic molecules have a long history of biological activity, including their use as pesticides in the agricultural industry [17]. These materials are essential in the quest for the development of new products that are biologically active, environmentally acceptable, sustainable, and provide an economic return [18]. These are some of the most important organic building blocks for technological materials, like liquid crystals [18-20]. The Grubbs catalyst is often used for olefin metathesis, and ligands are used in the Heck reaction [21]. These heterocyclic molecules and their derivatives have continued to attract great medicinal chemistry interest since the discovery of the first benzimidazole derivative used as a drug [22]. This chapter provides a crucial and elaborate account to expound on the importance of benzimidazole and its inorganic derivatives in the field of medicinal chemistry and also in the agricultural industry concerning the structural activity relationships, pharmacological studies, and various molecular modeling studies so far reported.

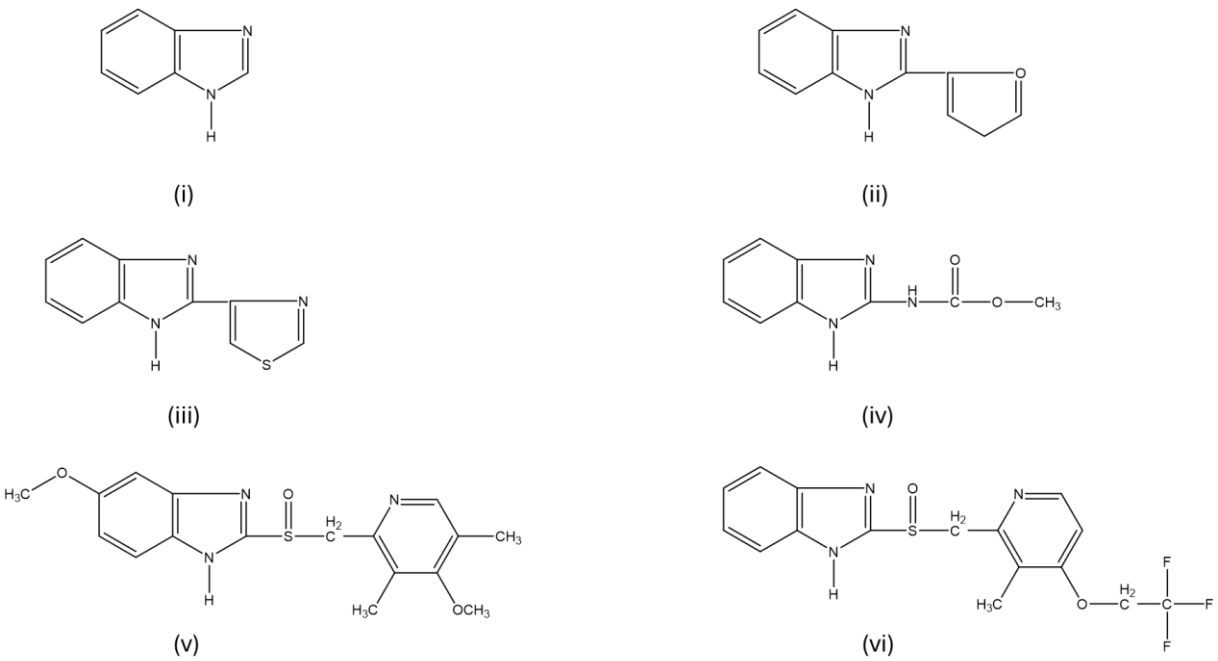

Fig.2 Benzimidazole derivatives such as
(i) Benzimidazole, (ii) Fuberidazole, (iii) Carbendazim, (iv) Thiabendazole, (v) Omeprazole, and (vi) Lansoprazole

1.3 Importance of Benzimidazole in Medicine and Agriculture: Benzimidazole plays a crucial role in both medicine and agriculture due to its diverse pharmacological properties and applications. Benzimidazole and its derivatives are crucial therapeutic agents in the field of

medicine [23]. They play a vital role as medications that treat ulcers, eliminate parasitic worms, combat microbial and viral infections, fight against cancer, reduce inflammation, and provide pain relief [23-25]. These chemicals are used to treat a variety of ailments, such as hypertension, malaria, cancer, microbial infections, and inflammatory disorders, demonstrating a diverse spectrum of biological actions [26]. In addition, benzimidazole derivatives have been utilized in agriculture, specifically as anthelmintic drugs to combat parasitic illnesses in animals [27]. The ongoing investigation of benzimidazoles and their analogs for their chemical and pharmacological properties highlights their importance in both the medical and agricultural sectors [28]. The antiparasitic activity of benzimidazoles is widely utilized as an anthelmintic drug for the treatment of parasitic infections in both humans and animals [29]. The antiparasitic drugs albendazole and mebendazole are standard treatment options for several parasitic diseases [30]. Since they possess antifungal properties, benzimidazole derivatives are extremely useful in the treatment of fungal infections [3].

Additional research has shown that several benzimidazole compounds possess anti-cancer properties, suggesting their potential as effective choices for cancer treatment [31]. Furthermore, benzimidazoles have demonstrated antiviral activity against specific viruses, which enhances their potential for use in the development of antiviral drugs [32].

Agriculture is the process of cultivating plants and rearing animals for food, fiber, medicinal plants, and other products used to sustain human life [33]. Furthermore, benzimidazole compounds, with their fungicidal properties, are widely used as agricultural fungicides to control fungal infections in crops [34]. They aid in safeguarding crops against several fungal diseases, hence enhancing agricultural productivity and quality [34].

Benzimidazoles exhibit potent nematocidal activity, targeting nematodes and pernicious parasites that inflict harm on plant roots and diminish agricultural yield [35]. Some work studies suggested that benzimidazoles aid in the regulation of nematode populations, hence promoting the overall health of crops [36].

Researchers also discovered the intricate activity of fuberidazole (ii) shown in **Figure 2**, and its wide-ranging uses in both medical and industrial agricultural fields [37]. Fuberidazole demonstrates great potential as an antifungal drug in medicine, namely in fighting a range of fungal diseases [37]. Endophytic fungi contain this substance, which has a role in protecting plants, promoting their growth, and competing with other microorganisms [37]. Its extensive distribution makes it suitable for use in medical applications [38]. Industrial agriculture uses fuberidazole and other fungal species as biofertilizers and biocontrol agents [39]. They can promote plant development and inhibit the growth of soil-borne diseases [39]. Ectomycorrhizae are essential in forestry as they enhance the growth of commercially significant crops and

decrease the need for fertilizers, thereby contributing to environmental sustainability [40]. All of these uses show how flexible and useful fuberidazole and related fungi can be in promoting environmentally friendly practices and improving plant health in a number of areas [40].

Therefore, benzimidazole compounds are essential in medicine and agriculture due to their diverse medicinal and preventive advantages.

1.4 Benzimidazole Compounds and Proton Pump Inhibitors (PPI) in the Medical and Agricultural Applications: Proton pump inhibitors (PPIs) are a class of drugs with a common structural foundation of a pyridine and benzimidazole ring as shown in **Figure 3**, differing only in the substituents attached to these rings [41]. Analgesics widely prescribe PPIs like Pantoprazole for conditions like gastritis and gastric irritation [42]. Studies have shown that PPI use is associated with increased risks of certain cancers, like gastric, pancreatic, colorectal, and liver cancer, while potentially decreasing the risk of breast cancer [43]. PPIs may interact with the cancer microbiome and affect the efficacy of antineoplastic agents, although only a few interactions are clinically significant [44]. Deprescribing PPIs when they are not clinically justified is advised to avoid unnecessary drug interactions and adverse effects [45].

The pharmacological relevance of benzimidazole compounds, especially proton pump inhibitors, is well-known [46]. Gastric acid-related illnesses like GERD and peptic ulcer disease are treated.

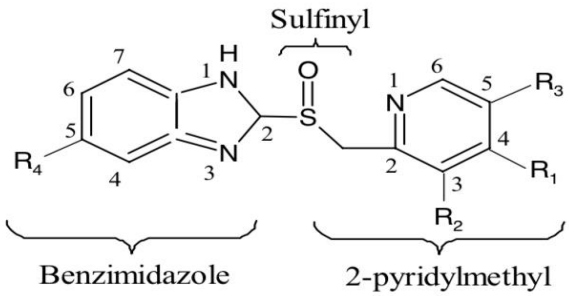

Figure 3. Structure of proton pump inhibitors (PPIs) that contain benzimidazole, sulfinyl, and 2-pyridylmethyl groups [41]

with PPIs [47]. PPIs such as omeprazole, lansoprazole, and pantoprazole are widely used benzimidazole derivatives [43]. These substances permanently block the action of the proton pump (H+/K+ ATPase) in the stomach lining cells, which stops gastric acid from entering the inside of the stomach [44]. Proton pump inhibitors (PPIs) alleviate symptoms of acid reflux and promote the healing of ulcers by reducing the production of stomach acid [48]. These proton pump inhibitors (PPIs) contain a benzimidazole molecule that forms covalent bonds with the proton pump enzyme. This stops the production of acid [45]. The correlation between benzimidazole compounds and PPIs underscores their clinical significance in treating acid-related gastrointestinal disorders [42].

The extensive spectrum of pharmacological activity exhibited by benzimidazole and its derivatives has also resulted in its use in the agriculture industry [43]. These chemicals have been used in the creation of proton pump inhibitors (PPIs) [44-45], which have shown associations with many types of cancer [46]. In addition, benzimidazole derivatives have demonstrated antibacterial capabilities, making them highly valuable for managing microbial infections in agricultural environments [47]. Research has been conducted on the manufacturing of benzimidazole PPIs using advanced methods such as catalytic reactions and catalysts utilizing graphene oxide [48]. These methods offer efficient and eco-friendly processes for industrial applications [48]. Benzimidazole compounds possess a diverse range of characteristics, which renders them highly favorable for use in agricultural applications [49]. They can be utilized to create innovative protein-protein interactions (P-PIs) to enhance crop protection and disease control [50].

2. Synthesis of Proton Pump Inhibitors

2.1 Omeprazole: Omeprazole (v), depicted in **Figure 2**, is scientifically known as 6-methoxy-2-[(4-methoxy-3,5-dimethylpyridin-2-yl) methylsulfinyl]. The compound -1H-benzimidazole exhibits a unique molecular structure [51]. Omeprazole, a widely used proton pump inhibitor, can be synthesized using various methods outlined in the research papers. One method involves the asymmetric oxidation of omeprazole thioether under specific conditions to generate esomeprazole, a more potent form of the drug [51]. Additionally, the synthesis of omeprazole involves the formation of coordination compounds with metal ions like copper, zinc, cadmium, and mercury, resulting in compounds with tetrahedral structures [52]. The structure and dynamics of omeprazole, particularly its chiral nature and molecular interactions, play a crucial role in its activity and stability, as revealed by NMR experiments [53]. Furthermore, novel synthesis processes have been developed to address impurities in omeprazole, enhancing its purity and efficacy for pharmaceutical use [54]. These diverse approaches contribute to the comprehensive understanding and efficient synthesis of omeprazole for proton pump inhibition.

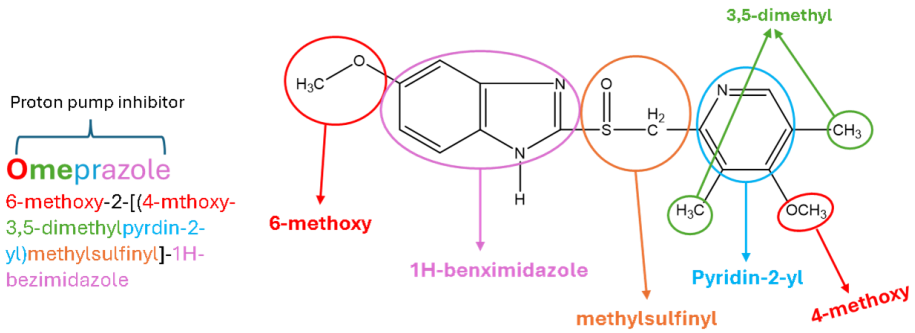

Fig. 4 Omeprazole functional groups structure

The substituted benzimidazole ring of omeprazole, shown in **Figure 4**, fights gastric acid **[55]**. Two strategically located nitrogens in this ring structure operate as a proton sponge, blocking H+/K+ ATPase and lowering stomach acid output **[54]**. The effectiveness of omeprazole relies on stomach acid activation, wherein the benzimidazole ring assumes a prominent role **[56]**.

2.2 Synthesis and Structure of Omeprazole: A reaction was carried out with 2-chloro-3,5-dimethyl-4-methoxy pyridine (121 g) to form the sulphide intermediate 3 **[57]**. Then, 2-(Lithium methyl sulphinyl)-5-methoxy-1H benzimidazole (220 g) was treated with m-CPBA, an oxidizing agent, which resulted in the conversion to omeprazole 4 [58]. After undergoing alkaline hydrolysis, the acetamide-sulfide compound was altered and produced the sulfinyl carboxylate or salts, which were then oxidized to yield the amide

sulfinyl compound **[59]**. Following decarboxylation, the target compounds were formed **[60]**. The purification process simply involved washing out the remaining unreacted salt, inorganic byproducts, and other minor byproducts, allowing for the easy purification of either omeprazole or lansoprazole **[61-63]**. Unlike the sulfides and sulfoxides of previously published techniques, the amide compounds were crystalline solids **[64-65]** as shown in **Figure 5**.

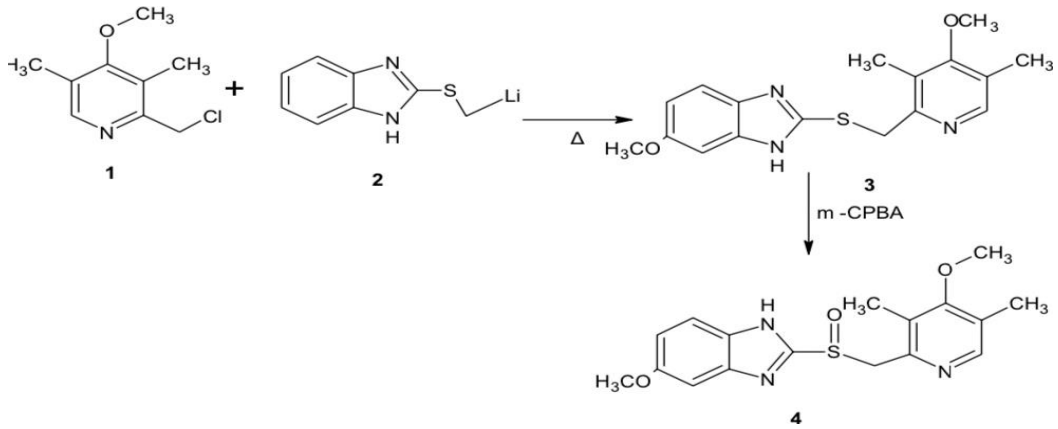

Fig. 5 The chemical reaction for preparing Omeprazole [64].

3. Conclusions:

In conclusion, benzimidazole and its derivatives are versatile molecules with great potential in medicine and agriculture. This study highlights the significance of benzimidazoles as powerful fungicides and insecticides in human health, pharmacology, disease treatment, and agriculture. This study has shown the importance of benzimidazole-based chemicals in medicinal and agricultural activities by investigating their modes of action, formulation obstacles, and regulatory issues. Further research into benzimidazole applications may lead to breakthroughs in these critical domains.

4. References:

[1] Jiyaul H, Amit A. Study on Benzimidazole: A Comprehensive Review. Int J Multidiscip Res. 2023. doi: 10.36948/ijfmr.2023.v05i02.1931.

[2] Sharma S, Dangi N, Mittal N, Kalra N. A Critical Analysis of the Modern Synthetic Procedures Used to Produce Benzimidazole Candidates. Curr Organocatal. 2023. doi: 10.2174/2213337210666230329103657.

[3] Rudolph A, Champa KA, Vishnumurthy, Yadav D, Bodke HS, Bhojya Naik, et al. Synthesis, characterization, and biological investigations of potentially bioactive heterocyclic compounds containing benzimidazole nucleus. Results Chem. 2023. doi: 10.1016/j.rechem.2023.101018.

[4] Choudhary A, Viradiya RH, Ghoghari RN, Chikhalia KH. Recent Scenario for the Synthesis of Benzimidazole Moiety (2020–2022). ChemSelect. 2023. doi: 10.1002/slct.202204910.

[5] Sharma S, Gupta MC, Gupta M, Sahu JK. Significance of Benzimidazole analogues for the creation of novel molecules in drug discovery. Curr Chem Lett. 2023. doi: 10.5267/j.ccl.2022.9.008.

[6] Benzimidazole [Internet]. Available from: https://en.wikipedia.org/wiki/Benzimidazole.

[7] Rudolph A, Champa KA, Vishnumurthy, Yadav D, Bodke HS, Bhojya Naik, et al. Synthesis, characterization, and biological investigations of potentially bioactive heterocyclic compounds containing benzimidazole nucleus. Results Chem. 2023. doi: 10.1016/j.rechem.2023.101018.

[8] Aralihalli S, Sudileti M, Aithal SJ. The medicinal panorama of benzimidazoles and their scaffolds as anticancer and antithrombotic agents: A review. Arch Pharm. 2023. doi: 10.1002/ardp.202300206.

[9] Chevallier F, Mongin F. Functionalization of Diazines and Benzo Derivatives Through Deprotonated Intermediates. ChemInform. 2008. doi: 10.1002/CHIN.200824242.

[10] Jeon BH. A Review of Approaches to the Metallic and Non-Metallic Synthesis of Benzimidazole (BnZ) and Their Derivatives for Biological Efficacy. Molecules. 2023. doi: 10.3390/molecules28145490.

[11] Sahu JK, Sharma S, Gupta M, Gupta MC. Impact of Benzimidazole containing scaffolds as Anticancer Agents through diverse modes of action. Curr Bioact Compd. 2023. doi: 10.2174/1573407219666230406082148.

[12] Saini A, Kumar G, Singh GD. A review of Benzimidazole derivatives' potential activities. Int J Pharm Clin Res. 2023. doi: 10.33545/26647591.2023.v5.i1a.51.

[13] Salahuddin, Shabana K, Mazumder A, Kumar R, Datt V, Tyagi S, et al. Review on the discovery of new Benzimidazole derivatives as Anticancer Agents: Synthesis and Structure-Activity Relationship (2010-2022). Lett Drug Des Discov. 2022. doi: 10.2174/1570180820666221017155955.

[14] Singh HP, Kumar R, Tiwari P, Singh A. Recent advances in Synthetic Strategies of Benzimidazole and Its Analogs: A Review. Curr Org Chem. 2022. doi: 10.2174/1385272827666221216113723.

[15] Aminov RI. A brief history of the antibiotic era: lessons learned and challenges for the future. Front Microbiol. 2010;1:134.

[16] Kale PA, Kaduskar SD. A REVIEW ON SYNTHESIS AND CHARACTERISATION OF BENZIMIDAZOLE. 2023.

[17] Rana NA, Zahraa L, Razzaq WI, Yahya I. Synthesis, Characterization and Studying Biological Activity of Heterocyclic Compounds. Int J Drug Deliv Technol. 2023. doi: 10.25258/ijddt.13.1.31.

[18] Thakur D. A Review on the Medicinal Significance of Heterocyclic Compounds. Int J Sci Technol Eng. 2023. doi: 10.22214/ijraset.2023.54569.

[19] Gulati S, Singh R, Sangwan S. A review on green synthesis and biological activities of medicinally important nitrogen and oxygen containing heterocycles. Curr Org Chem. 2022. doi: 10.2174/1385272827666221227114713.

[20] Sarria JJH. Synthesis of Bioactive Heterocycles Exploiting Modern Continuous Flow Chemistry. 2022. doi: 10.1002/9781119757153.ch12.

[21] Chérif SE, Ghosh A, Chelli S, Dixon IM, Kraiem J, Lakhdar S. Merging Grubbs second-generation catalyst with photocatalysis enables Z-selective metathesis of olefins: scope, limitations, and mechanism. Chem Sci. 2022. doi: 10.1039/d2sc03961c.

[22] Vasantha TS, Mani S, Pasha TY, Ramesh B. A comprehensive review on 2-substituted benzimidazole derivatives and its biological importance. 2023.

[23] Hak J, Agrawal A. Study on Benzimidazole: A Comprehensive Review. Int J Multidiscip Res. 2023. doi: 10.36948/ijfmr.2023.v05i02.1931.

[24] Pullagura MKP, Kanvinde A, Raja S. Potent biological agent benzimidazole-a review. Int J Pharm Pharm Sci. 2016;8:22-33.

[25] Sahu JK, Sharma S, Gupta M, Gupta MC. Impact of Benzimidazole containing scaffolds as Anticancer Agents through diverse modes of action. Curr Bioact Compd. 2023. doi: 10.2174/1573407219666230406082148.

[26] Abdullah AM, Dadoosh SA, Thani MZ, Fahad AS. Using Metal Oxide Nanoparticles as Catalyst in Benzimidazoles Synthesis. Earthline J Chem Sci. 2023;9(1):63-76.

[27] Venugopal S, Kaur B, Verma AK, Wadhwa P, Sahu SK. A Review On Modern Approaches To Benzimidazole Synthesis. Curr Org Synth. 2022. doi: 10.2174/1570179420666221010091157.

[28] Fujihara H, Fujii K, Fuchi S, Tanaka R, Akimoto K. Benzimidazole compound or salt thereof, agricultural and horticultural insecticidal and acaricidal agent comprising said compound, and method for using said insecticidal and acaricidal agent. 2021.

[29] Al Nasr I, Koko WS, Khan T, Schobert R, Biersack B. Antiparasitic Activity of Fluorophenyl-Substituted Pyrimido[1,2-a]benzimidazoles. Adv Cardiovasc Dis. 2023. doi: 10.3390/biomedicines11010219.

[30] Chai JY, Jung BK, Hong SJ. Albendazole and Mebendazole as Anti-Parasitic and Anti-Cancer Agents: an Update. Korean J Parasitol. 2021. doi: 10.3347/KJP.2021.59.3.189.

[31] Conaldnbww. Benzimidazole Zinc Complexes and Their Anticancer Activities. 2023. doi: 10.58830/ozgur.pub132.c673.

[32] Kotovskaya SK, Baskakova ZM, Charushin VN, Chupakhin ON, Belanov EF, Bormotov NI, Serova OA. Synthesis and antiviral activity of fluorinated pyrido[1,2-a]benzimidazoles. Pharm Chem J. 2005;39:574-8.

[33] Chiebuka P. Impacts of Environmental Challenges on Medicinal Plants and the Possibilities for Increased Sustainable Agriculture. Covenant J Entrepreneurship. 2020;4(1).

[34] Heneberg P, Svoboda J, Pech P. Benzimidazole fungicides are detrimental to common farmland ants. Biol Conserv. 2018;221:114-7.

[35] Agarwal SK. Pesticide Pollution. Vol. 3. APH Publishing; 2009.

[36] Abdel Gawad M, Eissa M, El-Gindi AE, Smart G. Development of plant-parasitic nematode populations on forage crops under field conditions. Egypt J Agronematol. 2017;16(2):51-62.

[37] Karunarathna SC, Ashwath N, Jeewon R. The Potential of Fungi for Enhancing Crops and Forestry Systems. Front Microbiol. 2021;12:813051.

[38] Jampílek J, Kráľová K, Campos EV, Fraceto LF. Bio-based nanoemulsion formulations applicable in agriculture, medicine, and food industry. In: Nanobiotechnology in bioformulations. 2019. p. 33-84.

[39] Dhevagi P, Ramya A, Priyatharshini S, Geetha Thanuja K, Ambreetha S, Nivetha A. Industrially important fungal enzymes: productions and applications. Recent Trends Mycol Res: Environ Ind Perspect. 2021;2:263-309.

[40] Aftab NF, Ahmad KS, Gul MM. Sorptive and degradative assessments of environmentally pestilential Benzimidazole fungicide Fuberidazole in pedosphere. Int J Environ Anal Chem. 2023;103(17):6097-114.

[41] Saïf EC, Ghosh A, Chelli S, Dixon IM, Kraiem J, Lakhdar S. Merging Grubbs second-generation catalyst with photocatalysis enables Z-selective metathesis of olefins: scope, limitations, and mechanism. Chem Sci. 2022. doi: 10.1039/d2sc03961c.

[42] He G, Deng S, Nooh MN, Ahmad BS, Yu R, Abram J, et al. Proton Pump Inhibitors and Cancer Risk. Am J Clin Oncol. 2022. doi: 10.1097/coc.0000000000000949.

[43] Ravindra BN, Sunny DS, Jain D. Study on Drug Utilization and Evaluation of Proton Pump Inhibitors in Surgery Unit of Tertiary Care Teaching Hospital. Int J Pharm Sci Rev Res. 2022. doi: 10.47583/ijpsrr.2022.v76i01.011.

[44] Singh HP, Kumar R, Tiwari P, Singh A. Recent advances in Synthetic Strategies of Benzimidazole and Its Analogs: A Review. Curr Org Chem. 2022. doi: 10.2174/1385272827666221216113723.

[45] He G, Deng S, Nooh MN, Ahmad BS, Yu R, Abram J, et al. Proton Pump Inhibitors and Cancer Risk. Am J Clin Oncol. 2022. doi: 10.1097/coc.0000000000000949.

[46] Patil GD, Nikam AR, Karanke NB, Shaikh AZ. A Short Review On Benzimidazole and Their Derivatives. 2020. doi: 10.46624/AJPHR.2020.V8.I3.002.

[47] Ahmad N, Azad MI, Khan AR, Azad I. Benzimidazole as a promising antiviral heterocyclic scaffold: a review. 2021. doi: 10.46939/J.SCI.ARTS-21.1-B05.

[48] Brishty SR, Hossain MJ, Khandaker MU, Faruque MRI, Osman H, Rahman SMA. A Comprehensive Account on Recent Progress in Pharmacological Activities of Benzimidazole Derivatives. Front Pharmacol. 2021;12:762807. doi: 10.3389/fphar.2021.762807.

[49] Bridoux M, Simon N, Turpin A. Proton Pump Inhibitors and Cancer: Current State of Play. Front Pharmacol. 2022. doi: 10.3389/fphar.2022.798272.

[50] Soong JTY. Proton pump inhibitors: When is it too much of a good thing? Ann Acad Med Singapore. 2022. doi: 10.47102/annals-acadmedsg.20226.

[51] Imparato RR, Toma TS. Proton pump inhibitor deprescription: A rapid review. Braz J Pharm Sci. 2022. doi: 10.1590/s2175-97902022e19989.

[52] Orel R, Benninga MA, Broekaert I, Gottrand F, Papadopoulou A, Ribes-Koninckx C, et al. Drugs in Focus: Proton Pump Inhibitors. J Pediatr Gastroenterol Nutr. 2021. doi: 10.1097/MPG.0000000000003063.

[53] Singh L, Kanwar K, Singh AP. Proton pump inhibitors: An incisive review. Int J Parallel Program. 2021. doi: 10.18231/J.IJPP.2021.019.

[54] Perry IE, Sonu I, Scarpignato C, Akiyama J, Hongo M, Vega KJ. Potential proton pump inhibitor–related adverse effects. Ann N Y Acad Sci. 2020. doi: 10.1111/NYAS.14428.

[55] Saini S, Majee C, Chakraborthy GS, Salahuddin. Novel Synthesis of Omeprazole and Pharmaceutical Impurities of Proton pump inhibitors: A Review. Int J PharmTech Res. 2019. doi: 10.20902/IJPTR.2019.120307.

[56] Cartee NMP, Wang MM. Binding of omeprazole to protein targets identified by monoclonal antibodies. PLoS One. 2020. doi: 10.1371/JOURNAL.PONE.0239464.

[57] Bruni AT, Ferreira MMC. Theoretical study of omeprazole behavior: Racemization barrier and decomposition reaction. Int J Quantum Chem. 2008. doi: 10.1002/QUA.21597.

[58] Malik S, Das S, Jain B. First-row transition metal complexes of omeprazole as anti-ulcerative drugs. Indones J Chem. 2010;10(3):382-9.

[59] Claramunt RM, López C, Alkorta I, Elguero J, Yang R, Schulman S. The tautomerism of Omeprazole in solution: a 1H and 13C NMR study. Magn Reson Chem. 2004. doi: 10.1002/MRC.1409.

[60] Claramunt RM, López C, Elguero J. The structure of Omeprazole in the solid state: a 13C and 15N NMR/CPMAS study. Arkivoc. 2005. doi: 10.3998/ARK.5550190.0007.502.

[61] Bruni AT, Ferreira MMC. Theoretical study of omeprazole behavior: Racemization barrier and decomposition reaction. Int J Quantum Chem. 2008. doi: 10.1002/QUA.21597.

[62] Murray IA, Perdew GH. Omeprazole Stimulates the Induction of Human Insulin-Like Growth Factor Binding Protein-1 through Aryl Hydrocarbon Receptor Activation. J Pharmacol Exp Ther. 2008. doi: 10.1124/JPET.107.13224.

[63] Singh SP, Siddiqui MJ, Mukarram D, Kulkami G, Purohit M. Synthetic procedure for 5-methoxy-2-[(4-methoxy-3,5-dimethyl-2-pyridinyl)-methylthio]-IH-benzimidazole hydrochloride and its conversion to omeprazole. 1999.

[64] Vora JJ, Trivedi KP, Kshatriya RS. Synthesis and Spectral Studies of 2-mercapto-5-methoxy-1H-benzimidazole: An Imperative Medicinal Intermediate. 2012.

[65] Nikiforova OV, Chistyakov VV, Shikh EV, Arzamastsev AP. Pharmacokinetics and bioaccessibility of gastrozole. Pharm Chem J. 1999. doi: 10.1007/BF02509933.

Al-Kitab Journal for Pure Sciences (2024); 8(2):138-152.
https://doi.org/10.32441/kjps.08.02.p12

Al-Kitab Journal for Pure Sciences
ISSN: 2617-1260 (print), 2617-8141(online)
https://isnra.net/index.php/kjps

The difference in the Physiological response of the wheat plant to the effect of algae extracts and hydrogel

Safaa Younis Mal Allah, Mira Ausama Al-Katib*

Department of Biology, College of Education for Pure Science, University of Mosul, Iraq

*Corresponding author: mirausama@uomosul.edu.iq

*ORCID ID: https://orcid.org/0000-0002-2234-1127

Citation: Mal Allah SY, Al-Katib MAA. The difference in the Physiological response of the wheat plant to the effect of algae extracts and hydrogel. Al-Kitab J. Pure Sci. [Internet]. 2024 Jul. 11 [cited 2024 Jul. 11];8(02):138-152. Available from: https://isnra.net/index.php/kjps/article/view/1193 https://doi.org/10.32441/kjps.08.02.p12.

Keywords: *Pithophora roettleri*, *Compsopogon caeruleus*, Bio Fertilization, Hydrogel, Wheat Growth Properties.

Article History

Received	18	May.	2024
Accepted	13	Jun.	2024
Available online	12	July	2024

Abstract:

The study aims to test the effect of two algae, Compsopogon *caeruleus*, and *Pithophora roettleri*, in three concentrations (2, 1, and 0.5). Hydrogel (4, 2) g/kg. The current study included vegetative growth characteristics: The wheat germination rate plant height, root length, water content, leave area, total chlorophyll content dry weight, root and shoot total, and. was affected by fertilization treatments. And their Interference with concentrations and gel. The treatments in which each alga was used alone outperformed the Interference treatment between them in terms of the dry weight of the shoot, as it reached 1.26 and 1.27 grams for C. *caeruleus* and P. roettleri, respectively, while the best treatment was for weight. Root dryness of P.roettleri alga amounted to 0.19 grams. As for plant height, the best treatments were recorded with P. roettleri and C. *caeruleus*, respectively, as they reached 50.03 and 49.17 cm. In root length, the highest length was recorded when treated with C. *caeruleus* algae and reached 13.19 cm. The highest leave area was also recorded when treated with P.roettleri algae and reached 12.47 cm. The highest total and total chlorophyll content was recorded. Chlorophyll a when treated with the alga C. *caeruleus* reached 22.70 and 8.44 mg/g, respectively, while chlorophyll's content reached the highest percentage in the algae P.roettleri and reached 15.15 mg/g. Adding the hydrogel at a concentration of 2g/kg soil had a significant effect on the mentioned characteristics, while it was the concentration of 4 gm/kg of soil for the gel had a significant increase in the concentration of chlorophyll a, b, and total chlorophyll an over the rest of the

treatments. Laboratory results showed the effect of aqueous extracts on the wet biomass of both algae, and with the two concentrations (1, 2%), there was a significant increase in (seed germination, length of the petiole, root, and dry weight for wheat. The results of the anvil experiments indicated the presence of varying effects of aqueous extracts of wet living mass. Both the interaction between the algae and the gel, along with their concentrations, played a stimulating and moral role in some of the studied traits.

Keywords: *Pithophora roettleri*, *Compsopogon caeruleus*, Bio Fertilization, Hydrogel, Wheat Growth Properties.

اختلاف الاستجابة الفسيولوجية لنباتات الحنطة لتأثير مستخلصات الطحالب والهلام المائي

صفاء يونس مال الله، مِرا اسامه الكاتب*

جامعة الموصل / كلية التربية للعلوم الصرفة / قسم علوم الحياة

mirausama@uomosul.edu.iq, safa.22esp8@student.uomosul.edu.iq

الخلاصة:

وتهدف الدراسة الى اختبار تاثير جنس *Compsopogon caeruleus* وجنس هو*Pithophora roettleri* ومعاملة التداخل (الطحلبين معاً) وبثلاث مكررات وفق تصميم القطاعات العشوائية الكاملة وثلاث تراكيز(٠,٥، ١، ٢٪)مع الهلام المائي (٢,٤) غم\كغم تربة لنباتات الحنطة صنف مودة نسبة انبات الحنطة ارتفاع النبات(سم)وطول المجموع الجذري(سم)والمحتوى المائي ومساحة الورقة (سم٢) ومحتوى الكلوروفيل الكلي ومحتوى كلوروفيل*a*ومحتوى كلوروفيل*b* الوزن الجاف(غم)للنبات(المجموع الجذري والمجموع الخضري) الى بهذه الطحالب اظهرت المعاملات وتداخلاتها مع التراكيز والهلام تفوق المعاملات التي استخدم فيه كل طحلب لوحده على معاملة التداخل بينهما في صفة الوزن الجاف للمجموع الخضري اذ بلغ١,٢٦,١,٢٧غم لكل من طحلب *C. caeruleus* وطحلب *P. roettleri* على التوالي في حين كانت افضل معاملة للوزن الجاف الجذري عند طحلب *P. Roettleri* إذ بلغ٠,١٩ غم اما ارتفاع النبات كانت افضل المعاملات *P. roettleri* و*C.caeruleus* على التوالي اذ بلغا ٥٠,٠٣,٤٩,١٧سم وفي طول المجموع الجذري بلغ اعلى طول عند المعاملة بطحلب *C. caeruleus* وبلغ١٣,١٩سم ولقد سجل اعلى مساحة ورقية عند طحلب *P. roettleri* وبلغ١٢,٤٧سم اما من حيث محتوى الكلوروفيل الكلي ومحتوى كلوروفيل*a*بلغت اعلى نسبة عند المعاملة بطحلب *C.caeruleus* وبلغا٢٢,٧٠و٨,٤٤ملغم\غم في حين بلغ محتوى كلوروفيل *b* اعلى نسبة عند الطحلب *P. roettleri* وبلغت١٥,١٥ملغم\غم .وان اضافة الهلام المائي عند التركيز٢غم\كغم تربة تاثير معنوي في الصفات المذكورة بينما كان التركيز٤غم\كغم تربة للهلام تفوق معنوي في كل من تركيز الكلوروفيل*a*و*b*والكلي على بقية المعاملات. واظهرت النتائج المختبرية لتاثير المستخلصات المائية للكتلة الحية الرطبة لكل من الطحلبين وبالتركيزين(٢،١)% زيادة معنوية في (انبات البذور,طول الرويشة,والجذير,والوزن الجاف. واشارت نتائج تجارب السنادين الى وجود تاثيرات متباينة للمستخلصات المائية للكتلة الحية الرطبة لكل من التداخل بين الطحالب والهلام مع تراكيزهما دوراً تحفيزياً ومعنوياً في بعض الصفات المدروسة.

الكلمات المفتاحية: *Pithophora roettleri*، *Compsopogon caeruleus*، التسميد الحيوي، الهلام المائي، خصائص نمو الحنطة.

1. Introduction:

Algae live in various environments in marine water, freshwater, and places where moisture is available. Algae differ among themselves, including small ones that cannot be seen without a microscope and consist of a single cell, and large ones **[1].** Algae have been used in the field of fertilization and can be defined as the process through which the plant is provided with nutrients according to the method in which they are added to the plant. Mixing fertilizer with the soil may be sprayed on the plant, and **[2]** .Algae bio-fertilization led to a significant increase in plant height, fresh and dry weight of the root and shoot mass, and leaf area of the plant after decomposition of the algae extracts. Algae work to increase soil fertility **[3]**. Currently, the great interest in agriculture has led to the use of algae extracts as a new system. Because these extracts are non-toxic and eco-friendly **[4]**. Wheat is one of the most prominent cereal crops and the most cultivated and productive in the world. It has a role in achieving food security and contains a percentage of protein ranging from 8-14% **[5]**. Hydrogel products do not contain a group of colloidal substances. Water-philic trap hydrogel and these polymers have gained a wide position in recent years in the fields of crops due to their high ability to retain water. A study **[6]** indicated the use of fertilizers at a concentration of 120 kg/ha not coated with gel and 120 kg/ha coated with gel, It showed that the concentrations of fertilizer coated with gel achieved a significant increase in grain yield.

2. Materials and Methods

2.1 Collecting algae samples: Samples were collected on September 15, 2023, from the Tigris River in the Qayyarah area, Mosul District, Nineveh Governorate. Then the samples were washed with liquefied water several times, as well as with distilled water, to clean them of dust and dirt, and they were dried. Diagnosis of algae: Algae genera were identified based on phenotypic diagnosis, and their phenotypic characteristics were noted based on the taxonomic keys of algae.

2.2 Source of wheat seeds: Mawaddah wheat seeds were obtained from the Seed Certification Center in Nineveh and tested for their vitality. Hydrogel: The gel was prepared from local markets by a Turkish company. Source of agricultural soil: The soil was prepared from the village of Al-Kasr, southeast of Mosul, Al-Hamdaniya district, and was sieved to get rid of the stones that hinder the growth of seeds.

2.3 Preparation of aqueous extracts: Aqueous extracts of the two algae *(P. rottieri* and *C. cearuleus)* were prepared at concentrations(2,1,0.5)% weight/volume by mixing the dry living mass with distilled water using an electric mixer (Sliver Crest) type for ten minutes. It was filtered using Whatman filter paper and the filtrate was collected for use in laboratory

experiments and the wire house. The experiment with the anvils (the wirehouse): Anvils with a capacity of (6 kg), a height of (24 kg), and a diameter of (21 cm) were used in the experiment, and 10 wheat seeds were planted At a depth of 0.5 cm from the soil surface, 11/7/2023, with three replicates, 400 ml of extracts were added to the soil, and the control treatment was prepared by adding water only.

2.4 Characteristics of vegetative growth of wheat plants:

1- Plant height and root system length (cm) were measured using a ruler.
2- Leave area (cm). Leaf area = length of Leave x maximum width of paper x 0.905 [8].
3- Water content: The water content was estimated using the method of [7]. The third leaf (homogeneous in age and shape) was taken from the seedlings, and to obtain the dry Relative water content %=100×(dry weight - wet weight)/(dry weight - swelling weight)weight (D.W), it was dried for 48 hours as in the following equation
4- Estimating the dry weight of the shoot and root system: using an electric oven at (70) for (48) hours for drying.
5- Determination of chlorophyll in leaves: The content of total chlorophyll a and b in plant leaves was estimated according to the method and the light absorption of the filtrate was read at wavelengths (645-663) nm using a spectrophotometer. Total chlorophyll content (mg/g) = (A645) +8.02) A663) +20.2 [9].

3. Results and Discussion

3.1 Plant height (cm): It was noted from the results (1) that there were significant differences in the effect of hydrogel on the height of wheat plants, as the highest height was reached when the soil was treated with hydrogel at a concentration of 2 g/kg of soil, except the control treatment. The reason for this is that the gel is considered a good storage of nutrients, as it led to the retention of both water and nutrients. Providing it to the plant as needed during the growth period [5] and between the effects of the type of algae, there are no significant differences when treated with two algae *C. caeruleus* and *P. roettleri* in the height of wheat plants, while the lowest height was reached when treated with the synergy recorded 47.26 cm. The table shows the effect of algae concentrations, which is 2% concentration, amounting to 48.31%, although it was not significantly superior to the control treatment. As for the interference (algae and gel concentration), it was observed when treating the soil with algae and gel that there were no significant differences between the treatments. And in the interference (concentrations of algae extract and gel concentration). There are significant differences, as the gel at the concentration of 2 g/kg soil was significantly superior to the rest of the treatments and recorded 55.00 cm. The table also showed that there was no significant difference between the

algae used and its concentrations are rising Plant. As for the binary interference (algae and its concentrations and gelatin and its concentrations) between the presence of significant differences in the height of wheat plants, the highest was recorded The height of the plant when treated with interference at a concentration of 2% reached 56.67 cm, while the effect of the gel levels at a concentration of 2 g/kg soil did not differ significantly with algae and their concentrations. This reflects the role of the extract in increasing the growth and elongation of cells and tissues, as it plays an important role in the height of the plant because it contains growth-regulating hormones, including auxins, which It has a role in cell division in topical meristem and thus increased plant length [2].

Table 1: The effect of aqueous extracts of algae and hydrogel on plant height (cm)

Algae type	Algae con(%)	Hydrogel con.gm\kg soil			Algae type Algae con.	Effect of algae type	Effect of algae con.
		Control	2	4			
C. caeruleus	0.0	1.44 cde	1.88 a	1.53 bc	1.62 a		
	0.5	1.19 f-i	1.67 b	0.84 k	1.23b		
	1	1.50 bcd	0.73 kl	0.73 kl	0.99 d		
	2	1.30 d-h	1.20 f-i	1.25 e-i	1.25 b		
P. roettleri	0.0	1.44 cde	1.88 a	1.53 bc	1.62 a		
	0.5	1.13 g-j	0.85 k	1.32 c-g	1.10 c		
	1	1.33 c-g	1.27 e-i	0.84 k	1.15 bc		
	2	1.40 c-f	1.35 c-g	0.76 kl	1.17 bc		
Algae Interference	0.0	1.44 cde	1.88 a	1.53 bc	1.62 a		
	0.5	1.11 hij	1.28 d-i	0.46 mn	0.95 d		
	1	1.08 ij	0.94 jk	0.36 n	0.80 e		
	2	1.21 e-i	0.61 lm	0.43 mn	0.75 e		
Algae type * Hydrogel con.	*C. caeruleus*	1.36 a	1.37 a	1.09 c		1.27 a	
	P. roettleri	1.33 a	1.34 a	1.11 bc		1.26 a	
	Interference	1.21 b	1.18 bc	0.70 d		1.03 b	
	0.0	1.44 b	1.88 a	1.53 b			1.62 a
Algae con. * Hydrogel con.		1.14 d	1.27 c	0.88 fg			1.10 b
	1	1.30 c	0.98 ef	0.64 h			0.98 c
	2	1.31 c	1.06 de	0.82 g			1.06 b
Effect of hydrogel con.		1.30 a	1.30 a	0.97 b			

*Values with different letters indicate significant differences at the 5% probability level according to the Duncan multiple range test.

3.2 The length of the root system Length (cm): It was noted in Table 2 that when the soil was treated with hydrogel, an increase in root length at a concentration of 2 g/kg of soil amounted to 12.96 cm. The reason for this is that the increase in the length of the root system indicates that the plant needs loose soil to grow taller. Hydrogel is considered one of the soil improvers, and thus the roots go deeper and curl. Within the hydrogel, this is consistent with [13], as he showed the role of the gels in the soil, as they work to retain water and fertilizers, improve soil aeration, reduce evaporation, and thus led to plant improvement. The effect of the type of algae was found to be higher root length when treated with *C. caeruleus* algae reaching 13.19 cm. It was also observed that there was a significant increase between (concentrations of algae extracts), as the highest length reached the 2% concentration, recording 12.46 cm, except for the comparison treatment, while the two concentrations (0.5 and 1)% did not differ

significantly in root length. As for the Interference The binary (algae and gel concentration) *C.caeruleus* outperformed the rest of the treatments significantly with a length of 14.17 cm, while between the Interference (concentrations of algae extracts and gel concentration), the best root length was reached when wheat plants were treated with the gel level of 2 g/kg Soil with a length of 16.43 cm and a concentration of 2%, which recorded 14.06 cm. The results of (the algae used and their concentrations) also showed a significant effect between the treatments, and the highest root length was recorded when treated with *C. caeruleus* algae at a concentration of 2% and a length of 13.81 cm. In the double Interference (algae and gel and their concentrations) it was observed when treating the soil with *C. caeruleus* alga at a concentration of 2% gave the best root length, which reached 17.25 cm and was significantly superior to the rest of the treatments. The reason for the increase in the length of the root system may be because the algae extracts contain growth hormones similar to plant growth hormones, which have a role in elongating and dividing the size of the cells and increasing the branching and growth of the roots within the soil, this agreed with the increase shown in results for length of the root system, as mentioned in **Table 3**, is that the algae *Cladophora sp*. with concentrations of (1,2,3) on the sesame plant led to a significant increase in the length of the root compared to the control treatment **[14]**.

Table 2: The effect of algae extracts and hydrogel on root system length (cm)

Algae type	(%).Algae con	Hydrogel con.gm\kg soil			Algae type Algae .con	Effect of algae type	Effect of .algae con
		Control	2	4			
C. caeruleus	0.0	12.42b-g	16.43 ab	11.50 d-g	13.45 ab		
	0.5	13.33 a-f	14.33 a-d	11.67 c-f	13.11 abc		
	1	13.67 a-f	10.50 d-g	13.00 a-f	12.39 a-d		
	2	17.25 a	12.67 a-g	11.50 d-g	13.81 a		
P. roettleri	0.0	12.42 b-g	16.43 ab	11.50 d-g	13.45 ab		
	0.5	10.00 d-g	11.00 d-g	12.67 a-g	11.22 b-e		
	1	16.25 abc	10.75 d-g	11.67 c-g	12.89 a-d		
	2	12.75 a-g	13.75 a-e	12.00 b-g	12.83 a-d		
Algae Interference	0.0	12.42 b-g	16.43 ab	11.50 c-g	13.45 ab		
	0.5	13.00 a-f	9.25 efg	9.50 efg	10.58 de		
	1	9.75 d-g	12.00 b-g	9.00 fg	10.25 e		
	2	12.17 b-g	12.00 b-g	8.05 g	10.74 cde		
Algae type * .Hydrogel con	*C. caeruleus*	14.17 a	13.48 ab	11.92 b		13.19 a	
	P. roettleri	12.85 ab	12.98 ab	11.96 b		12.60 b	
	Interference	11.83 b	12.42 ab	9.51 c		11.26 c	
Algae con. * .Hydrogel con	0.0	12.42 bcd	16.43 a	11.50 cd			13.45 a
	0.5	12.11 bcd	11.53 cd	11.28 cd			11.64 b
	1	13.22 bc	11.08 cd	11.22 cd			11.84 b
	2	14.06 b	12.81 bcd	10.52 d			12.46 ab
.Effect of hydrogel con		**12.95 a**	**12.96 a**	**11.13 b**			

*Values with different letters indicate significant differences at the 5% probability level according to the Duncan multiple range test.

3.3 Leave water content: The results of **Table 3** show that treating wheat plants of the Mawada variety with hydrogel at a concentration of 2 g/kg of soil resulted in an increase in water content by 6.73%. This may be due to the ability of the gel to retain water and moisture for a long period in addition to its role in improving the physical and biological characteristics of the soil. **[11]**. As for the effect of the type of algae, the algae *C. caeruleus* was significantly

superior to the rest of the treatments by 7.12%. It was noted that the effect of the concentration of the algae was that the concentration of 1% gave the best result, amounting to 5.28%, although it was not significantly superior to the treatment Control. Between the two-way Interference (algae and gel concentration), there were significant differences between the treatments, as the highest water content was recorded when the soil was treated with *C. caeruleus* algae, amounting to 8.88%. As for the interaction (algae concentrations with gel concentrations), the highest increase in water content was observed when using the gel concentration of 2 g/kg soil. In the Interference (the algae used and their concentrations), the highest increase in water content was reached when treated with *C. caeruleus* algae at a concentration of 2%, reaching a rate of 8.21%, while the lowest relative water content was reached when treated with Interference at the concentration was (1.2) % and reached 2.43 in the triple intervention (algae and gel and their concentration). There are significant differences between the treatments. The highest percentage was reached when treated with *C. caeruleus* algae, at 13.78%, which is the highest percentage compared to the treatments and gel. The reason for the increase in water content in the algae may be due to its containing of nutrients, including potassium, which increases the ability of plant leaves to retain water and moisture, as it plays a role in controlling the opening and closing of stomata. These results are consistent with the study **[9]** when using seaweed (Soluamine and Seamino) at a concentration of 2.5% gave a significant increase. In the water content of the urethral flora.

Table 3: The effect of algae extracts and hydrogel on the Leave water content %.

Algae type	(%)Algae con	Hydrogel con.gm\kg soil			Algae type .Algae con	Effect of algae type	Effect of .algae con
		Control	2	4			
C. *caeruleus*	0.0	3.56 j-m	11.59 b	6.43 def	7.19 b		
	0.5	9.04 c	3.32 j-m	3.55 j-m	5.30 cd		
	1	13.78 a	5.64 efg	3.86 i-l	7.76 ab		
	2	9.12 c	10.14 c	5.38 e-h	8.21 a		
P. *roettleri*	0.0	3.56 j-m	11.59 b	6.43 def	7.19 b		
	0.5	7.35 d	4.47 g-j	2.22 mno	4.68 de		
	1	6.80 de	4.21 h-k	5.88 ef	5.63 c		
	2	3.90 i-l	5.21 f-i	4.29 g-j	4.47 e		
Algae Interference	0.0	3.56 j-m	11.59 b	6.43 def	7.19 b		
	0.5	5.97 def	6.69 de	3.81 i-l	5.49 c		
	1	2.77 k-o	3.02 j-n	1.50 o	2.43 f		
	2	2.62 l-o	3.33 j-m	1.87 o	2.61 f		
Algae type * .Hydrogel con	C. *caeruleus*	8.88 a	7.67 b	4.81 de		7.12 a	
	P. *roettleri*	5.41 d	6.37 c	4.71 e		5.49 b	
	Interference	3.73 f	6.16 c	3.40 f		4.43 c	
Algae con. * .Hydrogel con	0.0	3.56 fg	11.59 a	6.43 c			7.19 a
	0.5	7.45 b	4.83 de	3.19 g			5.16 b
	1	7.79 b	4.29 ef	3.75 fg			5.28 b
	2	5.21 d	6.23 c	3.85 fg			5.10 b
.Effect of hydrogel con		6.00 a	6.73 a	4.31 b			

*Values with different letters indicate significant differences at the 5% probability level according to the Duncan multiple range test.

3.4 Leave area (cm): The data in **Table 4** indicated that there were significant differences in the leaf area of wheat plants growing in soil treated with hydrogel. The highest area was obtained with the gel at a concentration of 2 g/kg of soil, reaching 12.48 cm compared to the

control treatment. The reason for this may be that the gel provides good nutritional and water storage for the plant during the growth period, which leads to an increase in the leave area of the plant [5]. As for the effect of algae, it was observed when treated with *P. roettleri* algae, and it was significantly superior to the rest of the treatments with an area of 12.47 cm. As for the effect of algae concentrations, it reached the highest increase in leaf area was 11.34 cm, except for the control treatment. The two-way Interference (algae and gel concentration) was observed when treating the soil with *P. roettleri* algae with the gel at a concentration of 2 g/kg soil and with an area of 13.71 cm, and it significantly outperformed the rest of the treatments. In the Interference (algae extract concentrations and gel concentration), it was found that in the gel treatment at the concentration of 2 gm/kg of soil, the highest leaf area was recorded, amounting to 16.24 cm, compared to the control treatment. It was also noted from the results that there were significant differences between (the algae used and their concentrations). It was found that the highest concentration at 1% was for the algae *P. roettleri*, except for the control treatment. As for the binary Interference (the algae and the gel and their concentrations) The best leave area was recorded when the soil was treated with *P. roettleri* algae at a concentration of (0.5 and 1%) with gel at a concentration of 2 gm/kg of soil with an area of 14.25 cm compared to the treatment. The reason for this is that the algae stimulate cell division, elongation, and expansion, and increase the efficiency of the photosynthesis process, thus increasing the leave area [9]. These results are consistent with the study of the effect of foliar spraying of green pepper seedlings with extracts of green algae *Chlorella vulgaris* at a concentration of 0.4%, causing an increase in leaf area compared to the control treatment. [12].

Table 4: The effect of algae extracts and hydrogel on the leaf area (cm)

Algae type	Algae (%).con	Hydrogel con.gm\kg soil			Algae type .Algae con	Effect of algae type	Effect of algae con.
		Control	2	4			
C. caeruleus	0.0	11.73 b-f	16.24 a	13.19 bcd	13.72 a		
	0.5	10.13 f-h	10.83 d-g	7.69 ij	9.55 d		
	1	13.77 bc	6.98 ij	12.99 bcd	11.25 c		
	2	11.56 c-f	13.91 abc	12.82 bcd	12.77 ab		
P. roettleri	0.0	11.73 b-f	16.24 a	13.19 bcd	13.72 a		
	0.5	12.40 b-e	14.25 ab	10.07 e-h	12.24 bc		
	1	12.38 b-e	12.37 b-e	13.94 abc	12.90 ab		
	2	11.76 b-e	11.97 b-e	9.31 f-i	11.01 c		
Algae Interference	0.0	11.73 b-f	16.24 a	13.19 bcd	13.72 a		
	0.5	12.92 bcd	11.59 c-f	12.21 b-e	12.24 bc		
	1	7.09 ij	9.04 ghi	5.88 j	7.34 e		
	2	7.39 ij	10.09 e-h	8.26 hi	8.58 d		
Algae * type Hydrogel .con	C. *caeruleus*	11.80 b	11.99 b	11.67 b		11.82 b	
	P. roettleri	12.07 b	13.71 a	11.63 b		12.47 a	
	Interference	9.78 c	11.74 b	9.89 c		10.47 b	
	0.0	11.73 c	16.24a	13.19 b			13.72 a
Algae * con. Hydrogel .con	0.5	11.82	12.22 c	9.99 de			11.34 b
	1	11.08 cd	9.46 e	10.94cd			10.49 c
	2	10.24 de	11.99 bc	10.13 de			10.79 bc
.Effect of hydrogel con		11.22 b	12.48 a	11.06 c			

*Values with different letters indicate significant differences at the 5% probability level according to the Duncan multiple range test.

3.5 Estimation of chlorophyll content: Table 5 indicates that there are significant differences between the treatments when treating the soil with the gel, as it was given better at the concentration of 4 g/kg of soil, and its percentage reached 7.96%, except for the control treatment. The explanation for this is that the hydrogel can retain water and provide it to the plant with the property of osmosis, and this in turn works to provide suitable conditions for the plant in terms of moisture inside the plant, ventilation of the roots, and increased plant growth, and these results are consistent with **[15]**. It was noted that the effect of the type of algae reached the highest percentage when treated with *C. caeruleus* algae, reaching 8.44%. As for the concentrations of the algae extracts, the two concentrations (1.0.5%) were superior. morally in content Chlorophyll, except the control treatment, reached (7.31, 7.81) %, while the dual Interference (algae and gel concentration) reached the highest percentage when treating the soil with the synergistic treatment of 11.15% and the gel at a concentration of 4 g/kg soil. In the effect of the algae used and their concentrations on the chlorophyll content when treated with algae *C. caeruleus* at a concentration of 1%, the highest increase was recorded at 9.50%, although it was not significantly superior to the control treatment. As for the triple Interference (algae and its concentrations with the gel and its concentrations), there were significant differences, as the highest percentage was reached at the synergistic treatment at a concentration of 1%, reaching 16.54, followed by *C. caeruleus* algae with the gel at a concentration of 4 g/kg. Soil by 15.05%. This may be because these extracts work to increase the absorption of magnesium from the soil, which leads to improving root growth and increasing their efficiency in the Absorption of nutrients, as well as the fact that these extracts contain micro- and macro-nutrients, thus increasing the concentration of chlorophyll a in the plant **[9]**.

Table 5: The effect of algae extracts and hydrogel on the Leaves of chlorophyll a.

Algae type	Algae (%).con	Hydrogel con.gm\kg soil			Algae type .Algae con	Effect of algae type	Effect of .algae con
		Control	2	4			
C. caeruleus	0.0	8.68 c	7.61 cde	13.24 b	9.84 a		
	0.5	7.96 cd	4.70 fg	ت11. 55 b	8.07 b		
	1	8.83 c	4.61 fg	15.05 a	9.50 a		
	2	8.67 c	6.53 de	3.79 g	6.33 cd		
P. roettleri	0.0	8.68 c	7.61 cde	13.24 b	9.84 a		
	0.5	8.10 cd	8.61 c	4.34 fg	7.02 c		
	1	4.04 g	7.81 cde	4.52 fg	5.46 de		
	2	6.69 de	3.45 g	4.32 fg	4.82 ef		
Algae Interference	0.0	8.68 c	7.61 cde	13.24 b	9.84 a		
	0.5	13.28 b	3.11 g	4.13 g	6.84 c		
	1	16.54 a	4.62 fg	4.24 fg	8.47 b		
	2	6.08 ef	3.33 g	3.84 g	4.42 f		
Algae type * .Hydrogel con	*C. caeruleus*	8.54 b	5.86 d	10.91 a		8.44 a	
	P. roettleri	6.88 c	6.87 c	6.61 cd		6.79 c	
	Interference	11.15 a	4.67 e	6.36 cd		7.39 b	
	0.0	8.68 c	7.61 de	13.24 a			9.84 a
Algae con. * .Hydrogel con	0.5	9.78 b	5.47 f	6.67 e			7.31 b
	1	9.80 b	5.68 f	7.94 cd			7.81 b
	2	7.15 de	4.44 g	3.99 g			5.19 c
.Effect of hydrogel con		8.85 a	5.80 c	7.96 b			

*Values with different letters indicate significant differences at the 5% probability level according to the Duncan multiple range test.

3.6 Determination of chlorophyll b content: It was noted from **Table 6** that the highest increase in the effect of the gel at a concentration of 2 g/kg of soil in the chlorophyll b content reached 14.36%, although it was not superior to the control treatment. The reason for this may be attributed to the hydrogel, which works to dissolve the nutrients necessary for plant growth, which are included in the composition of Chlorophyll **[16]**. In terms of the effect of algae type, *P. roettleri* algae was significantly superior to the rest of the treatments, reaching 15.15%. As for the effect of the concentrations of algae extracts, there were no significant differences between the two concentrations (0.5 and 1%), as they were significantly superior to the rest of the treatments. In the Interference (algae and gel concentration), the highest percentage was reached when treating *P. roettleri* algac with the gel, and it reached 2 g/kg soil compared to the rest of the treatments. In the effect of the concentrations of algae extracts with the gel concentration, the highest percentage was reached at a concentration of 2 gm/kg of soil and was recorded at 21.71%. As for the effect of the algae used and their concentrations, it was observed when treating soil growing with wheat plants. The best result was recorded when treated with *P. roettleri* algae at a concentration of 2% and amounted to 18.88%. The Interference (algae and its concentrations and the gel and its concentrations) was found to have the highest increase when treating the soil planted with wheat plants when treated with *P.roettleri* algae at a concentration of 0.5% with the gel at a concentration of 2 g/kg soil and it reached 27.52%, which was significantly higher than the control treatment and the reason for the increase may be due to what the algae extracts contain and gibberellins which stimulate the opening and maturation of flower buds, and auxins, which have a role in cell division and elongation, which have a role in increasing the chlorophyll content of leaves **[17]**.

Table 6: The effect of algae extracts and hydrogel on the determination of Leaves chlorophyll b

Algae type	Algae (%).con	Hydrogel con.gm\kg soil			Algae type .Algae con	Effect of algae type	Effect of algae .con
		Control	2	4			
C. caeruleus	0.0	8.68 ijk	7.60 k	11.36 ghi	9.21 f		
	0.5	22.32 bc	12.72 fg	9.83 h-k	14.95 bc		
	1	15.18 ef	27.01 a	4.64l	15.61 b		
	2	8.68 bc	7.60 g-j	11.36ghi	9.21 cd		
P. roettleri	0.0	8.68 ijk	7.60	11.36 ghi	9.21 f		
	0.5	15.77 e	27.52 a	9.89 h-k	17.73 a		
	1	19.79 d	14.56 ef	9.94 h-k	14.76 bc		
	2	22.64 b	23.38 b	10.63 g-j	18.88 a		
Algae Interference	0.0	8.68 ijk	7.60 k	11.36 ghi	9.21 f		
	0.5	18.18 d	10.51 g-j	9.02 h-k	12.57 de		
	1	11.51 gh	14.96 ef	8.41 jk	11.63 e		
	2	20.07 cd	8.21 jk	7.57 k	11.95 e		
Algae type * .Hydrogel con	*C. caeruleus*	17.15 ab	14.48 c	8.62 e		13.42 b	
	P. roettleri	16.72 b	18.26 a	10.46 d		15.15 a	
	Interference	14.61 c	10.32 d	9.09 e		11.34 c	
	0.0	8.68 gh	7.60 h	11.36 f			9.21 c
Algae con. * .Hydrogel con	0.5	18.76 b	16.92 g	9.58 g			15.08 a
	1	15.50 d	18.84 b	7.66 h			14.00 b
	2	21.71 a	14.06 e	8.95 gh			14.91 a
.Effect of hydrogel con		16.16 a	14.36 b	9.39 c			

*Values with different letters indicate significant differences at the 5% probability level according to the Duncan multiple range test.

3.7 Estimation of total chlorophyll content (a+b): Table 7 shows that there were significant differences between the treatments in the effect of the gel, as the highest percentage was reached with the gel at a concentration of 2 g/kg of soil, at a rate of 20.90%, although it was not significantly superior to the control treatment. The reason for this may be that the hydrogel can retain moisture which makes the soil fragile and increases its permeability through the swelling process of the gel, which helps to make the soil brittle thus the roots can penetrate the soil and thus have a positive effect in increasing plant growth **[18]**. As for the effect of the type of algae, it reached the highest percentage of chlorophyll content when treated with *C. caeruleus* algae recorded at 22.70%. As for the effect of algae concentrations, the 2% concentration was significantly superior to the rest of the concentrations, except for the control treatment. As for the interaction between the algae types and the gel concentration, there were no significant differences between the algae *C. caeruleus* and the synergistic treatment in their effect on the chlorophyll content. As for the Interference between the concentrations of algae and the concentration of the gel, it reached the highest percentage at the concentration of 2% and reached 30.84%. The results showed that the algae used with its concentrations gave the best results Algae *C. caeruleus* at a concentration of 2% and 25.88%. The reason for this may be attributed to the fact that these extracts contain many nutritional elements that are involved in the synthesis of the chlorophyll molecule, such as magnesium and other elements that are involved in the construction of the chlorophyll molecule **[19]**.

Table 7: The effect of algae extracts and hydrogel on the total chlorophyll content (a + b)

Algae type	Algae (%).con	Hydrogel con.gm\kg soil			Algae type .Algae con	Effect of algae type	Effect of .algae con
		Control	2	4			
C. caeruleus	0.0	20.59 ij	22.22 hi	24.67 fgh	22.49 b		
	0.5	25.73 efg	16.40 kl	14.10 lm	18.74 c		
	1	28.87 cde	29.37 cd	12.81 mn	23.69 b		
	2	35.65 a	14.96 klm	27.02 def	25.88 a		
P. roettleri	0.0	20.59 ij	22.22 hi	24.67 fgh	22.49 b		
	0.5	22.60 ghi	33.93 ab	14.24 klm	23.59 b		
	1	23.83 f-i	21.03 i	14.46 klm	19.78 c		
	2	30.70 bc	26.65 def	14.93 klm	24.09 b		
Algae Interference	0.0	20.59 ij	22.22 hi	24.67 fgh	22.49 b		
	0.5	32.72 ab	12.70 mn	13.76 lm	19.73 c		
	1	31.41 bc	17.54 jk	9.56 n	19.50 c		
	2	26.18 def	11.54 mn	11.67 mn	22.49 d		
Algae type * .Hydrogel con	*C. caeruleus*	27.71 a	20.74 d	19.65 d		22.70 a	
	P. roettleri	24.43 c	25.96 b	17.08 e		22.49 a	
	Interference	27.72 a	16.00 ef	14.92 f		19.55 b	
Algae con. * .Hydrogel con	0.0	20.59 e	22.22 de	24.67 c			22.49 a
	0.5	27.02 b	21.01 de	14.03 g			20.69 b
	1	28.04 b	22.65 d	12.28 h			20.99 b
	2	30.84 a	17.72 f	17.87 f			22.14 a
.Effect of hydrogel con		26.62 a	20.90 b	17.21 c			

*Values with different letters indicate significant differences at the 5% probability level according to the Duncan multiple range test.

3.8 Shoots Dry weight of shoots (g): It was observed from **Table 8** that when treating the soil with hydrogel at a concentration of 2 g/kg soil, it gave an increase in dry weight, except for the control treatment. The reason for the increase may be attributed to the fact that the hydrogel

can retain plants with food materials for a longer period thus increasing their percentage in dry weight [5]. As for the effect of algae type, there was no significant difference between the algae *C. caeruleus* and P. *roettleri* in dry weight, and they outperformed the i Interference treatment, reaching (1.27, 1.26) mg, respectively, and in the effect of concentrations. Algae extracts gave the highest significant increase at the concentration of 0.5% and reached 1.10 mg, except for the control treatment. As for the Interference In the duo (algae and gel), there were no significant differences when treated with *C. caeruleus* algae**, *P.roettleri*** algae, and the gel at a concentration of 2 gm/kg soil in its effect on the dry weight of the shoot. In the Interference (algae and gel concentrations), there were significant differences. The highest increase was reached when treated with hydrogel at a concentration of 2 gm/kg soil, and it was recorded at 1.88 mg. When using (algae and their concentrations), when treating the soil with *C.caeruleus* algae, at two concentrations (1.2%), the highest increase in the dry weight of the shoots is highest. As for the Interference (algae and its concentrations and the gel and its concentrations), it gave the highest results when treating the soil with *C. caeruleus* algae at a concentration of 0.5% with the gel at a concentration of 2g/kg of soil and it reached 1.67mg. The reason for the increase in dry weight may be the result of increased absorption of Nutrients from the root leads to increased vegetative growth, and this positively affects the dry weight of the plant [10].

Table 8: The Effect of algae extracts and hydrogel on the shoot's dry weight

Algae type	Algae con(%)	Hydrogel con.gm\kg soil			Algae type Algae con.	Effect of algae type	Effect of algae con.
		Control	2	4			
C. caeruleus	0.0	1.44 cde	1.88 a	1.53 bc	1.62 a		
	0.5	1.19 f-i	1.67 b	0.84 k	1.23b		
	1	1.50 bcd	0.73 kl	0.73 kl	0.99 d		
	2	1.30 d-h	1.20 f-i	1.25 e-i	1.25 b		
P. roettleri	0.0	1.44 cde	1.88 a	1.53 bc	1.62 a		
	0.5	1.13 g-j	0.85 k	1.32 c-g	1.10 c		
	1	1.33 c-g	1.27 e-i	0.84 k	1.15 bc		
	2	1.40 c-f	1.35 c-g	0.76 kl	1.17 bc		
Algae Interference	0.0	1.44 cde	1.88 a	1.53 bc	1.62 a		
	0.5	1.11 hij	1.28 d-i	0.46 mn	0.95 d		
	1	1.08 ij	0.94 jk	0.36 n	0.80 e		
	2	1.21 e-i	0.61 lm	0.43 mn	0.75 e		
Algae type * Hydrogel con.	*C. caeruleus*	1.36 a	1.37 a	1.09 c		1.27 a	
	P. roettleri	1.33 a	1.34 a	1.11 bc		1.26 a	
	Interference	1.21 b	1.18 bc	0.70 d		1.03 b	
Algae con. * Hydrogel con.	0.0	1.44 b	1.88 a	1.53 b			1.62 a
		1.14 d	1.27 c	0.88 fg			1.10 b
	1	1.30 c	0.98 ef	0.64 h			0.98 c
	2	1.31 c	1.06 de	0.82 g			1.06 b
Effect of hydrogel con.		1.30 a	1.30 a	0.97 b			

*Values with different letters indicate significant differences at the 5% probability level according to the Duncan multiple range test.

3.9 Roots Dry weight of the root system (g): The results shown in **Table 9**: The best result was given when treating the soil in the gel at a concentration of 2 g/kg of soil compared to the control treatment which amounted to 1.15 mg. This may be attributed to the roots benefiting from the ability of the hydrogel to retain nutrients for the longest possible period. It also has a role in reducing the Loss of nutrients and increasing penetration of roots into the soil [11]. As

for the effect of algae type, *P. roettleri* algae was significantly superior to the rest of the treatments, reaching 0.19 mg. The effect of algae concentrations was observed, reaching the highest increase in dry weight At a concentration of 1%, it was recorded as 0.18 mg. As for the Interference between the types of algae and the concentration of the gel when treated with *P.roettleri* algae with the gel at a concentration of 2 gm/kg soil, the interaction was also observed between the concentration of the algae extract and the concentration of the gel. The highest concentration reached 2 gm/kg soil compared to the control treatment, and it was significantly superior to the rest of the treatments and recorded as 0.19 mg. The effect of the algae used and their concentrations was found when treated with *P.roettleri* algae, which gave the highest concentration of 1% and amounted to 0.24 mg, while the results of the triple Interference (algae and its concentrations) showed that the gel and its concentrations were better The result when treating the soil with *P.roettleri* algae at a concentration of 1% and the gel at a concentration of 2 g/kg of soil gave 0.31 mg, while the lowest weight was recorded when treating the Interference algae at a concentration of 0.5% with the gel at a concentration of 4% and it amounted to 0.05 mg. The reason for this may be that the algae extracts have a role in increasing the growth of the root system by increasing the number of lateral branches, which increases the absorption of nutrients and increases their percentage in dry weight **[2]**.

Table (9) the effect of algae extracts and hydrogel on the root dry weight.

Algae type	Algae (%)con	Hydrogel con.gm\kg soil			Algae type .Algae con	Effect of algae type	Effect of .algae con
		Control	2	4			
C. caeruleus	0.0	0.14 ij	0.12 kjl	0.11 lm	0.12 f		
	0.5	0.11	0.12 klm	0.23 c	0.15 d		
	1	0.14 ij	0.11 kl	0.21 d	0.15 d		
	2	0.13 ijk	0.12 klm	0.11 kl	0.12 f		
P. roettleri	0.0	0.14 ij	0.12 klm	0.11 kl	0.12 f		
	0.5	0.18 efg	0.21 d	0.20 d	0.20 b		
	1	0.24 bc	0.31 a	0.17 fgh	0.24 a		
	2	0.25 b	0.19 de	0.11 kl	0.19 c		
Algae Interference	0.0	0.14 ij	0.12 klm	0.11 kl	0.12 f		
	0.5	0.13 jk	0.12 jkl	0.05 n	0.10 g		
	1	0.14 ij	0.12 jkl	0.16 gh	0.14 e		
	2	0.18 ef	0.15 hi	0.09 m	0.14 e		
Algae type * .Hydrogel con	*C. caeruleus*	0.13 d	0.12 e	0.17 b		0.14 b	
	P. roettleri	0.20 a	0.21 a	0.15 c		0.19 a	
	Interference	0.15 c	0.13 d	0.10 f		0.13 c	
	0.0	0.14 e	0.12 f	0.11 fg			0.12 c
Algae con. * .Hydrogel con	0.5	0.14 de	0.15 cd	0.16 c			0.15 b
	1	0.17 b	0.18 ab	0.18 ab			0.18 a
	2	0.19 a	0.15 c	0.11 g			0.15 b
.Effect of hydrogel con		0.16 b	0.15 b	0.14 c			

*Values with different letters indicate significant differences at the 5% probability level according to the Duncan multiple range test.

4. Conclusions:

Isolating two genera of algae, one of which is a red algae, the genus *C. caruleus*, and the other genera belongs to the green algae *P. roettleri*. Adding algae extracts to the wheat crop led to a significant stimulation of the studied traits, treated with *C. caeruleus* algae at a

concentration of 2%, which exceeded significantly the rest of the treatments compared to the control treatment. Adding the gel, especially at a concentration of 2 grams, had a positive effect on most of the traits studied. We conclude that improving plant growth may be because algal extracts contain quantities of growth regulators, which include gibberellins and cytokinins, which work to increase plant growth.

5. References

[1] AlRawi, D.H. Antibiotic activity of extracts and nanoparticles of some green algae against types of bacteria and fungi in the City of Mosul M.SC.*College of Education, University of Mosul.* 2023.

[2] Yusief , H.M. Allelopathic activity of two green algae their effects in some growth features of three wheat Cultivars Ph.D. *Mosul University College of Science*. 2023.

[3] Agha, Q., Asrar, M., Leghari, S.K. and Somalani, M.A. Algae, soil fertility and physicochemical properties in agricultural fields of Balochistan, Pakistan. *Pak. J. Bot*, *52*(4), pp.1491-1495. 2020.

[4] Zamani, S., Khorasaninejad, S. and Kashefi, B. The importance role of seaweeds of some characters of plant. *International Journal of Agriculture and Crop sciences*.5 (16):1789-1793. 2013.

[5] Al-Abbar, A.T.K. Polymer (Hydrogel) and the effect of its use on Agricultural crops. *Iraq Journal of Agricultural Research, 27*(1). 2023.

[6] Muhammad Yaseen, M.Y., Aziz, M.Z., Asif Manzoor, A.M., Muhammad Naveed, M.N., Yasir Hamid, Y.H., Sobia Noor, S.N. and Khalid, M.A. Promoting growth, yield, and phosphorus-use efficiency of crops in maize-wheat cropping system by using polymer-coated diammonium phosphate. 2017.

[7] Turne, C. Tchniques and experimental approaches for the measurements of plant water status.*plant and soil*,58,339-366. 1981.

[8] Kemp, C.D. Methods of estimating the leaf area of grasses from linear measurements. *Annals of Botany London,*24(96),491-499. 1960.

[9] Saied, D.T. Studies of variation in primary productivity growth and morphology in relation to the selective improvement of broadlraved the species.Ph.D.*National Uni.Ireland*. 1990.

[10] Altaee, R.E. Effect sprying Two Seaweed extract Soluamine and *Sorghum halepense* are growth in Soils Polluted by heavy metals M.SC.*College of Education for pure Science ,Uneversity of Mosul.* 2017.

[11] Abobatta, W. Impact of hydrogel polymer in agricultural sector. Adv. Agric. Environ. *Sci. Open Access,* 1(2), 59-64. 2018.

[12] Tian, S. L., Khan, A., Zheng, W. N., Song, L., Liu, J. H., Wang, X. Q., & Li, L. Effects of Chlorella extracts on growth of *Capsicum annuum* L. seedlings. *Scientific Reports*, 12(1), 15455. 2022.

[13] Sarkar, D., Meena, V. S., Haldar, A., & Rakshit, A. Site-specific nutrient management (SSNM): a unique approach towards maintaining soil health. Adaptive soil management: *from theory to practices*, 69-88. 2017

[14] Alkhafaji, B. Y., Malih, H. R., & Elkheralla, R. J. Effect of fertilization by *Cladophora* algae on morphological characteristics of Vigna radiate & Sesamum indicum plants. *In Journal of Physics: Conference Series* (Vol. 1294, No. 7, p. 072024). IOP Publishing. 2019.

[15] Singh, A.S., Richa, S., Dubey, V., and Kumar, P. Efficacy of pusa hydrogel and chitosan on wheat(Triticum aestivum L.) physiological Pharmacognosy and phytochemistry 7(5) :1589-1591. 2018.

[16] Abass, M.F. The Role of Hydrogel in Assisting Resistance of wheat Plant *Triticum aestivum* L.*to Salinity and Drought College of Education .University of Mosul*. 2022.

[17] Tuhy, Ł., Samoraj, M., & Chojnacka, K. Evaluation of nutrients bioavailability from fertilizers in in vivo tests. Interdisciplinary, *Journal of Engineering Sciences*, 1(1). 2013.

[18] Moghadam, H. R. T. Super absorbent polymer mitigates deleterious effects of arsenic in wheat. *Rhizosphere*, 3, 40-43. 2017.

[19] Castellanos-Barriga, L.G., Sanacruz-Ruvalcaba, F., Hernandez-Carmona, G., Ramirez-Briones, E. & Hernandes-Herrera, R.M. Effect of seaweed liquid extract from *Ulva lactuca* on seedling growth of mung bean (*Vigna radiata). Journal of Applied Phycology, 29(5):2479-2488. 2017.*

Al-Kitab Journal for Pure Sciences (2024); 8(2):153-170.
https://doi.org/10.32441/kjps.08.02.p13

Al-Kitab Journal for Pure Sciences
ISSN: 2617-1260 (print), 2617-8141(online)
https://isnra.net/index.php/kjps

A Study on New Roulette and Special Forms of Cycloid and Laithoidal Curves

Laith H. M. Al-Ossmi*

Department of Civil Engineering, College of Engineering, University of Thi-Qar, Thi-Qar, IRAQ

*Corresponding author: laithhady@utq.edu.iq

*ORCID ID: https://orcid.org/0000-0002-6145-9478

CitationAl-ossmi LHM. A Study on New Roulette and Special Forms of Cycloid and Laithoidal Curves. Al-Kitab J. Pure Sci. [Internet]. 2024 Jul. 12 [cited 2024 Jul. 12];8(02):153-170. Available from: https://isnra.net/index.php/kjps/article/view/1194 https://doi.org/10.32441/kjps.08.02.p13.

Keywords: Cycloid, Geometrical Method, Laithoid, Roulette.

Article History

Received	19	May.	2024
Accepted	30	Jun.	2024
Available online	12	July	2024

Abstract:

This article deals with a new roulette of special curves formed by a circle rolling along a line which are given the name of Laithoid curves. The new curve is a new special form of cycloid produced by rolling a circle along a horizontal line of 4 times the rolling circle's radius. It is the locus traced out by a point fixed to a circle (where the point may be on, inside, or outside the circle), as it rolls along a straight line. In this paper, a set of 6 forms of new curvatures within two groups are produced depending on a rolling circle on the Laithoid's curve, and their geometrical and algebra proportions are graphically formed. Furthermore, the article provides the coordinate equations that govern the points along these curves. With the potential to pave the way for exploring additional geometric aspects relevant to this class of curves, and to enable comparative analyses across diverse mathematical and geometric domains, particularly in three-dimensional contexts in the future.

Keywords: Cycloid, Geometrical Method, Laithoid, Roulette.

دراسة حول المنحنيات الناتجة من حركة نقطة، توليد حالات خاصة من المنحنيات السايكلويدية، حالة المنحنيات الليثويدية

ليث هادي منشد العصامي*

كلية الهندسة / جامعة ذي قار/ محافظة ذي قار / العراق

laithhady@utq.edu.iq

الخلاصة:

يدرس هذا البحث حالة جديدة من المنحنيات الخاصة التي تتشكل عندما يتحرك دائرة على طول خط، وقد أُطلق عليها اسم منحنيات ليثويد. منحنى الليثويد هو حالة خاصة من منحنى السايكلويدي والذي ينتج عن طريق دوران دائرة بدون انزلاق على خط أفقي بطول ٤ مرات نصف قطر الدائرة المتحركة. وهذا المنحني هو المسار الذي يرسمه نقطة ثابتة على دائرة (حيث يمكن أن تكون النقطة على الدائرة أو داخلها أو خارجها)، أثناء تحركها على خط مستقيم.

في هذا البحث، تم إنتاج مجموعة من ٦ حالات جديدة من هذا المنحني ضمن مجموعتين تعتمد على دوران الدائرة على منحنى ليثويد، وتشكيلها بشكل هندسي وجبري بياني. علاوة على ذلك، يقدم المقال معادلات الإحداثيات التي تحكم النقاط على هذه المنحنيات. ويتيح ذلك الإمكانية لاستكشاف جوانب هندسية إضافية ذات صلة بهذا النوع من المنحنيات، وإجراء تحليلات مقارنة عبر مجموعات رياضية وهندسية متنوعة، لا سيما في السياقات ثلاثية الأبعاد في المستقبل.

الكلمات المفتاحية: منحني الدويري، طريقة إنشاء هندسية، منحني الليث.

1. Introduction:

In algebraic geometry, a cycloid is the curve traced by a point on a circle as it rolls along a straight line without slipping. Also, a cycloid is a specific form of trochoid and is an example of a roulette, a curve generated by a curve rolling on another curve. The cycloid generated by a rolling circle, which can be produced by different methods using a fixed point traced on a circle's circumference with the cusps pointing upward, is the curve of fastest descent under uniform gravity, known as the brachistochrone curve **[1]**. It is also the form of a curve for which the period of an object in simple harmonic motion (rolling up and down repetitively along the curve) does not depend on the object's starting position, known as the tautochrone curve **[2]**. Before describing this new special case of the cycloid, some historical background is in order. Historians of mathematics have proposed several candidates for the discoverer of the cycloid: English mathematician John Wallis, writing in 1679 **[3]**, Nicholas of Cusa **[4]**, Père Marin Mersenne **[5]**, Galileo Galilei **[6]**, Marin Mersenne **[7]**, Moritz Cantor [8], Siegmund Günther **[9]**, and the works of Charles de Bovelles **[10]**. During the seventeenth century, Pascal proposed three questions relating to the center of gravity, area, and volume of the cycloid **[11]**. Fifteen years later, Christiaan Huygens deployed the cycloidal pendulum and discovered that a particle would traverse a segment of an inverted cycloidal arch in the same amount of time, regardless of its starting point **[12]**.The cycloid curve in algebraic geometry, through the origin, generated by a circle of radius r rolling over the x-axis on the positive side ($y \geq 0$), consists of the points (x, y), where it is a real parameter corresponding to the angle through which the rolling circle has rotated. For given t, the circle's center lies at $(x, y) = (rt, r)$, with equations:

$$x = r\,(t - \sin t),$$
$$y = r\,(1 - \cos t),$$

The *Laithoid*'s curve is a special case of cycloid; it is the curve traced by a point on a circle as it rolls along a straight line with the length of ($2a$) where (a) is the radius of the rolling circle [13]. Also, *Laithoid* is not an example of a roulette because it is not a curve generated by a curve rolling on another curve, hence it is generated by a rolling circle (Drawing Circle), on a straight line with a specific length related to a circle's radius [14,15]. However, all these derivate forms of curvatures produced from *Laithoid* are examples of a roulette as they all are generated by a circle rolling on the *Laithoid* curve.

2. Drawing Method:

The method for drawing the new curve, *Laithoid*, involves several steps:

1. **Drawing the Initial Circle**: by drawing a circle with a specified radius a.
2. **Dividing the Vertical Diameter**: Divide the vertical diameter of the circle into equal parts, n_1, n_2, …
3. **Drawing Horizontal Lines**: Draw a horizontal line from the center of the circle with a length equal to $2a$. Extend this horizontal line to a length of $4a$ and divide it similarly into equal parts, c_1, c_2, …, matching the divisions of the vertical diameter.
4. **Drawing Moving Circles**: Draw circles representing the non-slipping movement of the initial circle, where the center moves sequentially to the points n_1, n_2, …,
5. **Drawing Rays**: From the uppermost point of the vertical diameter of each circle, draw a ray. This ray starts from the point that is a distance of $2a$ from the edge of the terminal circle.

The construction of a *Laithoid* using geometric tools is illustrated in **Figures 1** and **2**.

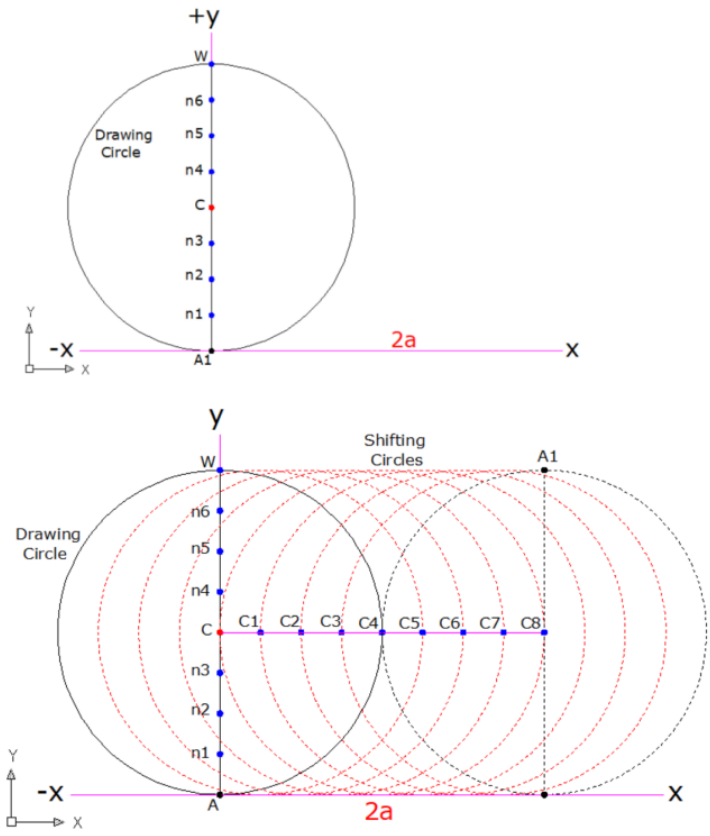

Figure 1: Construction of a *Laithoid* using a rolling disk's radius (a) along a path of ($4a$)

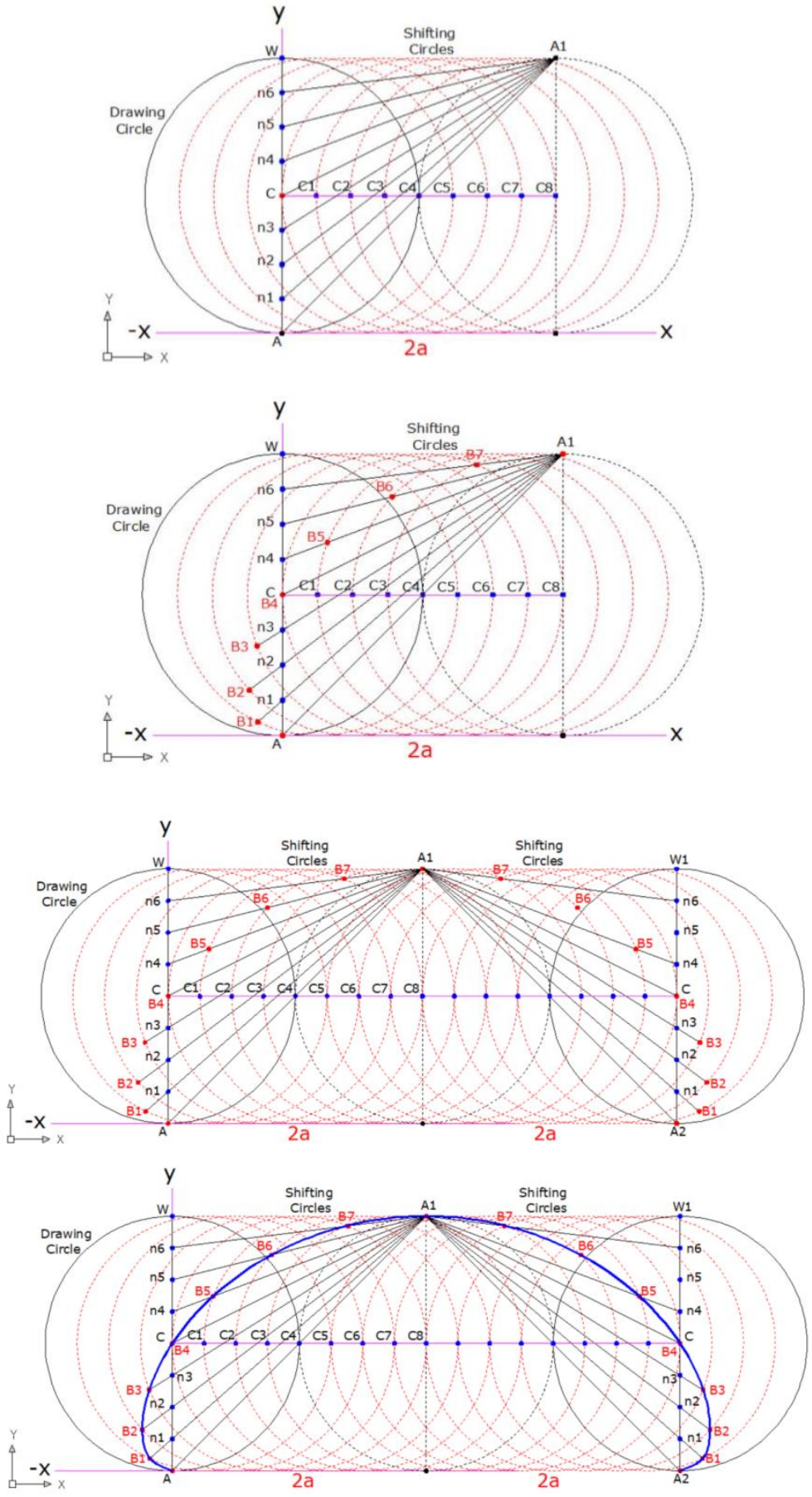

Figure 2: The plot of the construction of a *Laithoid* using a geometric method

2.1 Laithoid's Equations: Let a drawing circle with radius (a), and point (A) be the origin, (0,0). By drawing the Laithoid's arch passing from point (A) and (A_1) till (A_2), the horizontal distance is ($4a$). Each point on the curve is a result of rolling the drawing disk with angles; ($BNC_1 = t$) and ($BC1D_1 = u$), where point (B) lies at *Laithoid*, (see **Figure 3**).

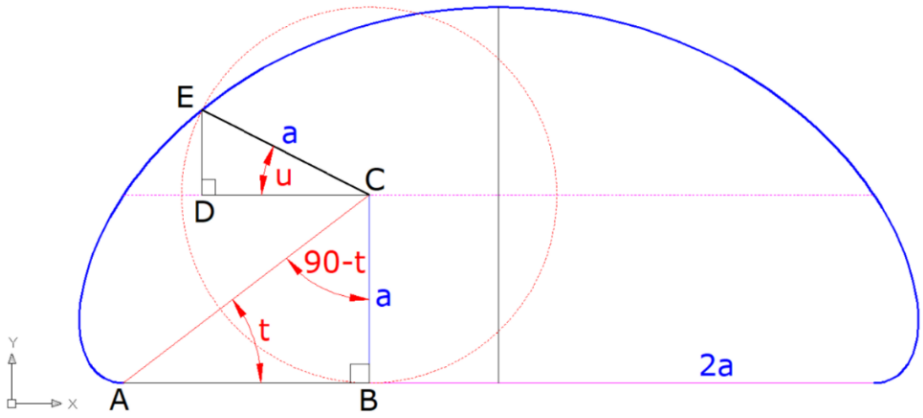

Figure 3: The plot of the Laithoid curve using a geometric method

Therefore, from **Figure 3** the *Laithoid* is the path traced out by a fixed point (B) on the boundary of a circular disk whose radius (a) rolls along a horizontal line ($4a$), to produce an arch with the length of (7.000700558440277713 a), as it is shown in **Table 1**.

Table 1: *Laithoid's* key properties

Properties Values	Properties Values
Rolling disk's radius, a	Rolling disk's radius, a
Start point (0,0)	Start point (0,0)
Top point ($2a$,$2a$)	Top point ($2a$,$2a$)
Cusp's intersection	(a,0)
Two arches cusp	$\pm(a, 0)$ and $\pm$ $(2a, a)$
End point ($4a$,0)	End point ($4a$,0)

From **Figure 3**, let (a) be the radius of the rolling circle and (t) be an angle between the segment line from the circle center (C) and the horizon line (AB) drawn from the origin point (A), this gives the Cartesian equations of the Laithoid's curve:

$$x = (AB - 2a) - DC, \quad (1)$$

$$y = ED + a, \quad (2)$$

$$\sin u = \frac{DE}{a},$$

$$\cos u = \frac{DC}{a},$$

$$DC = a \cos u,$$

Then by angle (t) and a simple trigonometry, we find:

$$\tan t = \frac{a}{AB},$$

$$AB = \frac{a}{\tan t},$$

Then for any point (x,y), we can find:

$$x = \left(\frac{a}{\tan t} - 2a\right) - a\cos u, \quad (3)$$

$$x = \left(\frac{a - 2a\tan t}{\tan t}\right) - a\cos u, \quad (4)$$

$$y = a\sin u + a, \quad (5)$$

$$y = a(\sin u + 1), \quad (6)$$

According to *Laithoid's* proportions, it shades region of area which can also be done by calculus, which is not exactly inconsequential. Then it must integrate this to get the required area covered by *Laithoid*:

$$A = \int_{x=0}^{2\pi a} y dx = \int_{u=0}^{2\pi} a^2 (1+\sin u)^2 du\,, \quad (7)$$

$$A = \int_{x=0}^{2\pi} a^2 (1 + 2\sin u + \sin^2 u)\, du\,, \quad (8)$$

$$Laithoid's\ Area = 2.2797365122\,\pi a^2\,, \quad (9)$$

This region under one *Laithoidal* arch and the horizontal line of (4*a*) is more than double times the area of the rolling circle. Obtained data from Table 1 indicates that the ratio between Laithoid's length and its rolling disk's circumference is precisely (1.1143102520478548*a*), nevertheless, this ratio related to cycloid is found to be (1.2978725139014964*a*), as shown in **Figure 3**. Along the coordinators of the y-axis and x-axis, (**Figure 3**), there is only one point (A) in which both curves, Cycloid and *Laithoid*, are intersected. Using the same rolling disk that rolls along a horizontal line, both curves make up an intersection point (V_1) which lies at (±2.56483 *a*, 1.94521 *a*), precisely it is:

$$AV_2 = 2.564834658174025\ a, \quad (10)$$

$$V1V_2 = 1.945206239700822\ a, \quad (11)$$

Similarly, to Trochoid **[12]**, the *Laithoidal* arches also have a cusp at point (A) whose intersection point (0, *a*) lies at the y-axis, whereas cycloid arches have not, **Figure 4**. Also, for each rolling of the drawing disk along the horizontal line (A_1A_2), the cycloid's arch requires a horizontal distance of (6.518839490783036347*a*), which is precisely (1.631668317375) time of *Laithoid's*, hence *Laithoid's* arch requires a horizontal distance of (4*a*), (as it is listed in **Table 2**).

Table 2: Comparison of the key proportions of Cycloid and Laithoid.

Key proportions	Cycloid	Laithoid	ratio
Curve's length.	$8a$	7.000699277711867699 a	1.142742986471309640
Covered area.	$3\pi a^2$	2.27973675122 πa^2	1.315941412268127658
Horizontal distance.	$2a\pi$	$4a$	1.570796326721501765
The hump height.	(3.2590a, 2a)	(2a,2a)	-
Cusp's length.	-	1.17507941583 a	-
Cusp's area.	-	2.4809340098320 πa^2	-
Cusp's intersection P.	(0, 0)	± (0, a)	1.000000000000000000
Where (a) is the rolling disk's radius.			

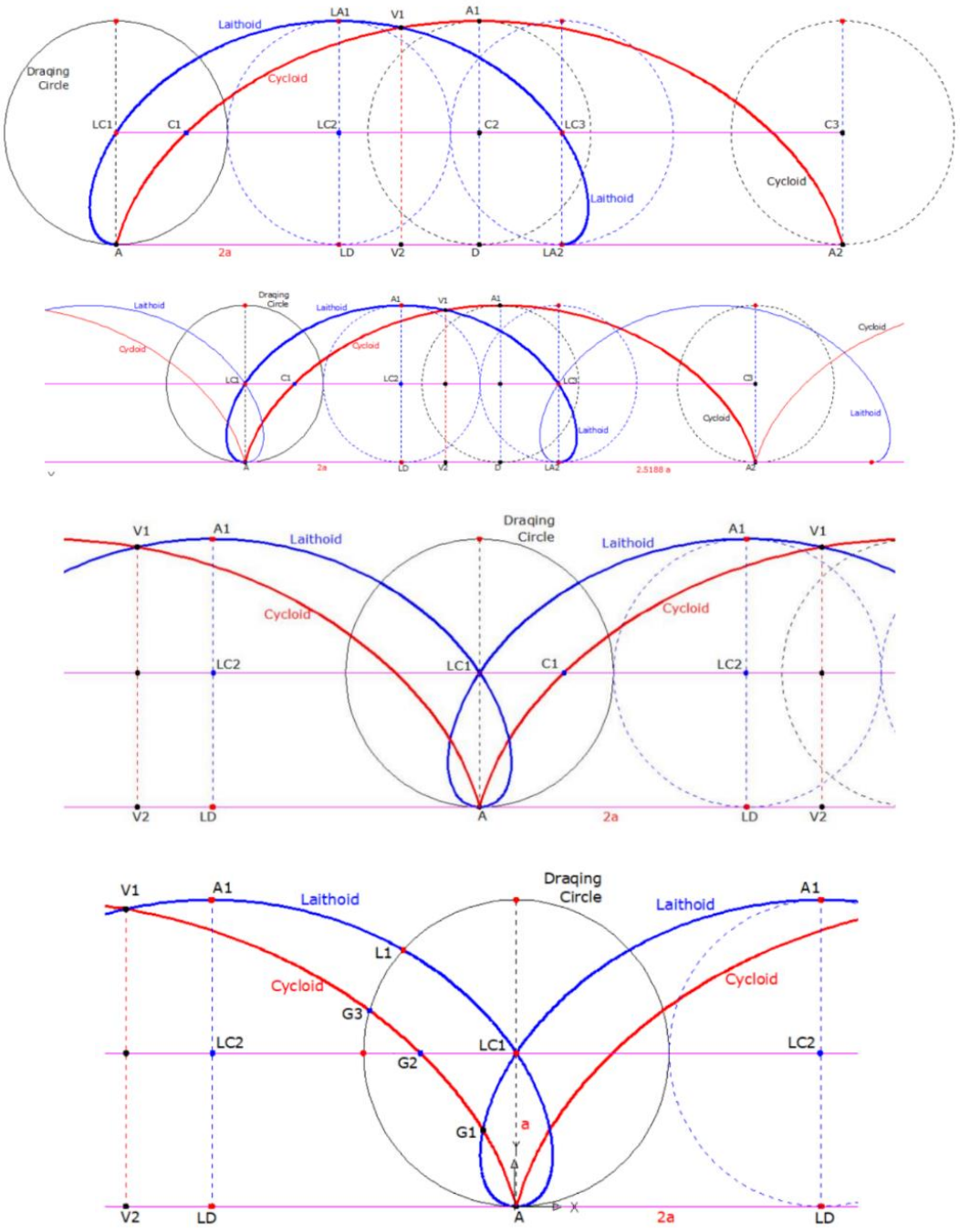

Figure 4: The plot of the comparison of the key points of Cycloid and *Laithoid*, where (*a*) is the rolling disk's radius

It is perceptible from **Figure 4** that from the origin point (A), the cycloid intersects with the drawing disk at two points,(G_1) and (G_2) in addition to point (G_3) through the horizontal distance from the center of the disk. While 3 points of Laithoid are; (A), (LC_1), and (L_1) with which the curve intersects with the disk's circumference. However, regardless of point (A), both curves intersect at two points; (G_2) and (V_1), more proportions are shown in **Table 3**.

Table 3: Comparison between the intersection points of Cycloid and Laithoid

Points	Cycloid	Laithoid
A	(0,0)	
G_1	± (0.2184a, 0.4993a)	
G_2	± (0.6297a, a)	-
G_3	± (0.9606a, 1.2776a)	-
LC_1	-	(0,a)
L_1	-	± (0.7398a ,1.6727a)
V_1	±(1.9399a, 2.5562a)	
Where (a) is the rolling disk's radius.		

In this paper, Laithoid's curve has been used to produce a set of new forms of curves, which are graphically studied and figured using AutoCad utility, (Version 2020).

3. Laithoid's family

There is a part of a new family of curves invented from the Laithoid curve that will be described here presently. In this paper, a new set of 6 curves are produced. In general, these 6 curves can be tabulated into two groups, the closed and opened curves. The first group is those curves that complete a full rolling at one point, (2a,0) without a cusp, while the second group is those that complete a full rolling at two points, (0,0) and (4a,0).

A- Group One: in this paper 3 forms of new curves were produced. Let a Laithoid and a given drawing circle with radius (a), let the drawing circle lie from its center at point (2a, a), where angle (u) is between line segment (BD) and x-axis. Let point (B) be a point at the Laithoid, then construct segment (BD), and from (B) draw a horizontal ray to intersect the circle at (B_1), then from point (B_1) draw a perpendicular to intersect the circle's circumference at (n_1), shown in **Figure 4**. Then;

$$Dn_1 = 2a\ sin(90 - u), \tag{12}$$

$$x = 2a\ \sin(90 - u)\ \sin(90 - u), \tag{13}$$

$$\boldsymbol{x} = sin(90 - u)\ (2a - 1), \tag{14}$$

$$\tan(90 - u) = 2a\ \cos(90 - u)\ \sin(90 - u)\ y\ , \tag{15}$$

And then we can obtain:

$$y = \left(\frac{2\ a\cos(90-u)\sin(90-u)}{\tan(90-u)}\right), \tag{16}$$

$$y = \left(\frac{2\,a\cos^2(90-u)\sin(90-u)}{\sin(90-u)}\right), \quad (17)$$

$$y = 2\,a\,cos^2(90-u), \quad (18)$$

$$\left(\frac{x}{y}\right) = \left(\frac{\sin(90-u)(2a-1)}{2\,a\,cos^2(90-u)}\right), \quad (19)$$

Then it is obtained that any point of the *laithoid's* curve can be described by ;

$$\boldsymbol{y} = \left(\frac{x\ 2\ a\,cos^2(90-u)}{sin(90-u)(2a-1)}\right), \quad (20)$$

$$\boldsymbol{x} = \left(\frac{y\ sin\ (90-u)}{2\ a\,cos^2(90-u)}\right), \quad (21)$$

Figure 5 shows that the heart-like curve is a closed curve without a cusp, and it intersects with the x-axis at (2a,0), and tangents with Laithoid by a single point (D1) at the top which is (2a,a). The coordination of any point of this curve can be determined by the ray drawn from a point (B) at laithoid and point (D), the intersection point between (BD) and the drawing disk (n_1), the horizontal and vertical segments from (B) and (n_1) will determine a point of the curve, (B_1). This new curve has a shaded region with an area of ($0.8223858140642\pi a^2$), and a length of ($6.127795789824198a$), where (a) is the rolling disk's radius, (**Figure 5**).

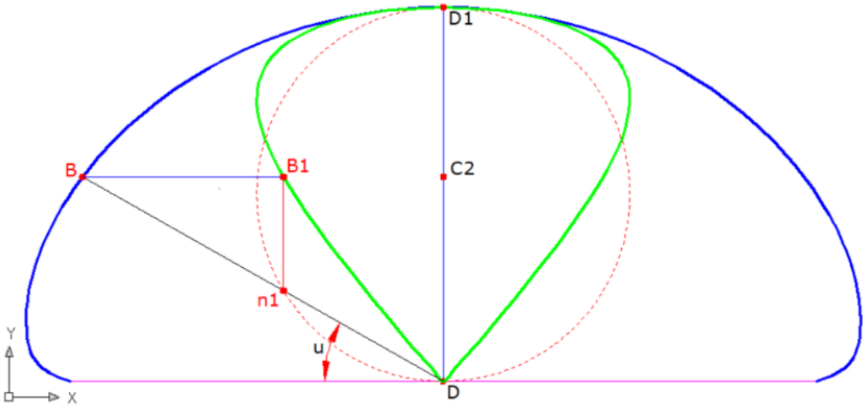

Figure 5: Construct a new form of curves from a point on Laithoid.
Where (a) is the rolling disk's radius, and (u) is the angle between the segment line from the origin (D) and the horizon line.

By changing the radius value of the rolling disk, another set of heart-like curves is formed. When the value of the radius of the rolling disk declined to (0.5 a), the curve tended to shrink from the top taking a shape of drop close to the y-axis, which decreased its shaded region area. In general, the length value of the curves depends on the value of the radius of the rolling disk regardless of that of drawing the circle of Laithoid. Correspondingly, the horizontal width of the curve is determined by the value of its rolling disk's radius.

When the radius of the rolling disk (0.5a) then the produced curve has a length of (4.7836971666054a) and a shaded region area of (0.4110219882904975 πa^2), while in case

radius of the rolling disk is (1.5a) the new curve is more inflated and has a length value of (5.412244557765046a), and more area in its shaded region of (0.6156407068172649πa^2), as it is shown in **Figure 6**.

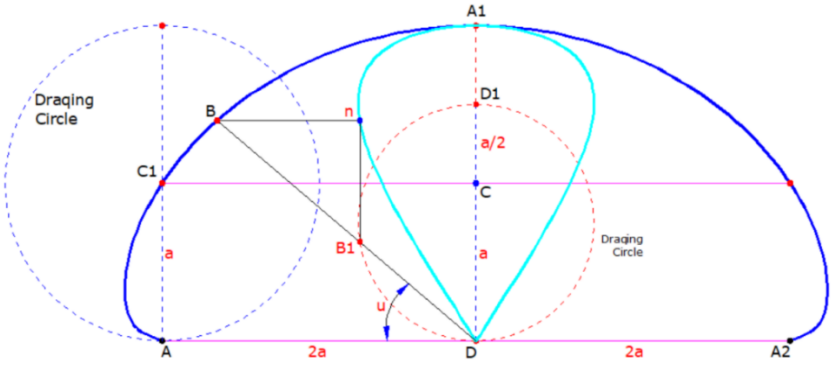

Where the rolling disk's radius is (1.5a)

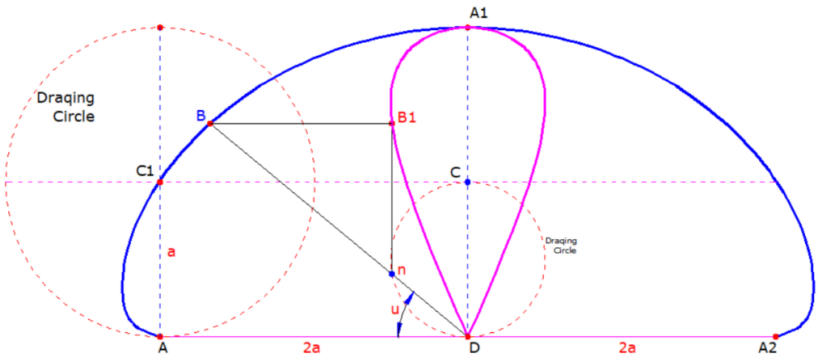

Where the rolling disk's radius is (0.5a)

Figure 6: Constructing a new form of curves from a point on Laithoid, where the rolling disk's radius is (1.5a) and (0.5a)

B- Group Two: In this group, 3 forms of new curves were produced. Let a *laithoid* and a given drawing circle with radius (a), let the drawing circle lie from its center at point (2a, a), where angle (u) is between line segment (BD) and the x-axis. Let point (B) be a point at the Laithoid, then construct segment (BD), and from (B) draw a horizontal ray to intersect the circle at (B_1), then from point (B_1) draw a perpendicular ton intersect with the circle's circumference at (n_1), shown in **Figure 6**. Then;

$$B_1(x) = B_1D \cos u, \tag{22}$$

$$DB_1 = 2a \cos (90 - u), \tag{23}$$

Then the value of y can be obtained by:

$$\boldsymbol{y} = 2a\ cos^2\ (90 - u), \tag{24}$$

Figure 7 shows that this form of the curve is an opened curve with a cusp between two arches along the y-axis, as it intersects with the x-axis at (0,0) and (2a,0), and tangents with *Laithoid* by a single point (D_1) at the top which is (2a, a). The coordination of any point of this

curve can be determined by the ray drawn from a point (B) at *Laithoid* and point (D), the intersection point between (BD) and the drawing disk is (n_1), the horizontal and vertical segments from (B) and (n_1) will determine a point of the new curve, (B_1).

This new curve has a shaded region and a length, where (a) is the rolling disk's radius, a set of these curves is illustrated in **Figures 6** and **7**. It is noticeable that all points of this form of curve are the intersection of these rays drawn between (D) and (B). Also, the produced curve (green in **Figure 7**), has a cusp with *Laithoid's* curve which is formed by two intersection points:

$$\pm(0.12968796501a,\ 0.2086584604810a),$$

$$\text{and } (4.129687965a,\ 0.2086584604810a).$$

Correspondingly, the intersection point of the curve's cusp lies at point (0, $0.416009485062a$), in addition, its cusp length is made up of ($1.37384011705a$), hence this form of curve correspondingly shaded region area of ($0.0357779584131759\ \pi a^2$), (see **Figure 7**, and **Tables 4**,**5**,**6**, and **7**).

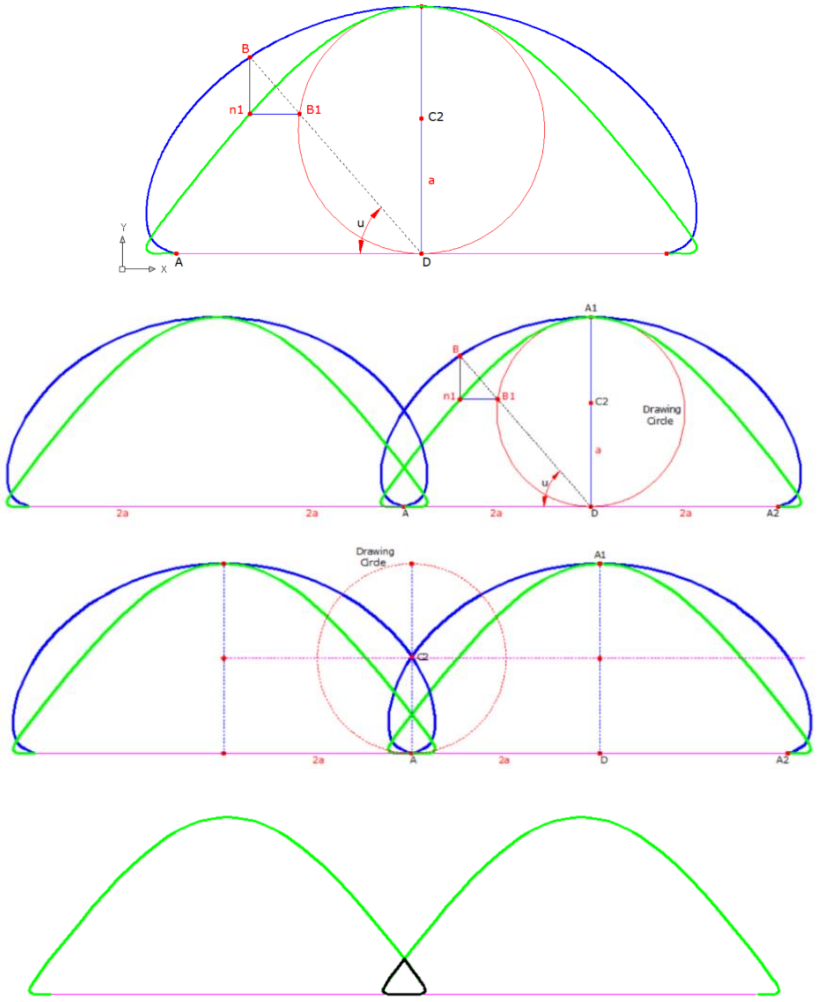

Figure 7: Constructing a new form of curves from a point on *Laithoid* where the rolling disk's radius is (a) and (n_1) a point on the curve

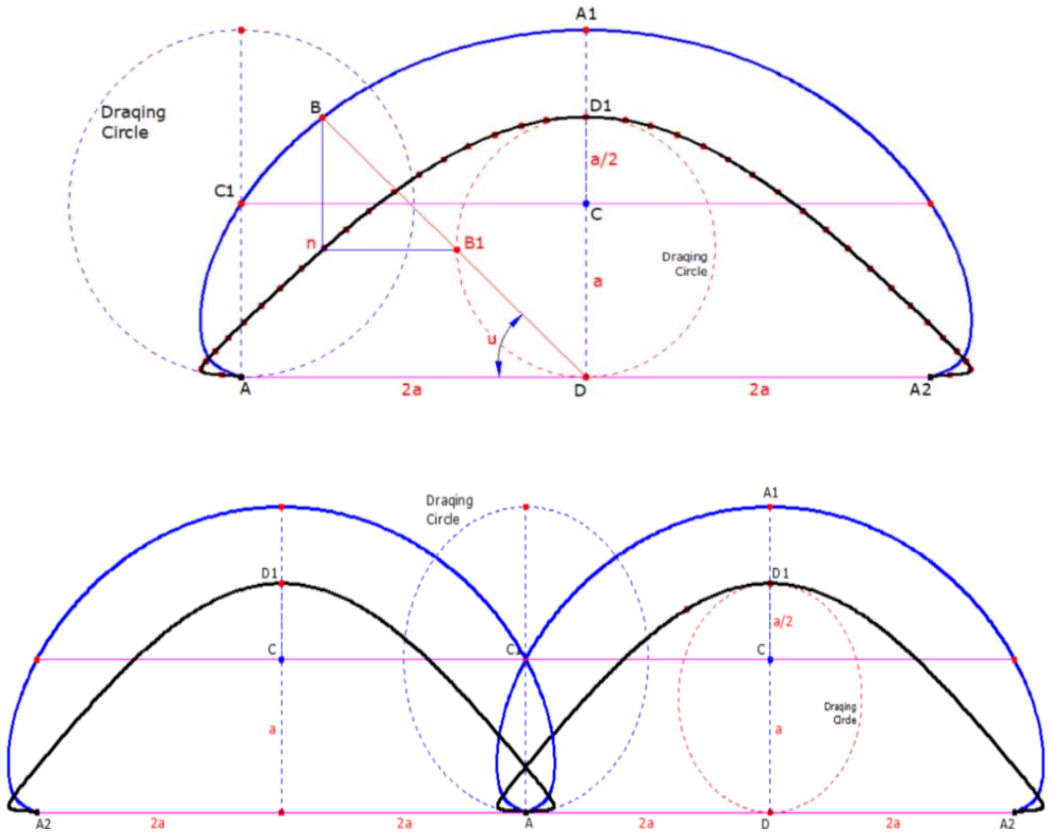

Where the rolling disk's radius is (1.5a).

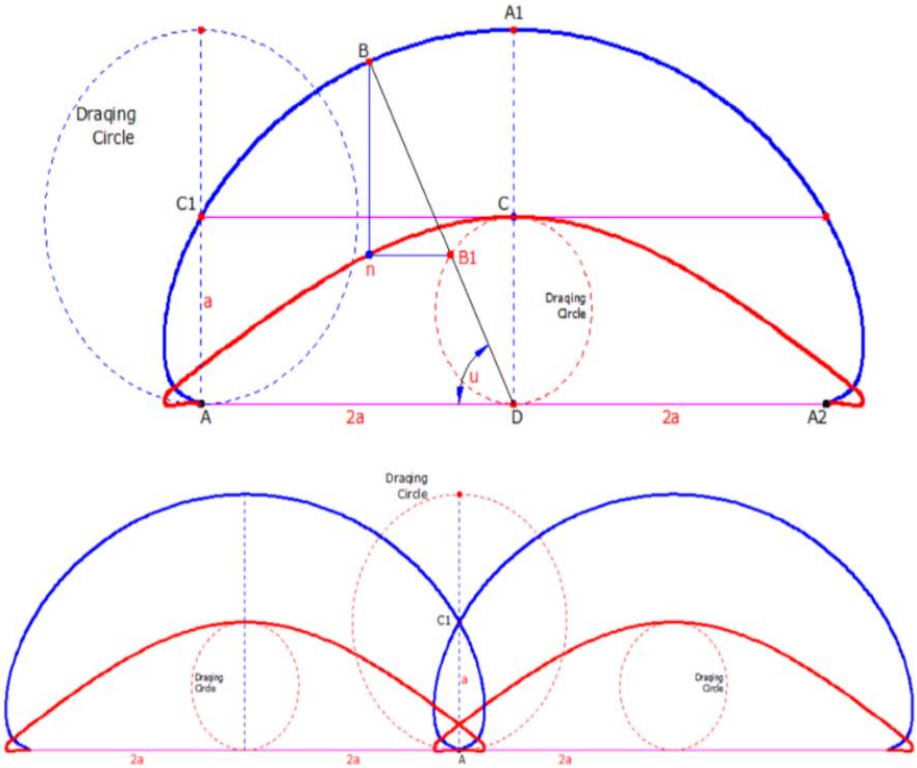

where the rolling disk's radius is (0.5a).

Figure 8: Constructing a new form of curves from a point on Laithoid, where the rolling disk's radius is (*a*) and (*n*) a point on the curve.

Table 4: Comparison of group one's curves related to Laithoid

Points	Group one's curves	Laithoid
Start point	(2a,0)	(0,0)
Top point	(2a,a)	(2a,a)
Endpoint	(2a,0)	(4a,0)
Length	(varied)	(7.000690251107a)
Shaded area	(varied)	(2.278887062739374 $\pi\ a^2$)
Cusp's area	-	(0.105913393319132167 πa^2)
Where (a) is the rolling disk's radius of Laithoid.		

Table 5: Comparison of group two's curves related to Laithoid

Points	Group Two's curves	Laithoid
Start point	(0,0)	
Top point	(2a,a)	
Endpoint	(4a,0)	
Length	(varied)	(7.000690251107a)
Shaded area	(varied)	(2.278887062739374 $\pi\ a^2$)
Cusp's area	(varied)	(0.105913393319132167 πa^2)
Where (a) is the rolling disk's radius of Laithoid.		

Table 6: Key properties of Group One's curves

Properties	L 1	L 2	L 3
Length	4.7836971666054 a	5.41224455776504 a	6.127795789824198 a
Shaded area	0.411021988290 πa^2	0.61564070279121 πa^2	0.82238581422668πa^2
Cusp's length	-	-	-
Cusp's area	-	-	-
Tangent point*	(2a, a)		
Intersection point*	-	-	-
**Shaded points with a Laithoid.* *Where (a) is the rolling disk's radius of Laithoid.*			

Table 7: Key properties of Group Two's curves

Properties	L 1	L 2	L 3
Length	6.654806579093416a	5.9604358927946a	5.47020227329001a
Shaded area	1.84053446580540πa^2	1.3774307432443πa^2	0.92072136146895πa^2
Cusp's length	1.3740375859635581a	1.10172429250216 a	0.551372160842206 a
Cusp's area	0.0188500927561 πa^2	0.0125071773814πa^2	0.00917801064989πa^2
Tangent point*	(2a, a)		
Intersection point*	± (0.2008444685a, 0.141708219704a)	± (0.1857509648141a, 0.1114055079789a)	± (0.169865928825a, 0.08678455016606a)
**Shaded points with a Laithoid.* *Where (a) is the rolling disk's radius of Laithoid.*			

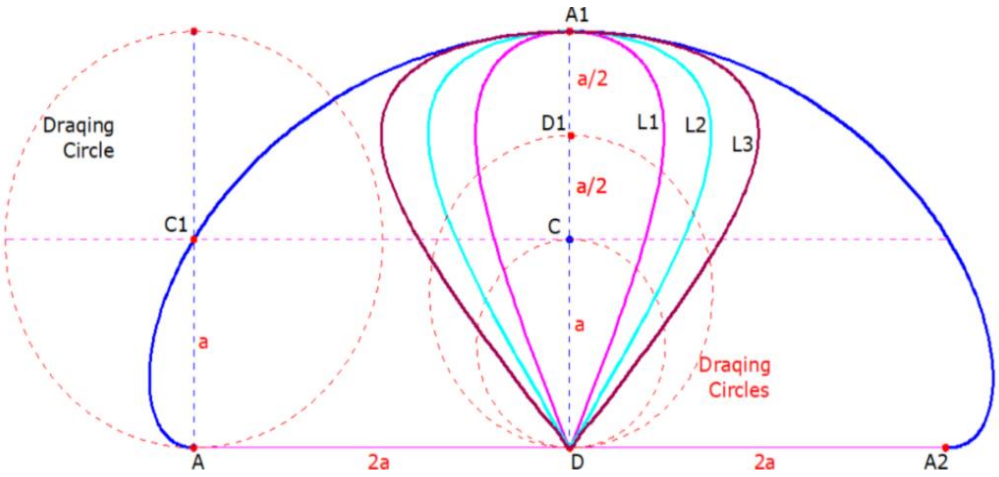

Group one; 3 curves of heart-like; (L_1), (L_2), and (L_3).

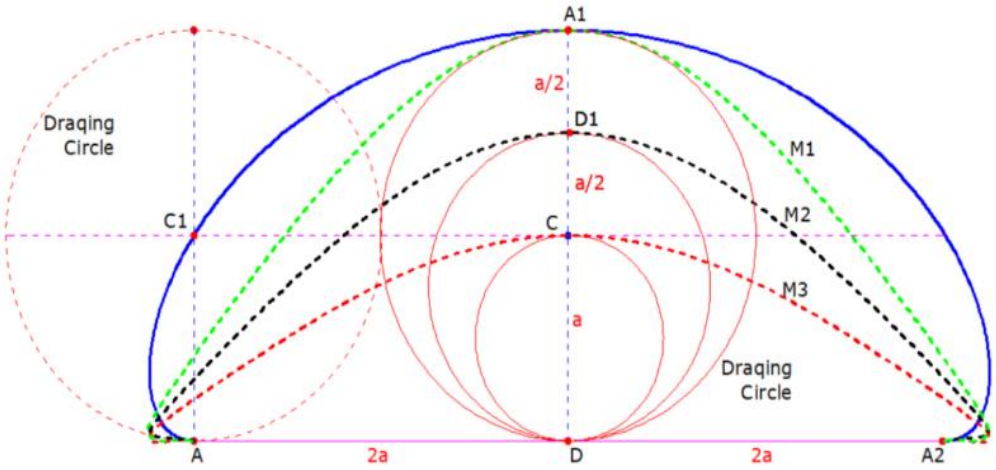

Group two; 3 curves of cusp; (M_1), (M_2), and (M_3).

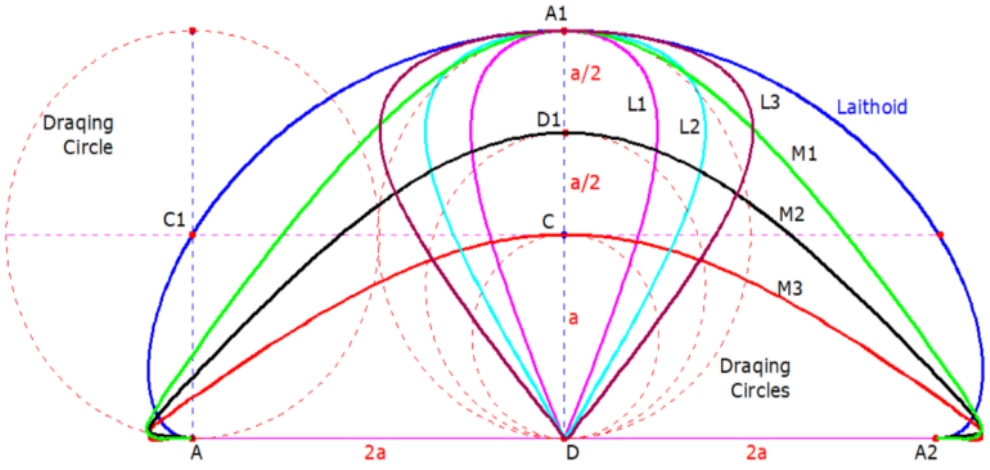

Figure 9: Constructing a set of two groups of new curves from a point on *Laithoid*, Where the rolling disk's radius is (*a*) and (*n*) a point on the curve

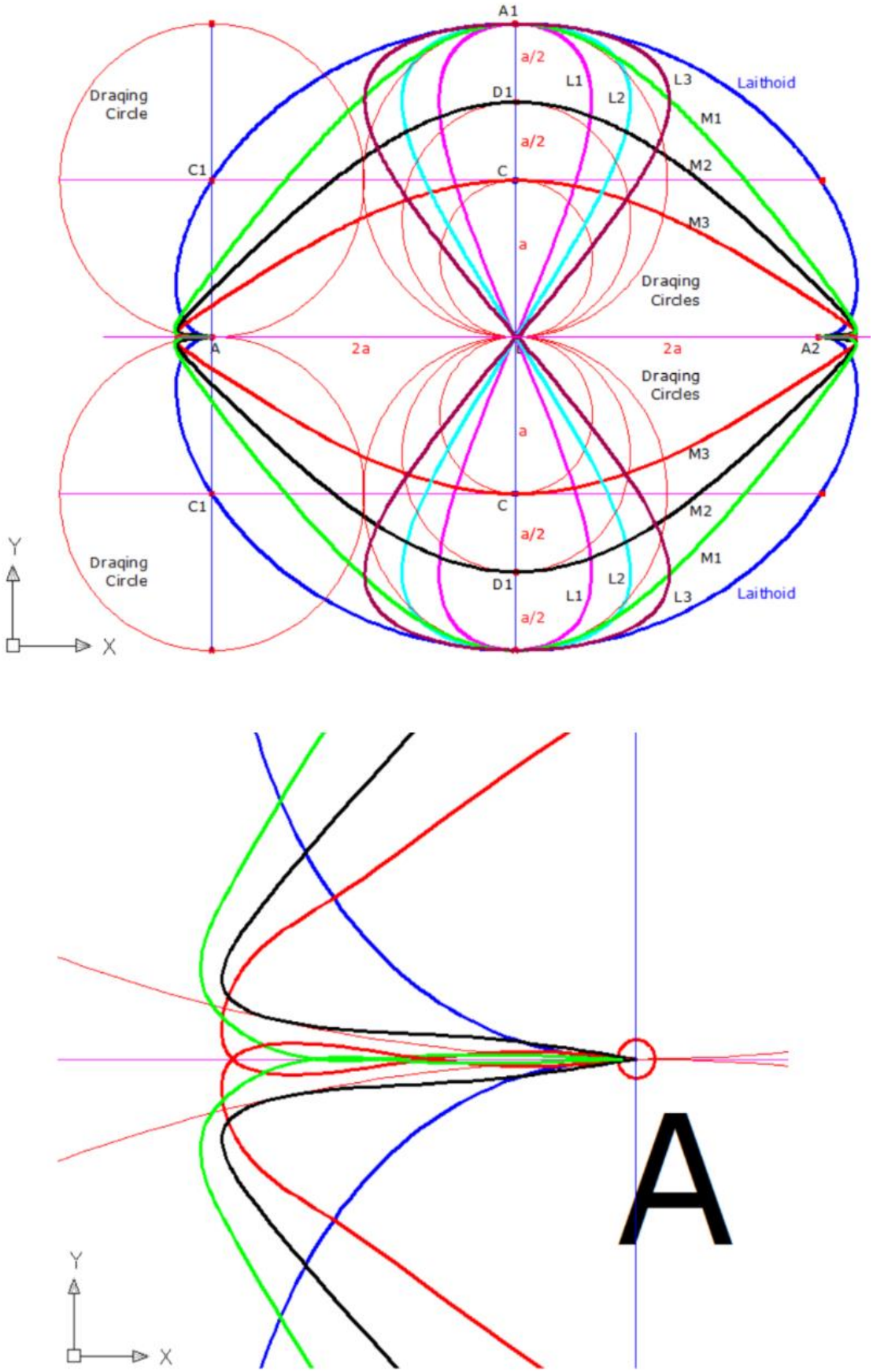

Figure 10: Plot all two groups of *Laithoid's* curves over ±y and x axis zooming in point of (A). Where the rolling disk's radius is (a)

4. Conclusion:

This paper delves into a specific aspect of 2D plane geometry, focusing on a special case of the cycloid, termed the "*Laithoid*". The paper utilizes geometric methods and mathematical analyses to investigate various aspects of the *Laithoid* curves. It explores equalities between different metrics in specific instances of the cycloid, indicating a rigorous analytical approach. The introduction of new curves and their properties demonstrates a comprehensive investigation of various geometrical aspects. The study explores various equalities between the Cassinian metric and other related metrics in specific instances of the cycloid. Additionally, the paper introduces six new curves and thoroughly investigates their properties. A rolling disk with a constant radius of 'a' is utilized to develop a geometric method for identifying points of curvature. These curves are categorized into two groups based on their rolling characteristics, with some completing a full rolling at one point ($2a$, 0) without a cusp, while others complete a full rolling at two points (0, 0) and ($4a$, 0).

The paper includes studying equalities between metrics related to the cycloid, introducing six new curves, investigating their properties, and examining the invariance and distortion properties of these curves using geometric methods. Additionally, the paper explores the creation of 3D surfaces from these curves through consistent revolution. The research also employs geometric methods to examine the invariance and distortion properties of these curves. Notably, certain curves are referred to as "heart-like *Laithoids*" due to their semi-cyclic nature, featuring arches with cusps along the y-axis. The study considers a more general form of relative distortion properties, incorporating the rolling disk's radius (a), distance ratio ($4a$), and ray segment angle (u). Furthermore, it is found that the curves generated in this study possess a cusp along with the *Laithoid*, where the cusp's intersection point lies on the y-axis. This observation defines a specific shaded region of area associated with the curve's cusp. The creation of 3D surfaces derived from these curves offers new insights into their geometric properties and applications. Furthermore, this study explores the generation of novel 3D surfaces (M_1, M_2, and M_3) from these curves by consistently revolving their shapes. The surface resulting from the revolution of the Laithoid's curves around the y-axis exhibits a simple and symmetric form, albeit requiring supplementary steps to adapt them to complex notation and operational calculus.

Regarding the limitations and future directions, further exploration of 3D and 2D practical applications and the need for adaptation to complex notation and operational calculus are taken into account. In conclusion, the findings presented in this paper hold potential for significant practical applications. The Laithoid's curves, especially in architectural engineering, show

promise for future practical use. The author's selection of conclusions is based on their extensive experience in this field.

Acknowledgments: It gives immense pleasure to thank all those who extended their coordination, moral support, guidance, and encouragement to reach the publication of the article. My special thanks to my family; my wife Angham S.M., and my daughters; Noor, Nada, Fatima, and Omneya, for their full support and coordination.

Author's declaration: Conflicts of Interest: None. I hereby confirm that all the Figures and Tables in the manuscript are mine. Besides, the Figures and images, which are not mine, have been permitted re-publication and attached to the manuscript.

5. References

[1] Stone TW, Smith J. A note on topological entropy. Appl Gen Topol. 2000;1(1):25-37.

[2] Cajori F. A History of Mathematics. New York: Chelsea; 2000. p. 177.

[3] Kabai S. Mathematical Graphics I: Lessons in Computer Graphics Using Mathematica. Püspökladány, Hungary: Uniconstant; 2002. p. 145.

[4] Apostol TM, Mnatsakanian M. New Horizons in Geometry. Washington, DC: Mathematical Association of America; 2012. p. 68.

[5] Mottola RM. Comparison of Arching Profiles of Golden Age Cremonese Violins and Some Mathematically Generated Curves. Savart J. 2011;1.(١)

[6] Lockwood EH. A Book of Curves. Cambridge, England: Cambridge University Press; 1967. p. 187-188.

[7] Roidt T. Cycloids and Paths [PDF]. Portland State University; 2011. p. 4. Available from: https://web.archive.org/web/20111022090445/http://www.someurl.com.

[8] Roberts C. Elementary Differential Equations: Applications, Models, and Computing. 2nd ed. Boca Raton, FL: CRC Press; 2018. p. 141.

[9] Choi H. Invariance of the Area and Volume of Cycloid Surfaces and Trochoid Surfaces. Am Math Mon. 2022. https://doi.org/10.1080/00029890.2022.2130677.

[10] Šajgalík M, Milena K. Analysis and Prediction of the Machining Force Depending on the Parameters of Trochoidal Milling of Hardened Steel. Appl Sci. 2020;10(5):1788. https://doi.org/10.3390/app10051788.

[11] Yang RG, Han B, Li FP, Zhou YQ, Xiang JW. Nonlinear dynamic analysis of a trochoid cam gear. J Mech Des. 2020;142(9):1-12.

[12] Yang RG, Li FP, Zhou YQ, Xiang JW. Nonlinear dynamic analysis of a cycloidal ball planetary transmission considering tooth undercutting. Mech Mach Theory. 2020;145:103694.

[13] Ronggang Y, Bo H, Jiawei X. Nonlinear Dynamic Analysis of a Trochoid Cam Gear with the Tooth Profile Modification. Appl Sci. 2020;10(5):1788. https://doi.org/10.3390/app10051788.

[14] Al-ossmi LH. Laithoid curve. Univ Thi-Qar J Eng Sci. 2010;1(1):29-43. Available from: https://jeng.utq.edu.iq/index.php/main/article/view/136.

[15] Al-ossmi LHM. Noor's Curve, a New Geometric Form of Agnesi Witch, a Construction Method is Produced. Baghdad Sci J. 2021;18(2 Suppl):1113. http://dx.doi.org/10.21123/bsj.2021.18.2(Suppl.).1113.

[16] Al-ossmi LHM. Nada's Curve Towards a new curvature produced by the tangent of a circle and an ellipse: The Nada's curve. IJCSM. 2022;4(1). DOI: 10.52866/ijcsm.2023.01.01.001.

[17] Al-ossmi LHM. An elementary treatise on elliptic functions as trigonometry. Alifmatika: J Pendidik Dan Pembelajaran Mat. 2023;5(1):1-20. https://doi.org/10.35316/alifmatika.2023.v5i1.1-20.

[18] Xu LX, Yang YH. Dynamic modeling and contact analysis of a cycloid-pin gear mechanism with a turning arm cylindrical roller bearing. Mech Mach Theory. 2016;104:327-349.